

**University of Strathclyde**  
**Department of Pure and Applied Chemistry**

# **Development of novel optical sensors**

by

**Graham A. Skinner**

A thesis presented in fulfilment of the requirements for the degree of  
Doctor of Philosophy

**2011**

This thesis is the result of the author's original research. It has been composed by the author and has not been previously submitted for examination which has led to the award of a degree.

The copyright of this thesis belongs to the author under the terms of the United Kingdom Copyright Acts as qualified by University of Strathclyde Regulation 3.50. Due acknowledgement must always be made of the use of any material contained in, or derived from, this thesis.'

Signed:

Date:

# Acknowledgements

---

I would like to express my thanks to my supervisor Prof. Andrew Mills, for his continued guidance and enthusiasm throughout all of my PhD. I have learned much throughout my time under his supervision and not least how to take a photograph with a perfectly white background! The Mills Group have been a constant source of friendship and guidance throughout, with each group member helping the other whenever needed. A special thanks to Chris O'Rourke for his patience helping me with many technical issues and also to Dr. Julie Bardin for proof reading this thesis.

Without Bob Fabian's constant ability to transfer our adventurous design ideas into high quality pieces, many of the results reported in this thesis would not exist. A big thanks to Bob for his patience and high quality craftsmanship. A special thanks to Robbie Macdonald for his help carrying out the fizzy drink experiments – definitely a young scientist in the making!

A wider thanks to all the technicians and support staff in the Chemistry Department who have helped me in many ways throughout my PhD.

Thanks also to EPSRC for funding this research.

My family and friends' constant support and interest have been a source of great encouragement throughout my studies and to them I give thanks. Throughout everything I have endeavoured in life, my parents Graham and Elaine, have continued to support me through prayer, advice and their love - Dad and Mam, thank you.

Lastly, I thank my wife Linda. I am so privileged to have such a loving and understanding wife who has sacrificed much to allow me to undertake my PhD. Her prayerfulness, gentle words of encouragement and constant support have been steadfast throughout. Linda, thank you for everything and to you I dedicate this thesis.

“Give thanks to the LORD, for he is good.

*His love endures forever...*” Psalm 136

# Abstract

---

A range of novel and innovative colourimetric optical indicators for commercially important analytes have been developed and characterised.

Water-based colourimetric indicator films are shown to have increased operational lifetimes under ambient conditions compared to similar solvent-based counterparts. Response and recovery times, as well as CO<sub>2</sub> sensitivity of a water-based, CO<sub>2</sub>-responsive ink are reported and compared to those of a similar solvent-based indicator. An investigation into the effect of humidity and temperature on CO<sub>2</sub> sensitivity was carried out, as well as the effect of plasticiser and base concentration on the response and recovery times.

The first example of a colourimetric indicator which detects CO<sub>2</sub> levels above ambient pressure is reported. The different sensitivities of the ink over the pressure range 1 - 8 bar are recorded, along with the effect of humidity on the response and recovery of the indicator. Its application as a 'fizziness' indicator is explored and a number of experiments using carbonated drinks demonstrated.

The coating of dyes onto inorganic supports, creating a range of intelligent pigments, has opened up a fresh way of developing a new family of intelligent materials. The incorporation of such intelligent pigments into thermoplastic polymers to create a range of flexible plastic indicators is described. The characterisation (e.g. response and recovery times, CO<sub>2</sub> sensitivity and effect of humidity and temperature on such sensitivity) of the indicator films revealed similar sensing capabilities as previously reported in the ink films.

Two polyoxometalate based indicators are described: an oxygen indicator and a UV dosimeter. The effects on the sensing characteristics of both inks by varying the key components (i.e. glycerol and polyoxometalate) are reported. Illustrations of the oxygen ink being used as a delayed oxygen indicator in food packaging applications are investigated. It is shown that the UV dosimeter can be tuned to match different skin types, by altering the ink formulation.

# Contents

---

<b>Acknowledgements.....</b>	<b>i</b>
<b>Abstract.....</b>	<b>ii</b>
<b>Contents.....</b>	<b>iii</b>
<b>List of Figures.....</b>	<b>ix</b>
<b>List of Tables .....</b>	<b>xviii</b>
<b>Chapter 1: Introduction .....</b>	<b>1</b>
1.1 Optical indicators .....	1
1.1.1 Carbon dioxide.....	3
<i>1.1.1.1 Capnography.....</i>	<i>9</i>
<i>1.1.1.2 Intelligent packaging.....</i>	<i>15</i>
<i>1.1.1.2.1 Modified Atmosphere Packaging (MAP) .....</i>	<i>17</i>
<i>1.1.1.3 Environmental Monitoring.....</i>	<i>22</i>
<i>1.1.1.4 Summary.....</i>	<i>24</i>
1.1.2 Oxygen .....	24
1.1.2.1 Food packaging.....	25
<i>1.1.2.1.2 Colourimetric Redox Dye-based Indicators .....</i>	<i>30</i>
<i>1.1.2.2 Polyoxometalates (POMs) .....</i>	<i>34</i>
1.1.3 Ultra Violet radiation .....	40
1.1.3.1 UV Index.....	41
1.1.3.2 UV dosimetry.....	43
1.2 Aims and objectives .....	48
1.3 References .....	48
<b>Chapter 2: Experimental.....</b>	<b>57</b>
2.1 Chemicals.....	57
2.2 Spectrophotometric Techniques.....	57
2.2.1 UV/Visible spectrophotometry.....	57

2.2.2 Diffuse Reflectance spectroscopy (DRS).....	61
2.2.3 Fluorimetry.....	63
2.3 UV light sources.....	63
2.4 General sample preparation.....	65
2.4.1 Ink preparation .....	65
2.4.2 Ink-film formation.....	65
2.4.2.1 <i>Spin coating</i> .....	65
2.4.2.2 <i>K-bar coating</i> .....	66
2.4.3 Pigment preparation .....	67
2.4.4 Pigmented polymer film preparation .....	67
2.5 Optical microscope.....	69
2.6 Film thickness measurements .....	70
2.6.1 Scanning electron microscopy (SEM) .....	70
2.6.2 Profilometry .....	70
2.6.3 Micrometry.....	72
2.7 Gas blending .....	72
2.8 Humid gas blends.....	73
2.9 Temperature studies .....	74
2.10 pH Measurement .....	75
2.11 Packaging sealer.....	75
2.12 References .....	76

### **Chapter 3: Water-based indicators for the detection of CO<sub>2</sub>..... 77**

3.1 Introduction.....	78
3.2 Experimental .....	80
3.2.1 Ink formulations .....	80
3.2.2 Dried ink films .....	81
3.3 Results and Discussion.....	82
3.3.1 Dye .....	82
3.3.2 Longevity .....	82
3.3.3 CO <sub>2</sub> sensitivity of water-based indicator .....	85
3.3.4 Indicator response and recovery times.....	90

3.3.5 Effect of base concentration.....	91
3.3.6 Effect of plasticizer .....	92
3.3.7 Effect of humidity .....	93
3.3.8 Effect of temperature.....	94
3.4 Applications .....	95
3.5 Conclusions .....	97
3.6 References .....	98

## **Chapter 4: High pressure CO<sub>2</sub> indicators ..... 100**

4.1 Introduction .....	100
4.2 Experimental .....	101
4.2.1 Ink formulations .....	101
4.2.2 High pressure gas cell set-up.....	102
4.2.3 Modified drinks bottles .....	104
4.2.3.1 'Artificial' pressurisation of drinks bottle .....	104
4.2.3.2 Bottle cap with incorporated pressure gauge .....	105
4.2.3.3 Bottle cap with glass window.....	106
4.2.4 Solar Simulator .....	106
4.3 Results and discussion .....	107
4.3.1 Identification of suitable dye.....	107
4.3.1.1 Phenol red.....	108
4.3.2 Ink optimization .....	109
4.3.3 CO <sub>2</sub> sensitivity of water-based ink.....	110
4.3.4 Indicator response and recovery times and effect of humidity .....	113
4.3.5 Development of a solvent-based ink.....	114
4.3.5.1 CO <sub>2</sub> sensitivity of ethanol-based ink .....	117
4.4 Applications .....	120
4.4.1 Typical headspace pressures .....	120
4.4.2 Relationship between headspace pressure and taste .....	123
4.4.3 Headspace pressurisation .....	124
4.4.4 Indicator trials .....	126
4.4.5 Temperature sensitivity.....	128

4.4.6 Stability .....	128
4.5 Conclusions .....	129
4.6 References .....	129
<b>Chapter 5: Intelligent pigments and plastics.....</b>	<b>131</b>
5.1 Introduction .....	131
5.2 Experimental .....	132
5.2.1 Colourimetric CO <sub>2</sub> Intelligent ink, pigment and plastic formulations ....	132
5.2.2 Colourimetric O <sub>2</sub> intelligent pigment and plastic formulations .....	134
5.2.3 Luminescent O <sub>2</sub> intelligent pigment and plastic formulations.....	134
5.3 Results and discussion .....	135
5.3.1 CO <sub>2</sub> -indicating pigments and plastics .....	135
5.3.1.1 CO <sub>2</sub> -sensitivity .....	138
5.3.1.2 Response and recovery times .....	143
5.3.1.3 Effect of temperature on CO <sub>2</sub> sensitivity.....	145
5.3.1.4 Effect of humidity on CO <sub>2</sub> sensitivity .....	147
5.3.1.5 Stability .....	148
5.3.2 Pressed pigment discs .....	149
5.4 Application.....	152
5.5 Further Work.....	153
5.6 Extended work on intelligent pigments and plastics.....	154
5.6.1 Breath responsive pigments .....	155
5.6.2 Oxygen indicating pigments and plastics.....	156
5.6.3 Luminescent oxygen indicating pigments and plastics.....	157
5.6.4 Volatile amine indicating pigments and plastics.....	164
5.7 Conclusions .....	164
5.8 References .....	165
<b>Chapter 6: Polyoxometalate based oxygen indicator .....</b>	<b>166</b>
6.1 Introduction .....	166
6.2 Experimental .....	167



6.2.1 Ink and pigment formulations .....	167
6.3 Results and discussion .....	168
6.3.1 PWA-based oxygen indicator .....	169
6.3.1.1 <i>Characteristics of standard PVA/PWA/glycerol indicator</i> .....	169
6.3.1.2 <i>Suitable UV light source</i> .....	173
6.3.1.3 <i>Effect of glycerol</i> .....	176
6.3.1.4 <i>Effect of humidity on response and recovery</i> .....	179
6.3.1.5 <i>'De-colouration' of the film</i> .....	182
6.3.1.6 <i>Application onto different substrates</i> .....	185
6.3.1.7 <i>Applications</i> .....	186
6.3.2 POM-based pigments and plastics .....	187
6.3.2.1 <i>Effect of SED on colourimetric response</i> .....	188
6.4 Conclusions .....	190
6.5 References .....	191
<b>Chapter 7: Polyoxometalate based UV dosimeter .....</b>	<b>193</b>
7.1 Introduction .....	193
7.2 Experimental .....	194
7.2.1 Ink formulations .....	194
7.3 Results and discussion .....	195
7.3.3 POM/Methylene blue based indicator.....	195
7.3.3.1 <i>Characterisation of standard PVA/MB/NaPWA/glycerol indicator</i> .....	195
7.3.3.2 <i>Indicator response and recovery times</i> .....	198
7.3.3.3 <i>Effect of humidity</i> .....	200
7.3.3.4 <i>Indicator optimisation as a personal UV-dosimeter</i> .....	202
7.4 Conclusions .....	206
7.5 References .....	207
<b>Chapter 8: Summary .....</b>	<b>208</b>
Further work.....	210

<b>Appendix – Published papers.....</b>	<b>212</b>
---	------------

# List of Figures

---

<b>Fig. 1.1</b> – Features of a dry optical indicator. ....	2
<b>Fig. 1.2</b> – Optical indicators for a range of applications. <sup>4,7,12-14</sup> .....	3
<b>Fig. 1.3</b> – Relationship between pH and CO <sub>2</sub> species.....	5
<b>Fig. 1.4</b> – Characteristics of a typical capnogram of a healthy patient. <sup>33</sup> .....	10
<b>Fig. 1.5</b> – Illustration of correct endotracheal tube placement. When the tube is inserted into position A, the indicator would show a colourimetric response (purple to yellow), however if inserted into position B, no colour change would occur, indicating incorrect placement. ....	11
<b>Fig. 1.6</b> - A.C.E STAT-Check™ CO <sub>2</sub> indicator. <sup>38</sup> .....	12
<b>Fig. 1.7</b> – Illustration of STAT-Check CO <sub>2</sub> indicator. <sup>37</sup> .....	13
<b>Fig. 1.8</b> - STAT-Check II™ illustrating the varying colour changes at different levels of CO <sub>2</sub> , 5%: yellow, 2%: brown and 0%: purple. <sup>39</sup> .....	14
<b>Fig. 1.9</b> – Mercury medical end tidal CO <sub>2</sub> detectors. <sup>41</sup> .....	14
<b>Fig. 1.10</b> – Chemical structure of the phosphazene base in equilibrium with water. ....	20
<b>Fig. 1.11</b> – Reaction of HPTS with H <sup>+</sup> . <sup>63</sup> .....	23
<b>Fig. 1.12</b> – Illustration of the ‘absorption’ of O <sub>2</sub> as it removes the oxygen content from air. <sup>69</sup> .....	26
<b>Fig. 1.13</b> – Ageless scavengers in a commercial pack of ham, and illustration of effectiveness of ageless scavengers on rice storage. <sup>70</sup> .....	27
<b>Fig. 1.14</b> – Schematic illustrations of the basic processes associated with colourimetric redox dye-based indicators: basic chemical reduction (top) and UV-activation (bottom). ....	31
<b>Fig. 1.15</b> – Illustration of Ageless Eye™ oxygen indicator showing the colour transition with varying oxygen levels. <sup>83</sup> .....	32
<b>Fig. 1.16</b> – UV activated oxygen indicator developed by Mills. <sup>75</sup> .....	34
<b>Fig. 1.17</b> – Keggin structure of polyoxometalates (left) and structure of commonly used POM, phosphotungstic acid (right). <sup>96</sup> .....	36
<b>Fig. 1.18</b> – Photocatalytic cycle of POM. <sup>99</sup> .....	37
<b>Fig. 1.19</b> – Solar Safe wrist band. <sup>128</sup> .....	44
<b>Fig. 1.20</b> - UV SunSignals® Sensor. <sup>129</sup> .....	45

<b>Fig. 1.21</b> - Flag-like warnings of the approach to erythema are observed. <sup>130</sup> .....	46
<b>Fig. 2.1</b> – Change in the electronic structure of phenolphthalein resulting in a dramatic change in colour. ....	58
<b>Fig. 2.2</b> – UV/vis absorption spectroscopy carried out on solutions and inks coated onto glass disks. ....	59
<b>Fig. 2.3</b> – Schematic of double beam UV/visible spectrophotometer. ....	60
<b>Fig. 2.4</b> – Picture of Varian Cary 50 spectrophotometer <sup>1</sup> (left) and gas cell which films are mounted onto, for recording of spectra (right).....	61
<b>Fig. 2.5</b> – Konica Minolta Cm-2500d portable spectrophotometer. <sup>2</sup> .....	61
<b>Fig. 2.6</b> – Schematic illustration of diffuse reflectance. ....	62
<b>Fig. 2.7</b> – Schematic of fluorimeter. ....	63
<b>Fig. 2.8</b> – Emission spectra of UVB lamp (—) and solar simulator (----). ....	64
<b>Fig. 2.9</b> - Typical spin coated ink film from ink solution.....	66
<b>Fig. 2.10</b> – Illustration of coating inks onto a substrate, using K-bars. ....	66
<b>Fig. 2.11</b> - Specac Atlas™ Series Heated Platens set-up.....	68
<b>Fig. 2.12</b> – Typical pigment and subsequent pigmented polymer film. ....	69
<b>Fig. 2.14</b> – SEM image of ink obtained from the Cambridge Stereoscan 90 SEM...	70
<b>Fig. 2.15</b> – Top: Dektak profilometer used for measuring the thickness of thin polymer films. Bottom: Sample result obtained from a 10% HEC spun onto quartz at 700 rpm, showing a film thickness of 2.5µm.....	71
<b>Fig. 2.16</b> – Picture of Mitutoyo digital micrometer. ....	72
<b>Fig. 2.17</b> - Cole-Parmer Rotameter.....	72
<b>Fig. 2.18</b> – Experimental set-up for obtaining different gas blends of CO <sub>2</sub> with varying humidity levels.....	73
<b>Fig. 2.19</b> – Optical arrangement for testing temperature sensitivity of ink films. <sup>6</sup> ...	74
<b>Fig. 2.20</b> – Food packager used to test indicators.....	75
<b>Fig. 3.1</b> – Solvent-based CO <sub>2</sub> -indicators as developed by Mills et al. in 1992. <sup>1</sup> .....	78
<b>Fig. 3.2</b> – Degradation of tetrabutylammonium hydroxide <i>via</i> Hoffman elimination. ....	79
<b>Fig. 3.3</b> – Photographs of water- and solvent-based ink and spun films. ....	81
<b>Fig. 3.4</b> – Structure of <i>m</i> -cresol purple. ....	82

<b>Fig. 3.5</b> – Comparison of film deterioration of water-based (top) and solvent-based indicators (bottom) when stored in the dark under ambient conditions.....	83
<b>Fig. 3.6</b> – Absorption spectra (recorded in triplicate) taken at various points across the radius of the film. ....	84
<b>Fig. 3.7</b> – Photographs of a standard CO <sub>2</sub> indicator and progressive colour response chart to CO <sub>2</sub> .....	86
<b>Fig. 3.8</b> – Photographs of the water-based CO <sub>2</sub> -indicator beside a sample of water where a pellet of dry ice has been inserted, rapidly evolving CO <sub>2</sub> gas.....	87
<b>Fig. 3.9</b> – UV/visible absorption spectra of the standard film as a function of %CO <sub>2</sub> at 21°C, for %CO <sub>2</sub> (from top to bottom) of 0, 2, 5, 10, 20, 30, 60, 100%, respectively. ....	88
<b>Fig. 3.10</b> – Plots of absorbance of film at 588 nm vs. %CO <sub>2</sub> at 21°C (insert: R vs. %CO <sub>2</sub> ). Data from Fig. 3.9. The solid lines are best fits to the data, assuming an $\alpha$ value of $0.052 \pm 0.001$ %CO <sub>2</sub> <sup>-1</sup> . ....	89
<b>Fig. 3.11</b> – Absorbance versus time plot for the typical water-based film, when exposed to alternating gas supply of air and 100% CO <sub>2</sub> (g) at 21°C.....	90
<b>Fig. 3.12</b> – Change in normalised absorbance (= $\Delta\text{Abs} / \Delta\text{Abs}_0$ ) versus %CO <sub>2</sub> at 21°C, as a function of varying sodium hydrogen carbonate concentration (from bottom to top: 0.1, 0.5, 0.7, 0.9 M and saturated respectively). The insert diagram is a plot of $\alpha$ (from the data in the main diagram) versus $1 / [\text{NaHCO}_3]$ . ....	91
<b>Fig. 3.13</b> - Relationship between response/recovery time and glycerol concentration (top: $\tau_{90}$ recovery and bottom: $\tau_{90}$ response).....	92
<b>Fig. 3.14</b> – Effect of humidity on sensitivity ( $\alpha$ ) for a water-based indicator (•) and solvent-based indicator (€) (21°C). The sensitivity of the water-based ink is directly proportional to %RH (a), whereas that of the solvent-based ink is mostly independent (b) or, at high %RH, negatively affected (c).....	93
<b>Fig. 3.15</b> – Van't Hoff plot of the temperature data from which $\Delta\text{H}$ and $\Delta\text{S}$ was calculated, knowing $m = -\Delta\text{H}/R$ and $c = -\Delta\text{S}/R$ .....	95
<b>Fig. 3.16</b> – Ink applied by pen onto a variety a substrates (top right: ceramic tile, middle right: metal foil, bottom right: cellulose based filter paper) all showing a distinct colour change when exposed to CO <sub>2</sub> (g). ....	96

<b>Fig. 3.17</b> – Illustration of the water-based CO <sub>2</sub> indicator at room temperature being used as a MAP packaging indicator. <b>A</b> – pork packaged under a high CO <sub>2</sub> atmosphere, indicator is yellow under these conditions. <b>B</b> – opened package, hence CO <sub>2</sub> concentration significantly reduced, hence indicator has changed colour to purple.....	97
<b>Fig. 4.1</b> – Top: Schematic of experimental set-up, where (a) is high pressure gas cell sample holder inside spectrophotometer and (b) is the front of the cell, showing indicator in line with beam, bottom: photographs of the high pressure gas cell.....	103
<b>Fig. 4.2</b> – Photographs of modified carbonated drinks bottle used to artificially pressurise the bottle.....	104
<b>Fig. 4.3</b> – Photographs of bottle cap with pressure gauge. ....	105
<b>Fig. 4.4</b> – Photographs of bottle cap with glass window. ....	106
<b>Fig. 4.5</b> - SS150W solar simulator (Sciencetech). <sup>10</sup> .....	107
<b>Fig. 4.6</b> – Structural change of phenol red in the presence of acid.....	109
<b>Fig. 4.7</b> – Photograph of optimised ink and spun film. ....	110
<b>Fig. 4.8</b> - UV/visible absorption spectra of film at different pressures of CO <sub>2</sub> at 21°C (from top to bottom: air, 1, 2, 4, 6, 8 bar respectively).....	111
<b>Fig. 4.9</b> - Plots of absorbance of film at 570 nm vs. <i>p</i> CO <sub>2</sub> at 21°C (insert: <i>R</i> vs. <i>p</i> CO <sub>2</sub> ). Data from Fig. 4.8. The solid lines in the two diagrams are best fits to the data, revealing an $\alpha$ value of $0.65 \pm 0.04 \text{ bar}^{-1}$ .....	112
<b>Fig. 4.10</b> – Change in absorbance of the film at 570 nm as the CO <sub>2</sub> pressure is increased and decreased stepwise (21°C).....	113
<b>Fig. 4.11</b> – Effect of humidity to response and recovery; higher %RH levels decrease response and recovery times (21°C).....	114
<b>Fig. 4.12</b> – UV/visible absorption spectra of film at different pressures of CO <sub>2</sub> at 21°C (from top to bottom: air, 1, 2, 3, 4, 6, 8 bar respectively).....	118
<b>Fig. 4.13</b> – Plots of absorbance of film at 570nm versus <i>p</i> CO <sub>2</sub> at 21°C (insert: <i>R</i> vs. <i>p</i> CO <sub>2</sub> ). Data from Fig. 4.12. Solid lines were best fit to the data, revealing an $\alpha$ value of $0.8453 \pm 0.06 \text{ pCO}_2^{-1}$ . ....	119
<b>Fig. 4.14</b> – Change in absorbance of the film as the CO <sub>2</sub> (g) pressure is increased and decreased stepwise (21°C).....	120
<b>Fig. 4.15</b> – Carbonation chart <sup>20</sup> .....	122

<b>Fig. 4.16</b> – Relationship between headspace pressure of lemonade bottle over time, along with average taste ratings. ....	123
<b>Fig. 4.17</b> – Plot of headspace pressure vs. time after re-sealing. ....	125
<b>Fig. 4.18</b> - Pictures of the laminated ink inside a plastic lemonade bottle with fizzy lemonade and the associated colour changes at three different pressures of CO <sub>2</sub> – air, 1 bar and 3 - 4 bar CO <sub>2</sub> respectively. ....	127
<b>Fig. 4.19</b> – Bottle cap changing colour with increasing pressure of CO <sub>2</sub> (g). ....	127
<b>Fig. 4.20</b> – Absorption spectra of water-based indicator when exposed to AM 1.5 solar simulated light. at 0, 1, 3, 6 and 24 hours at 22°C. ....	129
<b>Fig. 5.1</b> – Hydrophobation of silica. ....	132
<b>Fig. 5.2</b> – (a) - before exposure to CO <sub>2</sub> (g), (b) – during exposure to CO <sub>2</sub> , (c) – after exposure to CO <sub>2</sub> . ....	136
<b>Fig. 5.3</b> – Images of a large dye-coated fumed hydrophobic silica crystal, before and after exposure to CO <sub>2</sub> . ....	137
<b>Fig. 5.4</b> - Images of a dye-coated hydrophilic silica crystals, before and after exposure to CO <sub>2</sub> . ....	138
<b>Fig. 5.5</b> - UV/visible diffuse reflectance spectra of the powder as a function of %CO <sub>2</sub> at 21°C, for (from top to bottom) of 0, 1, 2, 3, 5, 10, 50, 100%CO <sub>2</sub> , respectively. .	139
<b>Fig. 5.6</b> – Plots of reflectance of powder at 588 nm vs. %CO <sub>2</sub> at 21°C (insert: <i>R</i> vs. %CO <sub>2</sub> ). Data from Fig. 5.5. The solid lines are best fits to the data, assuming an $\alpha$ value of $0.883 \pm 0.086$ %CO <sub>2</sub> <sup>-1</sup> . ....	140
<b>Fig. 5.7</b> - Colour change of CO <sub>2</sub> -sensing pigment incorporated into polyethylene plastic film, when exposed to 100 % CO <sub>2</sub> . ....	141
<b>Fig. 5.8</b> – UV/visible absorption spectra of the MCP/silica/PE plastic film as a function of %CO <sub>2</sub> at 21°C, for %CO <sub>2</sub> (from top to bottom) of 0, 1, 2, 3, 4, 5, 20, 30, 60, 100%CO <sub>2</sub> , respectively. Abs <sub>∞</sub> is ~ 0.44. ....	141
<b>Fig. 5.9</b> – Plots of absorbance of MCP/silica plastic film at 592 nm versus %CO <sub>2</sub> at 21°C. Data from Fig. 5.8. Solid lines were best fit to the data, revealing an $\alpha$ value of $0.185 \pm 0.02$ %CO <sub>2</sub> <sup>-1</sup> . ....	142
<b>Fig. 5.10</b> – Response of pigment when exposed to 100% CO <sub>2</sub> (g) at 21°C. ....	143
<b>Fig. 5.11</b> – Response and recovery of the MCP/silica/PE film when exposed to 100% CO <sub>2</sub> (g) and air at 21°C. ....	144

<b>Fig. 5.12</b> – Triplicate response and recovery of the MCP/silica/PE film when exposed to alternate 100% CO <sub>2</sub> and air purges at 21°C. ....	145
<b>Fig. 5.13</b> – The effect of temperature on the change of absorbance (at 592 nm) versus %CO <sub>2</sub> , where $\diamond = 20^{\circ}\text{C}$ , $\Delta = 25^{\circ}\text{C}$ and $+ = 30^{\circ}\text{C}$ .....	146
<b>Fig. 5.14</b> - Plot of $\ln \alpha$ versus $T^{-1}$ where $\alpha$ is the gradient of an R versus %CO <sub>2</sub> plot as a function of temperature. ....	147
<b>Fig. 5.15</b> – Effect of humidity on sensitivity ( $\alpha$ ) for MCP/silica/PE CO <sub>2</sub> -indicator at 22°C.....	148
<b>Fig. 5.16</b> – Colour change of pressed silica discs when exposed to CO <sub>2</sub> (g).....	150
<b>Fig. 5.17</b> – Diffuse reflectance spectra of wax/silica disc in the presence of air (—) and also carbon dioxide (- - -) at 22°C. ....	151
<b>Fig. 5.18</b> – Response and recovery of 30% w/w wax/silica disc towards carbon dioxide at 22°C.....	152
<b>Fig. 5.19</b> – Illustration of the intelligent plastic being used as a leak indicator in MAP packaged foods.....	153
<b>Fig. 5.20</b> – Photographs of pigment, polymer chips and extruded MCP film. ....	154
<b>Fig. 5.21</b> – CO <sub>2</sub> pigments responding to levels on CO <sub>2</sub> contained in human breath. Top: <i>o</i> -cresolphthalein based pigment, bottom: thymolphthalein based pigment. ..	155
<b>Fig. 5.22</b> – Solvent-based MB/TiO <sub>2</sub> /DL-Threitol pigment irradiated under UVA light and its recovery in air.....	156
<b>Fig. 5.23</b> – Solvent-based intelligent O <sub>2</sub> -indicating plastic irradiated under UVA light and its recovery in air.....	157
<b>Fig. 5.24</b> – Photograph of Pt (II) OEP coated hydrophobic silica and the silica dispersed in a polyethylene film. ....	158
<b>Fig. 5.25</b> – Observed change in the relative luminescent intensity at 644 nm ( $\lambda_{\text{excit}} = 535 \text{ nm}$ ), as a function of $p\text{O}_2$ for Pt(II)OEP/Silica/Polyethylene plastic indicator at 22°C. The insert diagram shows the corresponding Stern-Volmer plot of the data, revealing $m = 0.211$ , $c = 1.63$ and $R^2 = 0.9387$ . ....	159
<b>Fig. 5.26</b> - Photographs of the Pt (II) OEP/Silica/polyethylene sample (1) in normal lighting conditions (2) under UVA light in air (20% O <sub>2</sub> ) and (3) under UVA light in nitrogen. ....	159
<b>Fig. 5.27</b> – Response of the indicator to 100% O <sub>2</sub> and recovery at 21°C.....	160



<b>Fig. 5.28</b> – Observed change in the relative luminescent intensity at 644 nm ( $\lambda_{\text{excit}} = 535$ nm), as a function of $p\text{O}_2$ for Pt(II)OEP/Silica/Polyethylene oxide plastic indicator at 21°C. The insert diagram shows the corresponding Stern-Volmer plot of the data, revealing $m = 0.9963$ , $c = 1.7195$ and $R^2 = 0.9697$ .....	161
<b>Fig. 5.29</b> - Response of the indicator to 100% $\text{O}_2$ and recovery at 21°C.....	162
<b>Fig. 5.30</b> – (1) Pt(II)OEP coated silica luminescence under UVA light when nitrogen is being blown onto the sample, (2) silica dispersed in polyethylene oxide under normal lighting conditions and (3) the same sample exposed to UVA light with a stream of $\text{N}_2$ being blown onto the surface. ....	162
<b>Fig. 5.31</b> – Top left: $\text{Ru}(\text{dpp})_3^{2+} (\text{Ph}_4\text{B}^-)_2$ based powder under ambient conditions, top right: same powder under UVA light and exposed to a stream of nitrogen gas. Bottom left: $\text{Ru}(\text{dpp})_3^{2+} (\text{Ph}_4\text{B}^-)_2$ based powder dispersed in polyethylene, under ambient conditions, bottom right: same sample under UVA light and exposed to a stream of nitrogen gas. ....	163
<b>Fig. 6.1</b> – Structures of polyvinylalcohol (PVA) and polyacrylamide (PAM).....	168
<b>Fig. 6.2</b> – Photographs of a standard oxygen indicator.....	169
<b>Fig. 6.3</b> – Proposed general mechanism involved in the colour change of the indicator from colourless to dark blue. ....	170
<b>Fig. 6.4</b> – UV/vis spectra of the PVA /PWA /glycerol film at different time intervals during irradiation 0, 2, 4, 6, 8, 10, 15, 20, 24, 30, 40, 50 and 60 minutes at 22°C. .	171
<b>Fig. 6.5</b> – Irradiation and response of PVA /PWA /glycerol indicator in air at 21°C. ....	172
<b>Fig. 6.6</b> – Absorbance versus time plot for the typical indicator, when irradiated under UVB light and under $\text{N}_2$ , then left to recover in humid air (~90%RH) at 21°C; the start of the latter is depicted by the .....	173
<b>Fig. 6.7</b> – Absorbance spectra of aqueous phosphotungstic acid solution (—) and a standard PWA/PVA/glycerol indicator (---) before irradiation. ....	174
<b>Fig. 6.8</b> – Comparison of colour change after irradiation of standard indicator using UVA and UVB light for 4 minutes, $4 \text{ mWcm}^{-2}$ . ....	175
<b>Fig. 6.9</b> – Response and recovery of PVA/PWA/glycerol film under UVB ( $\circ$ ) and UVA light ( $\bullet$ ) irradiances at 22°C. Arrow depicts end of irradiation and subjection of the indicator to air (oxygen source). ....	176

<b>Fig. 6.10</b> – Pictures of PVA/PWA films with (top) and without (bottom) glycerol, whilst being irradiated under UVB light.....	177
<b>Fig. 6.11</b> – Response and recovery profiles at 21°C for PVA/PWA films with (○) and without (●) glycerol. Arrow depicts end of irradiation and subsection of indicator to air.....	178
<b>Fig. 6.12</b> – Basic reaction mechanism between POM and polymer (PVA) /glycerol to produce the blue $W^{5+}$ species. <sup>3</sup> .....	179
<b>Fig. 6.13</b> – Effect of humidity on the irradiation of the standard PVA/PWA/glycerol indicator (● = ~ 0 – 10 %RH and □ = ~ 90 – 100%RH) at 22°C.....	180
<b>Fig. 6.14</b> – Effect of humidity on the recovery of the indicator, where ● = 0, X = 40, Δ = 50 and ○ = 100%RH, at 20°C.....	181
<b>Fig. 6.15</b> - The PVA/PWA indicator exposed to alternate streams of humid nitrogen and humid air.....	182
<b>Fig. 6.16</b> - Spectra of the indicator before and after three consecutive cycles of irradiation and response to oxygen in air. ....	183
<b>Fig. 6.17</b> – Photographs of a glycerol (A) and glycerol-free (B) indicator before and after irradiation under UVB light for 4 minutes, then after their response to oxygen in air.....	184
<b>Fig. 6.18</b> – Structures of SEDs. ....	188
<b>Fig. 6.19</b> – Irradiation of PWA pigments with varying levels of SED (1,6-hexanediol) and their response to oxygen in air.....	188
<b>Fig. 6.20</b> - Photographs of an O <sub>2</sub> -sensitive pigment incorporated in a polyethylene plastic film, before and after irradiation to UVB light.....	189
<b>Fig. 6.21</b> – Effect of SED quantity on the response and recovery of POM pigment/PE films with 50 (○) and 125 (●) pphr of 1,6-hexanediol, at 21°C.....	190
<b>Fig. 7.1</b> – Photographs of a standard PVA/MB/NaPWA/glycerol ink film, before and after irradiation under UVB light for 4 mins. ....	196
<b>Fig. 7.2</b> – Proposed schematic illustration of the cycles involved in the PVA/MB/NaPWA/glycerol indicator. ....	196
<b>Fig. 7.3</b> – UV/vis absorption spectra of the standard PVA/MB/NaPWA/glycerol indicator as a function of irradiation time at 21°C. Spectra were recorded every 15 seconds for 3 minutes.....	197

<b>Fig. 7.4</b> – Comparison of irradiation of standard PVA/MB/NaPWA/glycerol indicator under UVA (o) and UVB (●) light, at 21°C.....	198
<b>Fig. 7.5</b> – Comparison of recovery in air (●) and oxygen (o), after irradiation under UVB light in nitrogen, at 21°C.....	199
<b>Fig. 7.6</b> – Four consecutive cycles of UVB irradiation for 4 minutes and then recovery for 24 hours, at 22°C. ....	200
<b>Fig. 7.7</b> – Effect of level of humidity in air on the response of indicator after 4 minutes irradiation under UVB light (4 mWcm <sup>-2</sup> ), where ■ (80%RH), ◇ (50% RH), ● (25%RH) and Δ (0%RH), at 21°C. ....	201
<b>Fig. 7.8</b> – Plot of ΔAbs (λ = 610 nm) against MED level of skin phototype II for indicator films containing 0 pphr (●), 10 pphr (□), 40 pphr (×), 75 pphr (■), 150 pphr (o) and 240 pphr (▲) glycerol, at 21°C. Inset diagram shows the variation of initial rate with [glycerol], calculated using the data in the main diagram. MED values on x-axis are directly proportional to irradiation time, with MED = 1 ≡ 33 mins. ....	203
<b>Fig. 7.9</b> – Plot of ΔAbs vs. MED Skin phototype II for a series of indicator films containing 0 pphr (o), 30 pphr (◆), 35 pphr (□), 40 pphr (■), 45 pphr (×) and 50 pphr (▲) NaPWA, at 21°C. The ink contained 12 mg methylene blue opposed to the standard 8 mg, in the attempt to make the colour change of the final dosimeter more striking. MED values on x-axis are directly proportional to irradiation time, with MED = 1 ≡ 33 mins.....	204
<b>Fig. 7.10</b> – Plot of initial rate (r <sub>i</sub> ) vs. [NaPWA], illustrating the optimum concentration of NaPWA. ....	205
<b>Fig. 7.11</b> – Plot of ΔAbs vs. MED for skin phototype II for original (o) and modified (●) ink, at 21°C. ....	206

# List of Tables

---

<b>Table 1.1</b> – List of recent colourimetric CO <sub>2</sub> indicators.....	8
<b>Table 1.2</b> – Shelf-life of a selection of MAP and non-MAPed foods. <sup>50</sup> .....	18
<b>Table 1.3</b> – The UVI exposure categories. ....	41
<b>Table 1.4</b> – Classification of skin types.....	43
<b>Table 3.1</b> – Summary table of dark storage conditions over 35 weeks for water- and solvent-based CO <sub>2</sub> indicators. ....	85
<b>Table 4.1</b> – List of dyes tested for their suitability to be used in high pressure CO <sub>2</sub> indicating inks. ....	108
<b>Table 4.2</b> – Summary table of solvent-based inks investigated as high pressure CO <sub>2</sub> indicating inks. ....	116
<b>Table 4.3</b> – Typical carbonation levels in fizzy drinks. <sup>20</sup> .....	121
<b>Table 4.4</b> – Correlation between drink volume and equilibrium headspace pressure .....	125
<b>Table 6.1</b> – Response of indicators to oxygen in air at 4 and 21°C.....	185

# Chapter 1: Introduction

---

## 1.1 Optical indicators

The growing need for novel, innovative and effective optical chemical indicators is becoming increasingly recognised by a range of industries e.g. medicine, food packaging technology, environmental analysis. The simple detection of important analytes, which are not readily picked up by the human nose and eye, have the potential to contribute significantly to a wide variety of applications.

Efforts in this area have focused on the development of indicators with specific industrial and commercial applications. For such indicators to become commercially relevant, they must possess a number of key features such as: suitable sensitivity, appropriate detection limits for the application (and also tuneable to various detection limits), a degree of robustness, portability, longevity, non-toxicity, and ease of use. To achieve these criteria, an interdisciplinary approach is essential to develop a product suitable for everyday use. In particular, a broad chemical expertise covering inorganic, organic, polymer science as well as material science is imperative.

Many types of optical indicators have been reported in the literature, and most can be classified under the three main classes: electronic, biological and chemical. Sub-types also exist within each category, such as chemical optical indicators, which can be classified further to luminescent, colourimetric and electrochemical indicators. This thesis will focus on the development of novel colourimetric optical indicators.

Such indicators are extremely portable, easily miniaturised and have the ability to be incorporated into existing technology with minimum disruption. Most importantly, colourimetric optical indicators can be easily detected by the human eye, without the need for specialised training or analytical equipment. Such features make these indicators highly desirable to many industries, such as biotechnology, food and packaging and security.

The common features of most dry optical indicators are illustrated in Fig. 1.1. Typically, a dye is imbedded into a solid phase supporting material such as polymer. The supporting material must be chosen appropriately so that its porosity allows the analyte to diffuse effortlessly, thereby allowing a timely response.

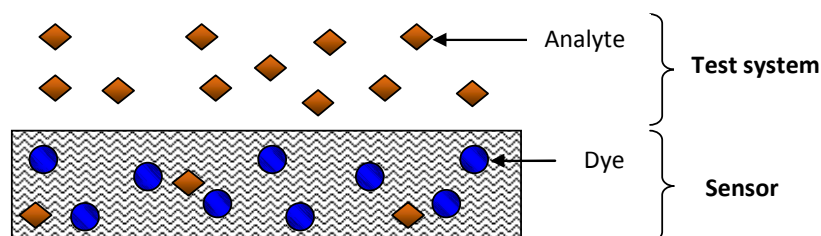


**Fig. 1.1** – Features of a dry optical indicator.

Recently developed optical indicators have been shown<sup>1-5</sup> to detect a wide range of analytes, indicative of the wide range of applications possible. For example, hydrogen peroxide ( $\text{H}_2\text{O}_2$ ) indicators can be used as effective anti-terrorism agents, specifically used in airport security.<sup>1,6</sup> The detection of ethylene gas by colourimetric indicators has shown that the ripening of fruit can be qualitatively analysed by observing the colour changes of the indicator incorporated into fruit packaging.<sup>7</sup> Volatile amines have been identified as the main analytes released during meat decomposition<sup>8</sup>, and are responsible for the characteristic ‘off’ smell that consumers recognise with putrefied food. Novel ammonia and volatile amine colourimetric indicators allow consumers to monitor the release of such gases, hence the freshness of the food contained within the food packaging.<sup>2</sup>  $\text{CO}_2$  sensitive indicators<sup>3,9-11</sup> able to colourimetrically detect  $\text{CO}_2$  in patients’ breath have found uses in medicine. Indicators which change colour with temperature have been shown to be useful in baby products<sup>12</sup> as well as chilled food packaging<sup>4</sup>. These examples demonstrate the versatility and impact such indicators can have in different areas of our lives. Fig. 1.2 illustrates some examples of commercially available optical indicators for a range of applications.

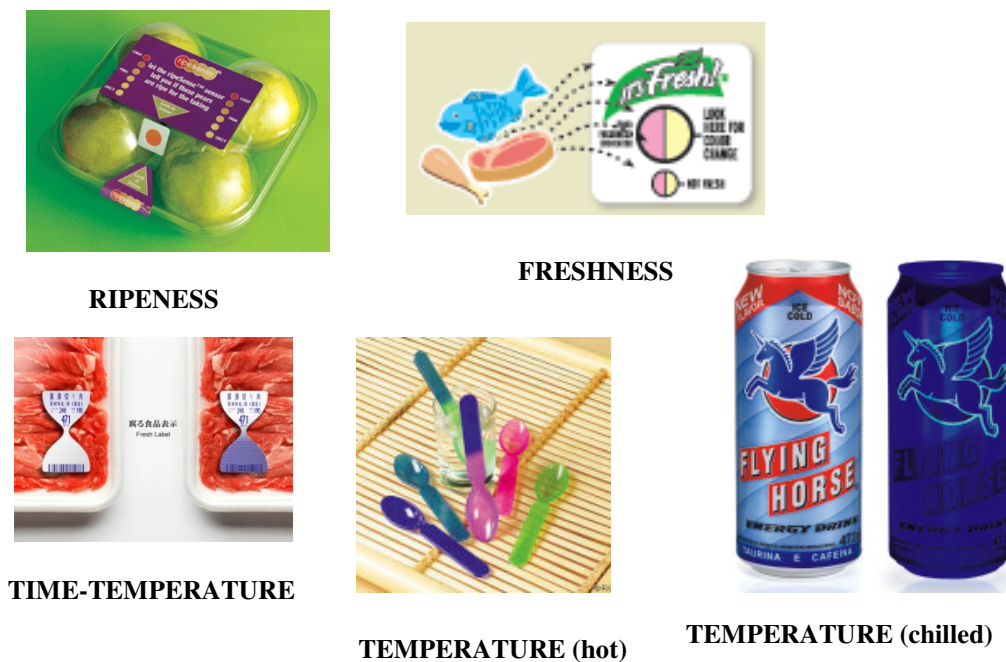
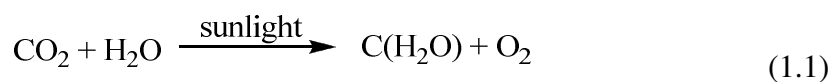


Fig. 1.2 – Optical indicators for a range of applications.<sup>4,7,12-14</sup>

The aim of this study is to develop novel colourimetric indicators for the detection of three commercially relevant analytes: CO<sub>2</sub>, O<sub>2</sub> and UV radiation. The importance of these analytes, along with their relevant applications, is discussed below and existing indicators reviewed.

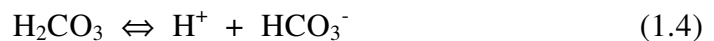
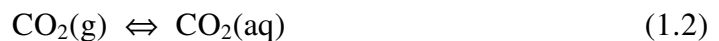
### 1.1.1 Carbon dioxide

Carbon dioxide is one of the most significant analytes in the world. Its importance can be easily demonstrated in reaction (1.1), where it supports the fine balance between plants, humans and animals in its use to generate the fuel and food necessary for the continued existence of most known forms of life.<sup>15</sup>



The reverse of reaction (1.1) is the basis of most cell metabolism, releasing the energy vital for life. The current global annual average concentration of carbon dioxide in the Earth's atmosphere is 386 ppm by volume and is rising between 1-2 ppm per year.<sup>16</sup> Although essential to life, CO<sub>2</sub> is toxic in high concentrations. Acute high-level CO<sub>2</sub> exposure in the presence of low-level O<sub>2</sub> can produce a range of adverse health effects in humans, including headaches, attacks of vertigo, poor memory and ability to concentrate, difficulty sleeping, double vision, photophobia, loss of eye movement, visual field defects, enlargement of blind spots, deficient dark adaptation, and personality changes.<sup>16</sup> Sufficiently high concentrations (typically >10%) can lead to unconsciousness in short periods of time.<sup>16</sup> In the UK the Short Term Exposure Limit (15-minute reference period) is 15,000 ppm.<sup>17</sup> Despite these health concerns, carbon dioxide's physical properties render its use vital to a number of industries, including food and beverage industry, fire extinguishing, welding, pharmaceuticals, lasers and refrigerants.

The high solubility of CO<sub>2</sub> in water (0.1449 g CO<sub>2</sub> / 100 ml H<sub>2</sub>O)<sup>18</sup> allows CO<sub>2</sub> to be easily detected if water is present in the sensing system, since carbonic acid (H<sub>2</sub>CO<sub>3</sub>) is formed when gaseous CO<sub>2</sub> is dissolved in water. Carbonic acid dissociates into hydrogen carbonate and carbonate ions, making the water slightly acidic. It is this change in ambient pH which enables quick and easy detection of CO<sub>2</sub>. The key reactions behind this acidification process are as follows,



Using carbonate mass balance and the acid equilibrium expressions, the fractional amounts of all carbonate species can be found as a function of [H<sup>+</sup>]. Fig. 1.3 illustrates the variation of carbonate species with increasing pH.



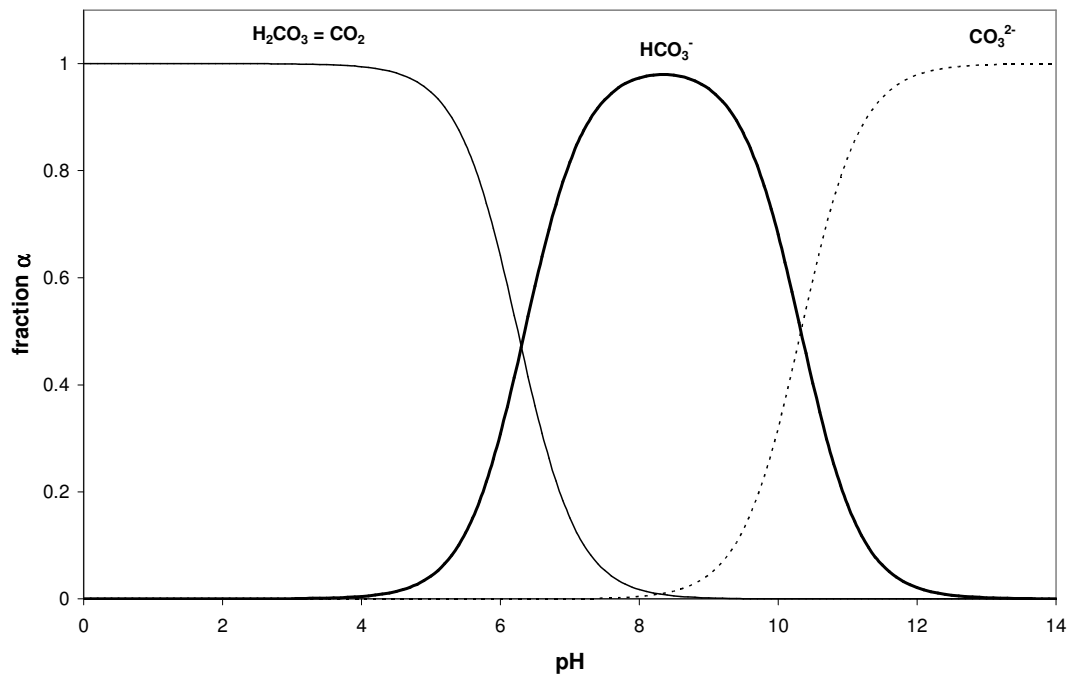


Fig. 1.3 – Relationship between pH and  $\text{CO}_2$  species.

The detection of carbon dioxide in the gas phase, historically, has been *via* infra-red (I.R.) spectroscopy. This is largely due to its strong infrared absorption band extending from 4200 to 4400 nm. However, I.R. spectroscopy requires long path lengths and bulky, expensive equipment. Gas chromatography has been used as an alternative to I.R., but as the technique still requires bulky, expensive equipment, it is not that widely used. Along with the expense, trained personnel are required to run these systems, which is far from ideal on a commercial scale. The measurement of dissolved carbon dioxide in an aqueous medium (e.g. riverwater, seawater or blood) using the above methods is very difficult, and other analytical methods are preferred. The Severinghaus electrode<sup>19</sup> currently dominates the routine monitoring of carbon dioxide, especially dissolved carbon dioxide. It is an analytical device which has been in common use for nearly 50 years without any serious challenge. The electrode utilises a pH electrode, placed in contact with a thin layer of an aqueous sodium bicarbonate solution, trapped behind a gas-permeable, ion-permeable membrane. Carbon dioxide in the test sample diffuses through the gas-permeable membrane, resulting in a change in the pH of the trapped bicarbonate layer which is measured by

the pH electrode. In the solution the equilibria described in reactions (1.2) – (1.5) are set up. The Severinghaus electrode is, unfortunately, fairly bulky, prone to electrical interference, affected by other acidic or basic gases and has fairly slow response and recovery times. Reference electrode contamination, osmotic pressure effects and liquid junction fouling also contribute to the problems faced when using the electrode on a daily basis. The initial cost and regular maintenance also contribute to the high expenditure required if such a system were to be used.

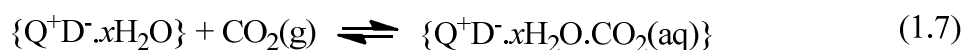
pH-sensitive colourimetric dyes have been recognised<sup>20</sup> as a method for CO<sub>2</sub> detection for many years. However the challenge remained as to how to incorporate these ionic dye species into a more useful medium, such as thin polymer films, which are largely hydrophobic. A breakthrough was achieved<sup>21</sup> through the addition of a phase transfer agent (PTA), which is able to extract the anionic form of a colourimetric pH indicator, from the highly polar protic medium into the less polar environment of the polymer/plasticizer. The water associated with the dye is also delivered to the hydrophobic polymer *via* the PTA and this appears to make possible a solvent-based solid, dry carbon dioxide sensors, based on reactions (1.2) – (1.5).

Thus, by utilising a PTA, the anionic form of the dye, D<sup>-</sup>, is rendered hydrophobic by ion-pairing with a quaternary ammonium cation, Q<sup>+</sup>, to form Q<sup>+</sup>D<sup>-</sup>. Therefore in a solid state CO<sub>2</sub> indicator, the equilibrium set up between the dye and carbon dioxide can be represented<sup>21</sup> by the following reaction.



Where  $\alpha'$  is the equilibrium constant associated with the process. It can be observed from the equilibrium that the presence of water is necessary for the sensor to function. In a dry gas atmosphere, although it might be expected that the solid thin film would lose the water of hydration and cease to function, this doesn't appear to

be the case. The water appears to be very tightly bound to the ion pair (i.e. the PTA cation and pH-sensitive dye anion), consequently allowing the sensor to be stored under very dry conditions without any appreciable loss in performance. The rate of diffusion of the carbon dioxide into the polymer network can be aided by using a plasticizer, which opens up the polymer network, whereby increasing the response rate of the sensor. A more detailed mechanism for the interaction of carbon dioxide and the dye has been proposed<sup>21</sup> in the following reactions (1.7) – (1.9):



The polymer ink films can be cast onto a variety of substrates using a range of techniques: e.g. doctor-blading, spin-coating, printing. This generates a range of thin, coloured plastic films containing a pH-sensitive dye in its highly coloured deprotonated anionic form i.e. as  $Q^+D^-$ .

$CO_2$  is widely used throughout a range of industries and its detection from trace quantities to high pressures is highly valued. The following discussion illustrates some of the applications for  $CO_2$  detection in greater detail, as well as some of the recent  $CO_2$  sensing technologies published in literature. Table 1.1, although not exhaustive, summarises some of the recent colourimetric  $CO_2$  indicators found in the literature.

**Table 1.1** – List of recent colourimetric CO<sub>2</sub> indicators

Dye	Sensor Type	PTA	Medium	Encapsulating medium	Application	Ref.
thymol blue	colourimetric	none	-	activated alumina	quantitative CO <sub>2</sub> determination in air.	20
phenol red, cresol red or thymol blue	colourimetric	none	aqueous	gel polymer - polyacrylamide or polyethyleneoxide supported on silicone rubber of PTFE, fiber optic.	does not specify	22
<i>m</i> -cresol purple or cresol red	colourimetric	tetraoctylammonium hydroxide	solvent	ethyl cellulose (EC)	adaptable to many	21
<i>p</i> -xylenol blue	colourimetric	tetraoctylammonium hydroxide	solvent	ethyl cellulose (EC)	dissolved CO <sub>2</sub> detection	23
$\alpha$ -naphtholphthalein or naphthol blue black or calmagite	colourimetric	tetraoctylammonium hydroxide	aqueous	Al <sub>2</sub> O <sub>3</sub> , SiO <sub>2</sub> or ZrO <sub>2</sub> dispersed in polyvinyl alcohol (PVA)	clinical applications e.g. breath analysis	24
quatarnary salts of various dyes e.g. <i>m</i> -cresol purple, phenol red	colourimetric	various quatarnary ammonium salts	solvent	polyvinyl butyral (PVB)/ polyethyleneimine	general CO <sub>2</sub> detection	25
bromothymol blue, thymol blue /8-hydroxypyrene-1,3,6-trisulfonic acid trisodium salt (HPTS)	colourimetric and fluorescent	tetrabutylammonium hydroxide	emulsion (RTIL in silicone matrix)	silicone matrix	high CO <sub>2</sub> concs. i.e. MAP	26
various e.g. thymol blue, bromothymol blue, <i>m</i> -cresol purple	colourimetric	none	aqueous	ink supported on borosilicate	breath analysis	27
<i>m</i> -cresol purple	colourimetric	none	aqueous	ink on whatman no. 1 filter paper	breath analysis	11
bromothymol blue	colourimetric	tetraoctylammonium hydroxide	ionic liquids	none	gas processing	28
cresol red	colourimetric	tetraoctylammonium hydroxide	solvent	polyvinyl butyral (PVB)	breath analysis	29
various, preferred is Alizarin Yellow R	colourimetric	none	alcoholic/ aqueous	ink on filter paper	ripening indicator	30
phenol red	colourimetric	tetraoctylammonium hydroxide	solvent	ethyl cellulose	breath analysis	31

Although a number of applications exist where the detection of CO<sub>2</sub> is important, from Table 1.1 it is evident that three areas remain the most significant and it is evident that indicators for these applications are continuing to be developed and new detection techniques explored. The first of these is capnography, a medical discipline which has been important in anaesthesia and intensive care for many years now. The second lies within the relatively new area of smart packaging. The potential of CO<sub>2</sub> detection in this area is very exciting and could have major impacts in the near future. Thirdly, the monitoring of CO<sub>2</sub> in the environment is becoming increasingly important as levels of CO<sub>2</sub> are continuing to rise and the subsequent consequences thereof. Each of these areas will be discussed briefly and existing detection techniques evaluated.

#### 1.1.1.1 Capnography

Carbon dioxide is often used as an indicator for the existence of life and as a measure of health. In medicine, the key, basic analytes that are routinely monitored in the blood of hospital patients are: dissolved oxygen, pH and carbon dioxide. Capnography is an area in medicine wholly devoted to the monitoring of levels of carbon dioxide in breath.<sup>31</sup> Not only does the presence of carbon dioxide provide important valued medical information, but also its temporal variations in the exhaled breath is used routinely to provide diagnostic information *via* capnography<sup>32</sup> (see Fig. 1.4). In anaesthesiology, one method to ensure the correct placement of the tube carrying the gases to the lungs into the trachea, rather than the oesophagus, is to monitor the level of carbon dioxide (typically 4 - 5% in exhaled breath).

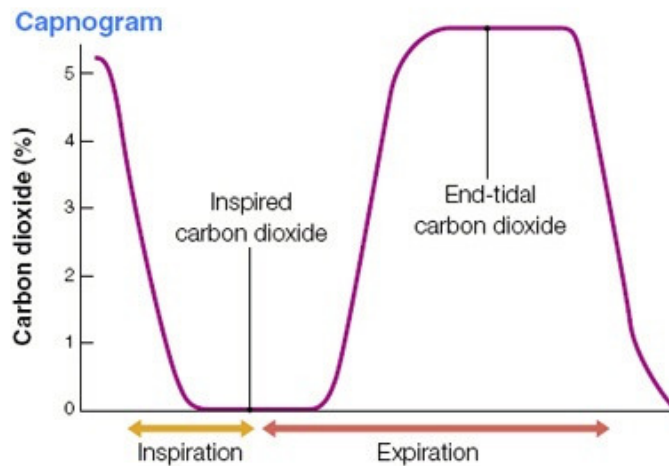


**Fig. 1.4** – Characteristics of a typical capnogram of a healthy patient.<sup>33</sup>

Esophageal intubation or misplaced endotracheal tube can result in unsuccessful resuscitation, or in worsening of cardio respiratory status. Therefore, it is essential to confirm the correct position of an endotracheal tube. One way to confirm its position is by detecting CO<sub>2</sub> in the exhaled breath from the lungs. A temporary colourimetric CO<sub>2</sub> indicator can be inserted at the top of this tube; if CO<sub>2</sub> is present in the patient's breath, the indicator will change colour instantaneously with every exhaled breath, ensuring the correct insertion of the tube.

One of the earlier attempts of developing an indicator for this application was reported in 1984 by Berman *et al.*<sup>34</sup>. Titled “The Einstein Carbon Dioxide Detector”, the paper described a solution based detector, which changed colour upon expired gas being bubbled through the solution. A colour change from red to yellow indicated tracheal intubation, whereas no colour change suggested esophageal intubation. However, many drawbacks were clearly evident using this detecting system, not least its impractical nature due to using a liquid solution. Raemer *et al.*<sup>35</sup> reported an improved system based on pH sensitive dyes bound to controlled pore glass particles. However, this system still had drawbacks due to the dye molecules not being encapsulated into a gas permeable membrane.

Significant improvements from these earlier examples have been made and a more recent, commercialised carbon dioxide semi-quantitative sensor which is currently being used by medical personnel is the EASY CAP<sup>TM</sup> and PEDI-CAP<sup>TM</sup> CO<sub>2</sub> indicators sold by Nellcor.<sup>3</sup> The inventors claim that the sensor can be used to determine whether respiratory gas is present in a gaseous sample by which the sample is brought into contact with an indicator which yields a response within a diagnostically effective time period<sup>11</sup>. They claim to be able to determine the presence of carbon dioxide in concentrations of at least 2%. The indicators are based on the sensor element comprising a pH-indicating dye, usually *meta*-cresol purple (MCP), dissolved into a 50:50 mixture of water containing either sodium carbonate or calcium hydroxide, and a non-aqueous, hygroscopic, non-volatile liquid such as glycerol<sup>11</sup>. This solution is then absorbed onto dry filter paper and dried over a stream of hot air. Nellcor Inc. developed this technology further by adding a borosilicate mesh substrate to aid CO<sub>2</sub> diffusion<sup>27</sup>. A photograph of the commercially available indicator (EASY CAP<sup>TM</sup>) and correct tracheal intubation is illustrated in Fig. 1.5.

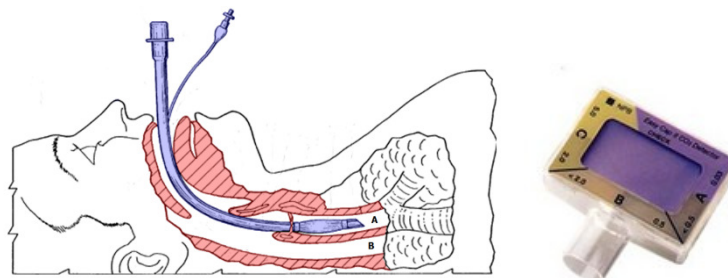


**Fig. 1.5** – Illustration of correct endotracheal tube placement. When the tube is inserted into position A, the indicator would show a colourimetric response (purple to yellow), however if inserted into position B, no colour change would occur, indicating incorrect placement.

A recent study was published<sup>9</sup> by a group of medics which assessed the performance of the PEDI-CAP<sup>TM</sup> during neonatal resuscitation, against the more traditional flow sensor measurements. The study revealed that in 60% of intubations both methods correctly identified successful intubation and in 9% both methods indicated unsuccessful tracheal intubation. In the remaining 31% of intubations, the

PEDICAP™ failed to detect a correct tracheal intubation, despite the flow sensor correctly revealing successful intubation. From these results, the researchers concluded that PEDICAP™ cannot always be depended upon to determine intubation positions, due to the high number (31%) of misleading results. The reason suggested for such a high number of failed tests was insufficient tidal volume ( $V_T$ ) to successfully produce a colour change. This problem, may be dramatically reduced when used on older patients, where the  $V_T$  would inevitably be higher due to an increased lung volume. However, this study demonstrates the need to design an indicator device which would need minimum amounts of  $CO_2$  to still effectively produce a striking colour change.

Another commercially available  $CO_2$  indicator is sold by Ventlab Corporation<sup>36-38</sup> is the A.C.E STAT-Check™, as pictured in Fig. 1.6. In the presence of  $CO_2$ , it changes from white to purple. Different shades of purple indicate different levels of end-tidal  $CO_2$ . It claims to have a shelf-life of 2 years at 25°C. Although it claims to have an impressive shelf life, the level of  $CO_2$  is determined by shades of the same colour, which often leads to a degree of subjectivity when trying to discern the  $CO_2$  level.



**Fig. 1.6** - A.C.E STAT-Check™  $CO_2$  indicator.<sup>38</sup>

A derivative of the same indicator is STAT-Check™, also sold by Ventlab Corporation, as illustrated in Fig.1.7.<sup>36</sup> The company claims that no special storage is required for the indicator as it is in-built onto the resuscitation bag. The indicator's



initial colour is pale lilac, which then gradually turns darker as the CO<sub>2</sub> level increases. Unfortunately the colour change is not distinct and could potentially cause a degree of ambiguity during the resuscitation process.

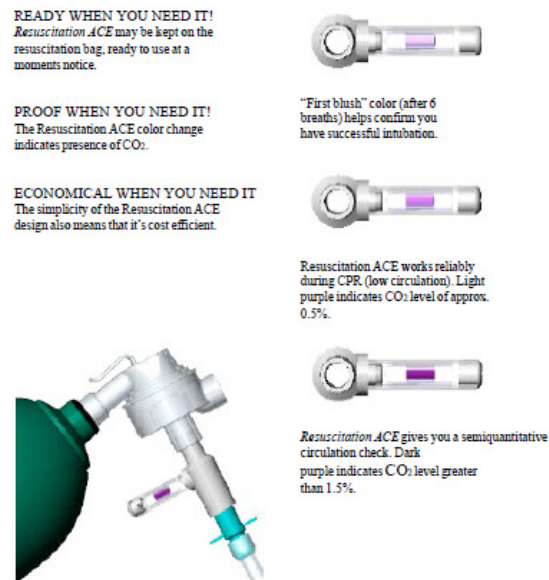


**Fig. 1.7** – Illustration of STAT-Check CO<sub>2</sub> indicator.<sup>37</sup>

More recently, Ventlab released a modified version of their indicator, which have addressed some of the initial disadvantages of STAT-Check<sup>TM</sup>.<sup>39</sup> STAT-Check II<sup>TM</sup> no longer uses the white to purple colour change, but rather purple to beige to yellow, as illustrated in Fig. 1.8. Although it is claimed that STAT-Check II<sup>TM</sup> also has significant clinical advantages, these all seem to be concerned with the design of the support, opposed to the choice of indicator. Unfortunately no patent allowing a better insight into the chemical make-up of the indicator could be found. However, the colour change may suggest the use of *m*-cresol purple.



**Fig. 1.8** - STAT-Check II™ illustrating the varying colour changes at different levels of CO<sub>2</sub>, 5%: yellow, 2%: brown and 0%: purple.<sup>39</sup>

Mercury medical<sup>10</sup> currently sell a variety of end tidal CO<sub>2</sub> detectors. Each indicator is designed to be suited to different patient weights i.e. StatCO<sub>2</sub>® (for patients over 15 kg), Mini StatCO<sub>2</sub>® (for patients within 1 - 15 kg) and Neo-StatCO<sub>2</sub>® (for patients within 0.25 - 6 kg).<sup>40</sup> As illustrated in the photographs below (Fig. 1.9), an initial blue colour indicates no CO<sub>2</sub>, green indicates 1.0 – 2.0% CO<sub>2</sub>, yellow/green indicates 2.0 – 5.0% CO<sub>2</sub> and yellow ≥ 5.0 %.



**Fig. 1.9** – Mercury medical end tidal CO<sub>2</sub> detectors.<sup>41</sup>

These series of indicators are designed and work in a similar manner to the previous commercially available CO<sub>2</sub> breath indicators. Although no patent giving more detailed description of the components involved could be found, given the colour changes and sensitivity, the pH indicator dye thymol blue would be a likely guess. It

is noted in the ‘instructions for use’ that that indicator cannot be used for more than 24 hours, since at this point the indicator fades to a yellow/light green, which is not surprising if the dye is continuously exposed in an environment where other acidic gases could be present.

Fernandez-Sanchez *et al.* developed<sup>24</sup> a series of CO<sub>2</sub> sensors based on a range of phenol dyes (e.g. a-naphtholphthalein (NAF), naphthol blue black (NBB), calmagite (CMG))<sup>24</sup>, using a phase transfer agent, PTA, and a metal-oxide nanoporous matrix e.g. AlOOH, SiO<sub>2</sub>, ZrO<sub>2</sub>. It was reported<sup>24</sup> that such nanoporous membranes provided higher dispersion and accessibility of the dye, which produced quicker response times. No major interferences were observed from NO<sub>x</sub> and SO<sub>x</sub> gases. It is thought that the nanostructured membrane provides a greater stability. Since the indicators have low detection limits and quick response times, these features adequately allow them to be utilised in breath-by-breath CO<sub>2</sub> analysis.

Breath CO<sub>2</sub> analysis have been the most successful application for colourimetric CO<sub>2</sub> indicators, boasting a number of commercial products<sup>3,36</sup>. Although commercial products have been made available to medical staff, it appears that the wide use of such products is still limited.

#### 1.1.1.2 Intelligent packaging

The principle function of traditional food packaging involves the reduction of food deterioration (thereby extending its shelf-life), maintenance of quality and safety, and the reduction/elimination of physical damage to food.<sup>42</sup> Packaging serves to protect the contents from factors such as heat, light, moisture, pressure, oxygen, enzymes, microorganisms, odours, insects, dust and dirt. The traditional secondary function of food packaging lies within the marketing of the product. Recent decades have increasingly demonstrated the importance of packaging in the advertisement and marketing of the product. Although a secondary function, this aspect of food packaging has a direct impact on the sales of the product.

Interestingly, all traditional packaging endeavours to minimize the contact between food and packaging, maintaining the functions as described above. However, due to increased consumer demands for mildly preserved, fresh tasting, convenient foods, along with changing retailing practises (i.e. globalisation of food distribution), the development of more sophisticated packaging solutions began to emerge.

With continued demand for high quality packaged food, significant advances in scientific research have arisen in recent years. Thus, the interaction between food and packaging has begun to change, often with the aim to provide the consumer with real time information about the food quality. This is the basis of intelligent packaging.

It is evident that there is some confusion surrounding the definition of intelligent packaging and it is often used interchangeably with similar, yet different terms such as smart and active packaging. Yam *et al.* define<sup>42</sup> intelligent packaging as “a packaging system that is capable of carrying out intelligent functions (such as detecting, sensing, recording, tracing, communicating, and applying scientific logic) to facilitate decision making to extend shelf life, enhance safety, improve quality, provide information, and warn about possible problems.” They highlight that the primary aim of an intelligent packaging system is to *communicate* a problem, whereas an active packaging system is primarily concerned with taking *action* (e.g. release of antimicrobial) to protect the food product. Robertson<sup>43</sup> defines active packaging as ‘packaging which subsidiary constituents have been deliberately included in or on either the package material or package headspace to enhance the performance of the package system.’ Examples of active packaging include the slow release of preservatives, the absorption of moisture or a component which maintains a desired temperature within the package. The term smart packaging is most commonly used as a broad definition which encompasses both intelligent and active packaging<sup>44</sup>, however is commonly used in place of intelligent packaging.

Intelligent food packaging has the potential to revolutionise the way supermarkets sell and we purchase our food. Ahvenainen suggests<sup>45</sup> that intelligent packaging will have a “bright future” due to the increasing significance of freshness and food safety, increasing consumer demands and increased globalization and expansion of marketing, leading to longer logistic chains and hence more demands on food

traceability. Intelligent packaging solutions may be a novelty to most consumers at first, but the true benefit of smart packaging will soon be apparent when it eliminates the need for the consumer to make a subjective judgement on whether the food is still safe to eat.

Although the potential advantages of smart packaging are numerous, there have been concerns<sup>46</sup> regarding the use of smart packaging. In an era where consumers are more aware of the environmental repercussions<sup>45</sup> from using excessive non-biodegradable plastics, concerns have been raised regarding the increased quantity of packaging which might be required for smart packaging to be widely used. Additionally, chemical migration from the indicators into the foodstuffs has also been raised<sup>46</sup> as a valid concern. Such concerns would have to be solved for indicators to be widely accepted within the packaging industry.

Until 2004 there was no formal legislation on the correct usage and production of smart packaging in Europe. Regulation 1935/2004/EC and more specifically the most recent Regulation 450/2009/EC, set out to define parameters for their development, safety and marketing<sup>47,48</sup>. These articles stressed the importance of migration testing on all products, ensuring no chemical migration occurred from the intelligent/active packaging to the foodstuff. They also stipulate that such packaging must not mislead the consumer.

#### *1.1.1.2.1 Modified Atmosphere Packaging (MAP)*

MAP packaging involves flushing the food packaging with an oxygen-free gas, usually carbon dioxide and sealed, ready for distribution to the wholesale and/or retail trader.<sup>49</sup> This prevents aerobic spoilage microbe growth, and usually allows food to stay fresh 3-4 times longer. It also reduces the amount of additives used in foods to prolong their shelf-life. A wide variety of foods are commonly packaged under MAP conditions e.g. meat, sweets, cakes, dairy products, nuts, fresh pasta, noodles. Table 1.2 illustrates the increase in shelf-life which is possible through MAP<sup>50</sup>.

**Table 1.2** – Shelf-life of a selection of MAP and non-MAPed foods.<sup>50</sup>

<b>Product</b>	<b>Non-MAP (days)</b>	<b>MAP (days)</b>
Fresh Red Meat (high O <sub>2</sub> )	2-3	6-10
Fresh Red Meat (low O <sub>2</sub> )	2-3	21
Fresh sausage	4-5	15-16
Fresh processed poultry	3-10	12-18
Cooked poultry	5-16	21-30
Cooked/cured meats	1	30-45
Cheese	7	180+
Fresh pasta	3	60+

Nowadays, MAP is the preferred method of food preservation over chemical treatment of food<sup>45</sup>. It is also preferred over vacuum packaging due to the lack of mechanical strain put on the package and the foodstuff. Mechanical pressure on the meat may increase drip loss, and if bone is present and not adequately covered with a suitable material, the pack may be ruptured<sup>51</sup>.

The choice of carbon dioxide as a flush gas is based upon its plentiful supply, and its antimicrobial action, i.e. it is an *active* packaging gas. The description ‘*active*’ indicates that carbon dioxide inhibits microbe metabolism when present in high enough concentrations, even if oxygen is present in the system. The first observations on the effect of carbon dioxide retarding the growth of bacteria were made in the early 1880s<sup>52</sup> and since that time, a large number of papers have been published on the effects of carbon dioxide on fresh foods and on the inhibitory properties of carbon dioxide<sup>53</sup>. It is thought that the carbon dioxide causes a decrease in inter- and intra-cellular pH and interferes with cellular metabolism. A side effect of using carbon dioxide as a flush gas when packaging meat is that the carbon dioxide dissolves into the meat. This is not thought to affect the meat in any way, but has to be considered when packaging such foodstuffs. The solubility of carbon dioxide in muscle tissue of pH 5.5 at 0°C is approximately 960 ml per kg of tissue at STP (standard temperature and pressure)<sup>54</sup>. As the temperature increases, the solubility decreases by 19 ml per kg for each °C rise. As the tissue pH increases, the

solubility decreases by 360 ml per kg for each pH unit. Therefore, an excess volume has to be added to the MAPed package to stop the package collapsing.

Detection of levels of carbon dioxide in MAP packaged food is essential to indicate the package integrity, since any leak will cause increased microbial growth due to the increased O<sub>2</sub> content. Thus accidental damage to the seal can cause the customer to buy spoiled food, without realising that the freshness has been compromised. By incorporating an intelligent colourimetric carbon dioxide indicator into the package, the consumer would be able to know that the package integrity has been upheld and that the quality of food inside is still as estimated by the 'use by' date.

A number of indicators for MAP have been developed which are less sensitive to CO<sub>2</sub> than the CO<sub>2</sub> breath indicators, and examples of these are discussed below. Typically there is 20-80% CO<sub>2</sub> in MAPed foods<sup>49</sup>, hence indicators which change colour when the concentration drops below these levels are suitable as leakage indicators.

For example, Balderston and Whitwood<sup>55</sup> describe a reversible CO<sub>2</sub> indicator designed to be used as a leak indicator in MAPed food packages. Their patent describes a progressive colour change of 5 indicator strips as the concentration of CO<sub>2</sub> inside the package changes. Details of the formulation were not found in the patent. The indicator was developed under Sealed Air Ltd<sup>56</sup>, but does not appear to be on the market.

A hybrid CO<sub>2</sub> indicator has been reported<sup>28</sup> recently, combining a PTA (i.e. tetraoctyl ammonium hydroxide) and the dye bromothymol blue, BTB, to create the ion pairs, along with an ionic liquid, (1-methyl-3-butylimidazolium tetrafluoroborate) into which is dissolved sodium bicarbonate. The resulting, non-volatile, liquid-based (although not aqueous) CO<sub>2</sub> indicator produces the usual characteristic variation in absorption spectra as a function of *p*CO<sub>2</sub> as observed with similar indicators. Ionic liquids have the benefit of being environmentally friendly and are 10-20 times better at dissolving carbon dioxide than other conventional solvents - this enhances the sensors' response and recovery. However, commercialisation of this formulation seems unlikely, given the high cost of the ionic liquids and the need to encapsulate a

liquid-based indicator. Similar work was carried out by Borisov *et al.*<sup>26</sup>, again utilising ionic liquids based on their negligible vapour pressure, excellent thermal stability, low toxicity and good CO<sub>2</sub> solubility. They reported<sup>26</sup> an emulsion-based optical sensor, where the dye and ionic liquid were trapped in a silicone matrix. This is evidently a vast improvement from the previous liquid-based indicator. Both absorption and fluorescence-based indicators were reported, where the sensitivity of the indicators could be tuned by varying the indicator pK<sub>a</sub>.

One recent attempt to add a lipophilic base to the solid state sensor produced some interesting results. Schroder *et al.*<sup>23</sup> investigated replacing the quaternary ammonium ion with a neutral phosphazene base and coupling it with the anion of the pH-sensitive dye *p*-xylenol blue (XB) to render it soluble in the polymer ethyl cellulose. The basic character of the base can be attributed to the lone pair of electrons on the tertiary nitrogen atom linked to the phosphorus atom by the double bond. For the basic character of the phosphazene to be activated, water needs to be present, as illustrated in Fig. 1.10. The basic character of the phosphazene along with the water forms a buffer for the sensor.

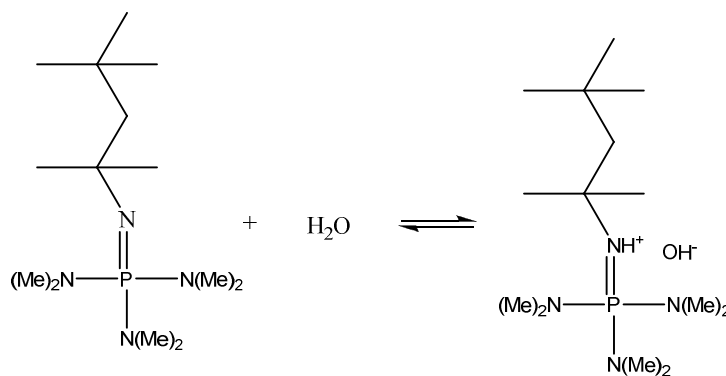


**Fig. 1.10** – Chemical structure of the phosphazene base in equilibrium with water.

The sensor showed similar response and recovery times compared to the tetraoctylammonium hydroxide analogue. One major drawback with the system is the volatility of the neutral form of the phosphazene base, which makes it very difficult for *p*CO<sub>2</sub> applications, since any indicator film rapidly loses the base and



therefore its sensitivity towards CO<sub>2</sub> in a flow gas stream. It is thus more ideally suited for dissolved CO<sub>2</sub> work.

Lines describes<sup>25</sup> the use of polyethyleneimine in a colourimetric sensor comprising of polyvinyl butyral, PVB, as polymer matrix, diphenyl-(2-ethylhexyl) phosphate as the plasticizer and ethanol as the solvent. Lines describes a process for preparing quaternary ammonium salts of anionic dyes, which enables the use of methanol to be avoided and allows the salt to be prepared, if desired, in the solvent in which it is to be used. This is carried out by mixing an aqueous solution of a salt of the dye with a solution of a water-insoluble salt in a water-immiscible organic solvent, and separating a solution of the 'onium salt of the anionic dye in the organic solvent. Thin films produced a striking dark blue to yellow colour change upon exposure to CO<sub>2</sub>(g). However, the films are relatively unstable in general lab conditions (acidification of films was observed). Adapted atmospheres need to be utilised to prolong the longevity of the films.

Although using mainly fluorescent CO<sub>2</sub> indicators (and indeed there are a vast number of fluorescent CO<sub>2</sub> indicators which have not been discussed), Leiner *et al.*<sup>57</sup> published an interesting patent illustrating classical dry optical indicators (e.g. ethylcellulose and 1-hydroxy-3,6,8-pyrenetrisulfonate (HPTS)) which incorporated various cationic species. The cation species was typically a metal cation (e.g. Rb<sup>+</sup> or Cs<sup>+</sup>), complexed to one or more ligands (e.g. typically crowns or calixarenes). It was the main objective of the study to improve the chemical stability of the previously reported<sup>21</sup> indicators. Although no stability data was shown, the writers suggest stability of the indicators was improved.

Despite many advances in colourimetric CO<sub>2</sub> detection, there are still many challenges to overcome before a range of CO<sub>2</sub> leak indicators will be commercially available. Smolander *et al.* correctly observes<sup>58</sup> that following a leak in a MAPed food package (decrease in CO<sub>2</sub>), an increase in microbial growth occurs due to the increased O<sub>2</sub> content, which consequently increases the CO<sub>2</sub> concentration within the package; thus in the worst case the CO<sub>2</sub> concentration will not change. This indeed is a challenge which needs to be addressed when designing CO<sub>2</sub> leakage indicators; ideally, they would be irreversible in response, whereas, in general, they are highly

reversible. Despite some criticisms<sup>45,58</sup>, there is an obvious opportunity to develop a range of low cost, colourimetric CO<sub>2</sub> indicators in food packaging applications. Cost and stability will play major influences as to whether these indicators will be adopted widely by food packaging companies which utilise MAP.

### 1.1.1.3 Environmental Monitoring

Combustion is the main source of carbon dioxide in the biosphere. Industry, domestic heating, burning, biomass degradation and fermentation are all large contributors to the levels of carbon dioxide. The levels of carbon dioxide in the oceans are as important as atmospheric levels, containing up to 60% more carbon dioxide than in the atmosphere<sup>59</sup>. The oceans play a big part in reducing the effect of carbon dioxide as a greenhouse gas and so lower the potential of global warming by acting as a carbon dioxide reservoir. However, the levels of carbon dioxide in the hydrosphere and atmosphere are not in equilibrium with each other and the rate of exchange between the two depends on a wide variety of parameters e.g. wind, atmospheric pressure, humidity and temperature<sup>59</sup>. Thus, the measurement of carbon dioxide levels in the biosphere is an important part of environmental monitoring. Dissolved CO<sub>2</sub> levels hold a particular interest to biologists as it can provide an indication of the health of aquatic life. High CO<sub>2</sub> levels can adversely affect fishes' metabolism, which can eventually lead to death.<sup>60</sup> Similarly, coral reefs, calcareous plankton and other organisms whose skeletons or shells contain calcium carbonate are directly affected by *d*CO<sub>2</sub> levels in ocean waters. There is an increasing need to monitor CO<sub>2</sub> levels in the environment and, as a consequence, there has been a wide interest in the development of optical indicators for this area.

The majority of the indicators are fibre optic based<sup>61-64</sup> and often use fluorescence based chemistry. One of the most commonly used dyes is 1-Hydroxy-3,6,8-pyrenetrisulfonate (HPTS) and its structure is shown in Fig. 1.11. The deprotonated



#### 1.1.1.4 Summary

From the discussion around these three main applications, the importance of CO<sub>2</sub> as an analyte has been highlighted. Given the significant interest in CO<sub>2</sub> indicators, it is surprising to note that few colour-based CO<sub>2</sub> indicators have been commercialised. One of the reasons for this may be the poor stability over time, i.e. most have shelf lives of less than six months under ambient air conditions due to, amongst other things, the poor thermal stabilities of the PTAs used. These weaknesses will be addressed and new substrates investigated.

### 1.1.2 Oxygen

Oxygen has been a key analyte in analytical chemistry for many centuries. Oxygen plays an important role in many areas of science.<sup>66</sup> For example, the measurement of oxygen, as with carbon dioxide, is an essential feature in the analysis of many biological systems, e.g. in environmental analysis, patient monitoring and a wide variety of biotechnological systems. The sensing of oxygen has become increasingly important in a wide range of industries, including food packaging, sewage treatment and brewing.<sup>66</sup>

Traditionally the detection of oxygen has been carried out using expensive and often bulky analytical equipment i.e. using the Clark electrode or thermal conductivity gas chromatography. Such techniques are time consuming and difficult and/or expensive to miniaturise. So in recent years there has been a drive to develop miniaturised, colourimetric oxygen indicators.

Although a number of applications exist, this review will concentrate on the use of oxygen indicators for use in food packaging applications.

### 1.1.2.1 Food packaging

The main cause of food spoilage is oxygen. Aerobic microorganisms, which are the main cause of food spoilage, require oxygen to grow and degrade the food. Oxygen also allows many enzyme-catalysed reactions to take place e.g. the browning of food and vegetables, or the degradation of flavours. The addition of lemon or lime juice has been common practise throughout history to hinder this undesirable effect – these juices work by lowering the pH, below the optimum pH of the food spoilage enzymes. Fats in foods are susceptible to oxidation or rancidity resulting in off-flavours and occasionally off-colours. Unsaturated fat is more prone to oxidation than saturated fats, which is unfortunate since unsaturated fats are healthier. Storing foods at low temperatures ( $\sim 4^{\circ}\text{C}$ ) also reduces these processes, but only increases their shelf-lives minimally.<sup>49</sup> Although such measures help maintain the quality of the foodstuffs, they have major limitations. In order to overcome these problems, it has become common practise to pack foodstuff in oxygen-free environments, such as achieved with modified atmosphere packaging (MAP).

After flushing the food package with inert gases (e.g.  $\text{N}_2$  and  $\text{CO}_2$ ), the residual level of oxygen in a package headspace is often still significant ( $\geq 2\%$ )<sup>67</sup>, due to the ability of food to retain oxygen and poor gas flushing. The oxygen level in the package can also increase over time due to inefficient sealing and the permeation of oxygen through the package material from the surrounding air. Although these increased levels of oxygen are minimal, it can significantly decrease the quality of the food inside. In order to overcome these problems, many manufacturers have added oxygen scavengers to food packaging, usually in the form of a sachet or a label. These sachets are used to maintain the level of oxygen in a food package at 0.1% or less.<sup>67</sup>

Oxygen scavengers work by undergoing a chemical reaction to remove any oxygen present in the headspace of the package. The scavengers can lower and sustain the oxygen content to approximately 0.01%.<sup>67</sup>

The most common type of oxygen scavengers used in food packaging are based on  $\text{FeO}$ <sup>68</sup>. In 1977 Mitsubishi Gas Chemical Company (MGC) introduced the ‘Ageless’

scavenger<sup>69</sup> based on FeO. The scavenger is based on the ‘rusting’ of iron powder, as illustrated in equation 1.10. As long as the FeO is in excess, the reaction is driven to the right, excluding all oxygen within the closed environment.

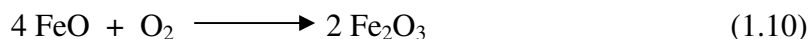
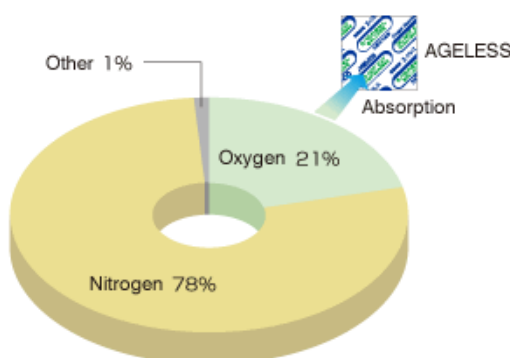


Fig. 1.12, illustrates how MGC have marketed their product, clearly demonstrating the scavengers’ ability to remove oxygen from the air.



**Fig. 1.12** – Illustration of the ‘absorption’ of O<sub>2</sub> as it removes the oxygen content from air.<sup>69</sup>

Scavengers based on FeO have been hugely successful, proven by the fact that many food manufactures still utilise similar scavengers today. Since 1977, MGC have expanded their range of O<sub>2</sub> scavengers so to include simultaneous O<sub>2</sub> and CO<sub>2</sub> absorption, CO<sub>2</sub> generation coincident with O<sub>2</sub> absorption, or temperature-prompted oxygen absorption.<sup>69</sup> They have also developed new substrates onto which the scavengers are dispersed. These sheets are not only resistant to microwave heating, but since the iron powder is attached on a resin, it also prevents spillage if the sachet were to be accidentally damaged. Fig.1.13 illustrates a typical oxygen scavenger label in a food package and an illustration of rice which has been packaged with an Ageless scavenger and one without, at 25°C for 1 month. It is clear that the control sample of rice has degraded significantly compared to the ageless packed one.<sup>70</sup>



**Fig. 1.13** – Ageless scavengers in a commercial pack of ham, and illustration of effectiveness of ageless scavengers on rice storage.<sup>70</sup>

In order for such scavengers to work effectively, there has to be a satisfactory flush of inert gas and also a durable seal to ensure no leakage. Secondly, the packaging material has to be well chosen, typically a flexible polymer with a high oxygen barrier property. However, if the food package integrity was compromised to the extent that a leak was formed – the oxygen scavenger would be considered useless, since there would be a constant influx of oxygen. Such leaks are often not visible to the human eye and only evident when moulds or discolouration occurs within the package, i.e. after food spoilage has taken place.<sup>71,72</sup>

Following these concerns, it is evident that there is a need for a leak detection system, which would detect a decreasing concentration of oxygen. In a typical MAP food package line, one in every 300 - 400 packages are tested routinely by a trained technician, often using expensive analytical equipment. If a leak was detected, the whole batch of packages would be scrapped or repacked. Such a system is time consuming and hugely wasteful. Developing a disposable, cheap, oxygen indicator able to detect key changes in oxygen levels, not only would reduce such waste, but would also supply consumers with real-time analysis of MAPed food quality.

There have been various examples of oxygen indicators reported<sup>73-77</sup> in literature. Typically these fall into two categories: colourimetric and lumophoric. Colourimetric based oxygen indicators depend on an observable colour change, commonly due to an oxygen-binding reaction, a redox reaction or a light-activated redox reaction. Lumophoric indicators rely on a changing intensity or lifetime of the indicator, which normally decreases with increasing partial pressure of oxygen. The focus of the work described in the thesis is on colourimetric oxygen indicators, so the introductory discussion of commercial and literature reported indicators will focus on colourimetric indicators.

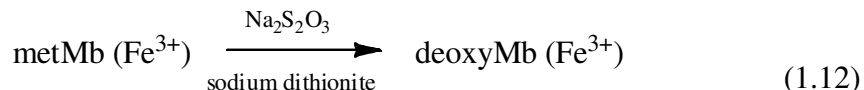
#### 1.1.2.1.1 Oxygen indicators based on oxygen-binding complexes

Earlier examples of colourimetric oxygen indicators were based on oxyhaemoglobin. The colour change between oxyhaemoglobin and deoxyhaemoglobin has been well documented throughout literature for many years. In 1986 Zhujun and Seitz reported an oxygen indicator which consisted of a 0.5 mm thick layer of deoxyhaemoglobin immobilized on a cation exchange resin, positioned at the end of a fibre optic bundle.<sup>78</sup> The indicator was found to be fully reversible, measuring  $pO_2$  levels from 20-100 Torr. Unfortunately, it was found to be unstable at room temperature, with a shelf-life of only 2 days. Storing the indicator at 4°C prolonged its shelf-life up to 1 week, but even at lower temperatures its lifetime was still significantly lower than desired. It was suggested that the main cause for such poor stability was largely due to the fact that under aerobic conditions, oxyhaemoglobin oxidised further to methaemoglobin.

This earlier design was improved by Chung *et al.*, who developed a dissolved oxygen indicator comprising myoglobin (Mb) encapsulated in a sol-gel glass matrix.<sup>79</sup> Unfortunately the colour changes were not striking due to the closeness of the absorption maxima of deoxyMb and oxyMb (432 and 418 nm, respectively). The indicator was formulated using metmyoglobin, metMb ( $Fe^{3+}$ ), and required an initial activation step to convert it to deoxyMb ( $Fe^{3+}$ ). Sodium dithionite was commonly

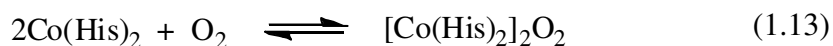


used as the reducing agent to initiate this conversion. The basic processes involved in the indicator are illustrated in reactions 1.11 and 1.12, below.



Although the lifetime of this indicator was better than in the previous work<sup>78</sup>, the authors<sup>79</sup> recommend storing the indicator in sodium dithionite, under argon at 4°C. Together with these less than ideal storage conditions and poor colour changes, this system has major limitations to its use.

In order to overcome these problems, some researchers have moved away from biological oxygen-binding agents and towards synthetic oxygen-binding metal complexes. Bis(histidinato) cobalt(II), Co(His)<sub>2</sub>, has proved particularly successful, showing a reversible colour change from almost colourless in its unbound form to pink in its oxygen-bound form.<sup>80</sup> The colour change is due to a charge transfer electronic transition between the oxygen and the metal, as illustrated in reaction 1.13.



The metal complex was immobilized onto a silica substrate, commonly a TLC plate. Whilst still wet, a gas-permeable, ion-impermeable silicon rubber coating was applied. This not only provided mechanical support for the sensitive detecting layer but also helped maintain a wet micro-environment which is essential for the sensing system. Unfortunately, the indicator is sensitive to both pH and humidity, which limits its use as a commercial MAP oxygen indicator.

*1.1.2.1.2 Colourimetric Redox Dye-based Indicators*

Colourimetric redox dye-based indicators have commonly been used in food packaging leak indicators for many years. A range of redox dyes have been employed in a range of indicators, e.g. 2,6-dichloroindophenol (DCIP)<sup>76</sup> and triphenyl tetrazolium chloride (TTC)<sup>81</sup>; however the most commonly used dye is methylene blue (MB). Methylene blue reversibly reverts from its colourless form (leuco-methylene blue, LMB) back to its blue, this distinct colour change provides the basis of a range of successful oxygen indicators. The colour change of the indicator depends on the oxidised and reduced forms of the dye. Typically, the oxidised form of the dye ( $D_{Ox}$ ) is the more coloured form and the reduced form ( $D_{Red}$ ). The transformation from one form to the other can be carried out in two ways. Firstly using a chemical reducing agent, e.g. glucose in an alkaline environment<sup>58,82,83</sup>. Alternatively, light-activation can be utilised, using a semiconductor and a sacrificial electron donor. In brief, upon UV light irradiation of the nanocrystalline finely dispersed semiconductor (SC) powder particles, electron-hole pairs are generated ( $SC^*$ ). These photogenerated holes are then able to irreversibly oxidise the sacrificial electron donor, allowing photogenerated electrons to accumulate on the semiconductor particles [ $SC(e^-)$ ]. These electrons are then able to reduce the oxidised form of the dye ( $D_{Ox}$ ) to its reduced form ( $D_{Red}$ ).

Both methods are effective at reducing a redox dye, causing a colour change. In both cases, oxygen is necessary to re-oxidise the reduced form of the dye which makes these systems successful oxygen indicators. Fig. 1.14 shows reaction schemes for the above types of processes.

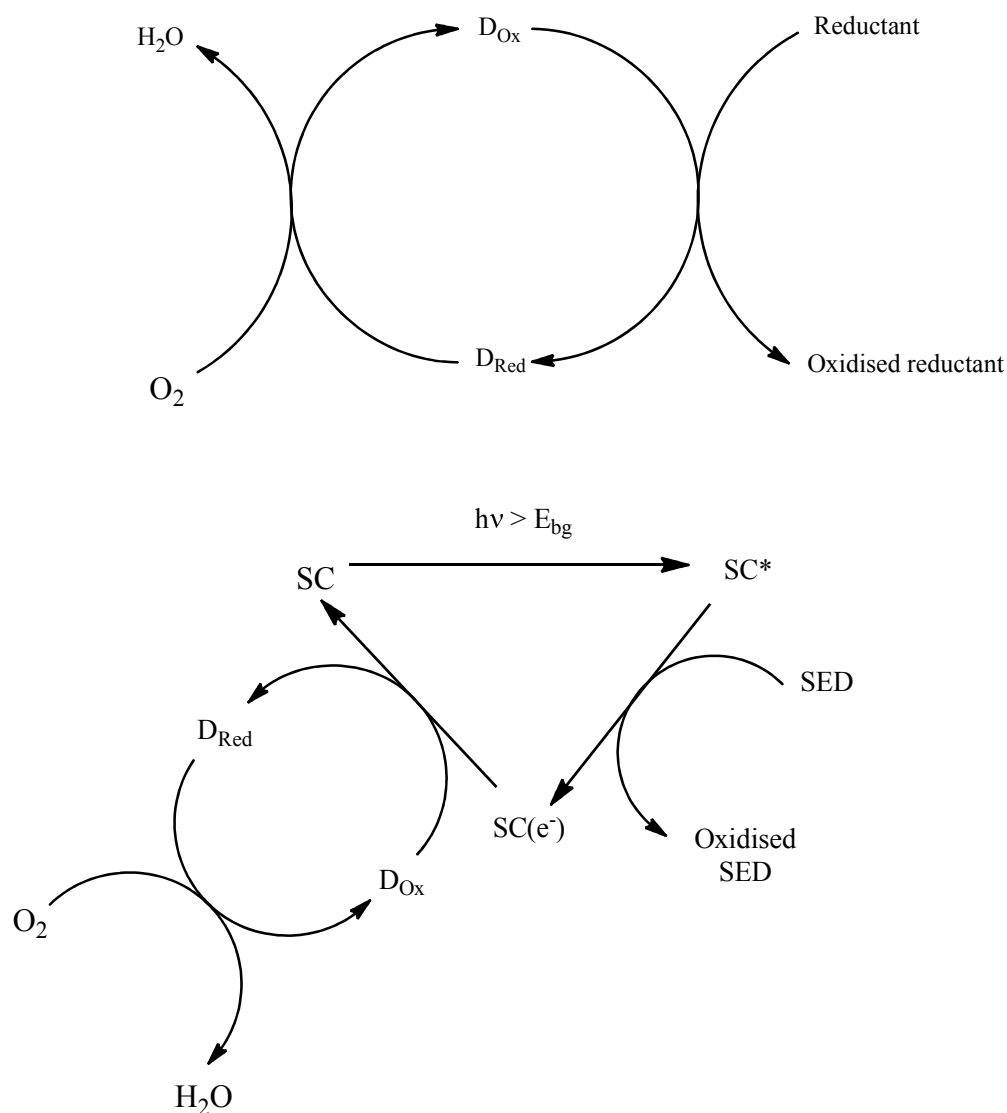


**Fig. 1.14** – Schematic illustrations of the basic processes associated with colourimetric redox dye-based indicators: basic chemical reduction (top) and UV-activation (bottom).

The Mitsubishi Gas Company developed the Ageless Eye™ oxygen indicator intended to enhance the already established range of Ageless™ oxygen scavengers.<sup>69</sup> It relies on a reducing agent (glucose in alkaline conditions) to convert methylene blue to the colourless form, leuco-methylene blue. In addition to methylene blue a non-redox dye, Acid Red 52, is usually added to provide the pink background colour<sup>82</sup>. The indicator components are pressed together to form a pellet which is then inserted into an oxygen-permeable sachet, as depicted in Fig. 1.15.

The main use of indicator is to monitor the level of oxygen in closed packages. Fig. 1.15 illustrates the colour changes involved as the oxygen concentration changes.

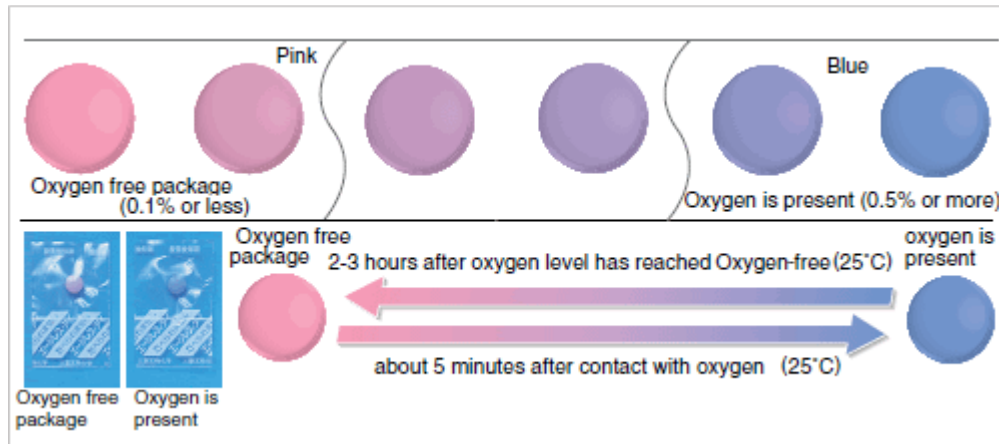


**Fig. 1.15** – Illustration of Ageless Eye™ oxygen indicator showing the colour transition with varying oxygen levels.<sup>83</sup>

As shown above, the indicator changes from blue to pink within 2-3 hours, when the oxygen level in the gas phase has reached  $\leq 0.1\%$ , and returns to its original blue colour within 5 minutes when exposed to an oxygen level of  $\geq 0.5\%$ . Although this indicator has many desirable qualities which have led to it being produced commercially, there are still several aspects of its design which limits its use. For example, unfortunately the cost of the indicator is fairly expensive relative to a standard item of food packaging and the indicators are required to be stored under anaerobic conditions.

Another example of a redox dye-based indicator was published by Eaton<sup>76</sup>, where she described an indicator comprised of the redox dye 2,6-dichloroindophenol, and the reducing sugar fructose in tetrabutylammonium hydroxide, all encapsulated in ethyl cellulose. The indicator works well as an oxygen indicator, showing good colour changes at varying levels of oxygen. However, over a fairly short time-period (*ca.* 10 hours), the indicator's response characteristics change markedly, due to dye degradation under aerobic conditions. To overcome this, the indicator requires

specialised storage (anaerobic conditions) which makes the indicator less than ideal for commercial applications.

This group have reported many examples of colourimetric oxygen indicators<sup>66,73-75</sup>, all of which require UV activation (see Fig. 1.14). The main advantage of UV activated indicators is their irreversible response to oxygen, without re-activation by UV light, which is highly desirable. If a small leak was created in a MAPed food package, the indicator would detect this increase in oxygen, producing a colour change. However, it is possible that this increase in oxygen would lead to an increase in microbial growth, which in turn leads to an increase in carbon dioxide. If these influxes of O<sub>2</sub> and formation of CO<sub>2</sub> were of comparable rates, the indicator would then indicate a low concentration of oxygen i.e. as found in a newly MAPed package, and suggest the package was intact and the food, therefore, fresh. This scenario is avoided by using an irreversible oxygen indicator.

As indicated in Fig. 1.14, for such a UV-activated indicator, a semi-conductor (SC), redox dye (D) and sacrificial electron donor (SED) all have to be present for the indicator to work. These components can be easily combined in a film forming polymer to create effective indicators. Commonly, the semi-conductor is titanium dioxide, usually P25 titania from Degussa, which is a mixture of two crystal structures of TiO<sub>2</sub> (80% rutile and 20% anatase). It has consistently been found that this combination of rutile to anatase exhibits enhanced photoactivity, in comparison to separate forms of titanium dioxide. Alternatively, SnO<sub>2</sub> can be used instead of TiO<sub>2</sub>. However SnO<sub>2</sub> has a larger band gap, hence requires UV light of higher energy i.e. typically UVB light is required to activate such indicators. Mills and Hazafy recognise this advantage when they report of a O<sub>2</sub> sensitive colour-based indicator consisting of nanocrystalline SnO<sub>2</sub>, methylene blue, glycerol, encapsulated in hydroxyethyl cellulose.<sup>74</sup> If used as a leakage indicator in food packaging, there is a possibility that small amount of UV light from supermarket shelf lights may re-activate TiO<sub>2</sub> based indicator. Since SnO<sub>2</sub> based indicators require higher energy than what would be typically emitted from such lights, this removes this concern.

Due to the high water content of many food items, in particular raw meat products, there is a fear that leaching may occur, since many of the indicator dyes are water soluble. To overcome this Mills and Hazafy published a solvent based oxygen indicator,<sup>75</sup> where each of the components in Fig. 1.14 were replaced using a non-aqueous counterpart, or a hydrophobically modified version of the existing component. For example, the water soluble dye, methylene blue, was rendered solvent soluble by ion pairing with dodecyl sulphate.<sup>75</sup> This system created an indicator more suitable to the environment often found in MAPed meat products. Fig. 1.16 clearly demonstrates the classical, blue to colourless colour change when 'activated' i.e. irradiated with UV light.

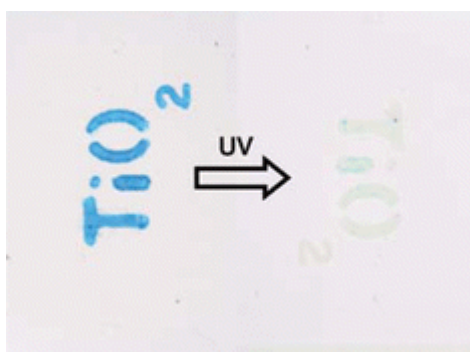


**Fig. 1.16** – UV activated oxygen indicator developed by Mills.<sup>75</sup>

Oxygen indicators as leak indicators appear to have much potential in the food packaging market. A drive to produce low cost, ease of use and appropriate market uptake could see such indicators succeed in this industry.

#### 1.1.2.2 Polyoxometalates (POMs)

In this work, in order to develop a new generation of novel colourimetric indicators, a group of compounds called polyoxometalates will be investigated. The chemistry

of these compounds form the basis of the O<sub>2</sub> indicator reported in Chapter 6 and the UV dosimeter technology reported in Chapter 7.

One of the first literature references which described the photosensitivity of compounds that were later known as POMs was published over 90 years ago<sup>84</sup> by M. Rindl. Since that time POMs have found applications in many areas of medicine, biology, catalysis and material science due to their chemical and structural versatility.<sup>85</sup> Polyoxometalates have received increasing attention in recent years due to the increased usage in a number of important industrial processes, most importantly as catalysts for the removal of organic pollutants.<sup>86</sup> Polyoxometalates have been used extensively in the degradation of dyes<sup>87-91</sup>, as well as coatings, analytical reagents, membranes, dopants and in radioactive processing.<sup>85</sup> Despite a wide variety of applications, the use of POMs in chemical sensors has been limited.

The best known<sup>92,93</sup> structure for POMs is the Keggin structure<sup>94</sup>, depicted in Fig.1.17. Among a variety of known structures, the Keggin structure is the most stable, thus most common and also most widely available as commercial products. The general formula of such polyoxometalates is [XM<sub>12</sub>O<sub>40</sub>]<sup>n-</sup>, where X is the heteroatom (most commonly are P<sup>5+</sup>, Si<sup>4+</sup>, or B<sup>3+</sup>), M is the addenda atom (most common are molybdenum and tungsten), and O is oxygen. Polyoxometalates exhibit fascinating redox chemistry, whereby they can be reduced, whilst keeping their structure intact. The Well-Dawson and Anderson-Evans structures are also reported<sup>95</sup> but are less frequent.

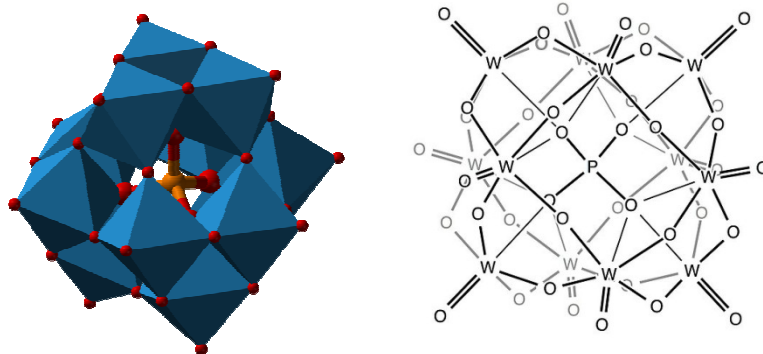


**Fig. 1.17** – Keggin structure of polyoxometalates (left) and structure of commonly used POM, phosphotungstic acid (right).<sup>96</sup>

It is well documented in the literature that when POMs are irradiated with visible and/or UV light, they become powerful oxidizing agents<sup>97</sup> with the ability to oxidise a great variety of organic compounds. In the process of being irradiated, the POMs are reduced, producing their characteristic blue colour. POMs continue to accumulate electrons until a species in the solution is able to accept the electrons from the POM, thus closing the photocatalytic cycle, or until the organic species can no longer be oxidized. POMs serve as excellent catalysts for redox reactions, as no bond breakage occurs, only electron transfer. It has been suggested<sup>98</sup> that the efficiency of POMs as catalysts is directly related to their 1-electron reduction potential. The photochemistry of POM can be described by the photocatalytic cycle shown in Fig. 1.18.



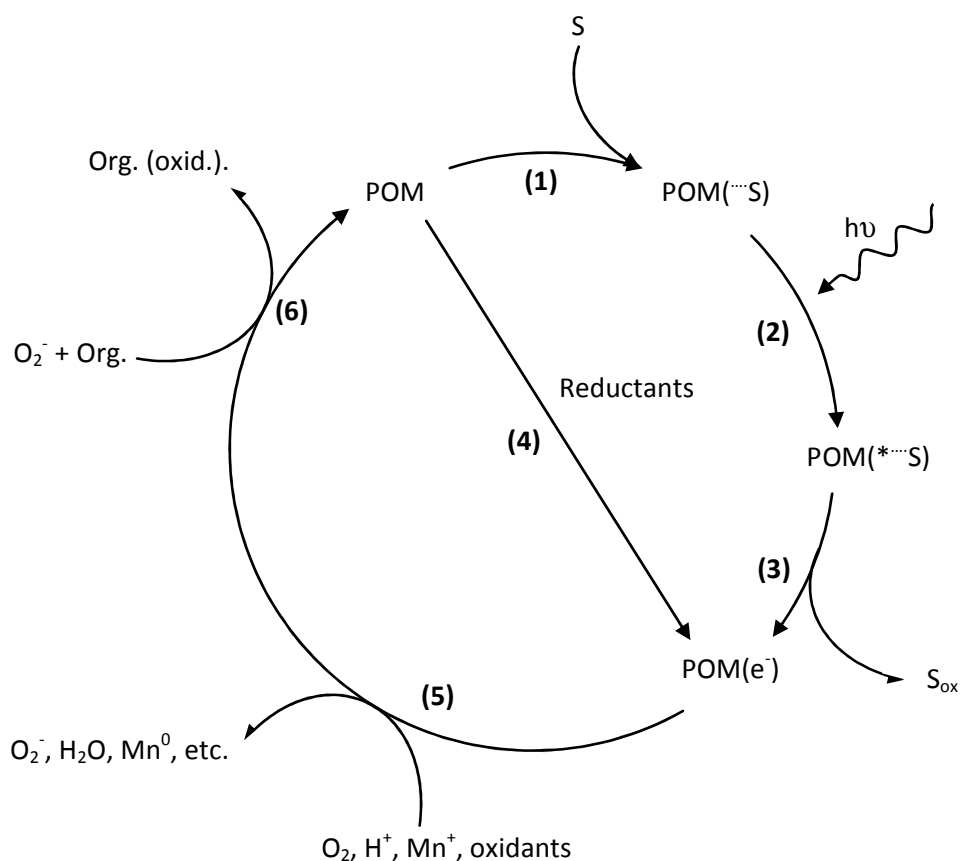
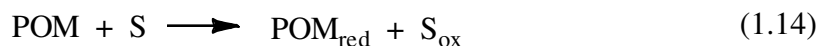


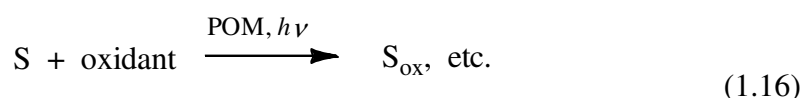
**Fig. 1.18** – Photocatalytic cycle of POM.<sup>99</sup>

Stage 1 shows the formation of a preassociation complex which occurs upon mixing POM with an organic substrate (S). Irradiation by UV light leads to oxidation of the organic substrate and reduction of the POM (stages 2 - 3). The reduced form of the POM can also be produced using various reducing agents (stage 4). Electrons accumulated on the POM can be withdrawn by a variety of electron acceptors, as shown in stage 5, thus closing the photocatalytic cycle. Dioxygen ( $O_2$ ) is the most common oxidant, which undergoes reductive activation in the process ( $O_2^-$ ), and can then initiate further oxidations.

The overall reactions<sup>99</sup> involved in the cycle are:



Overall:



where S = substrate.

As already suggested, oxygen is the most common oxidant, so according to equation 1.14, oxygen is carried mainly from the POM to the S, whereas in equation 1.15, the lost oxygen is replenished with atmospheric oxygen, or oxygen from other oxidants.

A number of papers have noted the similarity<sup>86,100</sup> between POMs and other photocatalytic metal oxides, in particular TiO<sub>2</sub>. POMs are well-defined anions that dissolve in water forming homogeneous solutions, whereas most metal-oxide particulates i.e. TiO<sub>2</sub>, disperse in water forming semi-heterogeneous solutions. Despite these differences POMs and TiO<sub>2</sub> share many similarities:

- They both absorb in the near-visible and UV regions. The absorption of light, for the POM, corresponds to O → M CT band, whereas for TiO<sub>2</sub> and other similar semi-conductors corresponds to the band gap i.e. promotion from the valence band to the conduction band, resulting in electron hole separation.
- They can both be reduced chemically, photolytically and electrochemically forming blue species.
- After irradiation by UV light, they are both powerful oxidising agents, able to oxidize many organic compounds, including organic pollutants to CO<sub>2</sub>.
- For both, the rate determining step is the removal of electrons<sup>100</sup>.

More detailed similarities and differences could also be noted, and indeed are discussed at length in a number of reviews.<sup>86,100,101</sup>

Following the wide use of POMs in many industries, research groups recognised the potential of capturing these properties into thin polymer films. Subsequently, there have been a number of papers<sup>92,102-107</sup> published on POMs being incorporated into thin polymer films; however surprisingly few suggest applications for their work.

Due to the high acidity of many POMs, the matrix used to construct the nanocomposites has to be carefully chosen. Matrices which have been used in literature are polyacrylamide<sup>105,106</sup>, polyvinyl pyrrolidone<sup>104</sup>, polyvinyl alcohol<sup>102</sup>, sol-gel, silica clusters<sup>108</sup>, polyether chains and various cross-linked polymer combinations<sup>103,107</sup>.

As referenced above, Feng *et al.* have published widely on a number of POM containing polymer films.<sup>92,105,106,109</sup> In all of the studies the polymer is used as the electron donor, as well as providing the support for the POM, with a range of POMs including phosphotungstic acid, silicotungstic acid and phosphomolybdic acid being used. All of the films show a gradual colouration process when irradiated with UV light, indicating the formation of the reduced POM species. They report full reversibility of colour in the presence of oxygen.

The use of polyoxometalates to photocatalytically degrade organic species which have potentially hazardous effects on the environment has been a major focus of research. Many research groups have focussed on the destruction of dyes<sup>88,90,91</sup>, and in particular azo containing dyes, due to their toxic and carcinogenic effects in nature. Groups have used POMs or combinations of POM and TiO<sub>2</sub> to effectively degrade these dyes into harmless by-products.

The recovery of metals has also been an area of research which POMs have been applied to<sup>98,110</sup>. Metal recovery is a topic of great interest from both environmental and economic aspects. Capturing metals from solution can both reduce the environmental risk, but also save precious infinite resources. When the POM gets reduced, they can become reoxidised by metal ions, closing the photocatalytic cycle and forming elemental metal.



The cycle (Fig. 1.18) and series of equations generalising the reactivity of POMs, (1.14) – (1.16), are key to the development of POMs into colourimetric indicators. It is clear that UV light is essential to produce a colour change and an oxidant (most notably oxygen) to produce the reverse colour change. It is the realization that these commercially useful analytes play an important role in the POMs chemistry that drives the development of POM-based indicators.

Realising the apparent limited use of POMs to create useful colourimetric optical sensors in the literature, it is aimed to development two indicators - a colourimetric UV dosimeter and an oxygen indicator.

### 1.1.3 Ultra Violet radiation

Solar ultraviolet radiation (UVR) is both essential and potentially detrimental to human health. UVB is required for the conversion of 7-deoxycholesterol to vitamin D, which is necessary to ensure good bone health.<sup>111</sup> If properly managed, artificial UVR can be used as a successful treatment of certain skin conditions e.g. psoriasis<sup>112</sup>. However, cosmetic use of artificial UV sources has become increasingly popular in recent years, which has caused a significant amount of concern amongst health professionals.<sup>113,114</sup> It is well documented that UVR can cause DNA lesions; such lesions are often repaired by the body's immunological response.<sup>115</sup> If these are not repaired or if the skin has been subject to chronic UVR exposure, irreversible mutations in the DNA sequence can occur, resulting in adverse effects. Such overexposure of UVR can lead to a variety of conditions e.g. skin aging<sup>115</sup>, skin cancer<sup>115-117</sup> and cataracts<sup>111</sup>; however the most common effect of overexposure is erythema (the reddening of the skin), more commonly known as sunburn. Erythema is a photochemical response by the skin normally resulting from overexposure of

wavelengths in the UVB and UVC regions. Sunburn occurs when skin cells are damaged by the absorption of energy from UV rays. The skin responds to this damage by sending extra blood to the damaged skin in an attempt to repair it - hence the redness that is associated with sunburn.

### 1.1.3.1 UV Index

The Global Solar UV Index (UVI)<sup>118</sup> was developed to help create a warning system, in the hope to reduce the occurrence of overexposure and therefore minimise the adverse effects of UVR. It describes the level of solar UVR at the Earth's surface, using an index range from zero upward – the greater the index value, the higher the intensity of UVR and the greater potential for damage to the skin and eye, and the less time it takes for harm to occur. Table 1.3 summarises the exposure categories which correspond to the UVI range.

**Table 1.3** – The UVI exposure categories.

<b>Exposure category</b>	<b>UVI range</b>
<b>LOW</b>	< 2
<b>MODERATE</b>	3 to 5
<b>HIGH</b>	6 to 7
<b>VERY HIGH</b>	8 to 10
<b>EXTREME</b>	11 +

Typically, the UV index on a summer's day in the UK will be around 5 or 6 (i.e. 125-150 mWm<sup>-2</sup>).<sup>119</sup> This system is now widely used by the media and other broadcasting organisations.

Erythemal dose is a term used to quantify the amount of erythemal radiation that has been cumulatively absorbed by the skin. It follows that the minimal erythemal dose (MED) is the minimum amount of UVR required to cause erythema (i.e. reddening of the skin). This value is largely dependent on the skin type, as defined by Fitzpatrick.<sup>120</sup> It is widely agreed that it is important to classify skin types, to ensure that the most vulnerable population groups are protected. It has been found that 90% of non-melanoma skin cancers occur in skin types I and II (see Table 1.4), hence much effort should be carried out to ensure this population group use the basic protective measure when out in the sun. Even though the incidence of skin cancer is reduced in dark-skinned people, they can also suffer the deleterious effects of UV radiation, especially on the eye and immune system.

The skin types are classified into six categories (I-VI). Type I being described as melano-compromised, which always burns in the sun and thereafter does not tan. Type IV describes skin which seldom burns and always tans, and type VI as naturally black skin. Types II, III, V lie in between these descriptions. Skin phototype II is the most prevalent skin type for the caucasian population. The MED for this skin type is equal to  $250 \text{ J m}^{-2}$ , i.e.  $69.4 \text{ mW m}^{-2}$  per hour. Since a UVI value of  $1 \equiv 25 \text{ mW m}^{-2}$ , it follows that even under mild UV conditions (i.e.  $\text{UVI} = 3$ ) persons with this skin type will burn within 1 hour, if not properly protected. Table 1.4 summarises the skin types.

**Table 1.4** – Classification of skin types.

<b>Skin Type classification</b>	<b>Burns in the sun</b>	<b>Tans after having been in the sun</b>
<b>I melano-</b>	Always	Seldom
<b>II compromised</b>	Usually	Sometimes
<b>III melano-</b>	Sometimes	Usually
<b>IV competent</b>	Seldom	Always
<b>V melano-</b>	Naturally brown skin  Naturally black skin	
<b>VI protected</b>		

### 1.1.3.2 UV dosimetry

Following the increasing awareness of the deleterious effects of UVR, there has been recognition<sup>121</sup> of the need for personal UV dosimeters which would give an alert when one's individual sunburn threshold is neared. Recent years have seen the development of a number of personal UV dosimeters. Electronic UV dosimeters provide the user with a quantitative digital display of how much UVR they have absorbed. Although such dosimeters provide detailed information for the user, they tend to be bulky and fairly expensive.<sup>122</sup>

Following the recognition that erythema is a consequence of damage to DNA, a number of groups developed UV dosimeters based on biological materials such as bacterial cells, bacteriophages and spores.<sup>123,124</sup> Unfortunately, such dosimeters need to be developed before the level of UV radiation can be determined. This is a major drawback when trying to develop a personal UV-dosimeter which can be easily used and interpreted by the general public.

UV-activated photochemical reactions were identified as a promising route to create effective personal UV-dosimeters. UV-activated chemical reactions have been well studied and employed in a number of areas throughout chemistry. A variety of photoactive chemicals have been identified and demonstrated to be effective UV-dosimeters. Such photoactive chemicals include polyphenylene oxide<sup>125</sup>, polysulphone<sup>126</sup>, phenothiazine<sup>5</sup>, 8-methoxypsoralen<sup>127</sup> and nalidixic acid<sup>126</sup>. One of the most widely used is polysulphone<sup>126</sup>, a polymer which upon exposure to UV radiation increases in its absorbance in the UV due to a photodegradation reaction. Polysulphone was particularly favourable as it has an initial spectral profile not too dissimilar to that of the human skin. However, to monitor the change in absorbance requires the use of a UV spectrophotometer, since the spectral change is not visible to the human eye.

UV dosimeters which provide a distinct colour change upon increasing UV exposure is highly desirable, as it provides the user with a clear and informative warning that sunburn may be imminent, without the need for bulky analytical equipment. There have been a number of commercialised colourimetric UV dosimeters developed<sup>128,129</sup>. One in particular was developed by Solar safe<sup>128</sup>, whereby they incorporated a photochromic compound into a polymer matrix, which could then be manufactured into a wristband. When the wristband is initially exposed to sunlight, it turns purple, as illustrated in Fig. 1.19. The manufacturing company describes this as the ‘activation’. When the band fades to light brown, it is recommended to reapply sunscreen on your body and also on the band. When the band turns pale yellow, it is recommended to cover up or get out of the sun.

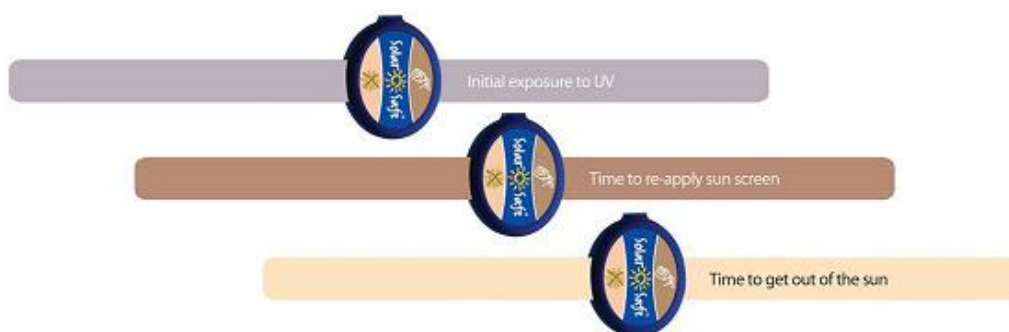


**Fig. 1.19** – Solar Safe wrist band.<sup>128</sup>



SunHealth Solutions LCC has produced a similar dosimeter as to the one above, whereby a sticker is applied to the skin and a colour change from yellow, through to orange and red, gradually indicating the increased absorption of UV radiation.<sup>129</sup> The dosimeters specifically respond to UVB light, necessary to initiate a reaction which releases at least one acidic product, typically an organic halogen capable of releasing an acidic product, such as HCl. The pH-sensitive dye incorporated into the dosimeter changes colour due to the change of pH incurred with the formation of such products. To aid the observation of the colour changes, often a graphic pattern is interposed amongst the radiation sensitive layer, where the pattern has the same colour as the ‘warning’ colour. Fig. 1.20 illustrates an example of the dosimeter and the associated colour changes.

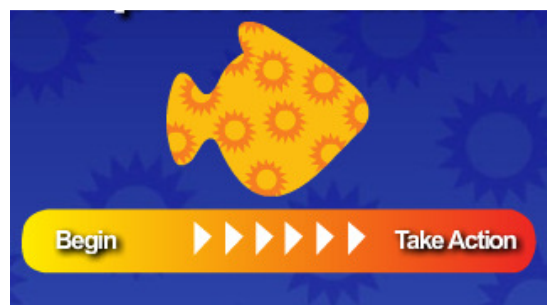


**Fig. 1.20** - UV SunSignals® Sensor.<sup>129</sup>

Similarly, our group reported a UV dosimeter which incorporated UV driven acid-release agents coupled to pH-sensitive dyes.<sup>130</sup> However, novelly they combined two UV dosimeter systems - one prompt and one delayed. The delayed response was achieved by adding a base to the system. The role of the base was to quench any acidic species formed, hence delaying the colour change. The colour change was only observed after all the base had reacted. The combined effect of using different coloured dyes, along with prompt and delayed dosimeters resulted in flag-like warnings as the MED level was increased. The arrangement created a system where

different combinations of colours were observed at different stages of the exposure process, as illustrated in Fig. 1.21.

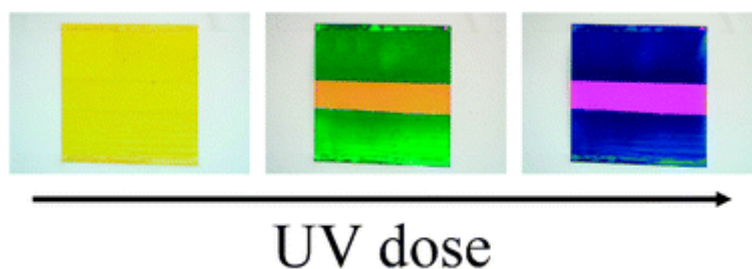


**Fig. 1.21** - Flag-like warnings of the approach to erythema are observed.<sup>130</sup>

The same group also developed a UV dosimeter based on neotetrazolium chloride.<sup>131</sup> Tetrazoliums are generally colourless, but transform to highly coloured formazans upon irradiation with UV light. By utilising a UV blocker (e.g. 2,2 dihydroxy-4-methoxy benzophenone), the colourimetric response to UVB light can be delayed and therefore calibrated to give an appropriate colour change when erythema is imminent. The resulting UV dosimeter changed colour from colourless to pink/red upon exposure to UVA and UVB light.

Another approach towards the development of colorimetric UV dosimeters is to utilise semiconductor photocatalysts. This work prompted the research discussed in this thesis, due to the similarity between inorganic photocatalysts and polyoxometalates.<sup>100</sup> One dosimeter previously developed in this group<sup>132</sup>, incorporated a redox dye, a mild reducing agent along with the photocatalyst, dispersed in a film forming polymer, i.e. methylene blue (MB)/triethanolamine (TEOA)/Titanium dioxide (TiO<sub>2</sub>) /hydroxyethyl cellulose (HEC). The TiO<sub>2</sub> nanoparticles absorb the UV light and photo-oxidise the TEOA. The resulting trapped photogenerated electrons photoreduce the methylene blue, from its blue form to its colourless leuco methylene blue. If oxygen is present, it re-oxidises the reduced colourless form to the original blue form. As a result the degree of bleaching can be directly correlated to the amount of UVR. In the presence of an oxygen impermeable barrier, the oxidation step is prohibited and the MB film acts as a successful UV

sensitive dosimeter. It is noted that the sensitivity can be altered by varying the amount of semi-conductor present. However, since  $\text{TiO}_2$  has band gap of  $3.2 \text{ eV}$ <sup>119</sup> it can absorb both UVA and UVB light. Since erythema is largely a result of exposure to UVB light, a system which responds to UVB light would be highly desirable as a commercial sunburn indicator. Such a system was recently developed in our group.<sup>119</sup> Tin (IV) oxide is a wide band-gap semiconductor ( $E_g = 3.5 \text{ eV}$ , i.e. absorption threshold  $354 \text{ nm}$ ), therefore is much more suitable to UVB detection. The indicator works in the same manner as the previously described system, however utilises the redox indicator 2,6-dichloroindophenol (DCIP) opposed to methylene blue. It is reported that the reduced form of DCIP is not readily oxidised by ambient oxygen in the film environment, creating an irreversible indicator. This feature is reported as a main advantage of the system, creating an unambiguous colour change in response to UVB light. However, this also means that the dosimeters can only be used once, and if only partially used, can never be used again. They report<sup>119</sup> that the response to UVB light can be tailored by varying the level of  $\text{SnO}_2$  contained within the indicator, so that UV dosimeters can be prepared for different skin types.

Surprisingly, UV dosimeters are not widely used by the general public, despite a number being commercial available. Along with the work described in this thesis and previous research, the area of UV dosimetry is becoming more sophisticated. It is hoped that with societies' increasing awareness of the deleterious effects of UV radiation, along with better product marketing, UV dosimeters will become popular among the general public in the very near future.

## 1.2 Aims and objectives

- To develop and extend the capabilities of previously reported ink-based colourimetric CO<sub>2</sub> indicators. In particular, to extend the shelf-life of CO<sub>2</sub> indicators, pressure range of CO<sub>2</sub> detection and hence making them more attractive for commercial development.
- To investigate extrudable plastic indicators or other possible substrates, apart from inks. Such indicators would ideally detect commercially useful analytes e.g. CO<sub>2</sub>, O<sub>2</sub>, UV light etc. This would begin a new phase in the development optical indicating, since it would eliminate the need for printing and/or adhering inks onto substrates.
- To investigate the capabilities of polyoxometalates to be used as colourimetric indicators for oxygen and UV light. Such indicators would produce optically clearer inks, since it would eliminate the need for powder dispersions of traditional semiconductors.

## 1.3 References

1. A. Mills, P. Grosshans and E. Snadden, *Sens. Actuator B-Chem.*, 2009, **136**, 458-463.
2. A. Mills, L. Wild and Q. Chang, *Mikrochim. Acta*, 1995, **121**, 225-236.
3. <http://www.nellcor.com/prod/product.aspx?id=176>, (accessed, 31/08/10).
4. <http://www.rexam.com/files/reports/2008ar/index.asp?pageid=28>, (accessed, 20/5/11).
5. K. Jia, A. V. Parisi and M. G. Kimlin, *Photochem. Photobiol. Sci.*, 2010, **9**, 1224-1227.

6. X. Q. Zhan, B. Y. Su, H. Zheng and J. H. Yan, *Anal. Chim. Acta*, **658**, 175-179.
7. <http://www.ripesense.com/>, (accessed 26/08/10).
8. A. Pacquit, K. T. Lau, H. McLaughlin, J. Frisby, B. Quilty and D. Diamond, *Talanta*, 2006, **69**, 515-520.
9. G. M. Schmolzer, D. A. Poulton, J. A. Dawson, C. O. F. Kamlin, C. J. Morley and P. G. Davis, *Resuscitation*, 2011, **82**, 307-312.
10. <http://www.mercurymed.com/catalog2/index.php?type=30>, (accessed 18/05/11).
11. C. G. Fehder, *US Pat.*, 5166075, 1992.
12. [http://www.polyvore.com/color\\_changing\\_spoons/thing?id=10146955](http://www.polyvore.com/color_changing_spoons/thing?id=10146955), (accessed 02/06/11).
13. <http://www.to-genkyo.com>, (accessed, 20/05/11).
14. <http://itsfreshinc.com>, (accessed, 20/05/11).
15. N. A. Campbell and J. B. Reece, *Biology*, Benjamin Cummings, 2001.
16. Dr. Pieter Tans, NOAA/ESRL ([www.esrl.noaa.gov/gmd/ccgg/trends](http://www.esrl.noaa.gov/gmd/ccgg/trends)) accessed, 30/08/10.
17. [www.hse.gov.uk/coshh/table1.pdf](http://www.hse.gov.uk/coshh/table1.pdf), accessed 14/05/2008.
18. *Lange's Handbook of Chemistry* McGraw-Hill , 10th edition, 1967.
19. J. W. Severinghaus and A. F. Bradley, *J. Appl. Physiol.* , 1958, **13**, 515-520.
20. E. C. Stanford, *US Pat.*, 3068073, 1962.
21. A. Mills, Q. Chang and N. McMurray, *Anal. Chem.*, 1992, **64**, 1383-1389.
22. M. Koch and R. C. Murray, *US. Pat.*, 4943364, 1990.
23. C. R. Schroeder and I. Klimant, *Sens. Actuators B*, 2005, **107**, 572-579.

24. J.F.Fernandez-Sanchez, R. Cannas, S. Spichiger, R. Steiger and U. E. Spichiger-Keller, *Sens. Actuators B*, 2007, **128**, 145-153.
25. R. Lines, *Int. Pat.*, 075498, 2007.
26. S. M. Borisov, M. C. Waldhier, I. Klimant and O. Wolfbeis, *Chem. Mater.*, 2007, **19**, 6187-6194.
27. R. Ostrowski and M. P. Debreczeny, *Int. Pat.*, 039424, 2008.
28. O. Oter, K. Ertekin, D. Topkaya and S. Alp, *Sens. Actuators B*, 2006, **117**, 295-301.
29. H. N. McMurray, *J. Mater. Chem.*, 1992, **2**, 401-406.
30. G. C. Upreti, Y. Wang and A. S. H. Kueh, *Int. Pat.*, 079024, 2008.
31. A. Mills, A. Lepre and L. Wild, *Sens. Actuators B*, 1997, **38-39**, 419-425.
32. <http://www.capnography.com/Homepage/HomepageM.htm>, (accessed, 19/06/08).
33. <http://www.frca.co.uk/article.aspx?articleid=100389>, (accessed, 19/06/08), .
34. J. A. Berman, J. J. Furgiuele and G. F. Marx, *Anesthesiology*, 1984, **60**, 613-614.
35. D. B. Raemer, D. R. Walt and C. Munkholm, *US Pat.*, 5005572, 1991.
36. <http://www.ventlab.com/ET%20Tube.htm>, (accessed 06/09/10).
37. <http://www.ventlab.com/ace.pdf>, (accessed, 23/09/10).
38. <http://www.ventlab.com/STAT-BAG.PDF>, (accessed, 15/07/11).
39. <http://www.ventlab.com/SCannouncement.pdf>, (accessed, 02/05/11).
40. [http://mercurymed.com/pdf/CO\\_Detector\\_dfu.pdf](http://mercurymed.com/pdf/CO_Detector_dfu.pdf), (accessed 18/05/11).
41. <http://www.officer.com/product/10045048/co2-detector>, (accessed, 18/05/11).

42. K. L. Yam, P. T. Takhistov and J. Miltz, *J. Food Sci.*, 2005, **70**, R1-R10.
43. G. L. Robertson, *Food Packaging - Principles and Practice. Second edition*, CRC Press, USA, 2006.
44. J. Kerry, P. Butler and MyiLibrary, *Smart Packaging Technologies for Fast Moving Consumer Goods*, Wiley Online Library, 2008.
45. *Novel food packaging techniques*, Woodhead Publishing Limited, 2003.
46. [http://www.azom.com/article.aspx?ArticleID=2152#\\_Possible\\_Concerns\\_over](http://www.azom.com/article.aspx?ArticleID=2152#_Possible_Concerns_over), (accessed, 31/08/11).
47. EU, Regulation 1935/2004/EC at <http://eur-lex.europa.eu/LexUriServ/LexUriServ.do?uri=OJ:L:2004:338:0004:0017:en:PDF> (accessed, 31/08/11).
48. EU, Regulation 450/2009/EC at <http://eur-lex.europa.eu/LexUriServ/LexUriServ.do?uri=OJ:L:2009:135:0003:0011:EN:PDF>, (accessed, 31/08/11).
49. R. Coles and M. Kirwan, *Food and beverage packaging technology*, Wiley Online Library, 2011.
50. <http://www.cptplastics.com/aboutMAP.html>, (accessed, 01/09/10).
51. G. L. Robertson, *Food Packaging - Principles and Practise*, Marcel Dekker, Inc., 1993.
52. G. Valley, *Q. Rev. Biol.*, 1928, **3**, 209-224.
53. C. N. R. Sankar, K. V. Lalitha, L. Jose, S. Manju and T. K. S. Gopal, *Food Microbiol.*, 2008, **25**, 518-528.
54. C. Gill, *Meat Sci.*, 1988, **22**, 65-71.
55. S. N. Balderson and R. J. Whitwood, Google Patents, 1995.
56. <http://www.sealedair.com/default.aspx>, (accessed 18/05/11).

57. M. J.-P. Leiner, J. Tusa and I. Klimant, *EP*, 1 965 198, 2008.
58. M. Smolander, E. Hurme and R. Ahvenainen, *Trends Food. Sci. Tech.*, 1997, **8**, 101-106.
59. P. V. Hobbs, *Introduction to Atmospheric Chemistry*, Cambridge University Press, 2000.
60. [http://pangea.stanford.edu/research/Oceans/GES205/Caldeira\\_Science\\_Anthropogenic%20Carbon%20and%20ocean%20pH.pdf](http://pangea.stanford.edu/research/Oceans/GES205/Caldeira_Science_Anthropogenic%20Carbon%20and%20ocean%20pH.pdf), (accessed, 24/09/10).
61. Y. Kawabata, T. Kamichika, T. Imasaka and N. Ishibashi, *Analytica Chimica Acta*, 1989, **219**, 223-229.
62. C. S. Chu and Y. L. Lo, *Sens. Actuator B-Chem.*, 2009, **143**, 205-210.
63. R. N. Dansby-Sparks, J. Jin, S. J. Mechery, U. Sampathkumaran, T. W. Owen, B. D. Yu, K. Goswami, K. L. Hong, J. Grant and Z. L. Xue, *Anal. Chem.*, 2009, **82**, 593-600.
64. O. S. Wolfbeis, B. Kovacs, K. Goswami and S. M. Klainer, *Mikrochim. Acta*, 1998, **129**, 181-188.
65. A. Mills and Q. Chang, *Sens. Actuator B-Chem.*, 1994, **21**, 83-89.
66. S. K. Lee, M. Sheridan and A. Mills, *Chem. Mat.*, 2005, **17**, 2744-2751.
67. A. Mills, *Chem. Soc. Rev.*, 2005, **34**, 1003-1011.
68. N. Church, *Trends in Food Science & Technology*, 1994, **5**, 345-352.
69. <http://www.mgc.co.jp/eng/products/abc/ageless/index.html>, (accessed 18/09/10).
70. <http://www.mgc.co.jp/eng/products/abc/ageless/effect/01.html>, (accessed 18/09/10).
71. K. Randell, R. Ahvenainen, K. Latvakala, E. Hurme, T. Mattilasandholm and L. Hyvonen, *J. Food Sci.*, 1995, **60**, 667-&.



72. M. Eilamo, R. Ahvenainen, E. Hurme, R. L. Heinio and T. Mattilasandholm, *Food Sci. Technol.-Lebensm.-Wiss. Technol.*, 1995, **28**, 62-71.
73. S. K. Lee, A. Mills and A. Lepre, *Chem. Commun.*, 2004, 1912-1913.
74. A. Mills and D. Hazafy, *Sensors and Actuators B-Chemical*, 2009, **136**, 344-349.
75. A. Mills and D. Hazafy, *Analyst*, 2008, **133**, 213-218.
76. K. Eaton, *Sensors and Actuators B-Chemical*, 2002, **85**, 42-51.
77. P. Hartmann, M. J. P. Leiner and M. E. Lippitsch, *Anal. Chem.*, 1995, **67**, 88-93.
78. Z. Zhujun and W. R. Seitz, *Anal. Chem.*, 1986, **58**, 220-222.
79. K. E. Chung, E. H. Lan, M. S. Davidson, B. S. Dunn, J. S. Valentine and J. I. Zink, *Anal. Chem.*, 1995, **67**, 1505-1509.
80. A. Delbianco, F. Baldini, M. Bacci, I. Klimant and O. S. Wolfbeis, *Sensors and Actuators B-Chemical*, 1993, **11**, 347-350.
81. S. Ebraheem, A. Abdel-Fattah, F. Said and Z. Ali, *Radiation Physics and Chemistry*, 2000, **57**, 195-202.
82. Y. Yoshikawa, T. Nawata, M. Goto and Y. Fujii, *US Patent*, 4169811, 1979.
83. <http://www.mgc.co.jp/eng/products/abc/ageless/eye.html>, (accessed 22/09/10).
84. M. Rindl, *S. Afr. J. Sci.*, 1916, **11**, 362.
85. D. E. Katsoulis, *Chem. Rev.*, 1998, **98**, 359-387.
86. A. Hiskia, A. Mylonas and E. Papaconstantinou, *Chem. Soc. Rev.*, 2001, **30**, 62-69.
87. C. Chen, Q. Wang, P. Lei, W. Song, W. Ma and J. Zhao, *Environ. Sci. Technol.*, 2006, **40**, 3965-3970.

88. A. Troupis, E. Gkika, T. Triantis, A. Hiskia and E. Papaconstantinou, *J. Photochem. Photobiol. A-Chem.*, 2007, **188**, 272-278.
89. A. Troupis, T. M. Triantis, E. Gkika, A. Hiskia and E. Papaconstantinou, *Appl. Catal. B-Environ.*, 2009, **86**, 98-107.
90. Y. Yang, Q. Wu, Y. Guo, C. Hu and E. Wang, *J. Mol. Catal. A-Chem.*, 2005, **225**, 203-212.
91. M. A. Zanjanchi, H. Golmojdeh and M. Arvand, *J. Hazard. Mater.*, 2009, **169**, 233-239.
92. W. Feng, T. R. Zhang, L. Wei, R. Lu, Y. B. Bai, T. J. Li, Y. Y. Zhao and J. N. Yao, *Mater. Lett.*, 2002, **54**, 309-313.
93. T. R. Zhang, W. Feng, Y. Q. Fu, R. Lu, C. Y. Bao, X. T. Zhang, B. Zhao, C. Q. Sun, T. J. Li, Y. Y. Zhao and J. N. Yao, *J. Mater. Chem.*, 2002, **12**, 1453-1458.
94. J. Keggin, *Nature*, 1933, **131**, 908-909.
95. I. Kozhovnikov, *Catalysis by polyoxometalates*, John Wiley & sons, 2002.
96. [http://en.wikipedia.org/wiki/Phosphotungstic\\_acid](http://en.wikipedia.org/wiki/Phosphotungstic_acid), (accessed, 03/09/11).
97. E. Papaconstantinou, *Chem. Soc. Rev.*, 1989, **18**, 1-31.
98. A. Troupis, E. Gkika, A. Hiskia and E. Papaconstantinou, *C. R. Chim.*, 2006, **9**, 851-857.
99. E. Papaconstantinou and A. Hiskia, *Polyoxometalate Molecular Science*, 2003, **98**, 381.
100. P. Kormali, A. Troupis, T. Triantis, A. Hiskia and E. Papaconstantinou, *Catal. Today*, 2007, **124**, 149-155.
101. J. J. Barra-Almenar, E. Coronado and A. Muller, *Polyoxometalate Molecular Science*, Kluwer Academic Publishers, 2001.
102. B. Xu, L. Xu, G. Gao and Y. Jin, *Appl. Surf. Sci.*, 2007, **253**, 3190-3195.

103. J. Chen, Y. Liu, W. Feng and W.-M. Cai, *J. Mater. Sci.: Mater. Electron*, 2008, **19**, 295-299.
104. T. R. Zhang, R. Lu, X. L. Liu, Y. Y. Zhao, T. J. Li and J. N. Yao, *J. Solid State Chem.*, 2003, **172**, 458-463.
105. W. Feng, Y. S. Ding, Y. Liu and R. Lu, *Mater. Chem. Phys.*, 2006, **98**, 347-352.
106. W. Feng, T. R. Zhang, Y. Liu, R. Lu, C. Guan, Y. Y. Zhao and J. N. Yao, *Mater. Chem. Phys.*, 2003, **77**, 294-298.
107. J. Chen, Y. Liu, D.-Q. Xiong, W. Feng and W.-M. Cai, *Thin Solid Films*, 2008, **516**, 2864-2868.
108. J. Huang, X. Dong, Q. Pan and Z. Cheng, *J. Shanghai. Univ.*, 2008, **12**, 368-371.
109. W. Feng, T. R. Zhang, Y. Liu, R. Lu and Y. Y. Zhao, *J. Mater. Sci.*, 2003, **38**, 1045-1048.
110. A. Troupis, A. Hiskia and E. Papaconstantinou, *Appl. Catal. B-Environ.*, 2003, **42**, 305-315.
111. R. P. Gallagher and T. K. Lee, *Prog. Biophys. Mol. Biol.*, 2006, **92**, 119-131.
112. M. Lebwohl and S. Ali, *J. Am. Acad. Dermatol.*, 2001, **45**, 487-498.
113. A. Gavin, C. Donnelly, A. Devlin, C. Devereux, G. O'Callaghan, G. McElwee, S. Gordon, T. Crossan, N. McMahon, P. Loan, S. Martin, L. McPeak, J. Caughey and A. H. O'Hagan, *Br. J. Dermatol.*, **162**, 627-632.
114. P. Mathys, M. Moser, D. Bressoud, B. Gerber and C. Braun-Fahrlander, *Sozial-und Pravent.*, 2002, **47**, 318-329.
115. Y. Matsumura and H. N. Ananthaswamy, *Toxicol. Appl. Pharmacol.*, 2004, **195**, 298-308.
116. R. M. MacKie, *Prog. Biophys. Mol. Biol.*, 2006, **92**, 92-96.

117. F. Urbach, *J. Photochem. Photobiol. B-Biol.*, 1997, **40**, 3-7.
118. <http://www.who.int/uv/publications/en/GlobalUVI.pdf>, (accessed 09/09/10).
119. A. Mills and P. Grosshans, *Analyst*, 2009, **134**, 845-850.
120. F. B. Fitzpatrick, *Arch. Dermatol.*, 1988, **124**, 869-871.
121. P. Autier, *Br. J. Dermatol.*, 2009, **161**, 40-45.
122. [http://www.cgmdirect.com.au/CGM\\_Main/Archive/SafeSun.htm](http://www.cgmdirect.com.au/CGM_Main/Archive/SafeSun.htm), (accessed 18/10/10).
123. L. E. Quintern, G. Horneck, U. Eschweiler and H. Bucker, *Photochem. Photobiol.*, 1992, **55**, 389-395.
124. P. Rettberg and C. S. Cockell, *Photochem. Photobiol. Sci.*, 2004, **3**, 781-787.
125. P. W. Schouten, A. V. Parisi and D. J. Turnbull, *J. Photochem. Photobiol. B-Biol.*, 2009, **96**, 184-192.
126. D. J. Turnbull and A. V. Parisi, *Phys. Med. Biol.*, **55**, 3767-3776.
127. B. L. Diffey and A. Davis, *Phys. Med. Biol.*, 1978, **23**, 318-323.
128. <http://www.solarsafewristbands.co.uk/>, (accessed, 20/10/10).
129. <http://www.sunsignals.com/>, (accessed, 25/10/10).
130. A. Mills, K. McDiarmid, M. McFarlane and P. Grosshans, *Chem. Commun.*, 2009, 1345-1346.
131. A. Mills, P. Grosshans and M. McFarlane, *J. Photochem. Photobiol. A-Chem.*, 2009, **201**, 136-141.
132. A. Mills, S. K. Lee and M. Sheridan, *Analyst*, 2005, **130**, 1046-1051.

## Chapter 2: Experimental

---

### 2.1 Chemicals

All chemicals were purchased from Sigma Aldrich, unless specified, and in the highest purity available. All solutions were prepared freshly using class A or B volumetric flasks, and all aqueous solutions were made up using double distilled and deionised water. The gases were obtained from BOC gases and of high purity.

### 2.2 Spectrophotometric Techniques

#### 2.2.1 UV/Visible spectrophotometry

Ultraviolet (UV) and visible light regions in the electromagnetic spectrum, encompass the range of wavelengths from around 200-750 nm. When this light interacts with molecules, it causes an electron to be promoted from its ground state to an 'excited state'. This process is called *absorption*. Molecules which absorb strongly in the visible region are highly coloured. The colour of a substance is dependent upon the wavelength of light it doesn't absorb; hence the observed colour is often called the 'complimentary colour'. The wavelengths of light which a substance absorbs, and hence the colour, is dependent upon the electronic structure of the molecule. The groups in a molecule which absorb the wavelengths in the UV and visible region are known as chromophores. Typically these groups contain  $\pi$ -electron groups or hetero atoms having non-bonding valence-shell electron pairs. Thus the electronic transitions which match the energy of UV and visible light are  $n \rightarrow \pi^*$  and  $\pi \rightarrow \pi^*$ . Dye molecules are highly coloured compounds, hence often contain a high level of  $\pi$ -conjugation and hetero atoms. pH indicating dyes are of most interest since a small change in the structure can cause significant electronic changes, causing it to absorb a different wavenegth of light, hence change its colour. One notable example is the phthalein dyes. In the acidic form (lactones) they are colourless, but deeply coloured (red, pink, violet, blue or green-blue) in the alkaline

form (quinone). This dramatic colour change can be explained with the loss of conjugation when the lactone is formed, as illustrated in Fig. 2.1.

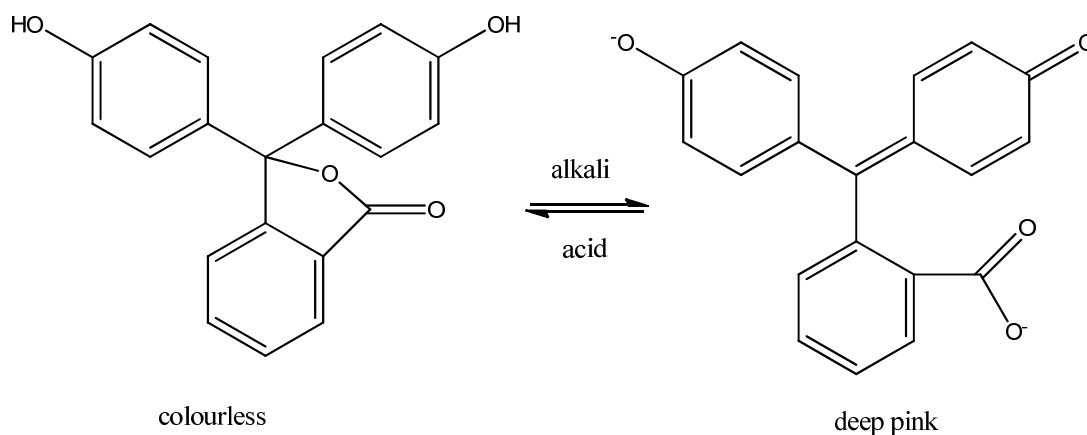


**Fig. 2.1** – Change in the electronic structure of phenolphthalein resulting in a dramatic change in colour.

UV/visible spectrophotometry is used to quantitatively analyse the colour changes. It does this by subjecting a sample to a beam of light of known intensity and wavelength. The light which is transmitted through the sample is then detected, hence the portion of the light which is absorbed is known, hence a value of absorption for a known wavelength is determined. This absorbance is taken to be a ratio of the incident light and transmitted light, as described in equation 2.1.

$$A = \log_{10} I_0/I \quad (2.1)$$

The Beer-Lambert law states that the concentration of a substance in solution is directly proportional to the absorbance of the solution. This relationship is expressed in below (2.2).

$$A = \epsilon bc \quad (2.2)$$

Where  $\epsilon$  = molar absorptivity ( $l \text{ mol}^{-1} \text{ cm}^{-1}$ ),  $b$  = cell pathlength (cm) and  $c$  = concentration ( $\text{mol l}^{-1}$ ). At low concentrations a plot of absorbance versus concentration gives a straight line, the gradient of which is the molar absorptivity.

The diagrams in Fig. 2.2 illustrate the measurements of absorbance for solutions and inks coated onto glass disks.

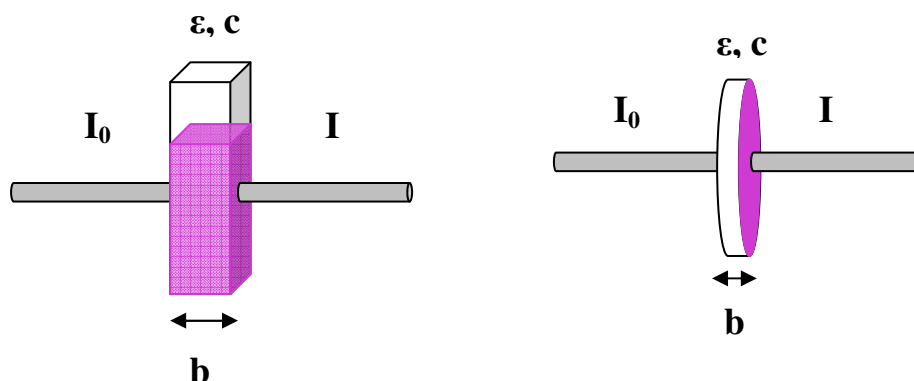


**Fig. 2.2** – UV/vis absorption spectroscopy carried out on solutions and inks coated onto glass disks.

A UV/visible spectrophotometer is used to perform these measurements and can either be configured as a single or double beam. In all experiments performed in this work a dual beam spectrophotometer was used and a schematic of the set-up is illustrated in Fig. 2.3. Typically, light is directed through a monochromator and then through the sample. Some of this light will be absorbed by the sample, however the remainder of this light passes through to the detector and the response recorded. By comparing the amount of light absorbed and transmitted, the absorbance spectrum can be produced, according to equation (2.1).

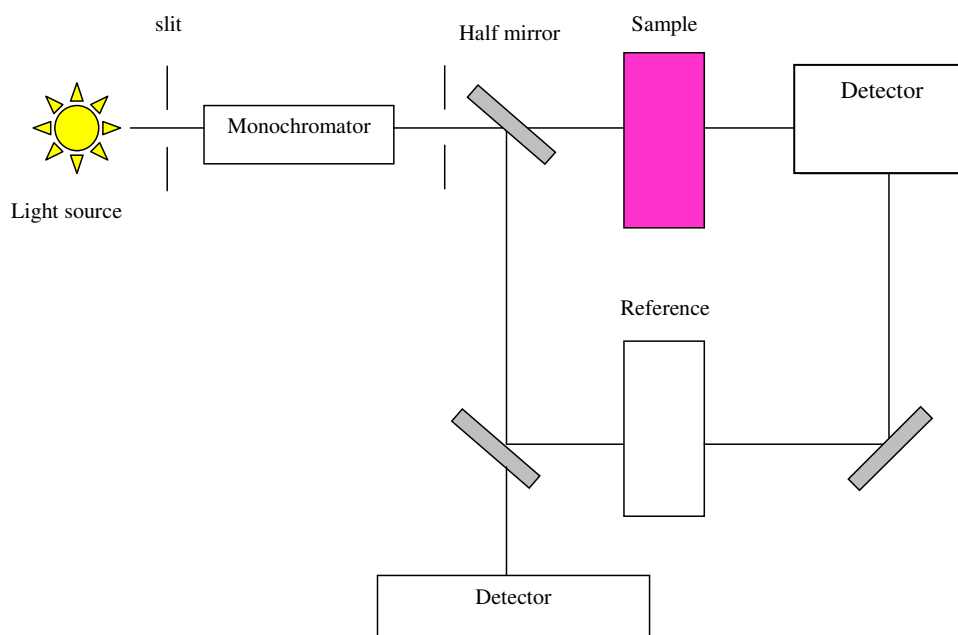


**Fig. 2.3** – Schematic of double beam UV/visible spectrophotometer.

UV/visible spectrophotometry allows quick analysis of the absorption and the intensity of the absorption of the films and any colour changes taking place, hence all of the inks were usually analysed using this method. Throughout the projects, Varian Cary 50 and Perkin Elmer Lambda 35 UV/Visible spectrophotometers were used. Typically, samples were fixed into a gas cell – the sample to the front and a blank glass disk to the back, as shown in Fig. 2.4, and then placed into the spectrophotometer for analysis. The cell comprises of a gas inlet and outlet, to allow the user to vary the gas composition and carry out continuous UV/Vis analysis.



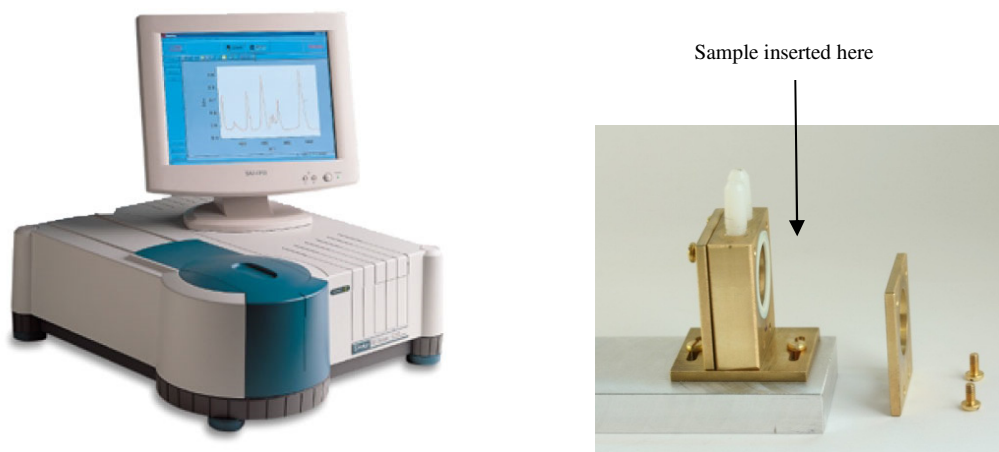


**Fig. 2.4** – Picture of Varian Cary 50 spectrophotometer<sup>1</sup> (left) and gas cell which films are mounted onto, for recording of spectra (right).

For colour studies, a portable spectrophotometer made by Konica Minolta (cm-2500d) was used. This spectrophotometer was useful when analysing samples which required quick, accurate, and convenient analysis.



**Fig. 2.5** – Konica Minolta Cm-2500d portable spectrophotometer.<sup>2</sup>

### 2.2.2 Diffuse Reflectance spectroscopy (DRS)

Unlike dye solutions and transparent ink films, pigments and inks printed into paper cannot be analysed by spectrophotometry. Many substances particularly rough surface solids exhibit diffuse reflection opposed to specular reflection i.e. when the

incident angle of light equals the angle of reflection. Diffuse reflectance is illustrated in Fig. 2.6.

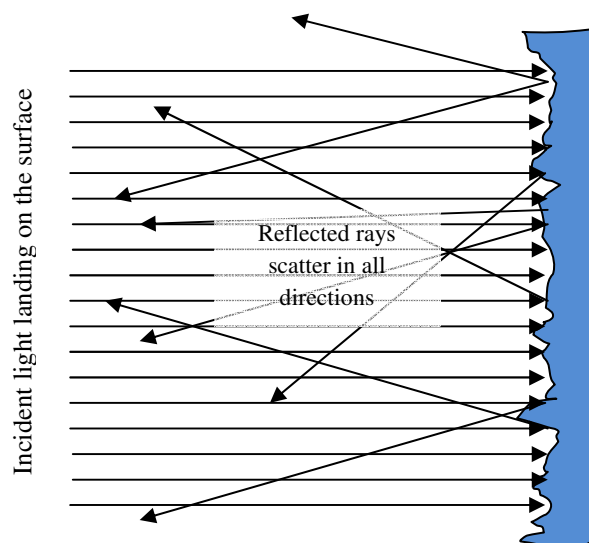


**Fig. 2.6** – Schematic illustration of diffuse reflectance.

DRS uses sphere technology to capture all of the reflected rays. A highly reflective white coating is used to coat the inside of the sphere to aid the reflection of the rays into the detector. DRS is a complicated measurement since many factors affect the results obtained; these include particle size, refractive indices, homogeneity, packing, and specular reflection.<sup>3</sup>

Typically, a Kubelka-Munk conversion is carried out where  $R$  = absolute reflectance.

$$f(R) = (1-R)^2 / 2R \quad (2.3)$$

Diffuse reflectance spectrophotometry was carried out a Labsphere RSA-PE-20 Reflectance Accessory which fits into the sample compartment of the Perkin Elmer Lambda 35 UV/Visible spectrophotometer.

### 2.2.3 Fluorimetry

Fluorescence occurs when the light emitted by a substance is of a different wavelength than the absorbed light. Fluorescence spectroscopy was carried out on a small number of samples, but not used extensively as UV/vis spectrophotometry, due to the limited use of fluorescing materials throughout the projects. A Perkin-Elmer LS50-B Luminescence spectrophotometer was used in all experiments, a schematic of such a fluorimeter is illustrated in Fig. 2.7.

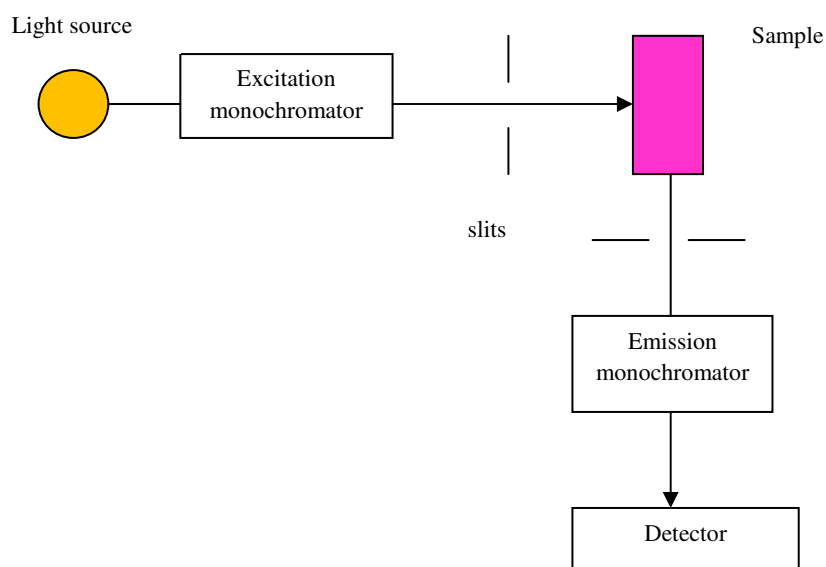
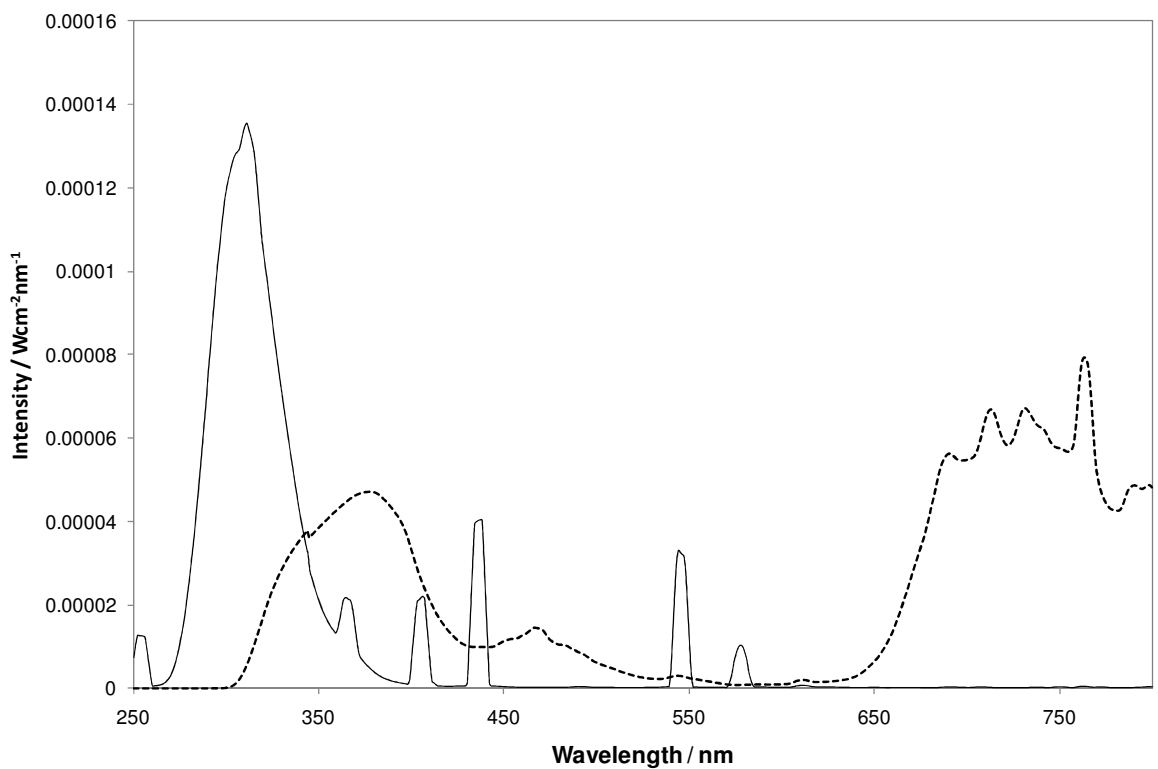


Fig. 2.7 – Schematic of fluorimeter.

## 2.3 UV light sources

UV irradiation of samples was carried out using UVA or UVB light provided by two 8 W fluorescence tubes (Vilber Lourmat), with the appropriate emission spectra maximum peak in these regions, *i.e.* at 365 and 315 nm respectively. For each of the UV light sources the sample–light source distance was set so that the irradiance (*i.e.* radiant power per unit area) was  $4 \text{ mWcm}^{-2}$ , as measured using a Multi-sense 100 UV light meter fitted with the appropriate UVA and UVB sensors.

The UV solar simulator used comprised a 180 W xenon arc lamp (Speirs Robertson), with UG5 and WG320 filters placed in-line as described previously by Diffey.<sup>4</sup> The UG5 filter allows transmission at UV wavelengths and absorbs in the visible region, while the WG320 filter absorbs in the short wavelength UVC region. The cumulative effect of both filters and the Xe arc lamp is an emission spectrum that provides a good match with the UV spectrum of the sun. The UVI of the UV solar simulated light was measured using a SafeSun™ solar meter<sup>5</sup> and was typically found to have a UVI value of 5 at the distance samples were irradiated. Fig. 2.8 illustrates the emission spectra of both the UVB and solar simulator.



**Fig. 2.8** – Emission spectra of UVB lamp (—) and solar simulator (----).

## 2.4 General sample preparation

### 2.4.1 Ink preparation

All of the intelligent inks used to prepare thin films were typically prepared by dissolving a few milligrams of dye/polyoxometalate in a small sample (2 - 10 g) of polymer solution. Other typical ingredients added to the ink solutions were phase transfer agents, base solutions, plasticizers and sacrificial electron donors. Each of the components were added with stirring and the inks were often placed in an ultrasonic bath to ensure good dispersion/dissolution of all components.

All polymer solutions, base solutions etc. were freshly prepared before being used in the ink formulation.

### 2.4.2 Ink-film formation

#### 2.4.2.1 Spin coating

Ink films were spun using the 'spin-coating technique', typically onto borosilicate or quartz glass disks using a Spin Coater Model 4000-1. Typically a few drops of ink were dropped onto a borosilicate or quartz glass slide which is mounted onto the spin coater. Speeds between 500 - 3000 rpm were selected for a spin time between 15 - 30 seconds. A photograph of a typical spin-coated film, along with the ink is shown in Fig. 2.9.

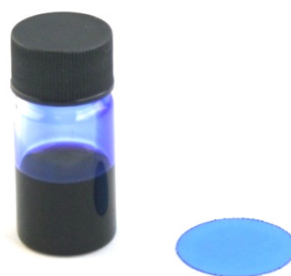


**Fig. 2.9** - Typical spin coated ink film from ink solution.

#### 2.4.2.2 K-bar coating

To obtain a uniform coating of ink on a range of substrates (e.g. paper, plastic, metal etc.), the K-bar coating technique was used. K-bars are metal rods with grooves, which control the wet film thickness. Closely wound grooves provide very thin coatings, whereas wider spaced grooves produce thicker coatings. Typically a set of K-bars can produce coating thicknesses of 4 to 120  $\mu\text{m}$ . The coating can be hand-drawn, as illustrated in Fig. 2.10, or alternatively drawn down using a mechanical K-bar coater.

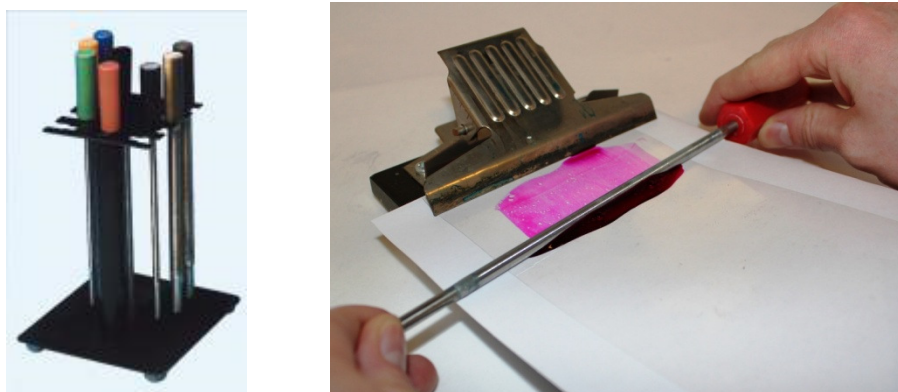


**Fig. 2.10** – Illustration of coating inks onto a substrate, using K-bars.

### 2.4.3 Pigment preparation

In order to prepare a typical intelligent pigment, a dye/polytungstate was mixed with silica and a solvent, until a uniform dispersion/solution was obtained. Other typical ingredients were base solutions and sacrificial electron donors, depending on the type of pigment. The solvent was then evaporated under reduced pressure using a Rotary Evaporator (Buchi, Rotavapor R-3), to produce a pigment, which was then oven dried (~50°C) until dry.

### 2.4.4 Pigmented polymer film preparation

In order to prepare small heat-pressed plastic pigmented films, Specac Atlas™ Series Heated Platens were used, as illustrated in Fig. 2.11. Firstly, the sample holder was assembled with the appropriate ring (depending on desired thickness of film) (4). Then approximately 0.3 - 0.4 g of sample was placed onto the sample holder. To avoid the sample sticking to the metal holder, small discs of aluminium foil were used to sandwich the sample, and easily peeled off after the sample is cooled. The temperature was set on the temperature gauge (2) close to the melting point of the polymer (typically 5°C lower than melt temperature). Once the press had reached the desired temperature, the sample holder, containing the sample was inserted (3). The sample was left to allow melting to take place, before being pressed using the hand lever (1). Typically the film is pressed to 3 - 5 tonnes, for approximately 3 minutes. After this time, the pressure is slowly released and the sample holder carefully transferred to the cooler (5). After ~10 minutes the sample was sufficiently cooled so that the sample could be safely removed.



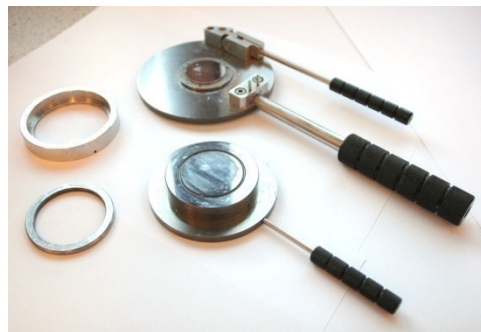
(1) Heated platens and pressure gauge



(2) Temperature controller



(3) Sample holder inserted into the press



(4) Sample holder, with metal ring which defines the film thickness



(5) Cooler

**Fig. 2.11** - Specac Atlas™ Series Heated Platens set-up.

This set-up allows the process temperature and pressure, along with the resulting film thickness to be easily adjusted dependent upon the sample type. The sample film



thickness is controlled by varying the ring size (0.015, 0.025, 0.050, 0.100, 0.250, 0.500 mm films of 29 mm diameter). Only a small sample size (approx 0.3 – 0.4 g) is required to obtain a high quality sample, as illustrated in Fig. 2.12.

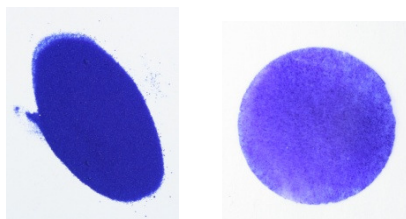


**Fig. 2.12** – Typical pigment and subsequent pigmented polymer film.

## 2.5 Optical microscope



Pigment particles were examined using an optical microscope (Olympus SZ-CTV). This allowed the photography of the individual pigments as they were exposed to the analyte. Examples of the photographs obtained are shown in Fig. 5.3.

**Fig. 2.13** – Optical microscope used to observed individual pigment particles.

## 2.6 Film thickness measurements

### 2.6.1 Scanning electron microscopy (SEM)

SEM produces detailed photographs of samples by directing a high energy beam of electrons onto surfaces. This effectively maps the surface of the sample and allows the determination of ink film thicknesses. All samples were analysed using a Cambridge Stereoscan 90 SEM, producing such images as shown in Fig. 2.14. All analyses were performed by technician, James Morrow.

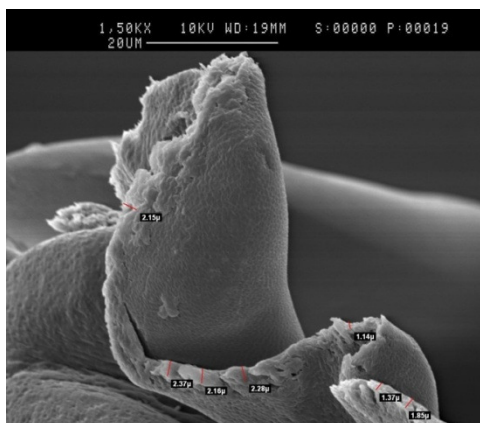


**Fig. 2.14** – SEM image of ink obtained from the Cambridge Stereoscan 90 SEM.

### 2.6.2 Profilometry

Alternatively, film thickness was determined by thin film profilometry. This method was used to compliment SEM, but was not used as the main technique due to not all samples being suitable for this technique. The instrument works by dragging a small diamond tip over a set distance, which detects any variation in the vertical axis of the tip. By coating a polymer film onto half of a quartz/glass substrate it is possible to drag the tip across a distance which includes the blank substrate and the coated film. The film will lift the tip and thus the machine records the thickness of the film. Problems with soft polymer films caused the tip to not correctly define the beginning of the polymer film, leading to inaccuracies in film thickness measurements. Hence this technique was only used for some samples. Fig. 2.15 shows a picture of the

Dektak profilometer along with a sample result obtained from a 10% HEC spun onto quartz at 700 rpm.

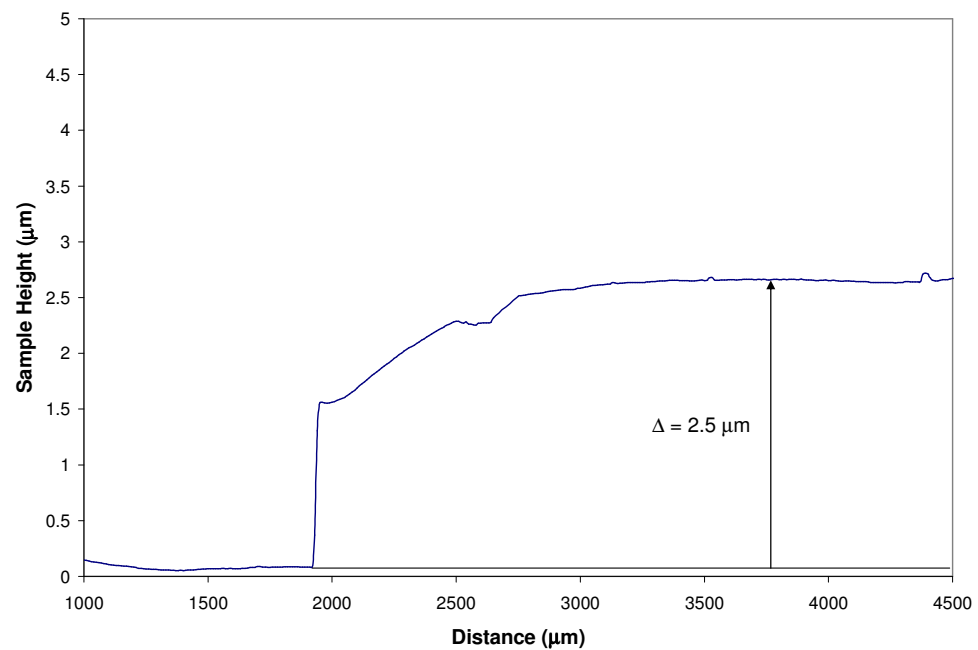


**Fig. 2.15** – Top: Dektak profilometer used for measuring the thickness of thin polymer films. Bottom: Sample result obtained from a 10% HEC spun onto quartz at 700 rpm, showing a film thickness of 2.5μm.

### 2.6.3 Micrometry

A Mitutoyo digital micrometer, as illustrated in Fig. 2.16, was used to determine the thickness of thicker samples, such as extruded or heat-pressed pigmented polymer films.



**Fig. 2.16** – Picture of Mitutoyo digital micrometer.

### 2.7 Gas blending

To obtain different concentration blends of gases, Cole-Parmer rotameters were used, as illustrated in Fig. 2.17. By simple ratiometric methods, different blends of gases were produced.

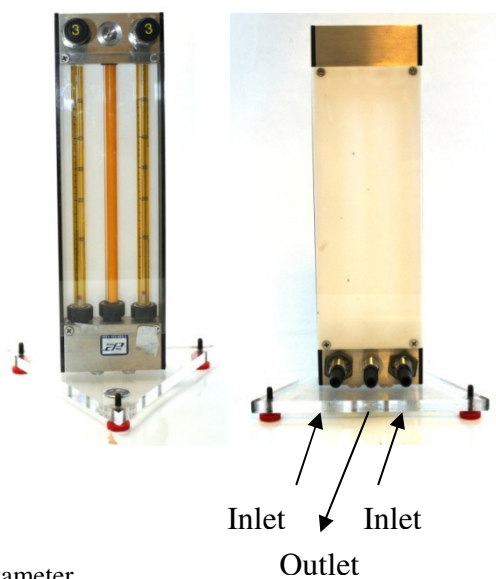


**Fig. 2.17** - Cole-Parmer Rotameter.

## 2.8 Humid gas blends

In order to achieve different blends of CO<sub>2</sub> at varying humidity levels, the experimental set-up as illustrated in Fig. 2.18 was used.

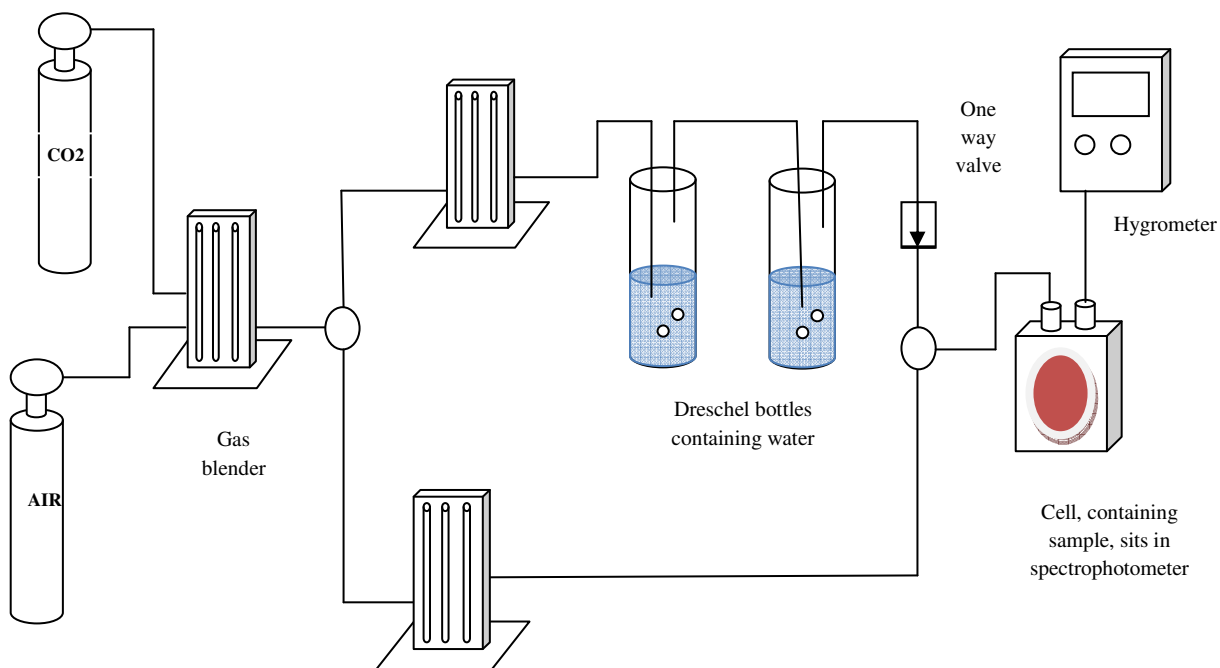


**Fig. 2.18** – Experimental set-up for obtaining different gas blends of CO<sub>2</sub> with varying humidity levels.

Firstly a gas blender is used to blend pure CO<sub>2</sub> with air to obtain the desired gas blend. This blend is then split into two lines: the first is flowed through two dreschel bottles filled with water to obtain a gas mixture with 100%RH, and the second line is not subjected to any further treatments, hence remains at 0%RH. By controlling the flow rates of these two gas streams (in this case by gas blenders) when they are combined together, gas blends with varying humidities can be obtained. To confirm the humidity of the gas stream, a hygrometer is placed at the end of the line, upon exit of the sample.

Similar experimental set-ups were used for other gases, with or without the need for initial gas composition blending.

## 2.9 Temperature studies

To investigate how temperature affected the sensitivity of the films to CO<sub>2</sub> (and indeed other gases, depending on the indicator), the same experimental set-up as described<sup>6</sup> in an earlier paper published by Mills' was adopted. Fig. 2.19 contains the diagram from the experimental section from this paper.

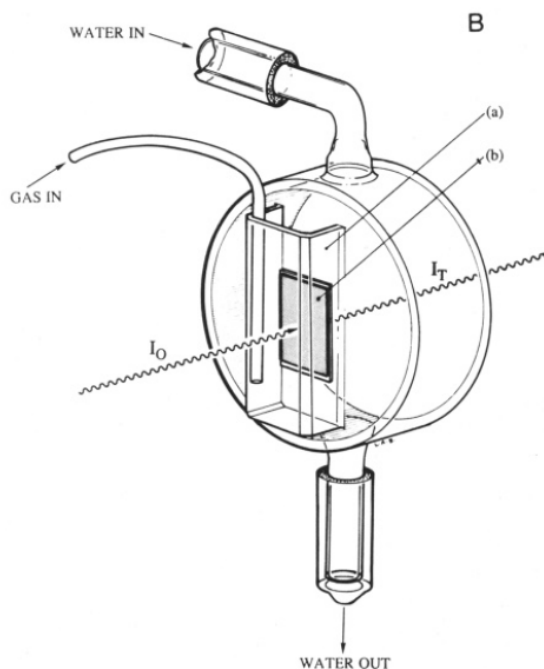


**Fig. 2.19** – Optical arrangement for testing temperature sensitivity of ink films.<sup>6</sup>

A film sample was glued/sellotaped onto the face of a cylindrical thermostated quartz cell covered with half of a 1 cm plastic cuvette which was glued into place and incorporated with the necessary gas inlet. The plastic film-thermostated cell arrangement was positioned in the spectrophotometer so that the film was perpendicular to the interrogating light beam. To confirm the temperature of the sample, a laser IR thermometer was used.

## 2.10 pH Measurement

The pH of solutions and inks were measured using a standard glass pH electrode, ensuring regular calibration with commercially supplied buffers.

## 2.11 Packaging sealer

In order to test the indicators as leak detectors, samples were tested by packaging the indicator in a high CO<sub>2</sub> gas environment using a VS 300 table top lidding commercial food packager, as shown in Fig. 2.20. The plastic lidding used is PET, which is known for its high barrier properties.



**Fig. 2.20** – Food packager used to test indicators.


## 2.12 References

1. <http://www.labwrench.com/?equipment.view/equipmentNo/1052/Varian/Cary-50/>, (accessed, 15/07/11).
2. <http://www.laboandco.com/controle-qualite/colorimetrie/spectrocolorimetre/colorimetrie-spectrocolorimetre-cm-2500-d-konica-minolta.html>, (accessed, 15/07/11).
3. [http://www.piketech.com/technical/application-pdfs/Diffuse\\_Theory&Appl.pdf](http://www.piketech.com/technical/application-pdfs/Diffuse_Theory&Appl.pdf), (accessed, 03/09/11).
4. B. L. Diffey, *Methods*, 2002, **28**, 4-13.
5. [http://www.cgmdirect.com.au/CGM\\_Main/Archive/SafeSun.htm](http://www.cgmdirect.com.au/CGM_Main/Archive/SafeSun.htm), (accessed 18/10/10).
6. A. Mills, Q. Chang and N. McMurray, *Anal. Chem.*, 1992, **64**, 1383-1389.



## Chapter 3: Water-based indicators for the detection of CO<sub>2</sub>

---



$$\text{CO}_2 + \text{H}_2\text{O} \rightleftharpoons \text{H}^+ + \text{HCO}_3^-$$
$$\text{H}^+ + \text{D}^- \rightleftharpoons \text{HD}$$

### 3.1 Introduction

An important step in the development of CO<sub>2</sub> solid-state indicators was in 1992 when it was established that phase transfer agents (PTA) could be used to incorporate hydrophilic pH-sensitive dyes into solvent-based inks to create a new range of CO<sub>2</sub> indicators.<sup>1</sup> PTAs work by extracting the dye from the highly polar protic medium into the less polar environment of the polymer/plasticizer. Such work created thin colourimetric polymer films which rapidly changed colour upon exposure to CO<sub>2</sub>. Photographs of typical films developed in this work are illustrated in Fig. 3.1.

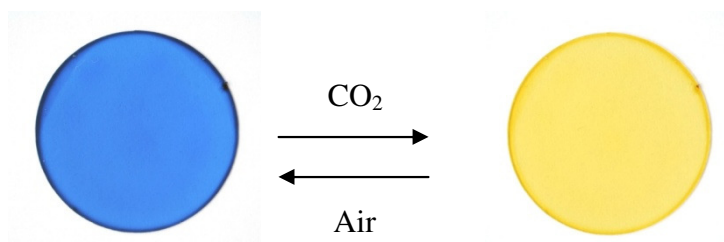


Fig. 3.1 – Solvent-based CO<sub>2</sub>-indicators as developed by Mills et al. in 1992.<sup>1</sup>

Most colourimetric CO<sub>2</sub> (g) indicators are reliant upon the change in pH which occurs when CO<sub>2</sub> (g) dissolves in water. In aqueous solution, this observed pH change is due to the following reactions



In such indicators, the colour change is usually due to the presence of a pH-sensitive dye which reacts with the protons generated *via* reactions (3.1) - (3.4), i.e.,



where A is the colour of the deprotonated dye (D<sup>-</sup>) and colour B is the colour of the protonated form of the dye (HD). Thus, upon exposure of such an indicator to CO<sub>2</sub> (g) at an appropriate level, the pH of the ambient environment decreases sufficiently to protonate the dye and so cause a measurable and observable change in absorbance of the indicator.

Many papers and patents have been published on the development of such colourimetric CO<sub>2</sub> optical indicators,<sup>2-8</sup> with the majority focused on solvent-based (i.e. non-aqueous) systems, incorporating a PTA.<sup>1</sup> However, it has been noted by many that a major drawback of such systems lies in their poor shelf-life stability<sup>1,9-13</sup> when stored under dark, but otherwise ambient, conditions. Thus, typically, the dye in such indicators will, over a period of a few hours/days, change irreversibly to its acidified form, rendering the indicator ineffective. There have been a number of theories as to why this occurs. Degradation of the commonly used phase transfer agent, tetrabutylammonium hydroxide, *via* the Hofmann elimination, has been proposed as a possible cause.<sup>1</sup> The mechanism for this degradation is shown in Fig. 3.2.

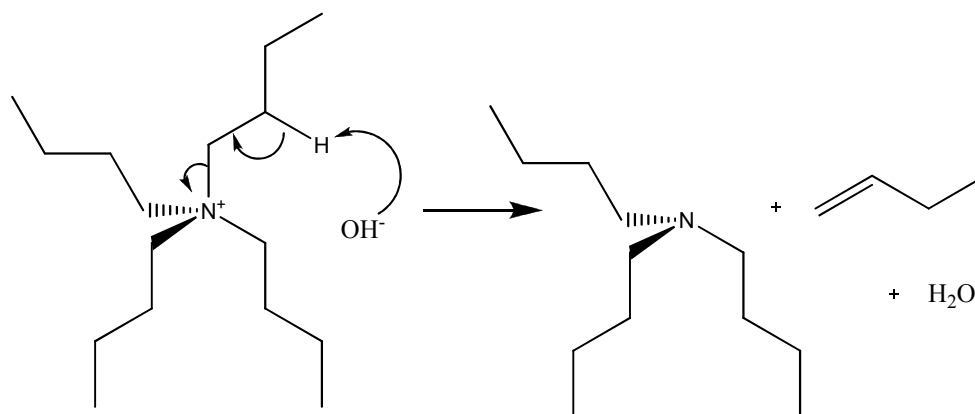


**Fig. 3.2** – Degradation of tetrabutylammonium hydroxide *via* Hoffman elimination.

It was further suggested<sup>1</sup> that this degradation step was enhanced by decreasing amounts of water within the film. However, most recent publications mostly agree that the short shelf-life of such indicators is likely due to acidic pollutant gases in the ambient air. Ambient SO<sub>2</sub> and NO<sub>2</sub>, have been suggested<sup>12,13</sup> to be

the main gases involved in such acidification, which is possible given typical levels of SO<sub>2</sub> and NO<sub>2</sub> in the atmosphere are in the range 150 and 50 μgm<sup>-3</sup>, respectively.<sup>10</sup> As a result, manufacturers of indicators have largely overcome this problem by packaging the indicators in an inert atmosphere,<sup>14,15</sup> but with an obvious added cost to production. Curiously, water-based CO<sub>2</sub> indicators have not been well studied, and we have found recently that such indicators have markedly greater lifetimes, when stored under ambient air conditions, than their solvent-based counterparts. Thus, in this chapter we report the characteristics of a typical example of a water-based CO<sub>2</sub> indicator compared and contrasted with those of a similar solvent-based indicator.

## 3.2 Experimental

### 3.2.1 Ink formulations

A typical water-based *meta*-cresol purple (MCP) ink was prepared by dissolving 0.100 g sodium salt of *m*-cresol purple in an aqueous solution comprising 2.5 ml distilled water and 1 ml of 0.7 M aqueous sodium hydrogen carbonate solution. The solution was stirred for 10-15 minutes, placed in a sonicating bath for 10 minutes, then stirred further until fully dissolved. To 2.0 ml of this solution were added 10 g of 5% w/v aqueous hydroxyethyl cellulose solution (HEC, medium viscosity, 80-125 cP, 2% in H<sub>2</sub>O at 20°C), 1 ml of the 0.7 M aqueous sodium hydrogen carbonate solution and 1.5 g glycerol; this solution was then stirred at room temperature for at least 30 minutes. The resulting ink was blue/purple in colour with a viscosity of approximately 1000 cP, as measured using a cone and plate rheometer (6 cm and 0.5°). The composition of the printed form of the water-based ink can be summarised by the ratio's HEC/MCP/NaHCO<sub>3</sub>/glycerol = 100/11/18/300 pphr, where pphr = parts per hundred resin.

A typical<sup>1</sup> solvent based *m*-cresol purple ink was also prepared at the same time by dissolving 0.036 g of *m*-cresol purple in 3 ml methanol and 0.5 ml 1M

tetrabutylammonium hydroxide in methanol (TBAH). This solution was stirred for 10-15 minutes, placed in the sonicating bath for 10 minutes, then stirred further until all the components were fully dissolved. To 2 ml of this solution were added 10 g of 10% w/v ethyl cellulose in toluene/ethanol (80:20) (EC, 45-55 cP, 5% toluene:ethanol (60:40) at 25°C), 1 ml tributyl phosphate (TBP), 0.5 ml of 1M tetrabutylammonium hydroxide in methanol and a further 0.5 ml methanol. The product was stirred at room temperature for at least 30 minutes. The resulting ink was dark blue with a viscosity of approximately 900 cP. The composition of the printed EC/MCP/TBAH/TBP ink was: 100/2/20/97 pphr.

### 3.2.2 Dried ink films

In preparation of dried colourimetric films of the above inks for CO<sub>2</sub> analysis, 1 – 2 drops of the ink were placed onto a borosilicate microscope slide and spun-coated at 1000 rpm for 15 seconds. Typical film thicknesses for the water- and solvent-based indicator films were ~1.0 and ~0.8 µm, respectively, as measured using scanning electron microscopy.

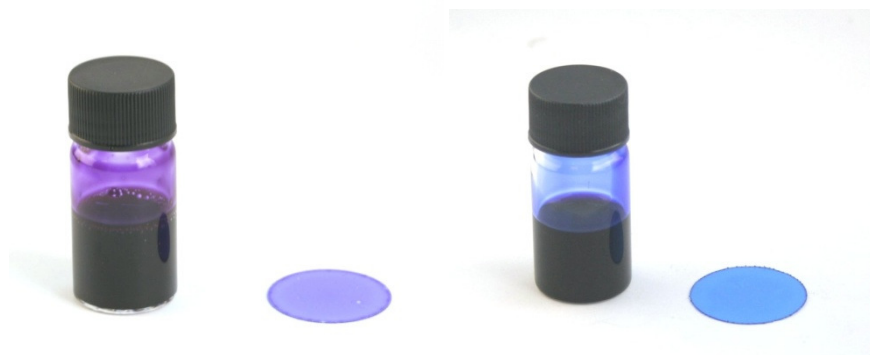


**Fig. 3.3** – Photographs of water- and solvent-based ink and spun films.

### 3.3 Results and Discussion

#### 3.3.1 Dye

The indicators described in this work use the dye *meta*-cresol purple (MCP) and its structure is shown in Fig. 3.4. It has been successfully used in a wide variety of applications in many areas of technology<sup>16-20</sup> e.g. determination of acidity of wine. Its versatility is most likely due to its pK<sub>a</sub> at 8.3<sup>21</sup>, which allows the detection of CO<sub>2</sub> for a range of commercially useful levels. It is a member of the sulfonphthalein dye family and so has the common quinoidal structure. It can be utilised in aqueous media, by using the sodium salt of the dye, which is more soluble in water than the neutral form. It can be synthesised by condensing one mole of *o*-sulfobenzoic acid anhydride with two moles of *m*-cresol<sup>22</sup>, but can be readily purchased from most major chemical suppliers.

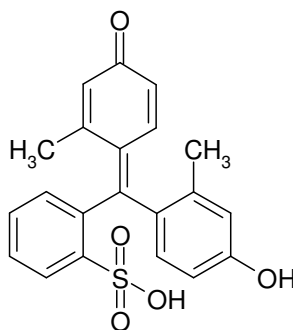
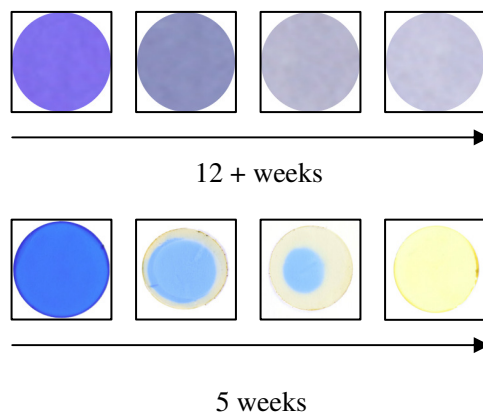


Fig. 3.4 – Structure of *m*-cresol purple.

#### 3.3.2 Longevity

As noted earlier, the well-known, limited shelf-life of most solvent-based CO<sub>2</sub> colourimetric films,<sup>9,10</sup> when stored under ambient dark conditions, is an obvious limitation to their application. Thus, longevity experiments were carried out on both the solvent- and water-based CO<sub>2</sub> indicators, whereby their absorbances were measured as a function of time over a period of 12 weeks when stored in the dark, but under otherwise ambient lab conditions. The results showed that

whereas the water-based indicator fades slowly and uniformly over time (but is still blue and working after 35 weeks), the solvent-based indicator fades much more quickly and changes irreversibly to the acidified yellow form of the dye, rendering it ineffective. As illustrated in Fig. 3.5, the solvent-based films have a characteristic ring pattern during this blue to yellow colour change ('yellowing') process.



**Fig. 3.5** – Comparison of film deterioration of water-based (top) and solvent-based indicators (bottom) when stored in the dark under ambient conditions.

As noted earlier, it has been suggested that this 'yellowing' is due to the irreversible acidification of the dye by interfering acidic gases found in air (e.g. SO<sub>2</sub> and NO<sub>2</sub>).<sup>12</sup> It is not clear why the yellowing/acidification occurs from the edge first, spreading inwards. However, additional work was carried out where the absorption spectra of a standard film was recorded at different points across its radius. The results illustrated in Fig. 3.6 show that the film is at least 20% thinner at the film edge compared to the centre and presumably, the thinner the film the faster the acidification process.

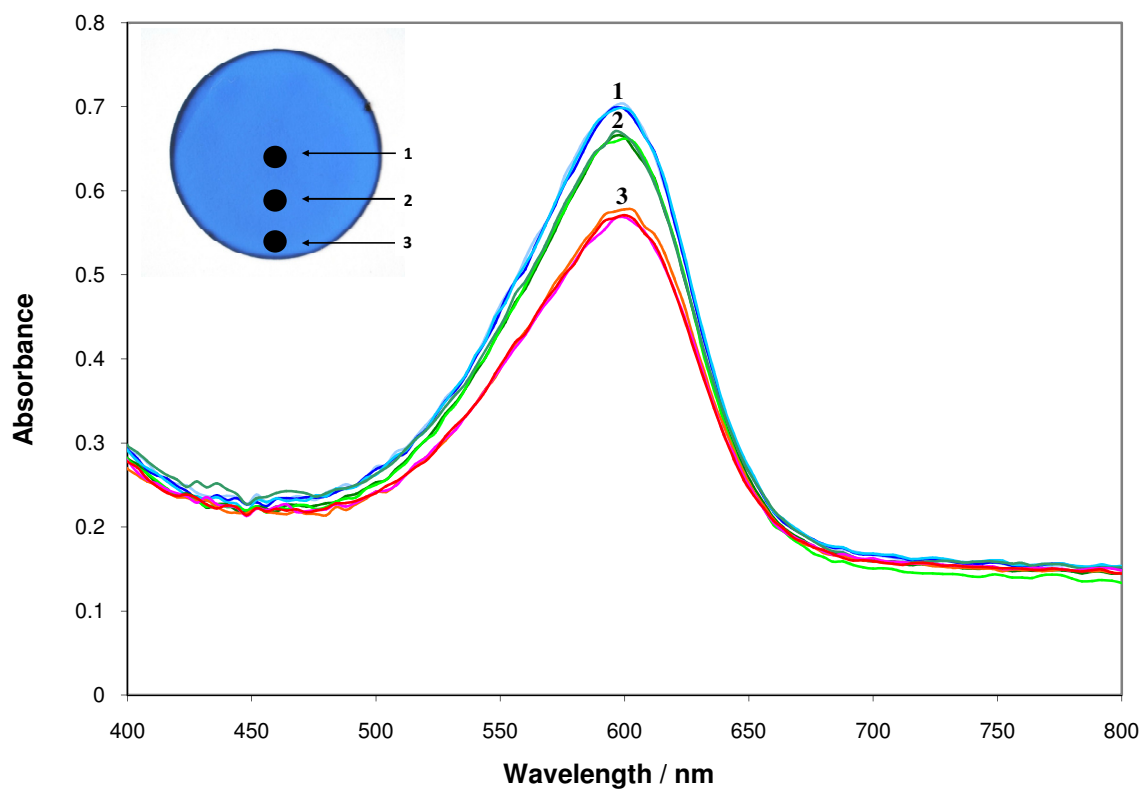


**Fig. 3.6** – Absorption spectra (recorded in triplicate) taken at various points across the radius of the film.

Interestingly, for reasons which remain unclear, the process of film fading appears very different for the water based ink. Thus, in contrast to the solvent-based CO<sub>2</sub> indicator, the water-based indicator, in its faded form, still gives a good, quantifiable colourimetric response to carbon dioxide, even after 9 months of storage.

The loss in colour of either indicator can be moderated if the indicator is stored under a modified atmosphere, as is usually the case for commercial forms of the CO<sub>2</sub> colourimetric indicator.<sup>23</sup> So, as part of this work, the effects of storage conditions on the colours of both solvent- and water-based indicators were further investigated and the results are given in Table 3.1.



**Table 3.1** – Summary table of dark storage conditions over 35 weeks for water- and solvent-based CO<sub>2</sub> indicators.

Storage Conditions	Water-based	Solvent-based
open atmosphere	Fades, but indicator performs well even after 35 weeks	Irreversible deterioration (yellowing) starts within one week – film permanently yellow and non-functioning within 6 weeks
sealed under air	Little fading, indicator works well	Irreversible deteriorating (yellowing) starts within 3 weeks – film permanently yellow and non-functioning within 7 weeks
sealed under vacuum	“	Little fading, indicator works well
open atmosphere in fridge	“	Starting to deteriorate after 20 weeks storage
sealed over NaOH pellets	“	Starts to deteriorate after 10 weeks
sealed under CO <sub>2</sub>	“	Little fading, indicator works well
sealed under Ar	“	“

From this work, it appears that by choosing suitable storage conditions, whereby most notably the permeation of permanent, film-acidifying species such as NO<sub>2</sub> and SO<sub>2</sub> is minimised, the longevity of the solvent- and water-based CO<sub>2</sub> indicators can be increased markedly, although the solvent-based film still appears much less stable than its water-based counterpart. From the results in Table 3.1, the water-based indicator alone appears to possess a significant longevity under ambient conditions and although additional storage conditions helps preserve the indicator, it is not essential.

### 3.3.3 CO<sub>2</sub> sensitivity of water-based indicator

Photographs of a standard water-based CO<sub>2</sub> ink were recorded in the absence and increasing presence of CO<sub>2</sub> and the results are illustrated below in Fig. 3.7.

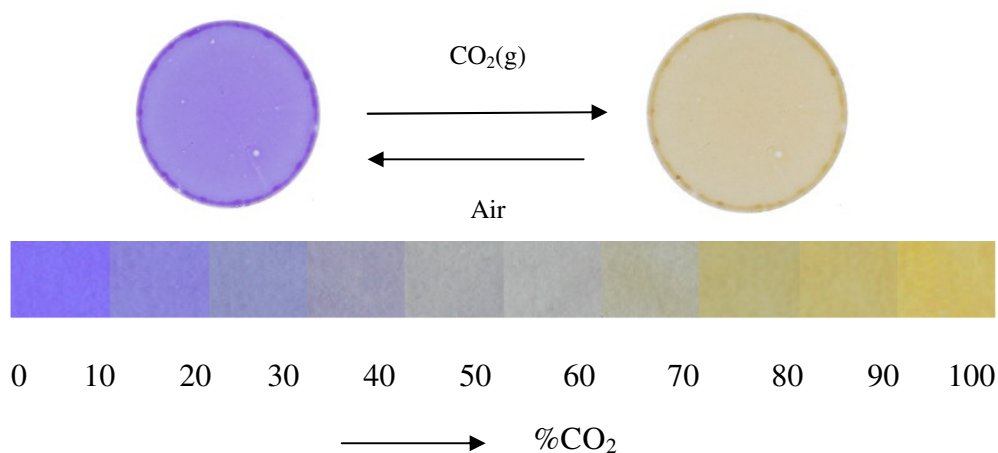


**Fig. 3.7** – Photographs of a standard  $\text{CO}_2$  indicator and progressive colour response chart to  $\text{CO}_2$ .

The results of Fig. 3.7 show that the initial blue indicator turns increasingly yellow when exposed to a gas stream containing an increasing partial pressure of  $\text{CO}_2$ . The process is reversible and so can be repeated many times with no sign of any deterioration in indicator response.

To further demonstrate the effect of  $\text{CO}_2$  on the indicator, a dry ice pellet was inserted into a small vial of water at room temperature, as illustrated by the photographs in Fig. 3.8. The presence of the condensed water vapour shown in the photographs is indicative of the presence of the  $\text{CO}_2$ . Hence, as the  $\text{CO}_2$  gas diffuses over the indicator, the water-based indicator changes from purple to yellow.

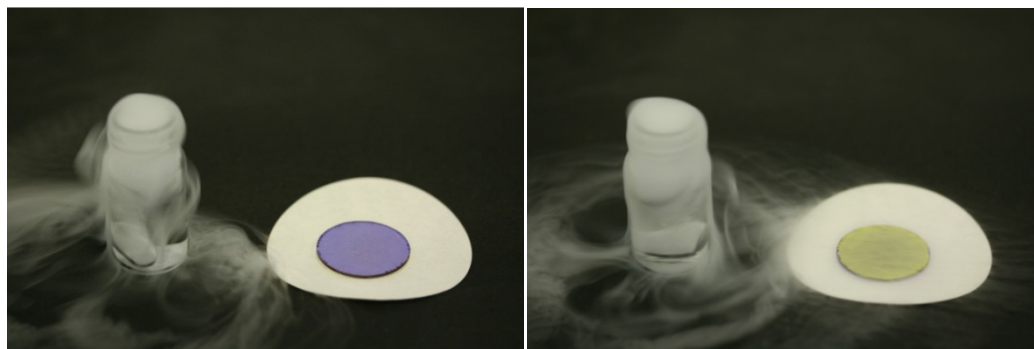


**Fig. 3.8** – Photographs of the water-based CO<sub>2</sub>-indicator beside a sample of water where a pellet of dry ice has been inserted, rapidly evolving CO<sub>2</sub> gas.

In this work, the absorbance spectrum of a standard CO<sub>2</sub> indicator film was also monitored by UV/vis absorption spectroscopy as a function of ambient %CO<sub>2</sub> (varied using a gas blender) and the results are illustrated in Fig. 3.9. A clear isosbestic point is observed (at  $\lambda = 490$  nm), indicating the conversion of the dye from its purple, deprotonated form, to its yellow protonated form by ambient CO<sub>2</sub> involves no other dye species, i.e. it is well described by reaction (3.5) as an equilibrium reaction between D<sup>-</sup> and DH.

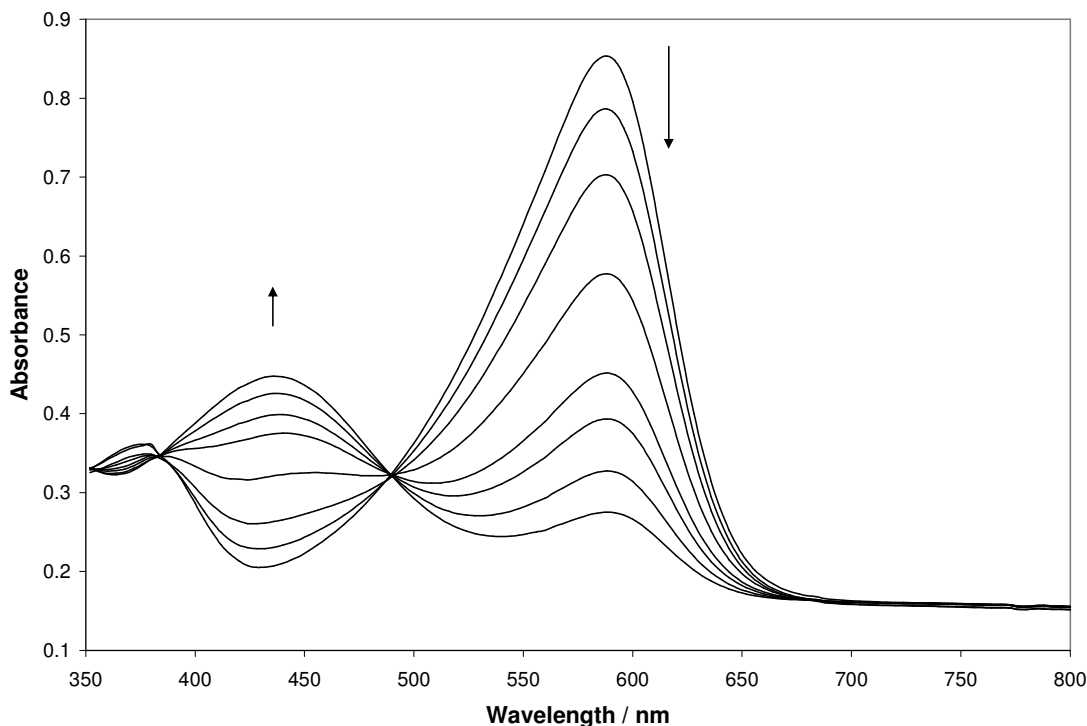


**Fig. 3.9** – UV/visible absorption spectra of the standard film as a function of %CO<sub>2</sub> at 21°C, for %CO<sub>2</sub> (from top to bottom) of 0, 2, 5, 10, 20, 30, 60, 100%, respectively.

It is usual<sup>1</sup> and useful to define the parameter,  $R$ , based on experimentally measurable absorbance values at  $\lambda_{\max}$  (due to  $D^-$  alone) at different %CO<sub>2</sub>, as follows:

$$R = (Abs_0 - Abs) / (Abs - Abs_\infty) = [HD] / [D^-] \quad (3.6)$$

Where  $[HD]$  and  $[D^-]$  are the concentration of the protonated and deprotonated forms of the dye, respectively.  $Abs_0$  is the value of absorbance of the dye at  $\lambda_{\max}$  ( $D^-$ ) when %CO<sub>2</sub> = 0 (i.e. when all the dye is in its deprotonated form) and  $Abs_\infty$  is the absorbance of the film when all the dye has been converted into DH, i.e. when %CO<sub>2</sub> =  $\infty$ . Since, with the dye concerned, HD does not absorb at  $\lambda_{\max}$  ( $D^-$ ), it is convenient to take  $Abs_\infty$  as that of the substrate (microscope slide) alone (i.e. no indicator film) at  $\lambda_{\max}$  ( $D^-$ ). From equation (3.7) the parameter,  $R$ , is a measure of the transformation of the dye from the deprotonated to protonated forms and is directly proportional to  $[HD]/[D^-]$ .<sup>1</sup> Based on reactions (3.1) – (3.5), for such indicators it can be shown<sup>23</sup> that:

$$R = [\text{HD}] / [\text{D}^-] = \alpha \cdot \% \text{CO}_2 \quad (3.7)$$

where  $\alpha$  is a proportionality constant, which is in turn inversely dependent upon the background base concentration, i.e.  $\alpha$  vs.  $1 / [\text{base}]$ , used in the film.<sup>24</sup> The absorbance (Abs) vs.  $\% \text{CO}_2$  plot arising from the data in Fig. 3.9 is illustrated in Fig. 3.10, along with the  $R$  vs.  $\% \text{CO}_2$  plot, calculated using this data and equation (3.6). The linear relationship between  $R$  and  $\% \text{CO}_2$  is in accordance with equation (3.7) and reveals an  $\alpha$  value of  $0.052 \pm 0.001 \% \text{CO}_2^{-1}$  at 21°C.

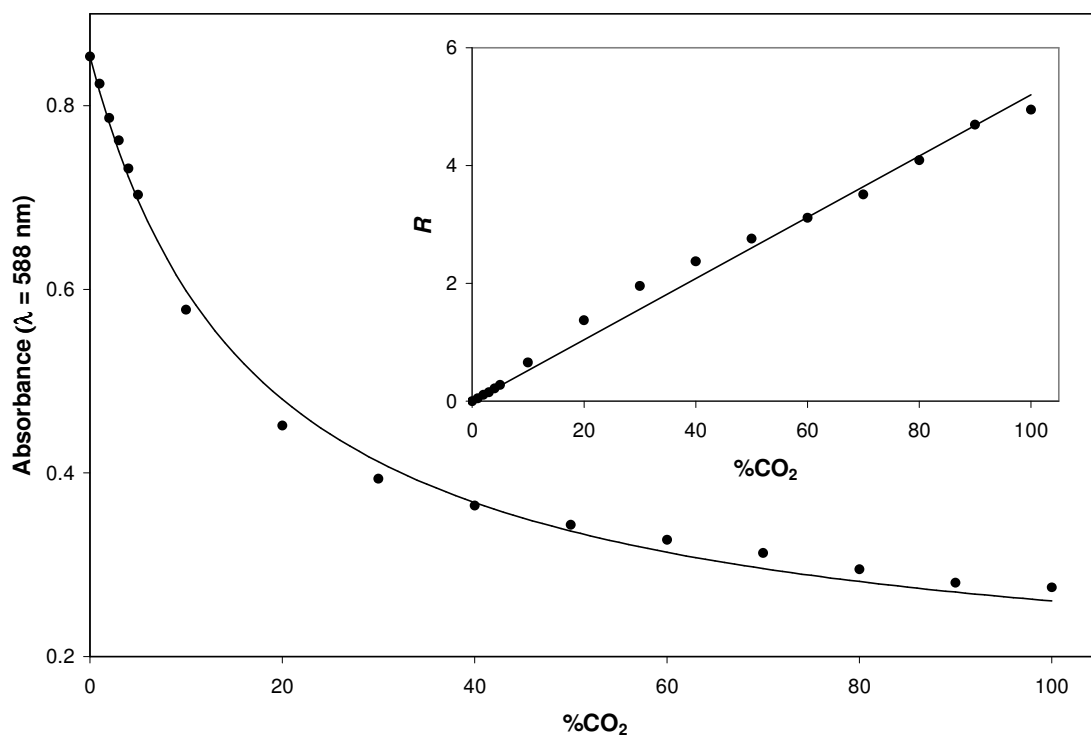


**Fig. 3.10** – Plots of absorbance of film at 588 nm vs.  $\% \text{CO}_2$  at 21°C (insert:  $R$  vs.  $\% \text{CO}_2$ ). Data from Fig. 3.9. The solid lines are best fits to the data, assuming an  $\alpha$  value of  $0.052 \pm 0.001 \% \text{CO}_2^{-1}$ .

In comparison, a typical solvent-based CO<sub>2</sub> indicator (using the same pH dye) revealed an  $\alpha$  value of  $0.33 \pm 0.01 \% \text{CO}_2^{-1}$  i.e. approximately 6 times more sensitive than the water based indicator, possibly due to the much greater solubility of CO<sub>2</sub> in hydrophobic medium of the solvent-based polymer.<sup>25</sup>

### 3.3.4 Indicator response and recovery times

In addition to indicator sensitivity (i.e. the value of  $\alpha$ ), another key characterisation parameter of any indicator is its response and recovery times. In one set of experiments the typical Abs (D<sup>-</sup>) response and recovery curves for a standard water-based ink were recorded by exposing it to an alternating gas stream of air and 100% CO<sub>2</sub> and the results are illustrated in Fig. 3.11, from which 90%,  $\tau_{90}$ , response and recovery times of 30 and 120 s, respectively, were determined.

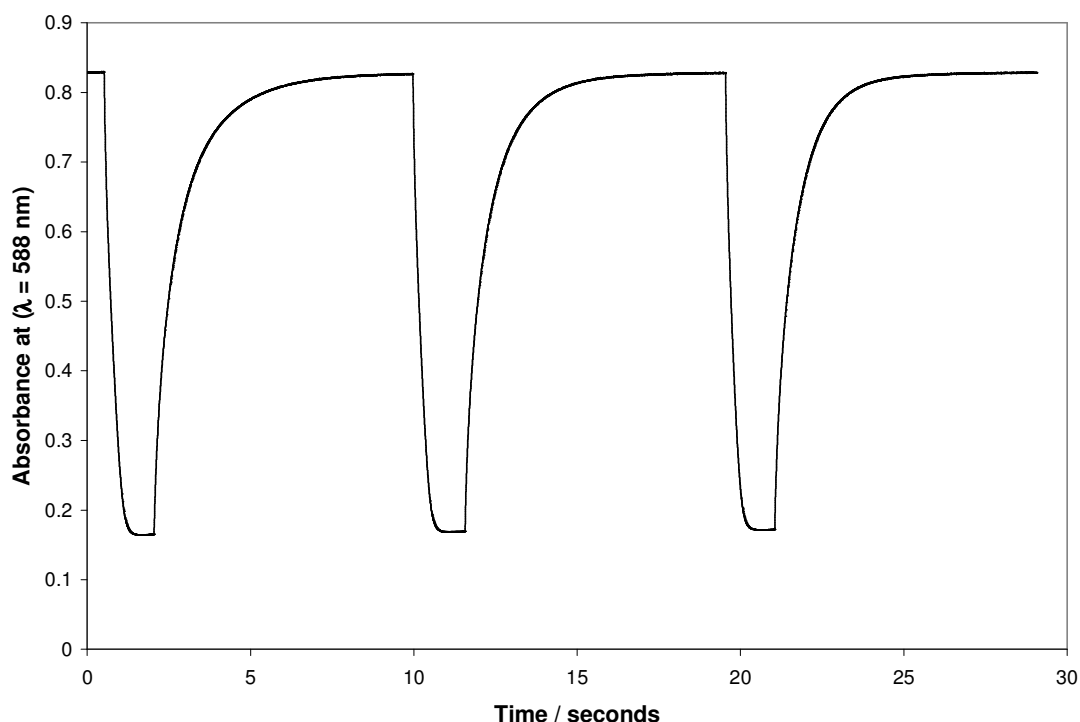


**Fig. 3.11** – Absorbance versus time plot for the typical water-based film, when exposed to alternating gas supply of air and 100% CO<sub>2</sub> (g) at 21°C.

In comparison, the  $\tau_{90}$  response and recovery times of a solvent-based ink were found to be < 1 and 3 s respectively. These much shorter response and recovery times may be due to a much greater plasticizer action of tributyl phosphate compared to that of glycerol.

## 3.3.5 Effect of base concentration

The sodium hydrogen carbonate concentration in a typical water-based ink was varied over the range 0.1 M to saturated (*ca.* 1.2 M) to create a series of water-based indicator films. The observed variation in absorbance versus %CO<sub>2</sub> recorded for each of these films is illustrated in Fig. 3.12. As expected, from other work on solvent-based CO<sub>2</sub> indicators<sup>13</sup> and predicted from reactions (3.1)-(3.5),<sup>24</sup> the sensitivity ( $\alpha$ ) of a typical water-based indicator is inversely proportional to [base] as illustrated by the plot of the data in this form shown as the insert diagram in Fig. 3.12.

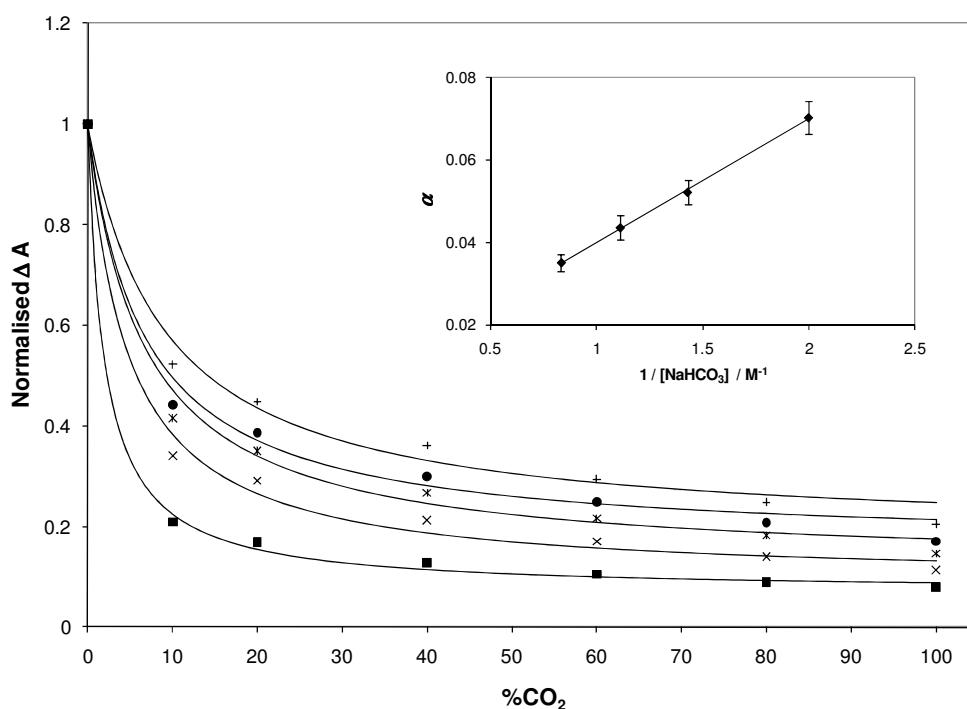


**Fig. 3.12** – Change in normalised absorbance ( $= \Delta\text{Abs} / \Delta\text{Abs}_0$ ) versus %CO<sub>2</sub> at 21°C, as a function of varying sodium hydrogen carbonate concentration (from bottom to top: 0.1, 0.5, 0.7, 0.9 M and saturated respectively). The insert diagram is a plot of  $\alpha$  (from the data in the main diagram) versus  $1 / [\text{NaHCO}_3]$ .

### 3.3.6 Effect of plasticizer

The use of plasticizers in solvent-based CO<sub>2</sub> film indicators is common,<sup>1,4,10,11</sup> and highly desirable as a method of decreasing the response and recovery times exhibited by the indicator films. They work by increasing the rate of diffusion of the CO<sub>2</sub> throughout the film. Glycerol is a colourless, odourless, viscous liquid which has wide applications in many pharmaceutical applications. Thus, increasing the level of plasticizer (i.e. glycerol) in the water-based CO<sub>2</sub> indicator should decrease the response and recovery times of the indicator. This feature was confirmed by the results illustrated in Fig. 3.13. The use of glycerol as a plasticizer is particularly favoured due to its hygroscopic properties. This ensures good hydration of the film, which is essential for the indicator to work effectively.

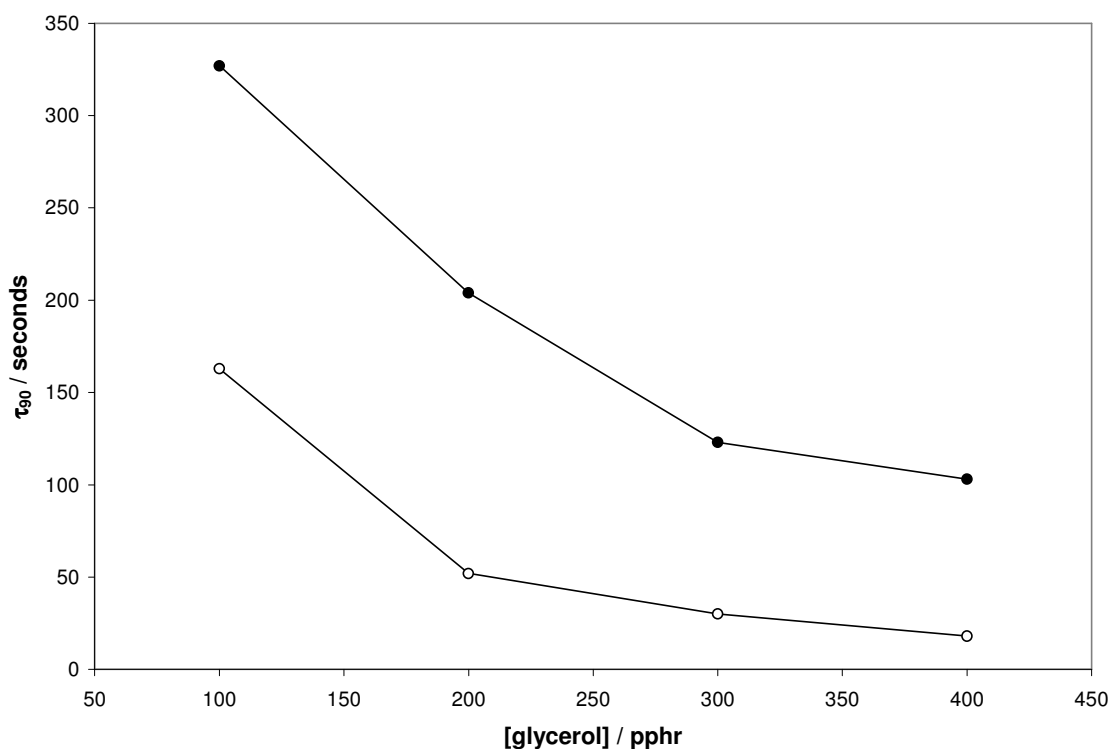


**Fig. 3.13** - Relationship between response/recovery time and glycerol concentration (top:  $\tau_{90}$  recovery and bottom:  $\tau_{90}$  response).

Solvent-based indicators are known to behave similarly using tributyl phosphate



as the plasticizer.<sup>11</sup>

### 3.3.7 Effect of humidity

Most CO<sub>2</sub> indicators exhibit some sensitivity towards relative humidity.<sup>12</sup> A brief study of a typical water-based indicator exposed to 0 and 40%CO<sub>2</sub> at different relative humidity (RH) values, spanning the range 25 up to 100%RH at 20°C revealed a clear increase in  $\alpha$  (i.e. sensitivity towards CO<sub>2</sub>) with increasing %RH, as illustrated in Fig. 3.14. Additional work showed this effect on  $\alpha$ , upon which increasing the relative humidity was completely reversible. In contrast, solvent-based *m*-cresol purple indicators exhibited an opposite trend in sensitivity with increasing humidity, as illustrated by the results in Fig. 3.14.

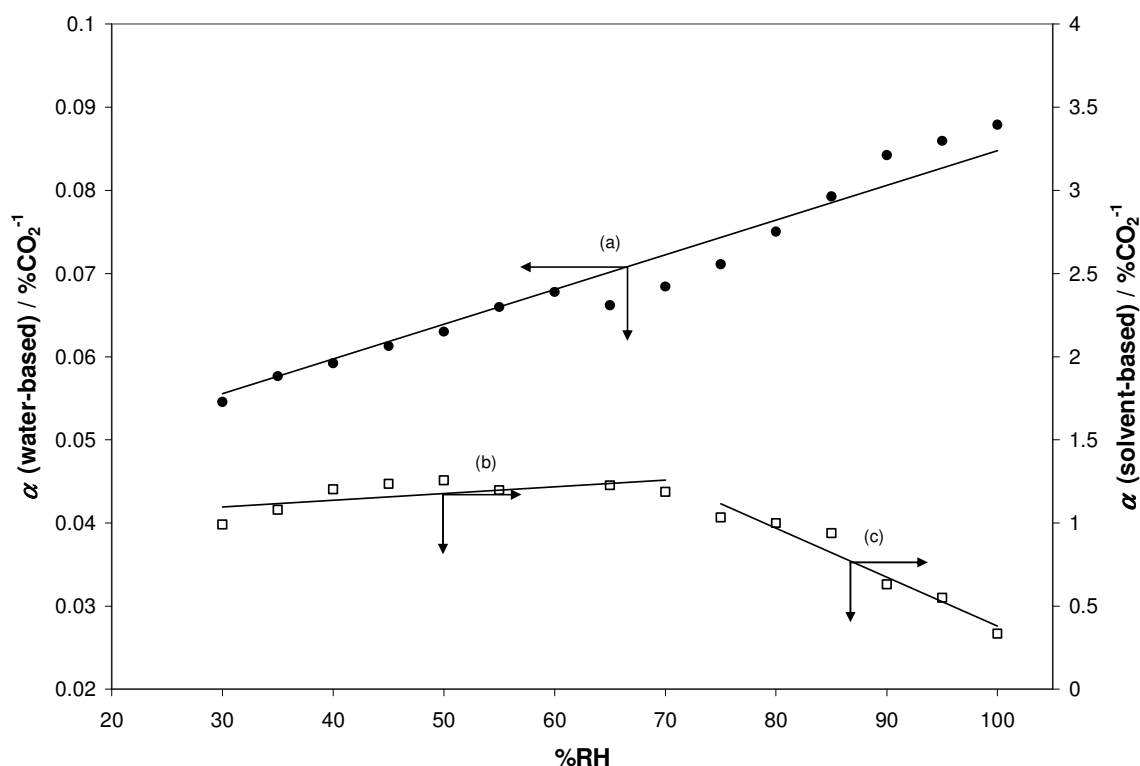


**Fig. 3.14** – Effect of humidity on sensitivity ( $\alpha$ ) for a water-based indicator (●) and solvent-based indicator (□) (21°C). The sensitivity of the water-based ink is directly proportional to %RH (a), whereas that of the solvent-based ink is mostly independent (b) or, at high %RH, negatively affected (c).

Similar findings to these have been reported by Schröder *et al.*,<sup>12</sup> studying

solvent-based CO<sub>2</sub> indicators with either quaternary ammonium or phosphazene bases. That the solvent-based indicator showed little or no sensitivity towards humidity over a wide range (20 – 70% for the indicator in Fig. 3.14) is suggested,<sup>12</sup> due to the presence of intrinsic molecules of water associated with the dye-base ion pair, i.e. D<sup>-</sup>Q<sup>+</sup>.xH<sub>2</sub>O, that enable reaction (3.5) to take place. In contrast, the same workers found a phosphazene indicator became increasingly CO<sub>2</sub>-sensitive with increasing RH, due to the need for water to promote reaction (3.5), and the lack of any bound water of hydration in the indicator. Thus, the water-based CO<sub>2</sub> indicator exhibits a similar humidity response as that noted<sup>12</sup> for a phosphazene-based CO<sub>2</sub> indicator, presumably due to the lack of bound water of hydration.

### 3.3.8 Effect of temperature

A series of experiments using a water-based CO<sub>2</sub> indicator were carried out in which the absorbance due to the deprotonated dye was monitored as a function of %CO<sub>2</sub> for indicators at different temperatures. The data was used to create *R* vs. %CO<sub>2</sub> plots from which different  $\alpha$  values as a function of temperature were extracted. A Van't Hoff plot of the data, as shown in Fig. 3.15, revealed a good straight line for which values of -27 kJ mol<sup>-1</sup> and -113 Jmol<sup>-1</sup>K<sup>-1</sup> were calculated for  $\Delta H$  and  $\Delta S$  respectively for the overall process, i.e.



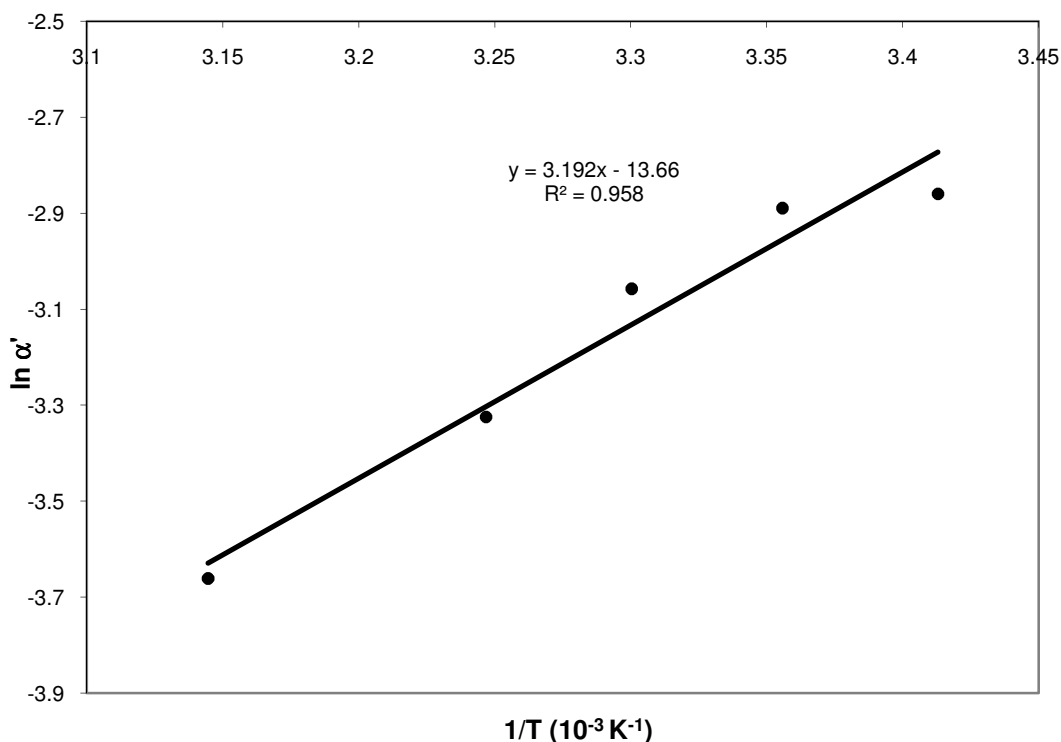


**Fig. 3.15** – Van't Hoff plot of the temperature data from which  $\Delta H$  and  $\Delta S$  was calculated, knowing  $m = -\Delta H/R$  and  $c = -\Delta S/R$ .

Typical solvent-based CO<sub>2</sub> indicators, have similar values of  $-(28 \text{ to } 80) \text{ kJmol}^{-1}$  and  $-(211 \text{ to } 80) \text{ Jmol}^{-1} \text{ K}^{-1}$  for  $\Delta H$  and  $\Delta S$  respectively.<sup>1,12</sup> Thus, water based indicators, like solvent-based ones, exhibit a strong temperature dependence, becoming less sensitive with increasing temperature.

### 3.4 Applications

Most promising, in terms of possible applications, the indicator can be applied readily (e.g. *via* felt-tipped pens) to a variety of different materials, including ceramics, paper and tin foil as illustrated in Fig. 3.16. A typical, water-based CO<sub>2</sub> sensing ink was incorporated into a refillable felt-tipped pen and prepared using a thinner polymer solution and increased dye, base and plasticizer content. This felt-tipped pen ink formulation is summarised as follows HEC/MCP/NaHCO<sub>3</sub>/glycerol = 100/43/55/750 pphr.

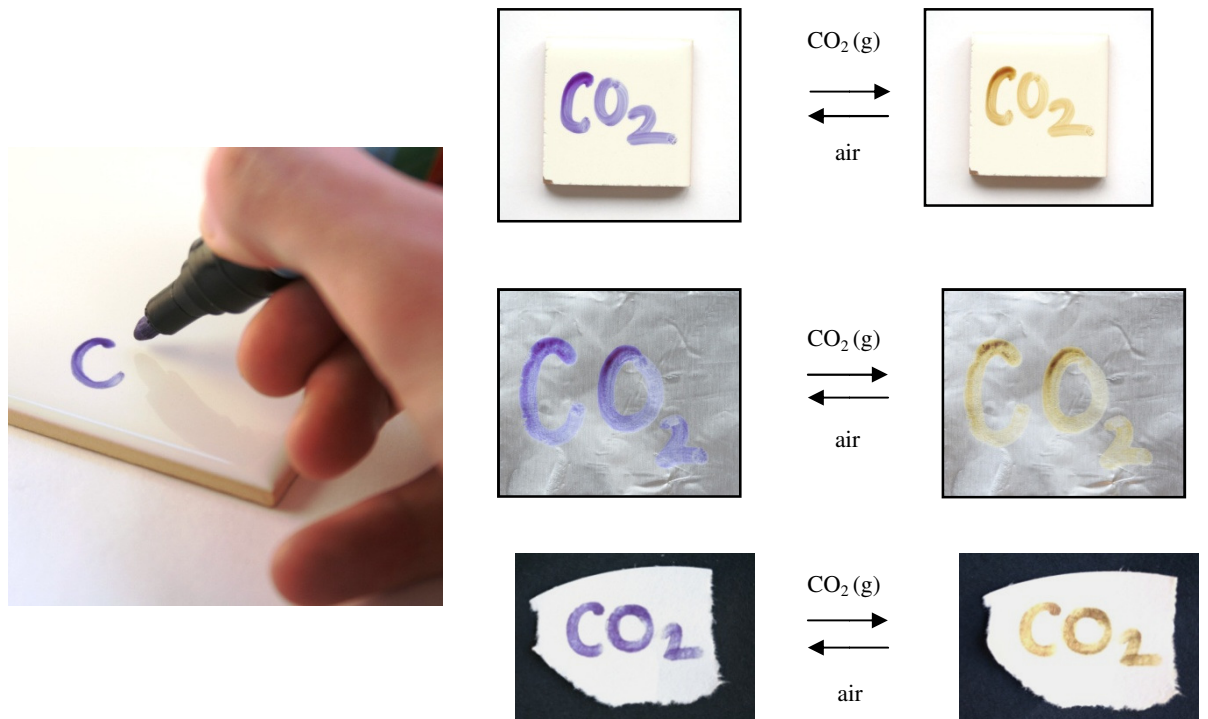


**Fig. 3.16** – Ink applied by pen onto a variety a substrates (top right: ceramic tile, middle right: metal foil, bottom right: cellulose based filter paper) all showing a distinct colour change when exposed to CO<sub>2</sub>(g).

The ink when stored in a sealed container (such as a bottle or pen) under otherwise ambient conditions is extremely stable and showed no deterioration even after one year. It might find applications in modified atmosphere packaging (MAP), with a suitable coating to prevent dye leaching and direct food contact. Fig. 3.17 illustrates the use of the indicator in MAP applications. In this experiment, the indicator was packaged along with pork meat in a high CO<sub>2</sub> concentration gas atmosphere (photo **A**). Under these conditions, the indicator was yellow as expected. Upon opening the package, the CO<sub>2</sub> concentration decreased significantly, causing the indicator to change colour from yellow to purple (photo **B**).

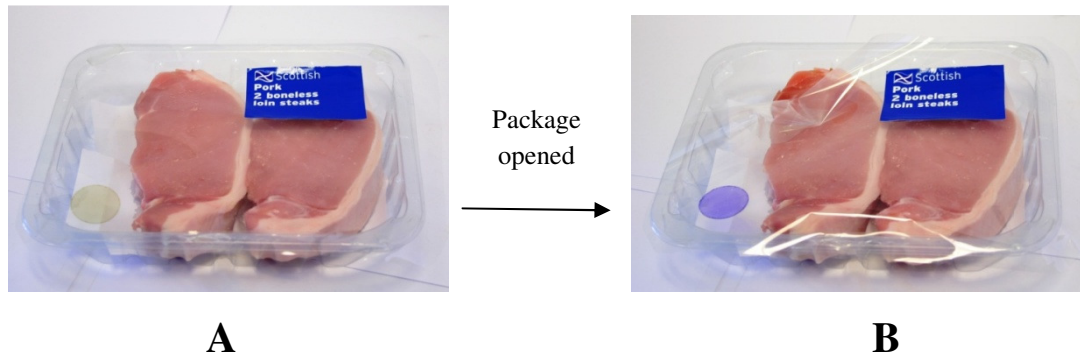


**Fig. 3.17** – Illustration of the water-based CO<sub>2</sub> indicator at room temperature being used as a MAP packaging indicator. **A** – pork packaged under a high CO<sub>2</sub> atmosphere, indicator is yellow under these conditions. **B** – opened package, hence CO<sub>2</sub> concentration significantly reduced, hence indicator has changed colour to purple.

Although the humidity and temperature sensitivity of the ink are a drawback, fortunately, in MAP often the food package is maintained at a fixed (usually chilled, 4°C) temperature and (for meat and fish) high and largely unchanging %RH. Thus, under such conditions a water-based CO<sub>2</sub> indicator may find applications in MAP, if not as a quantitative indicator of ambient CO<sub>2</sub>, at least as a semi-quantitative CO<sub>2</sub> indicator of the package integrity.

### 3.5 Conclusions

The water-based CO<sub>2</sub> indicator ink is less sensitive towards CO<sub>2</sub> than a typical solvent-based counterpart, but much more stable in terms of shelf life. The water-based CO<sub>2</sub> indicator is still quick in its response and recovery ( $\leq 2$  minutes), but rendered less sensitive by increasing base concentration. Increasing the amount of plasticizer improves the indicator's response and recovery times. As is common with most CO<sub>2</sub> indicators, the water-based indicator's sensitivity toward CO<sub>2</sub> decreases with increasing temperature. The response of a water-based CO<sub>2</sub> indicator is directly related to relative humidity, roughly increasing by 80% as the RH is increased from 20% to 100%. In contrast, a solvent-based CO<sub>2</sub> indicator is largely humidity insensitive over the RH range 20 – 70%, which is an obvious

advantage. The water-based inks have much improved operational lifetimes compared to the more, well-studied solvent-based indicators<sup>1,2</sup> and can be applied to a variety of different surfaces, using a simple applicator, such as felt-tipped pen.

### 3.6 References

1. A. Mills, Q. Chang and N. McMurray, *Anal. Chem.*, 1992, **64**, 1383-1389.
2. R. Lines, *Int. Pat.*, 075498, 2007.
3. O. Oter, K. Ertekin and S. Derinkuyu, *Talanta*, 2008, **76**, 557-563.
4. M. J.-P. Leiner, J. Tusa and I. Klimant, *EP*, 1 965 198, 2008.
5. G. C. Upreti, Y. Wang and A. S. H. Kueh, *Int. Pat.*, 079024, 2008.
6. R. Ostrowski and M. P. Debreczeny, *Int. Pat.*, 039424, 2008.
7. Y. Amao and N. Nakamura, *Sens. Actuators B*, 2004, **100**, 347-351.
8. S. M. Borisov, M. C. Waldhier, I. Klimant and O. Wolfbeis, *Chem. Mater.*, 2007, **19**, 6187-6194.
9. J.F.Fernandez-Sanchez, R. Cannas, S. Spichiger, R. Steiger and U. E. Spichiger-Keller, *Sens. Actuators B*, 2007, **128**, 145-153.
10. H. N. McMurray, *J. Mater. Chem.*, 1992, **2**, 401-406.
11. A. Mills and L. Monaf, *Analyst*, 1996, **121**, 535-540.
12. C. R. Schroder and I. Klimant, *Sens. Actuators B*, 2005, **107**, 572-579.
13. B. H. Weigl and O. S. Wolfbeis, *Sens. Actuators B*, 1995, **28**, 151-156.
14. F. Colin, T. J. N. Carter and J. D. Wright, *Sens. Actuators B*, 2003, **90**, 216-221.
15. C. G. Fehder, *US Pat.*, 5166075, 1992.
16. E. N. Gaiao, R. S. Honorato, S. R. B. Santos and M. C. U. Araujo, *Analyst*, 1999, **124**, 1727-1730.
17. D. R. Walt, G. Gabor and C. Goyet, *Anal. Chim. Acta*, 1993, **274**, 47-52.
18. L. M. Mosley, S. L. G. Husheer and K. A. Hunter, *Marine Chemistry*, 2004, **91**, 175-186.
19. S. Kaltin, L. G. Anderson, K. Olsson, A. Fransson and M. Chierici, *J. Mar. Sys.*, 2002, **38**, 31-45.

20. M. Chierici, A. Fransson and L. G. Anderson, *Mar. Chem.*, 1999, **65**, 281-290.
21. M. Qian, J. N. Earnhardt, N. R. Wadhwa, C. Tu, P. J. Laipis and D. N. Silverman, *Biochim. Biophys. Acta*, 1999, **1434**, 1-5.
22. F. J. Green, *The Sigma-Aldrich handbook of stains, dyes, and indicators*, 1990.
23. A. Mills, A. Lepre and L. Wild, *Sens. Actuators B*, 1997, **38-39**, 419-425.
24. A. Mills and Q. Chang, *Anal. Chim. Acta*, 1994, **285**, 113-123.
25. J. Brandrup, E. H. Immergut and E. A. Grulke, *Polymer handbook*, 1999.





Chapter 3 it was found that water-based CO<sub>2</sub> inks, utilising the same dye, exhibit much lower CO<sub>2</sub> sensitivities than solvent-based inks; the water-based inks are also much more stable towards irreversible acidification under ambient conditions. This feature opens up the possibility of creating the first example of a stable, high pressure ( $\geq 1$  bar) CO<sub>2</sub> colourimetric indicator.

These indicators could have a significant impact on areas associated with the measurement of high levels of carbon dioxide. It is envisaged that the carbonated drinks industry is the most promising area of application for such indicators, but applications can easily be foreseen in biotechnology (especially fermentation), fire extinguishers and aerosols.

## 4.2 Experimental

### 4.2.1 Ink formulations

All chemicals were purchased from Sigma Aldrich, unless specified, and in the highest purity available. The water used to make all aqueous solutions was double distilled and deionised. The gases were obtained from BOC gases and of high purity. All films were produced using a spin coating technique, with a Spin Coater Model 4000-1 (Electro-Micro Systems).

A typical water-based, high  $p\text{CO}_2$  ink was prepared by dissolving 0.400 g of phenol red (sodium salt, PR) in 10 cm<sup>3</sup> of distilled water and adding 4 cm<sup>3</sup> of 1.0 M sodium hydroxide (aq). The solution was stirred for 10 - 15 minutes and then 4 cm<sup>3</sup> of this solution added to 6.00 g of 15% w/v polyvinyl alcohol in water (PVA, MW 146,000-186,000), along with 0.600 g glycerol. The resulting solution was stirred at room temperature for at least 30 minutes. The composition of the PVA/PR/glycerol/NaOH ink can be summarised as 100/12.7/66.7/5.6 pphr, where pphr = parts per hundred resin. In order to characterise the dried form of the ink, the ink (bright pink) was spun-coated onto borosilicate glass discs using a spin coater operated at 2000 rpm for 10 seconds, forming a dry  $\sim 2$   $\mu\text{m}$  thick film.

Another formulation of the ink was prepared by adding 0.400 g of phenol red in 10 cm<sup>3</sup> of ethanol and 1.5 cm<sup>3</sup> of 1.0 M sodium hydroxide in ethanol solution. The solution was stirred for 10-15 minutes. 4 cm<sup>3</sup> of this solution was added to 6.00 g of a 50% w/v polyvinyl butyral in ethanol (PVB, Acros organics, MW = 40,000 – 70,000), along with 0.600 g of glycerol. The resulting solution was stirred at room temperature for at least 30 minutes. The resulting ink can be summarised in pphr as PVB/PR/glycerol/NaOH – 100/4.7/20/0.6 pphr. The ink (bright pink) was spin coated onto borosilicate glass discs using a spin at 2000 rpm for 10 seconds, forming a ~2 µm thick film.

#### 4.2.2 High pressure gas cell set-up

To characterise the ink films under high gas pressures *via* UV/vis spectrophotometry, a specially designed high pressure sample cell was used. A schematic of the experimental set-up and photographs of the gas cell are shown in Fig 4.1. The high pressure gas cell is made from stainless steel, which encases two thick borosilicate glass windows, which are bolted securely by eight bolts. The inks were spin coated onto the glass discs which were then fitted into the cell. Alternatively, when analysing thin polymer films, the samples were laid on top the glass discs and secured into the cell. The gas cell has the ability to be pressurised to different pressures of CO<sub>2</sub> (g) and placed inside a spectrophotometer so that the colour changes can be monitored *via* UV/vis spectroscopy.

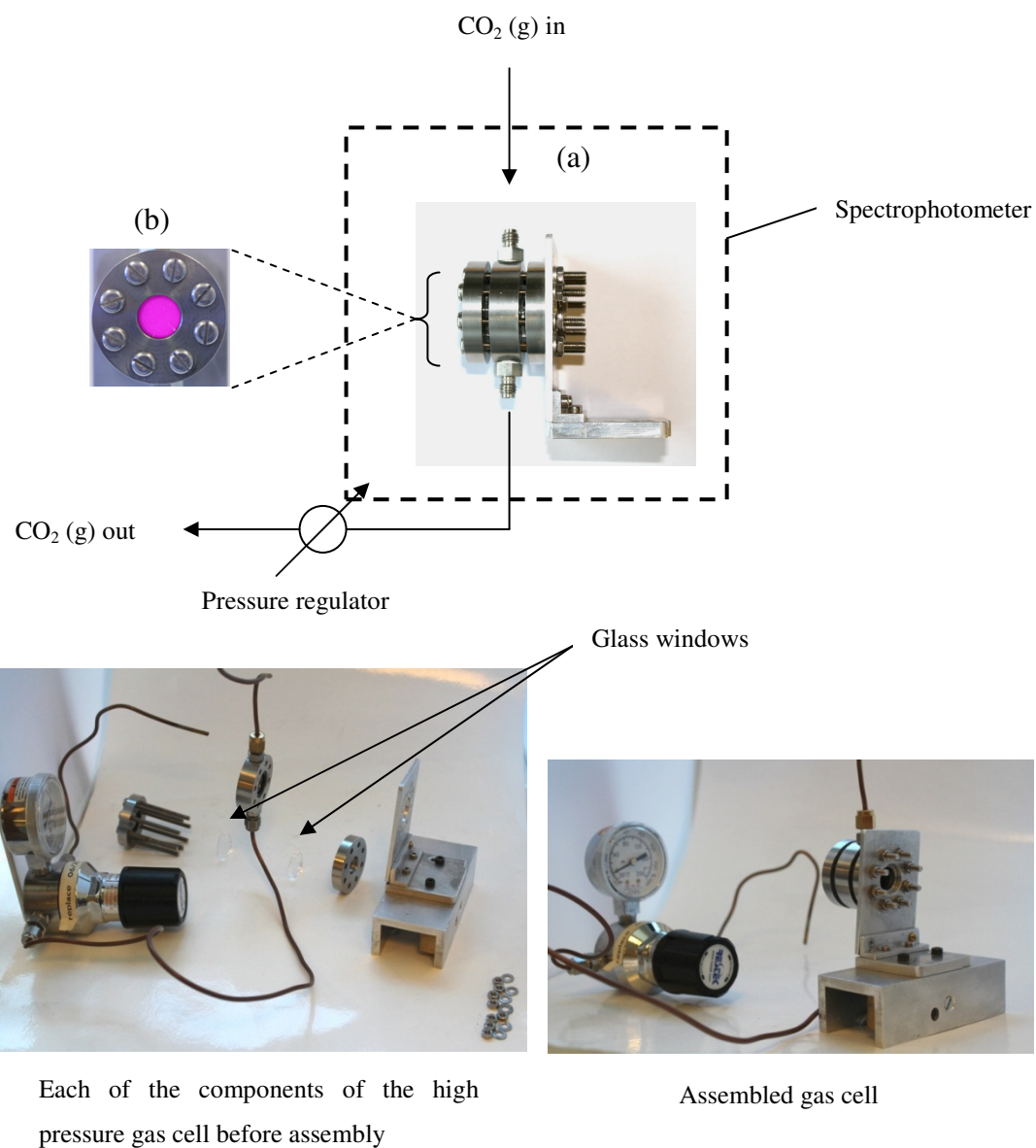


**Fig. 4.1** – Top: Schematic of experimental set-up, where (a) is high pressure gas cell sample holder inside spectrophotometer and (b) is the front of the cell, showing indicator in line with beam, bottom: photographs of the high pressure gas cell.

### 4.2.3 Modified drinks bottles

To test the effectiveness of the indicators' use in a realistic application (e.g. colourimetrically detect the fizziness of drinks), a range of modified carbonated drinks bottles were designed.

#### 4.2.3.1 'Artificial' pressurisation of drinks bottle

The re-pressurisation of bottles containing carbonated drinks can take a number of hours, and the final equilibrium pressure varies depending on the headspace volume, temperature and level of initial carbonation of the beverage. During the developmental stage of the project, it was necessary to trial the indicators in known pressures of CO<sub>2</sub>. This was adequately done by artificially pressurising a carbonated drinks bottle with CO<sub>2</sub> from a gas cylinder. The bottle consisted of inlet and outlet valves, which were attached to the bottle top. As illustrated in Fig. 4.2, the inlet valve can easily be connected to a CO<sub>2</sub> gas cylinder. The pressure in the bottle is determined by the outlet pressure gauge on the gas cylinder.

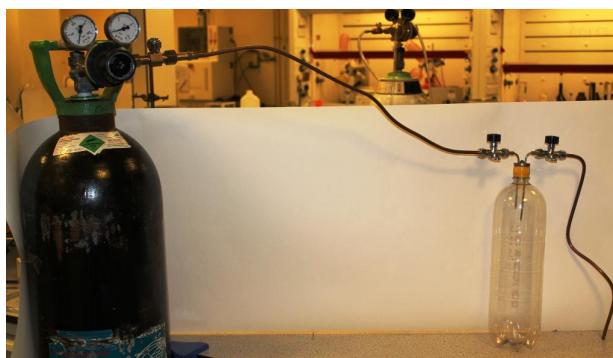


**Fig. 4.2** – Photographs of modified carbonated drinks bottle used to artificially pressurise the bottle.

Typically the bottle is connected to a CO<sub>2</sub> gas cylinder with the inlet and outlet valves opened. CO<sub>2</sub> gas is then flowed through the bottle at ambient pressure in order to saturate the bottle with CO<sub>2</sub> and expel the air from the bottle. After 10 minutes, the outlet valve is closed and the pressure increased using the pressure gauge on the CO<sub>2</sub> cylinder. After a few minutes, the inlet valve is also closed, sealing off the pressure inside the bottle. The CO<sub>2</sub> cylinder valves are closed and the copper piping carefully removed from the bottle. Although this experimental set-up is highly useful when determining the effectiveness of the samples, it does not perfectly simulate the conditions inside a real carbonated drinks bottle, since the humidity levels would be much higher inside bottles containing drinks.

#### 4.2.3.2 Bottle cap with incorporated pressure gauge

In order to determine the pressure inside carbonated drinks bottles and to easily monitor the headspace pressure as it re-pressurises, a bottle cap was designed which incorporated a pressure gauge. The cap can be easily tightened onto regular drinks bottles, allowing pressure versus time experiments to be carried out.



**Fig. 4.3** – Photographs of bottle cap with pressure gauge.

#### 4.2.3.3 Bottle cap with glass window

A bottle cap which contains a borosilicate glass window was designed. Inks can be coated onto the inside of the glass, which is in direct contact with the headspace. Photographs of the modified cap can be seen in Fig. 4.4.



**Fig. 4.4** – Photographs of bottle cap with glass window.

#### 4.2.4 Solar Simulator

To carry out light stability studies on the indicators, a SS150W solar simulator (Sciencetech) was used. Fig. 4.5 below illustrates a picture of the instrument. To accurately simulate solar light a AM1.5D Filter was inserted in simulator. This filter simulates the direct solar spectrum on the ground when the sun is at 48.2° zenith angle.<sup>9</sup>



Fig. 4.5 - SS150W solar simulator (Sciencetech).<sup>10</sup>

## 4.3 Results and discussion

### 4.3.1 Identification of suitable dye

As discussed in the introduction, to successfully achieve an ink which would colourimetrically detect high pressures of CO<sub>2</sub>, it was necessary to identify a dye with a lower pK<sub>a</sub> than that of the previously used *m*-cresol purple (pK<sub>a</sub> = 8.3), and one which also has a distinct colour change upon exposure to CO<sub>2</sub>. A ‘broad-stroke’ preliminary set of experiments were carried out, where a standard ink was prepared using a wide variety of dyes. Each ink was tested as to whether any colourimetric response was observed when a thin film of the ink was exposed to 1 bar of CO<sub>2</sub>, and then at 5 bar CO<sub>2</sub>. Table 4.1 illustrates the initial findings.

**Table 4.1** – List of dyes tested for their suitability to be used in high pressure CO<sub>2</sub> indicating inks.

Dye	Colour change	pKa	Ref.	Colourimetric response from 1 – 5 bar CO <sub>2</sub> (g)?	
				air to 1 bar CO <sub>2</sub> (g)	1 to 5 bar CO <sub>2</sub> (g)
bromocresol green	blue/green → yellow	4.6	11	some	×
chlorophenol red	purple → yellow	6.3	12	some	×
bromocresol purple	purple → yellow	6.3	11	✓	×
4-nitrophenol	yellow → colourless	7.1	13	×	×
brilliant yellow	orange → yellow	-	-	some	×
phenol red	pink/red → yellow	7.6	11	✓	✓
bromothymol blue	blue → yellow	7.0	11	✓	-
phloxine B	purple → colourless	-	-	×	×
nitrazine yellow	blue → yellow	6.4	14	×	×
orange II	yellow → amber	~8	-	×	×
cresol red	yellow → orange	8.2	11	✓	-

From these results, only one dye displayed a colourimetric response when exposed to both 1 and 5 bar CO<sub>2</sub>. The ink containing phenol red, when exposed to 1 bar CO<sub>2</sub>, changed from a fuchsia pink to a deep red colour. When the pressure of CO<sub>2</sub> was increased to 5 bar, it continued to change colour to a light orange/yellow colour. This result established that phenol red had the potential to be used as a high CO<sub>2</sub> pressure indicator.

#### 4.3.1.1 Phenol red

Phenol red, also known as phenolsulfonphthalein, belongs to the sulphonphthalein family of dyes. Its structure, shown in Fig. 4.6, is typical of many pH-sensitive dyes, showing the classical conjugated three-ring structure, which accounts for the intense colour of these dyes.



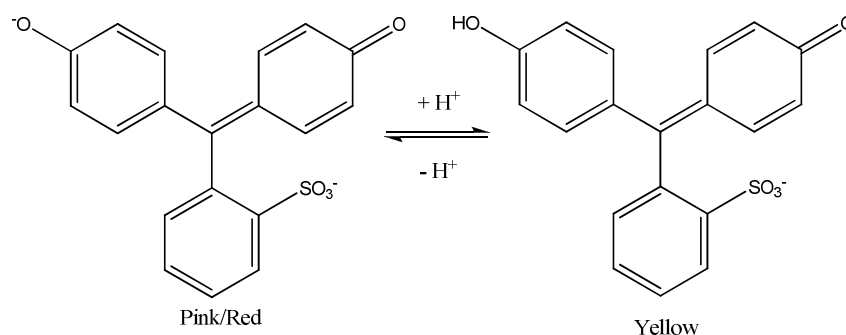


**Fig. 4.6** – Structural change of phenol red in the presence of acid.

Phenol red's ability as a colourimetric pH indicator has been widely utilised in many areas in biology and medicine.<sup>11</sup> Its applications include the determination of soil acidity<sup>15</sup> and the incorporation into microbiological culture media, for bacterial identification<sup>16</sup>. The free acid form of the dye is sparingly soluble in water and ethanol, however the sodium salt is soluble in both water and ethanol, making it a very versatile dye.

### 4.3.2 Ink optimization

Optimisation of the ink formulation was carried out in order to achieve a definitive colour change between air, 1 and 5 bar CO<sub>2</sub>. Polyvinyl alcohol (PVA) was identified as a suitable polymer, due to its high water solubility and good permeability towards CO<sub>2</sub><sup>17</sup>. Sodium hydroxide was chosen as a suitable base due to its low cost and high solubility in water and ethanol. Glycerol had previously been reported<sup>8</sup> as a successful plasticiser, so was utilised in the ink formulation as a way of controlling the response and recovery times. The optimised ink formulation, as summarised in the experimental (section 4.2.1), is PVA/PR/glycerol/NaOH ink 100/12.7/66.7/5.6 pphr. The resulting ink is fuchsia pink in colour, as shown in the photograph in Fig. 4.7.

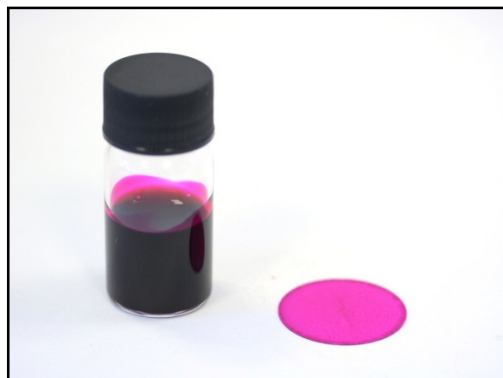


**Fig. 4.7** – Photograph of optimised ink and spun film.

### **4.3.3 CO<sub>2</sub> sensitivity of water-based ink**

The absorbance spectrum of such a typical high pressure CO<sub>2</sub> indicator film was monitored *via* UV/vis absorption spectroscopy as a function of CO<sub>2</sub> pressure and the results are illustrated in Fig. 4.8, along with the associated recorded colours of the indicator at the different  $p\text{CO}_2$  values. The results of this work reveal a very effective high pressure CO<sub>2</sub> colour-based indicator.

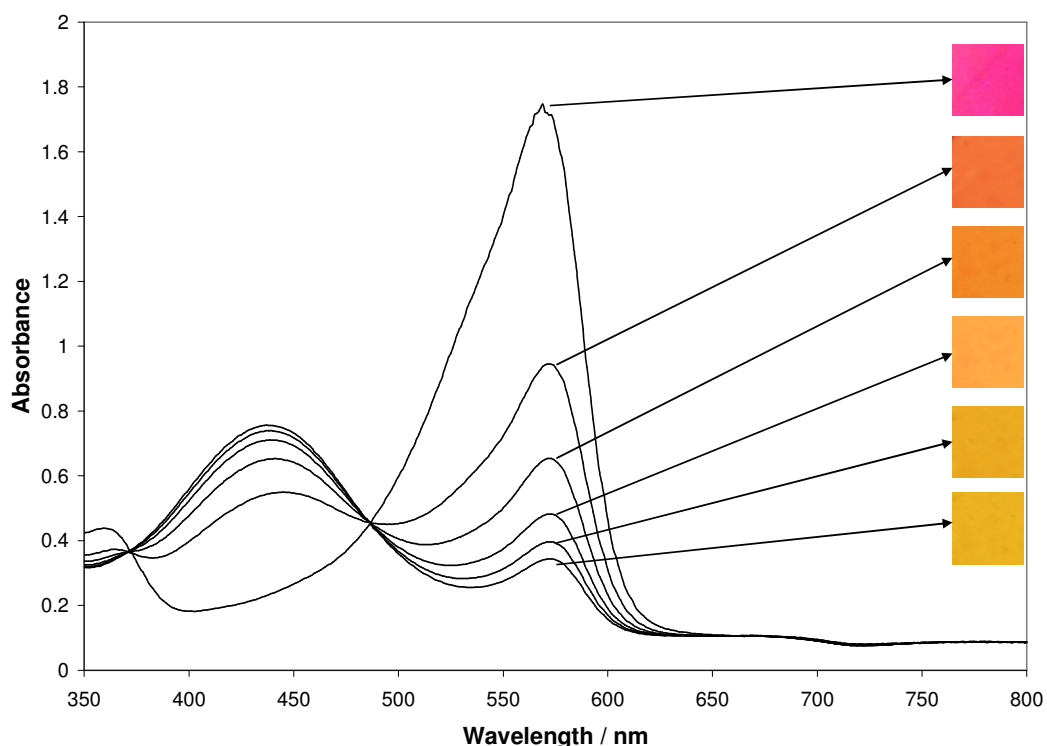


**Fig. 4.8** - UV/visible absorption spectra of film at different pressures of CO<sub>2</sub> at 21°C (from top to bottom: air, 1, 2, 4, 6, 8 bar respectively).

The absorbance of the dye at the wavelength of its maximum absorbance in its deprotonated, D<sup>-</sup> form,  $\lambda_{\max}$  (D<sup>-</sup>), 570 nm, as a function of  $p\text{CO}_2$ , decreases in a hyperbolic manner as illustrated in Fig. 4.9. It is usual<sup>18</sup> and useful to define the parameter,  $R$ , based on experimentally measurable absorbance values at  $\lambda_{\max}$  (due to D<sup>-</sup>) at different  $p\text{CO}_2$ , as follows:

$$R = (\text{Abs}_0 - \text{Abs}) / (\text{Abs} - \text{Abs}_\infty) = [\text{HD}] / [\text{D}^-] \quad (4.2)$$

Where,  $\text{Abs}_0$  is the value of absorbance of the dye at  $\lambda_{\max}$  (D<sup>-</sup>) when  $p\text{CO}_2 = 0$  (i.e. when all the dye is in its deprotonated form), and  $\text{Abs}_\infty$  the absorbance of the film when all the dye has been converted into its protonated form (HD). Since the protonated form of the dye does not absorb significantly at  $\lambda_{\max}$ , it is convenient to take  $\text{Abs}_\infty$  as that of the substrate (in this case the glass disc) alone (i.e. no indicator

film) at  $\lambda_{\max}$ .  $R$  is a measure of the transformation of the dye from its deprotonated to protonated form and for such indicators it can be shown<sup>18</sup> that:

$$R = [\text{HD}] / [\text{D}^-] = \alpha \cdot p\text{CO}_2 \quad (4.3)$$

where  $\alpha$  is the proportionality constant. The absorbance versus  $p\text{CO}_2$  plot arising from the data in Fig. 4.8, is illustrated in Fig. 4.9, along with the  $R$  versus  $p\text{CO}_2$ , calculated using this data and equation (4.2). The linear relationship between  $R$  and  $p\text{CO}_2$ , as expected from equation (4.3), reveals an  $\alpha$  value of  $0.65 \pm 0.04 \text{ bar}^{-1}$ .

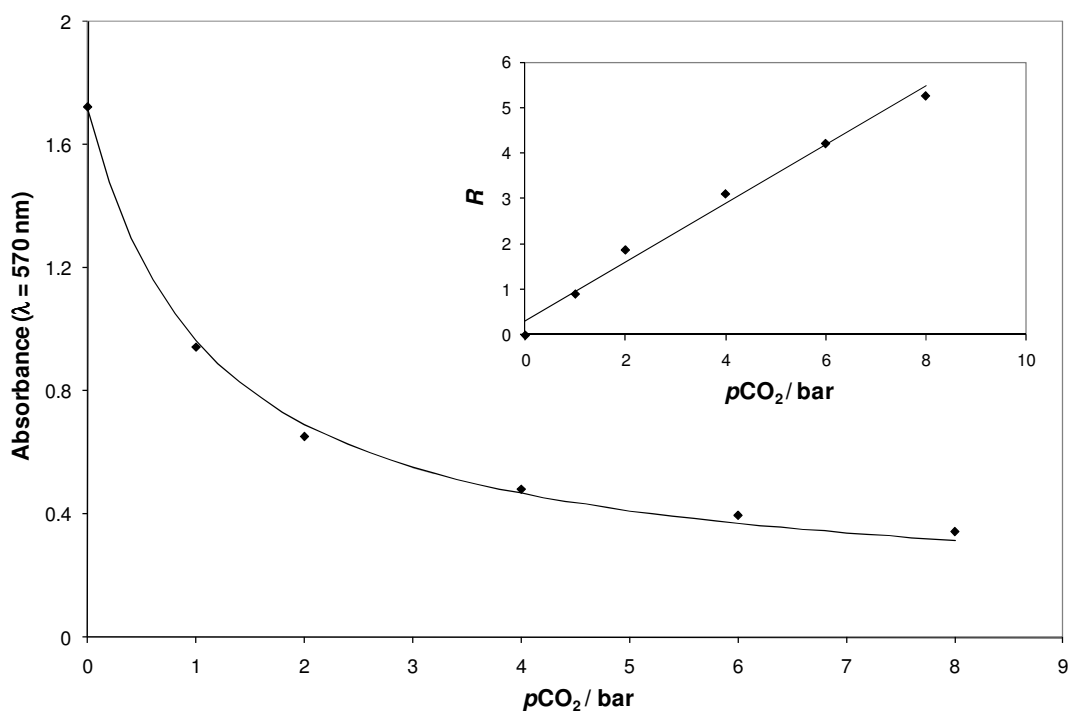


**Fig. 4.9** - Plots of absorbance of film at 570 nm vs.  $p\text{CO}_2$  at 21°C (insert:  $R$  vs.  $p\text{CO}_2$ ). Data from Fig. 4.8. The solid lines in the two diagrams are best fits to the data, revealing an  $\alpha$  value of  $0.65 \pm 0.04 \text{ bar}^{-1}$ .

An experiment was carried out to confirm that the indicator colourimetrically indicates different *pressures* of CO<sub>2</sub>, proving that the eventual colour change is not simply quickened by increasing the pressure. The change in absorbance at the  $\lambda_{\max}$  (= 570 nm) was monitored as a function of time as the pressure of carbon dioxide was firstly increased step-wise and then decreased step-wise. The results in Fig. 4.10

clearly illustrate that the indicator is indeed an effective pressure indicator, since the absorbance levels off after each exposure to different pressures of CO<sub>2</sub>. When exposed to higher pressures of CO<sub>2</sub> the absorbance decreases further. These results also illustrate that each colour change can be reproduced by decreasing the CO<sub>2</sub> pressure in a similar step-wise manner. The change in absorbance mirrors that of the first half of the experiment, hence it is confirmed that each colour of the indicator succinctly represents a different pressure of CO<sub>2</sub>.

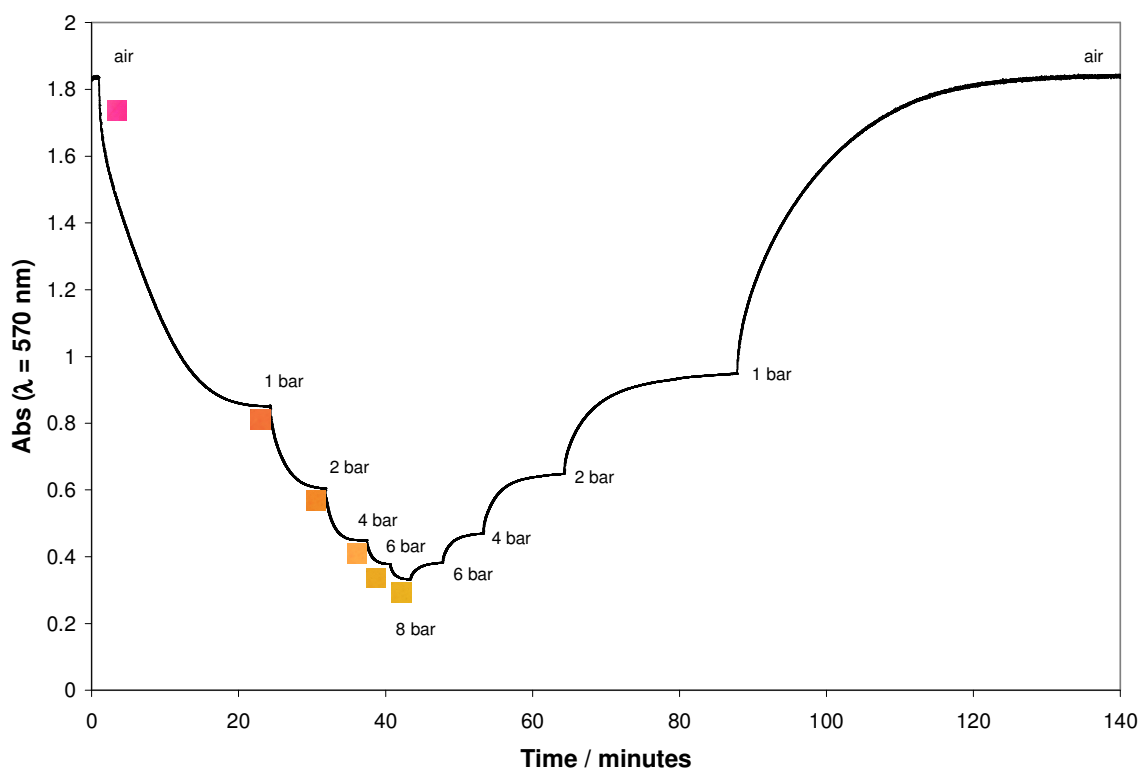


**Fig. 4.10** – Change in absorbance of the film at 570 nm as the CO<sub>2</sub> pressure is increased and decreased stepwise (21°C).

#### 4.3.4 Indicator response and recovery times and effect of humidity

Typical response and recovery times for the indicator when exposed to 3 bar of dry (~0%RH) CO<sub>2</sub> and then back to ambient, are 22 and 54 minutes, respectively. To investigate the effect of humidity of the response and recovery of the indicator, an experiment was carried out where the indicator was exposed to 1 bar of CO<sub>2</sub> which

had been bubbled through a bottle of water, producing a gas stream with ~80-90%RH. The results of this experiment are illustrated in Fig. 4.11.

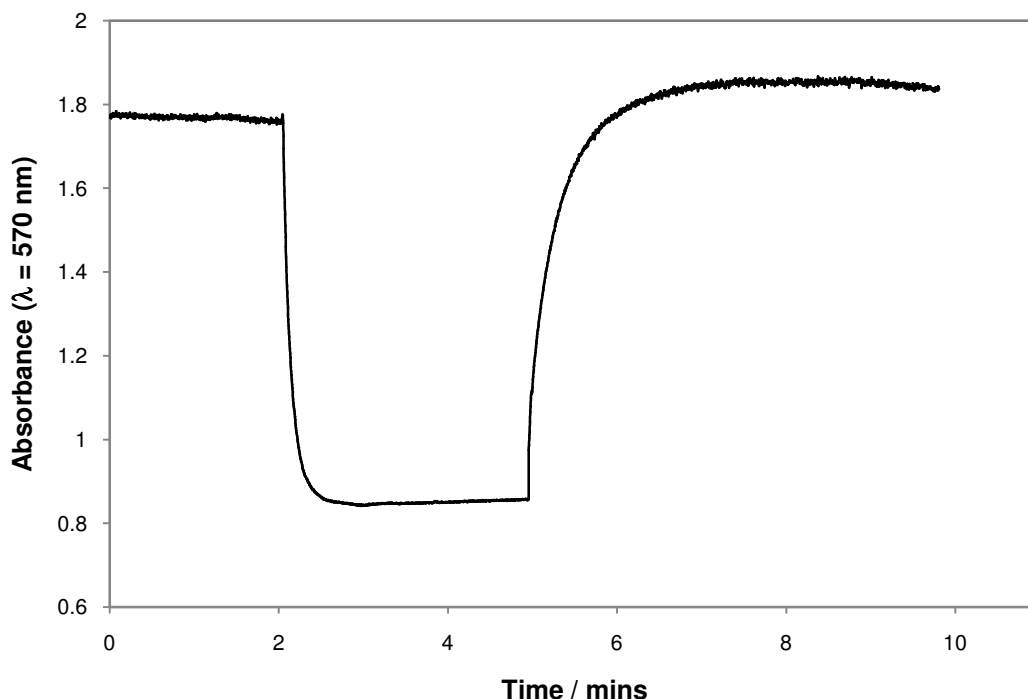


**Fig. 4.11** – Effect of humidity to response and recovery; higher %RH levels decrease response and recovery times (21°C).

The results show that the response and recovery of the indicator decreased dramatically. Within 30 seconds the film had fully responded to CO<sub>2</sub> and recovered within 3 minutes when exposed to humid air. This effect is possibly due to the ability of water to act as a plasticiser.<sup>19</sup> With dry or humidified gases, the indicator is fully reversible and can be used repeatedly without any loss in performance.

#### 4.3.5 Development of a solvent-based ink

It is recognised that commercial manufacturers which utilise inks in packaging prefer solvent-based inks due to their greater ability to be applied to a greater variety of surfaces. In light of this, work was carried out to develop a similar, non-aqueous, high pressure CO<sub>2</sub> indicating ink. Solvent-based indicators are typically more

sensitive to CO<sub>2</sub> than their water-based counterparts, so it was envisaged that developing an insensitive solvent-based CO<sub>2</sub> indicating ink would prove problematic.

Much work was carried out to develop a solvent-based ink, of which the attempts are summarised in Table 4.2. Each row summarises the components in each of the inks investigated. The concentrations of some of the components were varied (i.e. base concentration and polymer viscosity), however details of each variation are not given here for reasons of conciseness.

**Table 4.2** – Summary table of solvent-based inks investigated as high pressure CO<sub>2</sub> indicating inks.

Dye	Solvent	Polymer	Base	Plasticizer	Comment
Phenol Red	MeOH	ethylcellulose in Tol:MeOH	TBAH in MeOH	-	full colour change at 1 bar CO <sub>2</sub>
Nitrazine Yellow	MeOH	ethylcellulose in Tol:MeOH	TBAH in MeOH	tributyl phosphate	no response to 0 - 6 bar CO <sub>2</sub>
Rosolic acid	MeOH	ethylcellulose in Tol:MeOH	TBAH in MeOH	tributyl phosphate	no further colour response when CO <sub>2</sub> pressure increased
Rosolic acid	EtOH	polyvinyl butyral in EtOH	KOH in EtOH	-	no further response to > 1 bar CO <sub>2</sub>
Bromocresol purple	MeOH	ethylcellulose in Tol:MeOH	TBAH in MeOH	-	no response to 0 - 6 bar CO <sub>2</sub>
Phenol Red	MeOH	ethylcellulose in Tol:MeOH	KOH in EtOH	-	
Cresol Red	EtOH	polyvinyl butyral in EtOH	KOH in EtOH	-	full colour change at 1 bar CO <sub>2</sub>
Bromothymol blue	MeOH	ethylcellulose in Tol:MeOH	TBAH in MeOH	tributyl phosphate	no significant colour change to CO <sub>2</sub>
Phenol Red	EtOH	polyvinyl butyral in EtOH	NaOH in EtOH	(glycerol)	distinct colour changes observed from air, 1 and 5 bar CO <sub>2</sub>

Initial efforts were focused on converting the present water-based system directly into the equivalent solvent-based version (see row 1 of Table 4.2). Unfortunately, the ink was far too sensitive, showing a full colour change even at ambient pressures of CO<sub>2</sub>. Realising the higher sensitivity of solvent-based inks, dyes with a similar or lower pK<sub>a</sub>s that phenol red were tried. Unfortunately, no alternative dye was



identified to successfully give a colourimetric response at the desired pressures of CO<sub>2</sub>. Finally, phenol red was re-visited, this time using an ethanol-based system. The general ink formulation is summarised in the last row of Table 4.2. Successfully, the spun ink film showed gradual colour changes to increasing pressures of CO<sub>2</sub>, similar to the water-based ink. Although not truly 'solvent-based' (since ethanol also dissolves typical water-soluble compounds due to its high polarity), the ethanol-based ink has a greater ability to adhere to hydrophobic surfaces compared to the water-based ink. However, it was noted that the colour changes observed using the ethanol-based ink were not as distinct compared to the water-based ink. For example, upon exposure to 1 bar CO<sub>2</sub>, the film changed from pink to orange, whereas the water-based equivalent changes from pink to red, then changes to orange/yellow at higher pressures of CO<sub>2</sub>. Further details of the colour changes and the characterisation of the ethanol-based ink are described below.

#### *4.3.5.1 CO<sub>2</sub> sensitivity of ethanol-based ink*

Similar analyses were carried out for the ethanol-based ink as were performed for the water-based ink. Fig. 4.12 illustrates distinct colour changes as the pressure of CO<sub>2</sub> is increased from 0 to 8 bar and a clear isosbestic point at 484 nm is observed.

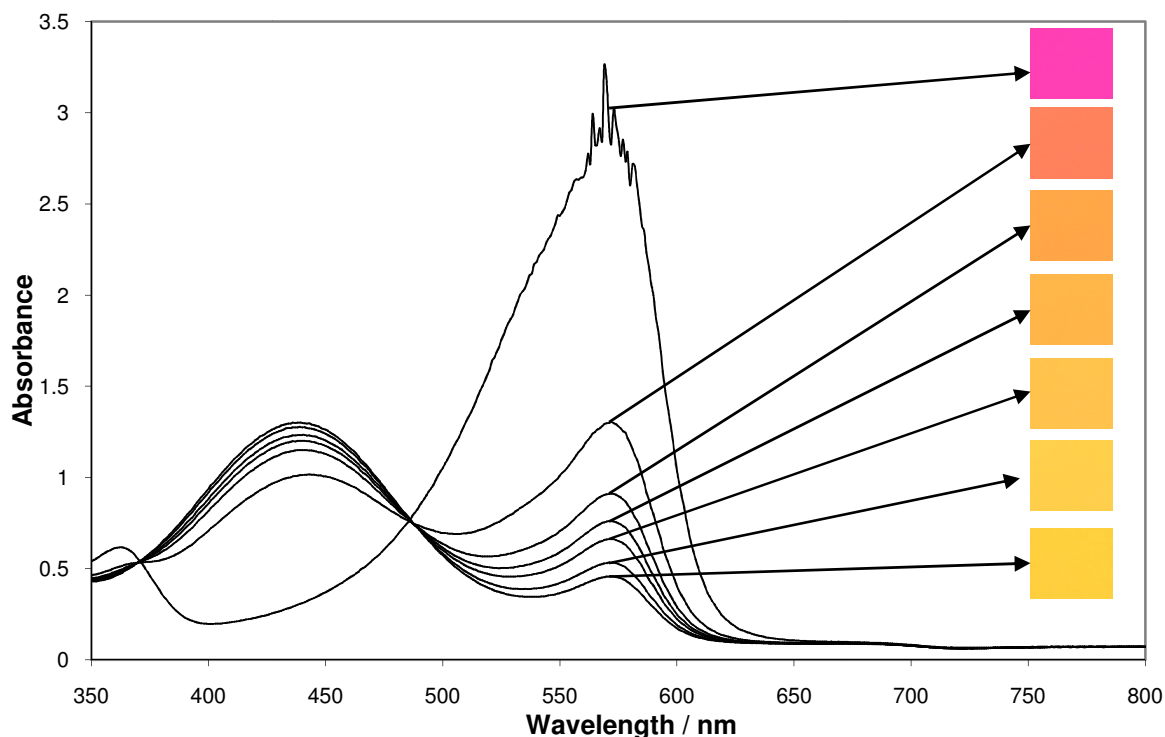


**Fig. 4.12** – UV/visible absorption spectra of film at different pressures of CO<sub>2</sub> at 21°C (from top to bottom: air, 1, 2, 3, 4, 6, 8 bar respectively).

The absorbance vs.  $p\text{CO}_2$  plot arising from the data in Fig. 4.12 is illustrated in Fig. 4.13, along with the  $R$  vs.  $p\text{CO}_2$ , calculated using this data and equation (4.2). The linear relationship between  $R$  and  $p\text{CO}_2$ , as expected from equation (4.3), reveals an  $\alpha$  value of  $0.8453 \pm 0.06 p\text{CO}_2^{-1}$ . Since the value of  $\alpha$  is often taken to be an indication of the films sensitivity, it is evident that the solvent based ink is 1.3x more sensitive than the water based ink. This observation is consistent with results obtained in previous work reported in Chapter 3, where it was suggested that the difference in sensitivity may be due to the much greater solubility of CO<sub>2</sub> in the hydrophobic medium of the solvent-based polymer.

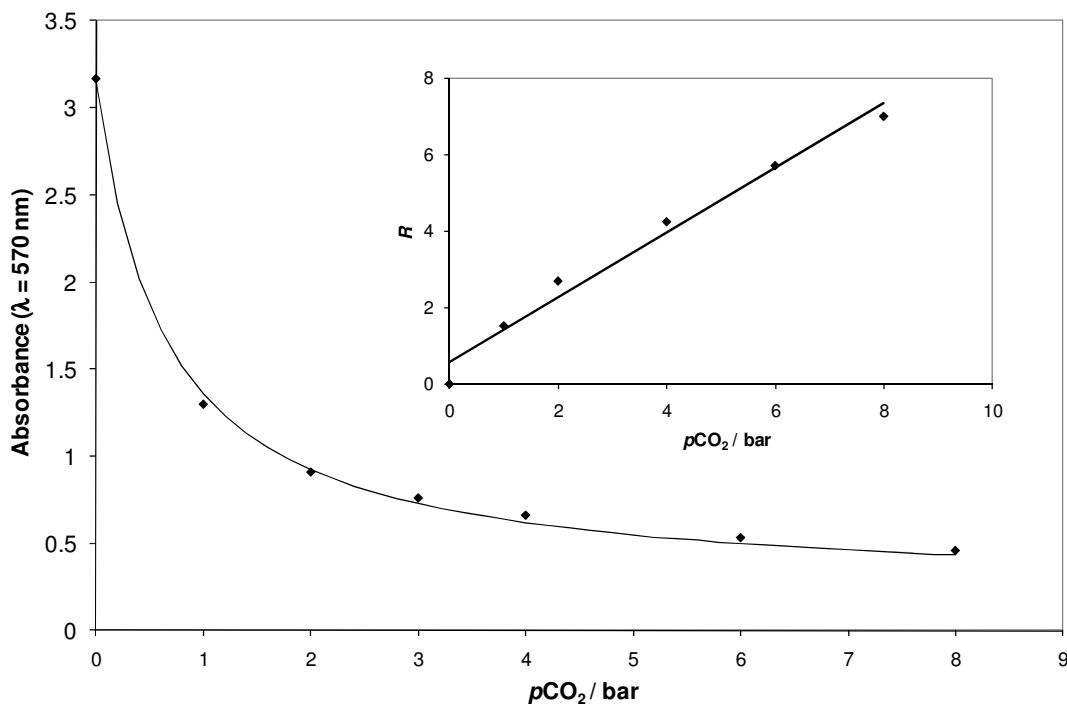


**Fig. 4.13** – Plots of absorbance of film at 570nm versus  $p\text{CO}_2$  at 21°C (insert:  $R$  vs.  $p\text{CO}_2$ ). Data from Fig. 4.12. Solid lines were best fit to the data, revealing an  $\alpha$  value of  $0.8453 \pm 0.06 p\text{CO}_2^{-1}$ .

The indicator's increased sensitivity is also evident in Fig. 4.14, where the  $\lambda_{\text{max}}$  absorbance (570 nm) is monitored as the CO<sub>2</sub> pressure is increased and decreased step-wise. Whereas it took approximately 15 minutes for the water-based indicator to respond fully to 1 bar of CO<sub>2</sub> (Fig. 4.11), it only took approximately 1 minute for the solvent based to respond to the same pressure of CO<sub>2</sub>.

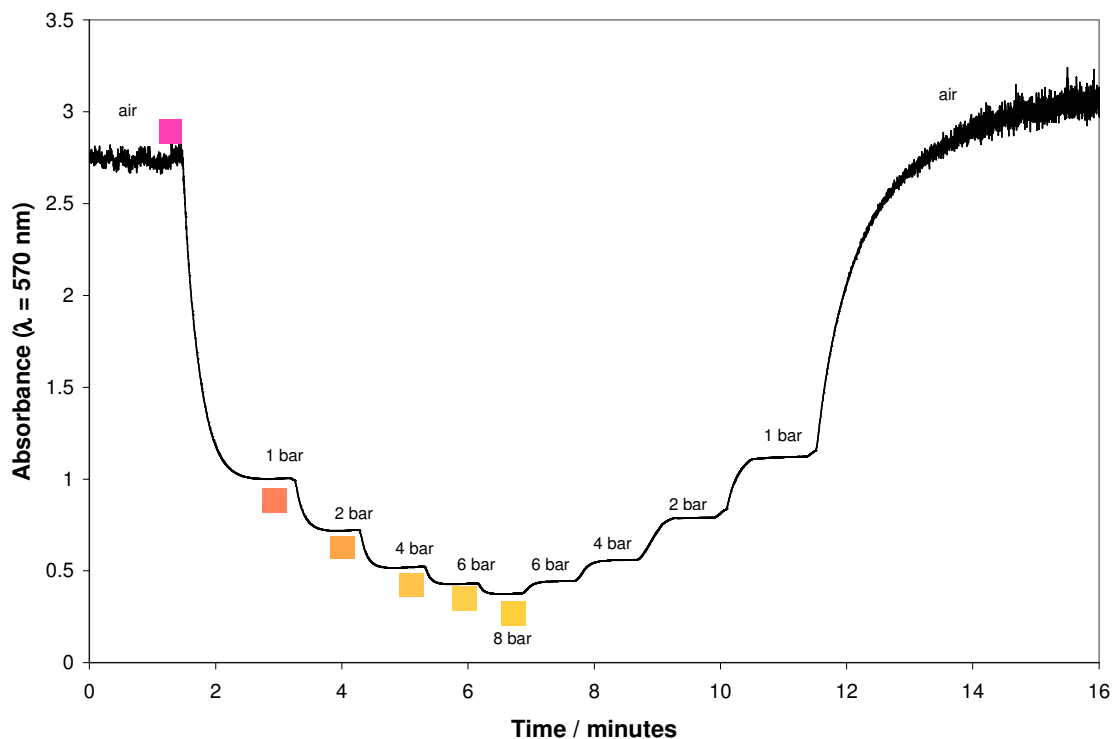


**Fig. 4.14** – Change in absorbance of the film as the CO<sub>2</sub> (g) pressure is increased and decreased stepwise (21°C).

## 4.4 Applications

The detection of carbon dioxide at pressures over the range 1 - 5 bar is very relevant in many areas. As previously mentioned there are many applications that high pressure CO<sub>2</sub> indicators could be applied to e.g. biotechnology (especially fermentation), refrigeration, fire extinguishers and aerosols. However the main application of this study is the measurement of ‘fizziness’ in carbonated drinks.

### 4.4.1 Typical headspace pressures

The data in Table 4.3 lists the typical pressure of CO<sub>2</sub> in the headspace of different classes of carbonated drinks. The range of pressures listed in this table correlates well with the colourimetric responses given by the indicators described above, and

therefore has the potential to become a useful quality assurance tool to both the retailer and consumer.

**Table 4.3** – Typical carbonation levels in fizzy drinks.<sup>20</sup>

Degree of 'fizziness'	Approximate $p\text{CO}_2$ / bar at 20°C
Flat	$\sim \leq 1.0$
Lightly sparkling	1.5
Typical fizzy drink (e.g. cola)	3.5
Highly carbonated (e.g. mixer)	4

For a given volume of liquid, the amount of CO<sub>2</sub> which a solution can contain is dependent upon temperature and pressure. It is well known that the solubility of CO<sub>2</sub> in water decreases as the temperature increases, but increases with increasing pressure i.e. a specific carbonation level will generate a higher pressure as the temperature increases. Henry's law states that 'the amount of gas dissolved in a given volume of solvent is proportional to the pressure of gas with which the solvent is in equilibrium', whilst Charles' law states, 'the volume of an ideal gas at constant pressure is directly proportional to the absolute temperature'.

Using these theories, an estimation of the headspace pressures in carbonated beverages can be determined. Knowing the number of volumes of CO<sub>2</sub> dissolved in the drink (volumes is defined as number of times the total volume of dissolved gas can be divided by the volume of the container) and the storage temperature of the drink, Henry's constant can be determined for that specific temperature (using Van't Hoff equation). Applying Henry's law i.e.

$$p = k_H c \quad (4.4)$$

where  $p$  = pressure,  $k_H$  = Henry's constant and  $c$  = concentration of solute, the headspace pressure can be estimated.

Fig. 4.15 illustrates a carbonation chart published<sup>20</sup> by D. P. Steen and P. R. Ashurst which is typical of charts used in industry.

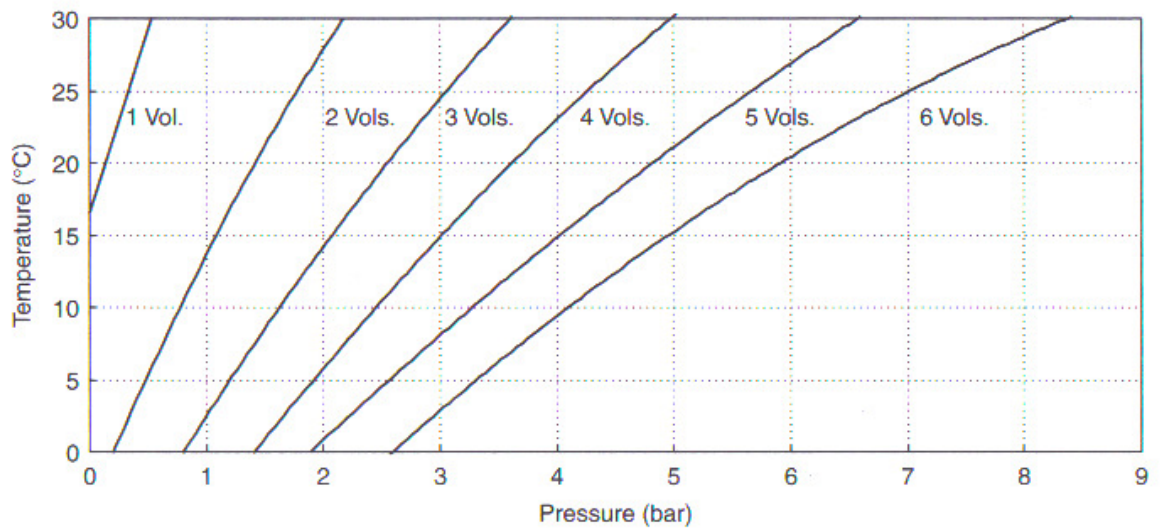


Fig. 4.15 – Carbonation chart<sup>20</sup>.

Applying this chart to a bottle of cola at 25°C with approximately 4.0 volumes of carbon dioxide, this corresponds to a headspace pressure of approximately 4.3 bar. This pressure decreases over time as the bottle is repeatedly opened and closed. The colourimetric high pressure CO<sub>2</sub> indicator would visually give a colour change which would monitor these changing pressures inside the bottle, which corresponds to the relative ‘fizziness’ of the drink.

According to studies<sup>20</sup>, a standard 2 litre PET bottle normally loses 15% of carbonation in 12 weeks. This is then reduced to *ca.* 9 weeks for a 500 ml bottle and only 7 weeks for a 250 ml bottle.

Obviously, with such drinks, the headspace pressure decreases everytime the bottle is opened, or decreases with time in the case of faulty packaging. Such, usually unwanted, degassing increases with increasing temperature and time. The longer the bottle is left opened – the more CO<sub>2</sub> is lost from the system and the lower the eventual equilibrium headspace pressure when the bottle is eventually resealed.

#### 4.4.2 Relationship between headspace pressure and taste

To consolidate the usefulness of a fizziness indicator and relate the pressure of the bottle's headspace to the level of carbonation someone experiences when drinking (i.e. fizziness), a small scale experiment was set up within our research group in the University of Strathclyde. The pressure inside a bottle of lemonade was monitored using a pressure gauge connected to a bottle top (see section 4.2.3.2). Every two days, the pressure was noted and a sample of the lemonade was given to each participant in the group (resulting in a loss of approximately 40 ml per day). Each taster rated the level of carbonation on a scale from 1 to 10 every two days. The highest rating 10, described the expected level of carbonation of a newly opened bottle and the lowest rating 1, described the drink when it had lost all carbonation (i.e. totally flat). The group of tasters were also asked to comment at what point they would normally no longer drink the lemonade, primarily due to lack of carbonation. The results of this work are illustrated in Fig. 4.16.

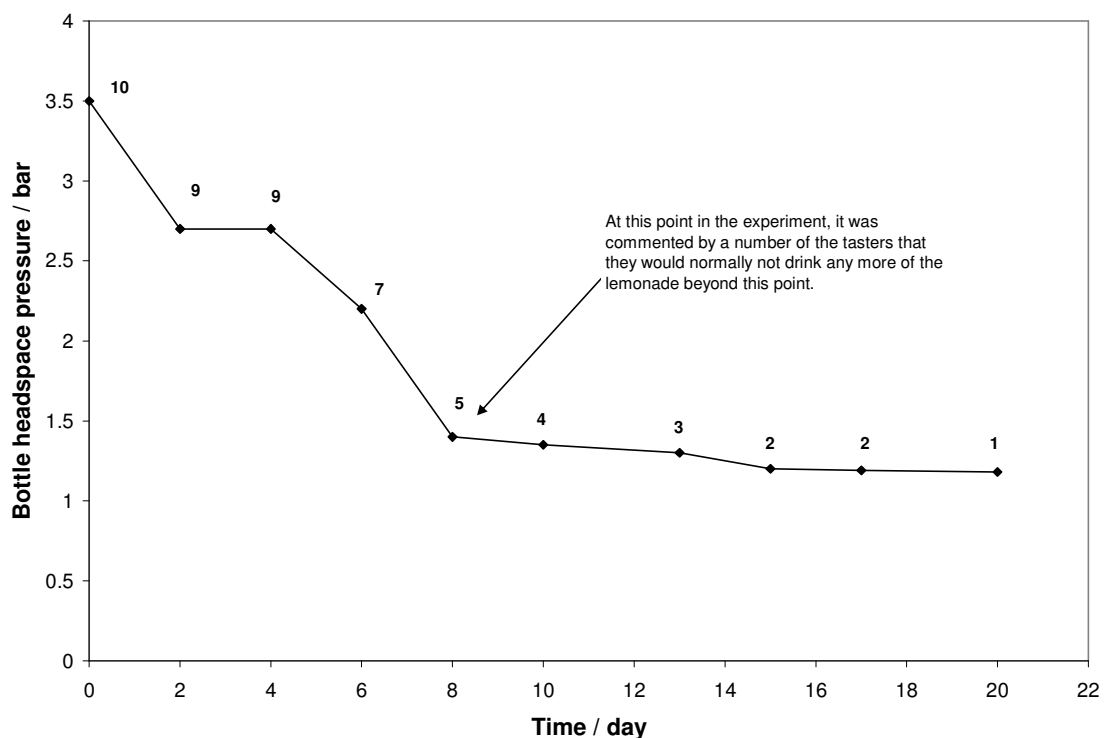


**Fig. 4.16** – Relationship between headspace pressure of lemonade bottle over time, along with average taste ratings.

The ratings of each taster are averaged and noted on the graph beside each pressure. It is clearly evident that there is a clear decrease in headspace pressure over the time period, as well as a decrease in average taste rating. From the results, it is understood that the pressure inside the bottle when the drink is described as 'flat' is approximately 1 - 1.2 bar. This is an encouraging result since the CO<sub>2</sub> indicator changes colour around the point the group of tasters would classify the drink as flat. Obviously, this small scale experiment doesn't give a complete and definitive result; however it does serve as a marker to suggest that the pressures of CO<sub>2</sub> the indicator can colourimetrically respond to, are indeed the key pressures involved in the de-carbonation of carbonated drinks.

#### **4.4.3 Headspace pressurisation**

It has previously been noted that each time the carbonated drink is resealed, the headspace pressure proceeds to re-pressurise, as the equilibrium re-establishes. The increase in headspace pressure after a carbonated drinks bottle had been resealed was recorded in a similar manner using the bottle top with the incorporated pressure gauge. The pressure was monitored at regular intervals over a 38 hour period. The results of this work are illustrated in Fig. 4.17. Due to these long (~20 hours) re-pressuring times, the response and recovery times of the indicator are not a cause of concern to the technology.



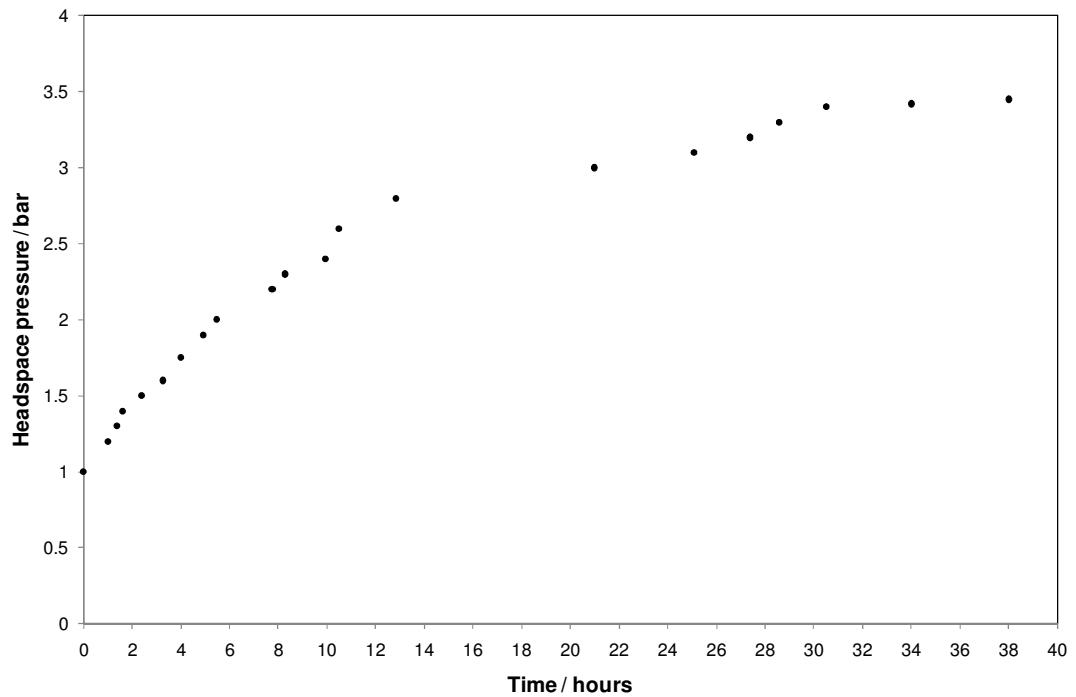


Fig. 4.17 – Plot of headspace pressure vs. time after re-sealing.

The eventual equilibrium headspace pressure also decreases as the carbonated drink is consumed. As the drink volume is decreased, the headspace volume is increased. Hence more of the dissolved CO<sub>2</sub> equilibrates into the headspace volume, increasing the headspace pressure, and decreasing the amount of dissolved CO<sub>2</sub>, i.e. ‘fizz’, in the drink. To consolidate this, bottles of lemonade with varying liquid volumes were shaken until equilibrium headspace pressure was reached. Table 4.4 Summarises these results.

Table 4.4 – Correlation between drink volume and equilibrium headspace pressure

Fraction volume of lemonade	Equilibrium headspace pressure after 30 s of shaking
1	3.6
2/3	2.9
1/3	2.1

It is evident from Table 4.4 that as the headspace volume increases, the equilibrium headspace pressure decreases. This change in pressure would be indicated by the

colour change of the indicator, which reflects the level of carbonation within the drink.

#### 4.4.4 Indicator trials

To demonstrate the use of the ink as a possible ‘fizziness’ indicator for carbonated drinks, it was necessary to coat the ink onto a flexible polymer sheet which could be easily inserted into a bottle. The high pressure water-based CO<sub>2</sub> indicator ink was coated onto biaxially orientated polypropylene sheets (Goodfellow, 0.075 mm), which had been pre-treated with a 1µm coating of polyvinyl butyral in ethanol (20% w/v) to improve film adhesion. The water-based ink was chosen to demonstrate the indicator, since it is slightly less sensitive to CO<sub>2</sub> pressures, therefore giving more distinct colour changes at the key levels of CO<sub>2</sub>. The samples were then laminated using commercially available PET lamination pouches (80 µm thick) in order to render them as water-proof.

The product coloured strip was inserted into a full fizzy drinks bottle and the headspace allowed to pressurise. The ink changed, over a period of 2 hours from magenta to yellow/orange indicating a high fizz level. The liquid content of the fizzy drink bottle was then progressively allowed to lose its fizz (by removing cap and allowing to stand, then sealing up again). The results illustrated in Fig. 4.18, showed a gradual colour change from yellow/orange to magenta, with yellow/orange and magenta indicating the extremes of a ‘very fizzy’ and ‘flat’ state, respectively, in a commercial carbonated drink.

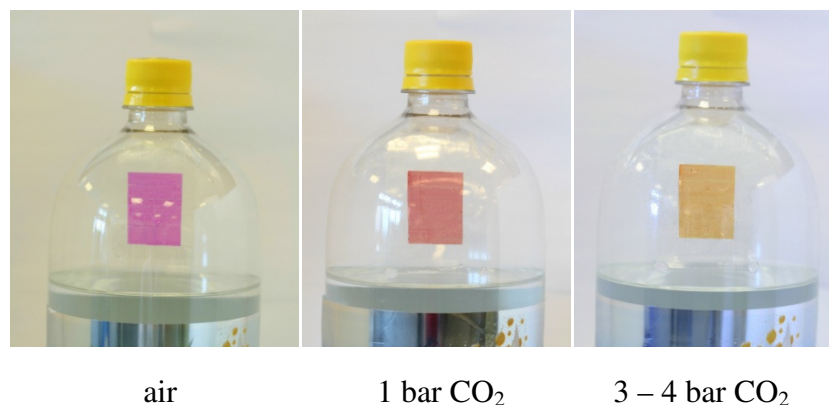


**Fig. 4.18** - Pictures of the laminated ink inside a plastic lemonade bottle with fizzy lemonade and the associated colour changes at three different pressures of CO<sub>2</sub> – air, 1 bar and 3 - 4 bar CO<sub>2</sub> respectively.

The ink has potential to be either incorporated into the plastic packaging of the bottle, or the bottle cap. The incorporation of the ink in this manner was unfortunately beyond the scope of this project, as it would involve the integration of the ink into the laminate polymer system of the drinks bottle. However to envisage a colour changing bottle cap, a modified bottle cap was designed as described in section 4.2.3.3. The cap incorporates a glass disc which acts as a window, on which the ink can be coated and easily observed by the consumer. Since the ink is in direct contact with the headspace of the drink, the ‘cap’ changes colour as the headspace pressure changes. Fig. 4.19 illustrates photographs of the cap as the indicator changes colour with changing headspace CO<sub>2</sub> pressure.

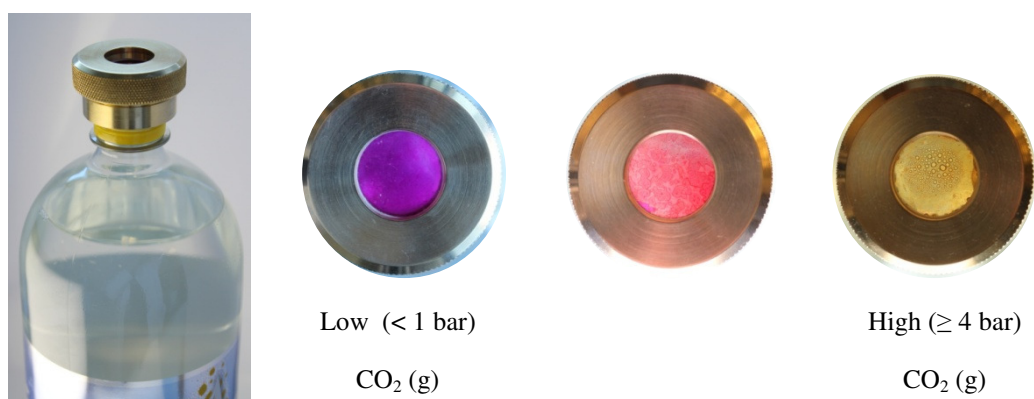


**Fig. 4.19** – Bottle cap changing colour with increasing pressure of CO<sub>2</sub> (g).

#### 4.4.5 Temperature sensitivity

The effect of temperature on the indicator's sensitivity was recognised as an important feature to characterise, since the temperature at which the indicators may be used may vary from room temperature to a chilled fridge (~ 4°C). However, the measurement of colour using spectrophotometry with varying temperatures (as carried out on similar indicators) proved difficult and potentially hazardous, due to the high pressures involved in the experimental set-up. Therefore, the colours of an indicator inserted into an 'artificially' pressurised drinks bottle (see section 4.2.3.1) were observed visually at different storage temperatures. As is common with most CO<sub>2</sub>-sensitive inks<sup>18</sup>, a degree of temperature sensitivity is observed, whereby the CO<sub>2</sub> sensitivity increases with decreasing temperature. Distinct colour differences were still observed between 1 and 3 bar *p*CO<sub>2</sub> values over the temperature range 5 – 25°C.

#### 4.4.6 Stability

Both water- and solvent-based inks are stable under ambient conditions and require no specialised storage conditions. Previously reported CO<sub>2</sub> indicators show deterioration within a few days due to interfering acidic gases, however, only after approximately one year being left out in ambient, unprotected conditions, is any sign of deterioration observed. This is not surprising due to the levels of acidic gases the indicators are designed to detect is very high.

When the indicator is incorporated into a drinks bottle it should only be used when the product is stored under the manufacturers recommended conditions, since failure to do so would possibly compromise the indicator as well as the product. In the case of fizzy drinks it is the recommendation of most manufacturer's to keep the product 'cool and store out of direct sunlight'. Saying that, under ambient room light conditions, or when exposed to AM 1.5 solar simulated light for 24 h, the indicator showed minimal evidence of photobleaching or change of sensitivity, as illustrated in Fig. 4.20.

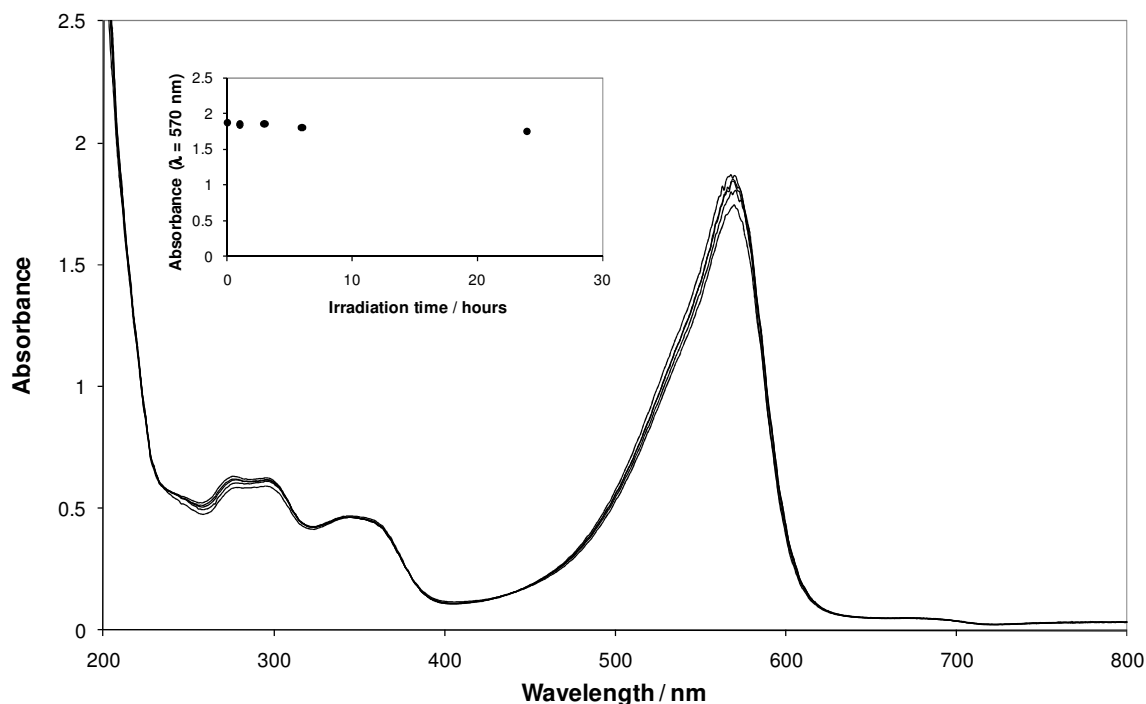


**Fig. 4.20** – Absorption spectra of water-based indicator when exposed to AM 1.5 solar simulated light. at 0, 1, 3, 6 and 24 hours at 22°C.

## 4.5 Conclusions

Water- and solvent- based CO<sub>2</sub> indicator inks have been developed, which progressively change colour from deep pink to yellow over a 0 - 8 bar CO<sub>2</sub> pressure range. High pressure CO<sub>2</sub> indicating inks have exciting new applications into a new range of smart packaging for carbonated drinks. By observing the colour of the ink, after the headspace pressure has equilibrated, an indication of the level of carbonation will be known. They are stable, easy and cheap to prepare and highly reversible.

## 4.6 References

1. R. Lines, *Int. Pat.*, 075498 2007.
2. O. Oter, K. Ertekin and S. Derinkuyu, *Talanta*, 2008, **76**, 557-563.

3. M. J.-P. Leiner, J. Tusa and I. Klimant, *EP*, 1 965 198, 2008.
4. G. C. Upreti, Y. Wang and A. S. H. Kueh, *Int. Pat.*, 079024 2008.
5. R. Ostrowski and M. P. Debreczeny, *Int. Pat.*, 039424 2008.
6. Y. Amao and N. Nakamura, *Sens. Actuators B*, 2004, **100**, 347-351.
7. S. M. Borisov, M. C. Waldhier, I. Klimant and O. Wolfbeis, *Chem. Mater.*, 2007, **19**, 6187-6194.
8. A. Mills and G. A. Skinner, *Analyst*, 2010, **135**, 1912-1917.
9. [http://www.sciencetech-inc.com/en/catalog/86/solar\\_filters/AM15D-3S](http://www.sciencetech-inc.com/en/catalog/86/solar_filters/AM15D-3S), (accessed 15/03/11).
10. [http://www.sciencetech-inc.com/en/catalog/3/fully\\_reflective\\_solar\\_simulators](http://www.sciencetech-inc.com/en/catalog/3/fully_reflective_solar_simulators), (accessed 15/03/11).
11. R. W. Horobin and J. A. Kiernan, *Conn's Biological Stains*, Taylor & Francis, 2002.
12. X. Zhang, R. van Eldik, T. Koike and E. Kimura, *Inorganic Chemistry*, 1993, **32**, 5749-5755.
13. L. E. Janes, A. C. Löwendahl and R. J. Kazlauskas, *Chemistry-A European Journal*, 1998, **4**, 2324-2331.
14. T. D. Rhines and M. A. Arnold, *Analytica Chimica Acta*, 1989, **227**, 387-396.
15. A. R. Coscione, J. C. de Andrade and B. van Raij, *Commun. Soil Sci. Plant Anal.*, 1998, **29**, 1973-1982.
16. D. H. Kang and D. Y. C. Fung, *J. Food Prot.*, 1999, **62**, 313-317.
17. J. Brandrup, E. H. Immergut and E. A. Grulke, *Polymer handbook*, 1999.
18. A. Mills, Q. Chang and N. McMurray, *Anal. Chem.*, 1992, **64**, 1383-1389.
19. F. Franks, *Water Science Reviews 3: Water Dynamics*, Cambridge University Press, 1988.
20. D. P. Steen and P. R. Ashurst, *Carbonated Soft Drinks - Formulation and Manufacture*, Blackwell Publishing, 2006.

## Chapter 5: Intelligent pigments and plastics

---

### 5.1 Introduction

The majority of novel indicators reported for applications in food packaging technology have largely been ink based (as has previous work described in this thesis). Inks are often the accepted choice since they can be easily printed onto a number of surfaces, however some limitations exist. Intelligent inks are typically printed and manufactured as separate labels which are then attached to food packaging. This method has been criticised<sup>1</sup> since this process can add extra time and elevate manufacturing costs, which has led to some packaging companies not supporting such technology.

This part of the project aims to investigate the capabilities of intelligent pigments to be used in smart packaging and investigate the scope for such indicators to be used in a variety of other applications. Pigments have been used as colourants in plastics for many centuries and the incorporation of pigments into polymers has become a standard manufacturing step in the process of producing coloured plastic materials. The incorporation of *intelligent* pigments into polymers, commonly used in food packaging (i.e. polyethylene), would potentially develop a new range of intelligent materials with a direct application in industry.

To create such an indicating system, it was proposed that the appropriate dye could be supported on a suitable particulate inorganic substrate, thereby creating an intelligent pigment. The pigment could then be incorporated into a hydrophobic thermoplastic such as polyethylene. The main aim of this study is to develop a new series of CO<sub>2</sub>-indicating intelligent pigments and plastics which could easily be converted into MAP leakage indicators for use in food packaging. However, realising that a vast range of intelligent inks<sup>2-5</sup> have been reported in recent years for a variety of analytes and applications, it is envisaged that a range of intelligent pigments and plastics could be developed for a variety of applications. Some of these are reported and brief characterisations carried out.

## 5.2 Experimental

### 5.2.1 Colourimetric CO<sub>2</sub> Intelligent ink, pigment and plastic formulations

To 2.0 g of hydrophobic silica (Degussa/Evonik Aerosil R812, specific surface area =  $260 \pm 30 \text{ m}^2/\text{g}$ , average particle size = 7 nm), 0.08 g of *m*-cresol purple (MCP), 100 ml of ethyl acetate and 5 ml of 1 M tetrabutylammonium hydroxide in methanol were added. (The silica employed has been rendered hydrophobic, by the manufacturer, by reacting the surface hydrophilic silanol groups (Si-OH) with dimethyldichlorosilane to produce hydrophobic Si-Me groups, as illustrated in Fig. 5.1).

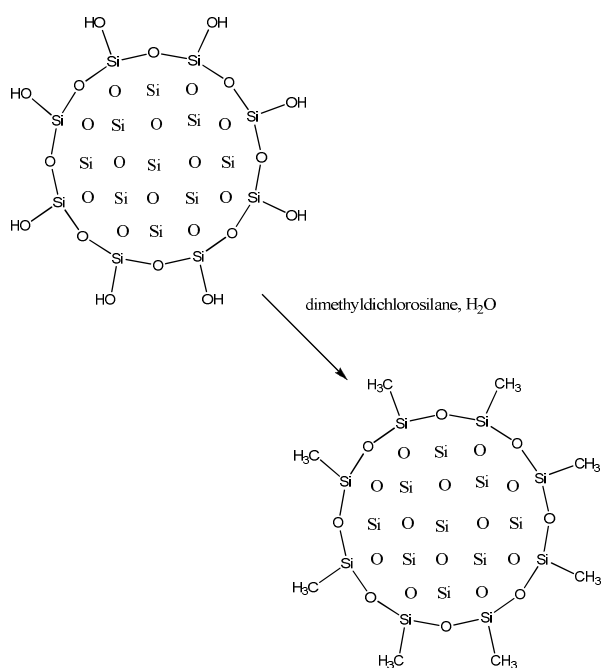


**Fig. 5.1** – Hydrophobation of silica.

This mixture was mixed thoroughly and the solvent (ethyl acetate) then removed under reduced pressure using a rotary evaporator. The resultant powder was dried in the oven at 70°C for ~2 hours, then ground up using a pestle and mortar to generate a fine blue powder. The anionic form of MCP, MCP<sup>-</sup>, is rendered hydrophobic by ion-pairing with the quaternary ammonium cation, Q<sup>+</sup>, to form Q<sup>+</sup>MCP<sup>-</sup>.xH<sub>2</sub>O; note: the



presence of a few water molecules of water are known<sup>6</sup> to associate with such ion-pairs.

As a result, rotary evaporation of this solvent-soluble ion-pair with the hydrophobic silica, generates particles with a coating of  $Q^+MCP^-.xH_2O$ , which are able to respond rapidly and reversibly to the presence of  $CO_2$  via the following equilibrium reaction:



This same key reaction features<sup>6</sup> in MCP, solvent-based  $CO_2$ -sensitive plastic films. Thus, as illustrated by the photographs in Fig. 5.2, in the absence of  $CO_2$  the MCP is in its blue anionic ( $MCP^-$ ) state, but in the presence of  $CO_2$  it is converted, via the reversible reaction (5.1), to its yellow, protonated form (MCPH).

In order to make the corresponding intelligent *plastic*, 0.6 g of the hydrophobic *pigment* were added to 4.0 g of powdered polyethylene (Alfa Aesar, LDPE, 1000  $\mu m$ ) and the mixture ground up using a mortar and pestle until the colour was a uniform blue colour. A small sample (*ca.* 0.3 - 0.4 g) of the powder mixture was heat pressed using a Specac Atlas™ Series Heated Platens at 115°C to create a blue polyethylene film (0.1 mm thick) which was used in subsequent indicator work. The composition of the final  $CO_2$  intelligent plastic, in terms of parts per hundred resin (pphr), was PE/MCP/SiO<sub>2</sub>/TBAH = 100/0.6/15/9.6.

For comparison purposes, a similar solvent-based ink was prepared by dissolving 0.08 g of *m*-cresol purple in 3 ml methanol and 1.5 ml 1M tetrabutylammonium hydroxide in methanol (TBAH). This solution was stirred for 15 minutes, placed in a sonicating bath for 10 minutes, then stirred further until fully dissolved. This solution was added to 20 g of 10% w/v ethyl cellulose in toluene:ethanol (80:20) (EC, 45-55 cP, 5% toluene:ethanol (60:40) at 25°C), along with 2 ml of tributyl phosphate. The final ink solution was stirred for at least 30 minutes. The composition

of the deposited dried ink film in terms of pphr, was EC/MCP/TBAH/tributyl phosphate = 100/4/19.5/97.

Pigments which colourimetrically indicated levels of CO<sub>2</sub> typically found in breath (~5%) were prepared. Thus, 0.25 g of thymolphthalein were added to 4 g of hydrophobic silica, along with 3 ml 1M tetrabutylammonium hydroxide solution in methanol. Approximately 100 ml methanol were added and the mixture stirred. The solvent was removed under a reduced pressure, forming a fine blue powder.

Alternatively 0.25 g of *o*-cresolphthalein were added to 4 g of hydrophobic silica, along with 3 ml 1M tetrabutylammonium hydroxide solution in methanol. Approximately 100 ml methanol were added and the mixture stirred. The solvent was removed under a reduced pressure, forming a fine purple powder.

### 5.2.2 Colourimetric O<sub>2</sub> intelligent pigment and plastic formulations

To 2.0 g of titanium dioxide (P25, Degussa), 10 mg of methylene blue (MB), 1.0 g of DL-threitol and approximately 100 ml of ethanol were added. The mixture was mixed thoroughly and then the solvent (ethanol) removed under reduced pressure using a rotary evaporator. The resultant powder was ground up using a pestle and mortar to generate a fine blue powder. 0.2 g of the methylene blue coated TiO<sub>2</sub> pigment (solvent-based) was then mixed with 1.0 g of powdered polyethylene, and ground up using a pestle and mortar. A small sample (*ca.* 0.3 - 0.4 g) of the powder mixture was heat pressed at 115°C and under 5 tonnes pressure using a Specac Atlas™ Series Heated Platens. A thin (0.1 mm) blue, flexible plastic film was formed.

### 5.2.3 Luminescent O<sub>2</sub> intelligent pigment and plastic formulations

To 4.0 g of hydrophobic silica (Degussa/Evonik R812, S.S.A. = 260 +/- 30 m<sup>2</sup>/g, average particle size = 7 nm), 15 mg of Platinum (II) octaethyl porphyrin (Pt(II)OEP)

was added. Approximately 100 ml THF were added. The solution was mixed thoroughly and then the solvent (THF) removed under reduced pressure using a rotary evaporator. The resultant powder was then ground up using a pestle and mortar to generate a fine, light pink powder.

To 15.0 g of hydrophilic silica (BDH, average particle size 50 nm), 15 mg of Platinum (II) octaethyl porphyrin were added. Approximately 100 ml THF were added. The solution was mixed thoroughly and then the solvent (THF) removed under reduced pressure using a rotary evaporator. The resultant powder was then ground up using a pestle and mortar to generate a fine, light pink powder.

Similar fluorimetric O<sub>2</sub>-sensing pigments, based on Ru(dpp)<sub>3</sub><sup>2+</sup> (Ph<sub>4</sub>B<sup>-</sup>)<sub>2</sub> were also prepared, following the same procedure as for Pt(II)OEP pigments.

The hydrophobic and hydrophilic pigments were mixed with polyethylene and polyethyleneoxide, respectively, and heat pressed into pigmented plastic films in a similar manner as described earlier.

## 5.3 Results and discussion

### 5.3.1 CO<sub>2</sub>-indicating pigments and plastics

The standard *m*-cresol purple pigment turns from bright blue to yellow immediately when exposed to CO<sub>2</sub>. As captured in the photographs in Fig. 5.2, the pigment immediately changes colour as the CO<sub>2</sub> gas permeates through the silica, and all of the sample quickly becomes yellow. The colour change is distinct and dramatic, which makes it very appealing as an indicator for commercial applications.

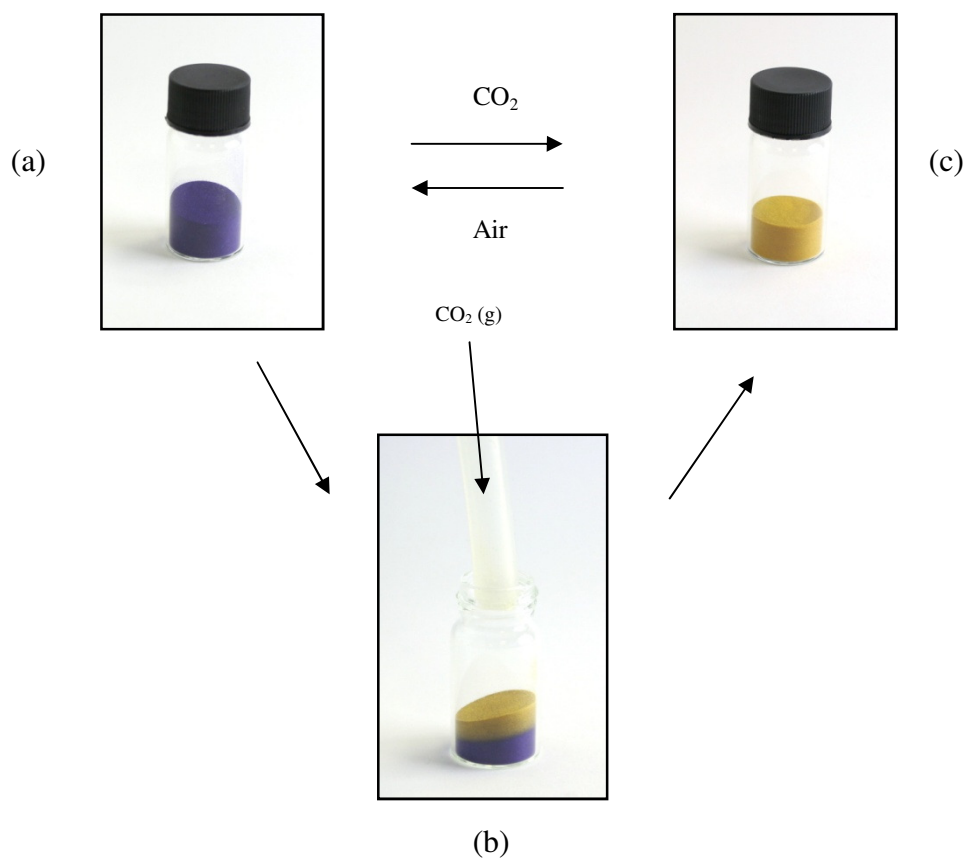


**Fig. 5.2** – (a) - before exposure to CO<sub>2</sub> (g), (b) – during exposure to CO<sub>2</sub>, (c) – after exposure to CO<sub>2</sub>.

Pictures of the hydrophobic silica crystals under an optical microscope (x220 magnification) show that the indicating solution is a coating on the silica crystals and that the coating changes colour (purple to yellow) upon exposure to CO<sub>2</sub>, as illustrated in Fig. 5.3. The crystals are typically 10 – 60  $\mu\text{m}$ , however due to the amorphous nature of the silica, smaller or larger particle sizes are often observed. Fig. 5.3 below shows a good colour change of one of the larger crystals viewed under the microscope.

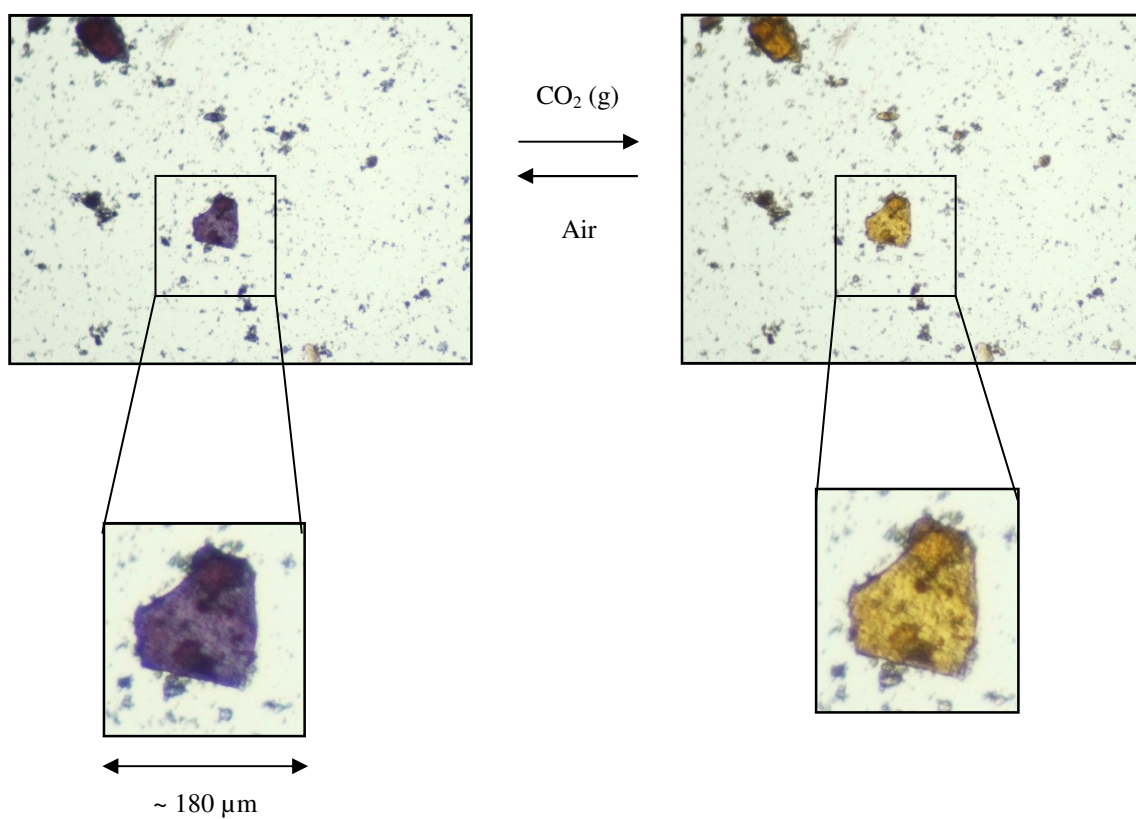


**Fig. 5.3** – Images of a large dye-coated fumed hydrophobic silica crystal, before and after exposure to CO<sub>2</sub>.

A similar pigment was prepared using larger particle sized hydrophilic silica. These silica crystals are more uniform so the colour change can be easily observed under the microscope, as shown in Fig. 5.4.

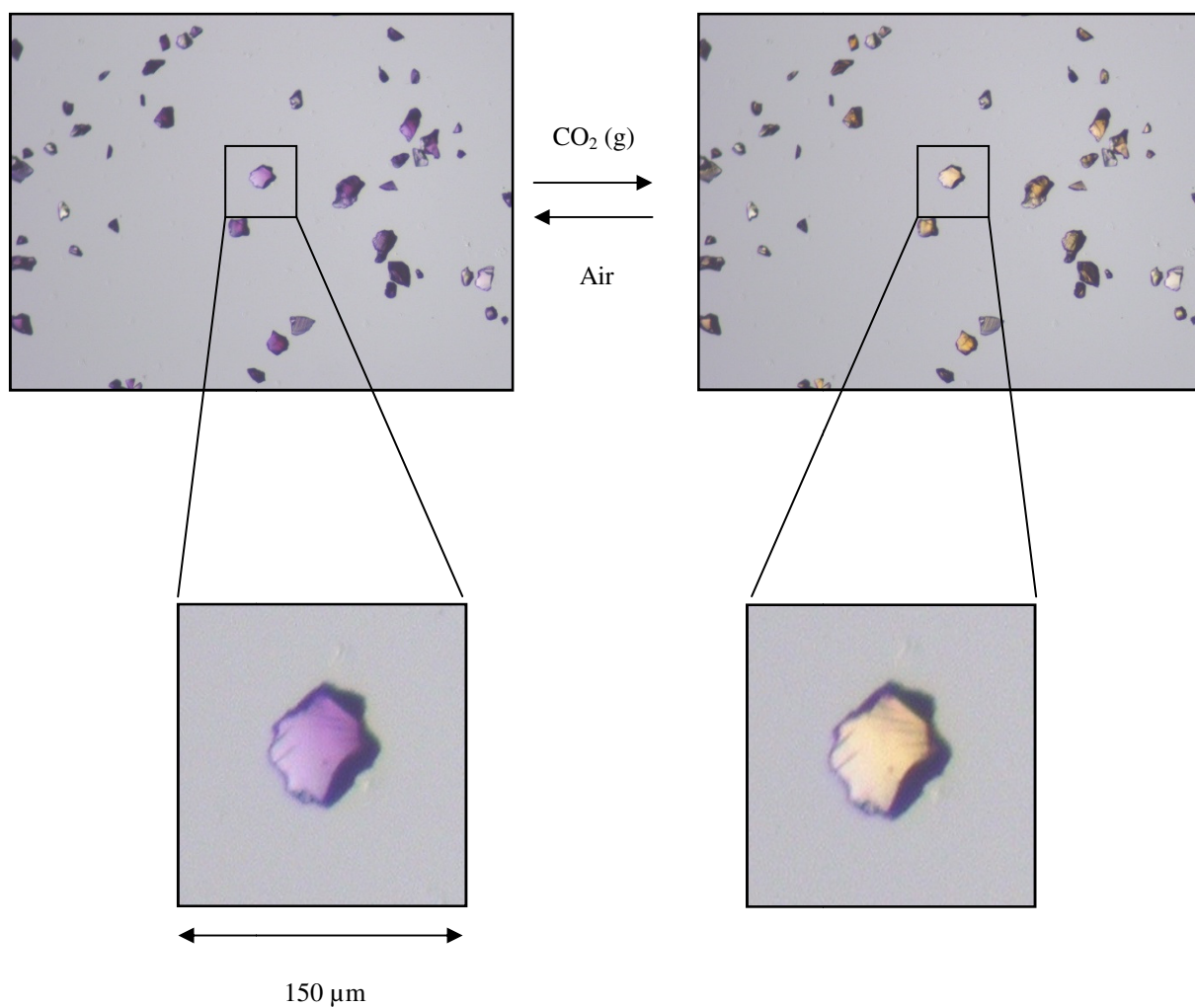


**Fig. 5.4** - Images of a dye-coated hydrophilic silica crystals, before and after exposure to CO<sub>2</sub>.

### 5.3.1.1 CO<sub>2</sub>-sensitivity

To measure the diffuse reflectance spectra of the pigment with varying levels of ambient CO<sub>2</sub>, the pigment was smeared onto filter paper. The transition of the dye from the deprotonated form (D<sup>-</sup>,  $\lambda_{\text{max}} = 588 \text{ nm}$ ) to the protonated form (HD,  $\lambda_{\text{max}} = 430 \text{ nm}$ ) as the %CO<sub>2</sub> increased, is illustrated in Fig. 5.5.

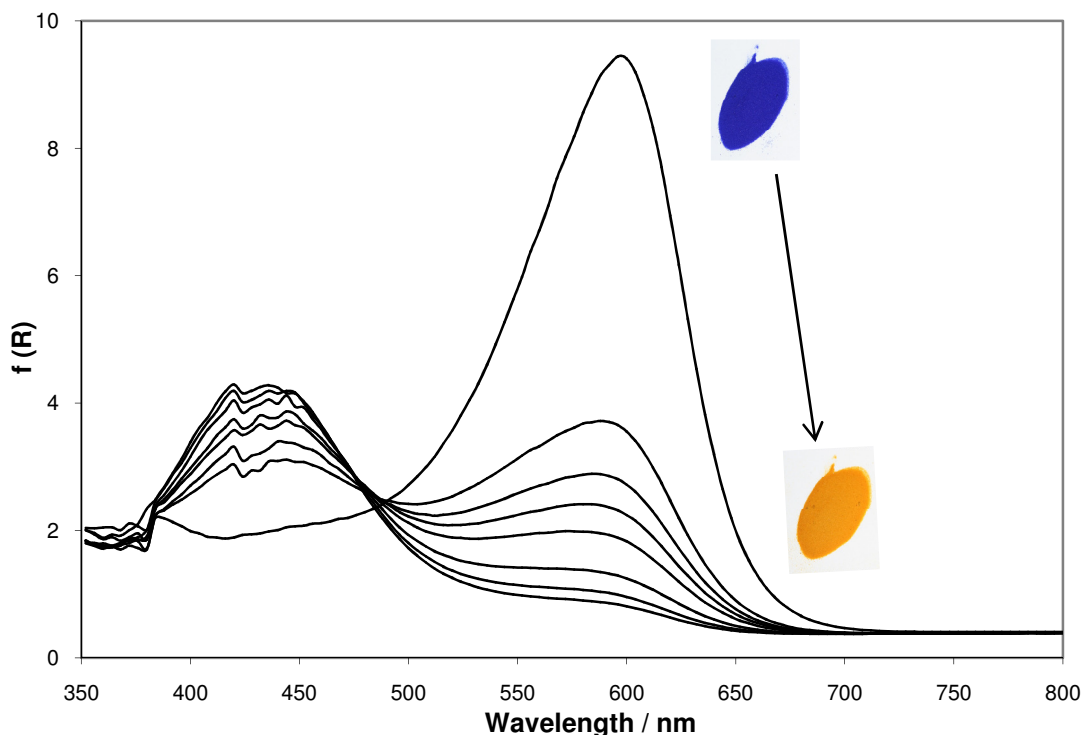


**Fig. 5.5** - UV/visible diffuse reflectance spectra of the powder as a function of %CO<sub>2</sub> at 21°C, for (from top to bottom) of 0, 1, 2, 3, 5, 10, 50, 100%CO<sub>2</sub>, respectively.

Similar to the work carried out in previous analyses of CO<sub>2</sub> indicators, it is useful to define the parameter,  $R$ , based on experimentally measurable absorbance or reflectance values at  $\lambda_{\max}$  (due to  $D^-$ ) at different %CO<sub>2</sub>, as follows:

$$R = (f(R)_0 - f(R)) / (f(R) - f(R)_\infty) = [HD] / [D^-] \quad (5.2)$$

Where  $[HD]$  and  $[D^-]$  are the concentration of the protonated and deprotonated forms of the dye, respectively.  $f(R)_0$  is the value of reflectance of the dye at  $\lambda_{\max}$  ( $D^-$ ) when %CO<sub>2</sub> = 0 (i.e. when all the dye is in its deprotonated form) and  $f(R)_\infty$  is the reflectance of the film when all the dye has been converted into  $DH$ , i.e. when %CO<sub>2</sub> =  $\infty$ . Since, with the dye concerned,  $DH$  does not reflect at  $\lambda_{\max}$  ( $D^-$ ), it is convenient to take  $f(R)_\infty$  as that of the substrate (filter paper) alone (i.e. no indicator) at  $\lambda_{\max}$  ( $D^-$ ). From equation (5.2) the parameter,  $R$ , is a measure of the transformation of the dye from the deprotonated to protonated forms and is

directly proportional to  $[HD]/[D^-]$ . The relationship between  $R$  and  $\%CO_2$  is normally linear<sup>6</sup> for a direct indicator, as is the case of most similarly based  $CO_2$  indicators<sup>7</sup>. Thus, as described for previous  $CO_2$ -indicators, it can be shown that:

$$R = [HD] / [D^-] = \alpha \cdot \%CO_2 \quad (5.3)$$

where  $\alpha$  is a proportionality constant, which in turn is inversely dependent upon the background base concentration, i.e.  $\alpha$  vs.  $1 / [\text{base}]$ , used in the film.<sup>8</sup> The reflectance ( $f(R)$ ) vs.  $\%CO_2$  plot arising from the data in Fig. 5.5 is illustrated in Fig. 5.6, along with the  $R$  vs.  $\%CO_2$ , calculated using this data and equation (5.2). The linear relationship between  $R$  and  $\%CO_2$  is in accordance with equation (5.3) and reveals an  $\alpha$  value of  $0.883 \pm 0.086 \%CO_2^{-1}$  at  $21^\circ C$ .

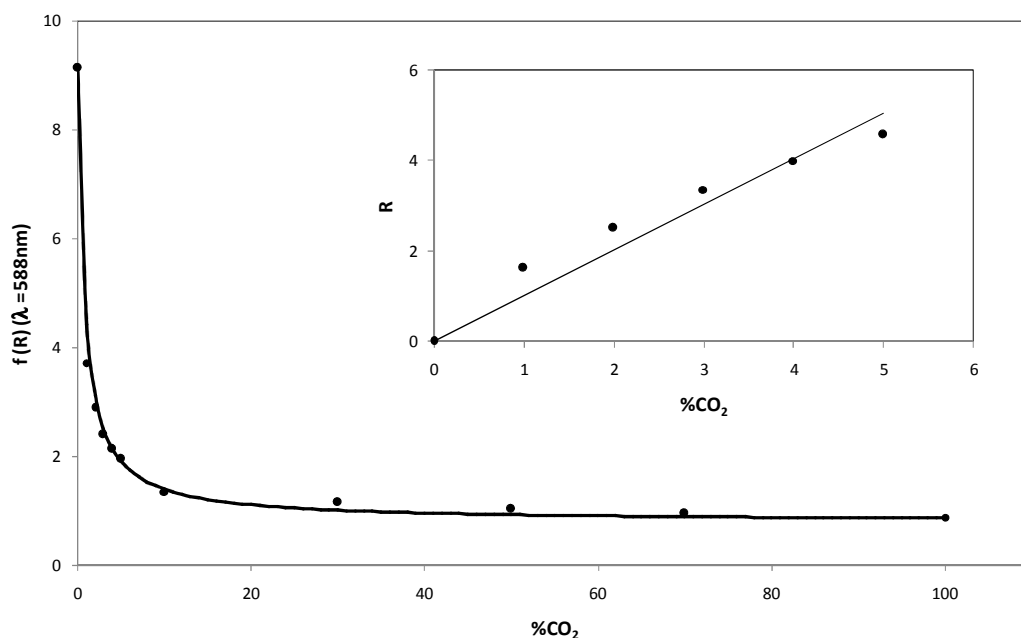


**Fig. 5.6** – Plots of reflectance of powder at 588 nm vs.  $\%CO_2$  at  $21^\circ C$  (insert:  $R$  vs.  $\%CO_2$ ). Data from Fig. 5.5. The solid lines are best fits to the data, assuming an  $\alpha$  value of  $0.883 \pm 0.086 \%CO_2^{-1}$ .

A striking colour change is also observed when the pigment is incorporated into a thin polymer film, as illustrated in Fig. 5.7. This characteristic, blue to yellow colour change was also observed for the MCP solvent-based ink, which uses the same quaternary base.



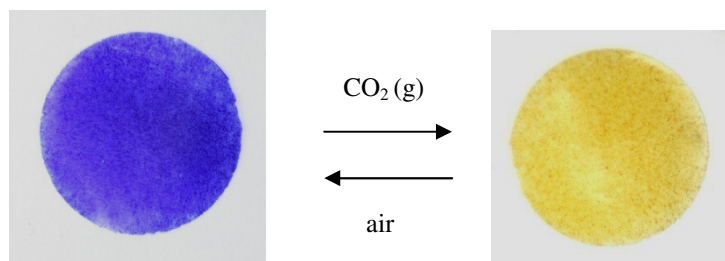


**Fig. 5.7** - Colour change of CO<sub>2</sub>-sensing pigment incorporated into polyethylene plastic film, when exposed to 100 % CO<sub>2</sub>.

The absorbance spectra of the plastic film as a function of %CO<sub>2</sub> was recorded and the Fig. 5.8 shows the recorded UV/vis spectra of the MCP/silica plastic film as a function of %CO<sub>2</sub>. As with its solvent ink-based film counterpart, the change in colour, due to  $\lambda_{\max}$  shifting from 592 to 424 nm, is a result of the deprotonated form of the dye becoming protonated *via* reaction (5.1).

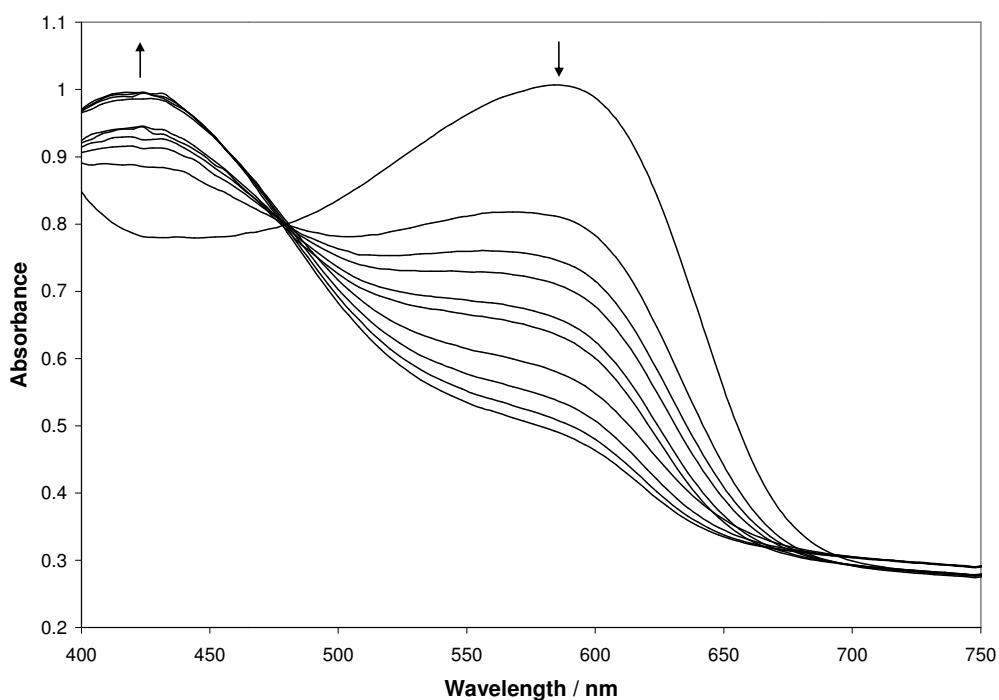


**Fig. 5.8** – UV/visible absorption spectra of the MCP/silica/PE plastic film as a function of %CO<sub>2</sub> at 21°C, for %CO<sub>2</sub> (from top to bottom) of 0, 1, 2, 3, 4, 5, 20, 30, 60, 100%CO<sub>2</sub>, respectively. Abs<sub>∞</sub> is ~ 0.44.

The linear relationship between  $R$  and  $\%CO_2$ , as illustrated in Fig. 5.9, reveals an  $\alpha$  value of  $0.185 \pm 0.02 \ \%CO_2^{-1}$ .

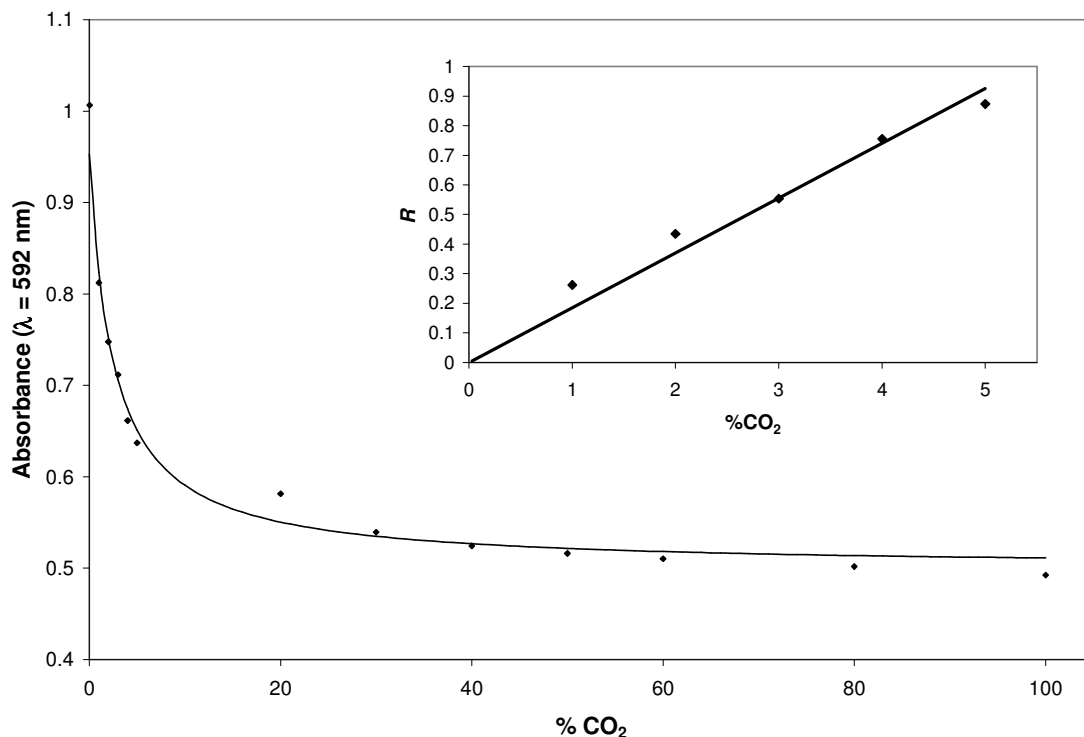


**Fig. 5.9** – Plots of absorbance of MCP/silica plastic film at 592 nm versus  $\%CO_2$  at 21°C. Data from Fig. 5.8. Solid lines were best fit to the data, revealing an  $\alpha$  value of  $0.185 \pm 0.02 \ \%CO_2^{-1}$ .

The  $CO_2$  sensitivity was also determined for the solvent-based ink, using the same methods as discussed previously. The results showed that the MCP solvent-based ink had a very similar sensitivity ( $\alpha = 0.799 \pm 0.076 \ \%CO_2^{-1}$ ) to the powder  $CO_2$ -indicator. Since  $\alpha$  is a measure of indicator sensitivity, it appears that the solvent-based sensor shows a greater sensitivity (4 times) towards  $CO_2$  compared to the MCP/silica pigment plastic film, possibly due in part to the greater permeability of  $CO_2$  (by a factor of *ca.* 9) in ethylcellulose compared to polyethylene.<sup>9</sup> Although the two indicator systems tested have markedly different dye levels ( $[dye] = ca. 7$  times more – in terms of pphr in the solvent based indicator), this is unlikely to be responsible for the difference in sensitivity for two reasons. Firstly, the sensitivity of such indicators is expected<sup>8</sup> to be independent of dye concentration, except at very high dye levels. Secondly, at high dye concentrations the dye will buffer the system

and so the indicator would appear less sensitive (not more, as found for the higher dye-containing solvent-based indicator).

### 5.3.1.2 Response and recovery times

The determination of response and recovery times towards the presence of CO<sub>2</sub> is key to the characterisation, and eventually the application, of any indicator. The response and recovery times of the three indicators were determined by monitoring the absorbance (or reflectance) at  $\lambda_{\max}$  of the deprotonated, D<sup>-</sup>, form of the dye, over time as the indicator is exposed to alternating streams of CO<sub>2</sub> and air.

Due to limitations of the experimental set-up when recording the response and recovery characteristics of the powder, only the response time could be recorded. The  $\tau_{90}$  response time is < 1 s, as illustrated in Fig. 5.10 and the  $\tau_{90}$  recovery time is approximately 3 s. These fast response and recovery times are most likely due to the ability of the gas to permeate into the powder quickly. Similarly, the solvent-based CO<sub>2</sub>-indicator has response and recovery times of both <1 and 3 s respectively.

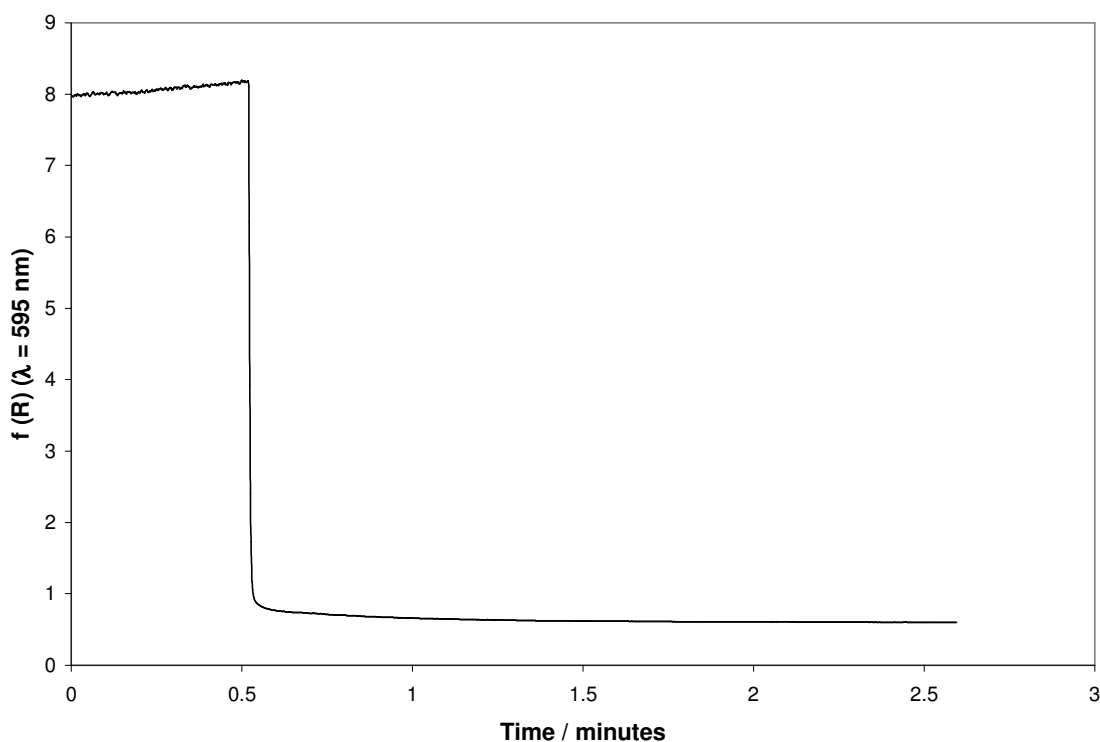


**Fig. 5.10** – Response of pigment when exposed to 100% CO<sub>2</sub> (g) at 21°C.

The MCP/silica/PE indicator is also fully reversible and responds quickly (few minutes) when exposed to 100% CO<sub>2</sub>, but has a slower recovery (*ca.* 2 hours to reach full recovery), as illustrated in Fig. 5.11. The differences in response and recovery times of the three indicators are due to diffusion effects, therefore variances are expected with different film thicknesses.

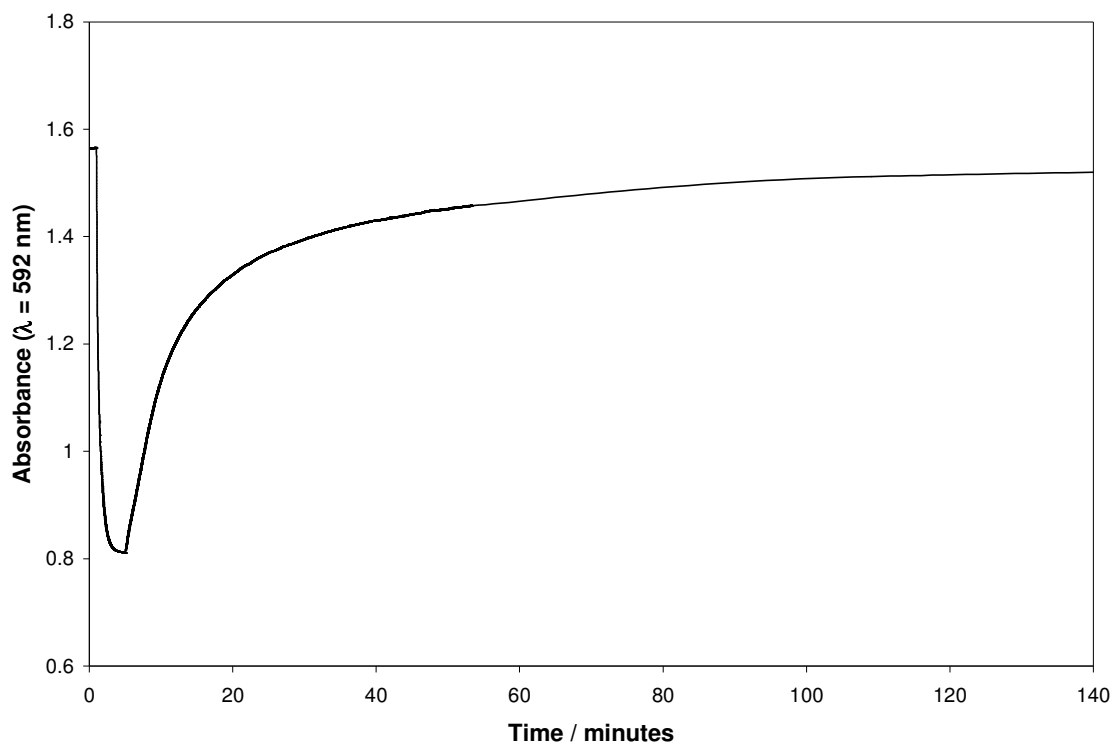


**Fig. 5.11** – Response and recovery of the MCP/silica/PE film when exposed to 100% CO<sub>2</sub>(g) and air at 21°C.

The plastic MCP/silica/PE film can be used repeatedly without any significant loss in performance, as is illustrated in Fig. 5.12, for such a film when exposed to a repeated cycle of air and 100% CO<sub>2</sub>.

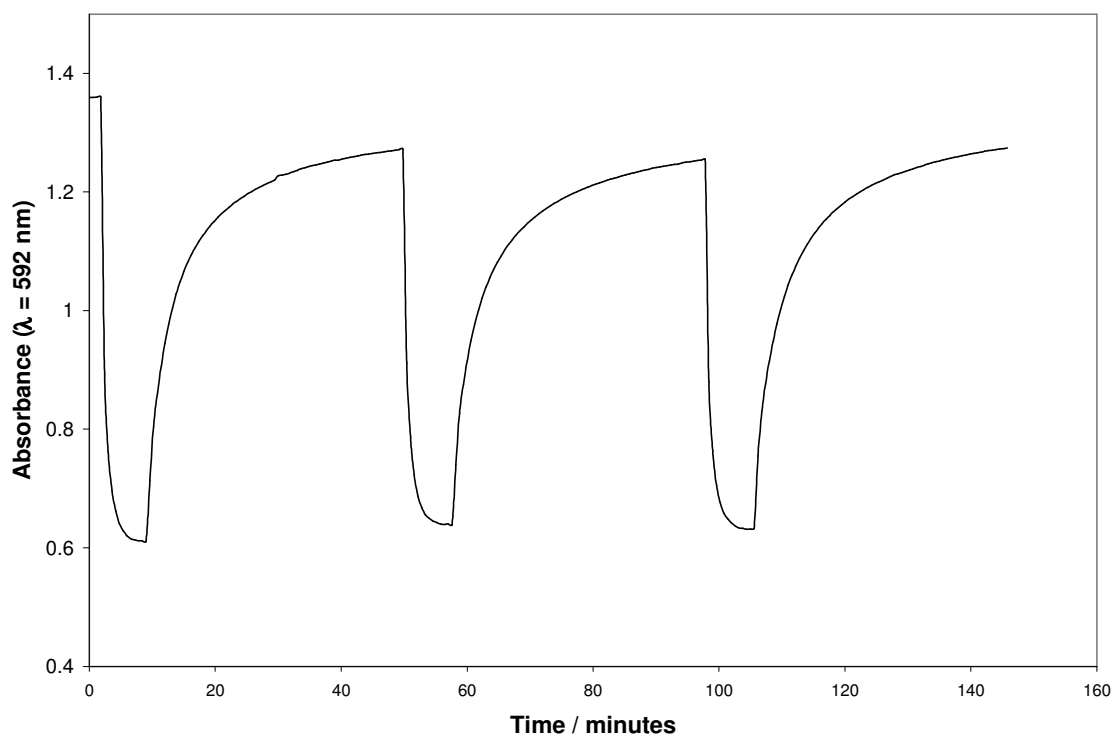


**Fig. 5.12** – Triplicate response and recovery of the MCP/silica/PE film when exposed to alternate 100% CO<sub>2</sub> and air purges at 21°C.

### 5.3.1.3 Effect of temperature on CO<sub>2</sub> sensitivity

A series of experiments were carried out on the MCP/silica/PE films in which the absorbance due to the deprotonated dye was recorded as a function of %CO<sub>2</sub> over a range of different temperatures. The absorbance versus %CO<sub>2</sub> curves for a range of different temperatures are illustrated in Fig. 5.13, along with the corresponding  $R$  versus %CO<sub>2</sub> plots. Values of  $\alpha$  (which is a measure of sensitivity), as a function of temperature were extracted from these plots.

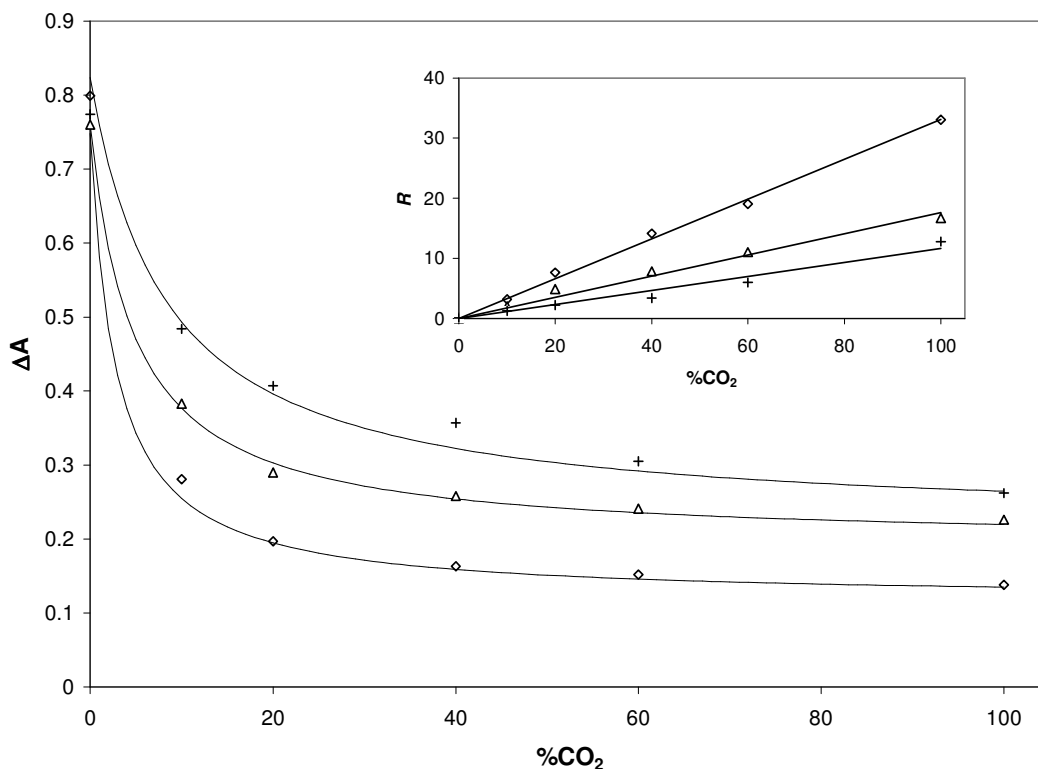


**Fig. 5.13** – The effect of temperature on the change of absorbance (at 592 nm) versus %CO<sub>2</sub>, where ◇ = 20°C, Δ = 25°C and + = 30°C.

As is common with most reported<sup>6,10</sup> CO<sub>2</sub>-indicators, the MCP/silica/PE indicator exhibits greater CO<sub>2</sub>-sensitivity as the temperature decreases (*ca.* 0.06% per °C). Assuming that the enthalpy and entropy changes associated with each of the equilibrium constants for the series of equilibria associated with the colour change, are not changeable within the temperature range studied, a Van't Hoff plot (i.e.  $\ln \alpha$  versus  $T^{-1}$ ) can be used to determine  $\Delta H$  and  $\Delta S$  for the overall reaction. The plot, as illustrated in Fig. 5.14, resulted in a good straight line from which values of  $-77 \pm 8$  kJmol<sup>-1</sup> and  $-288 \pm 57$  Jmol<sup>-1</sup>K<sup>-1</sup> were calculated for  $\Delta H$  and  $\Delta S$  respectively.

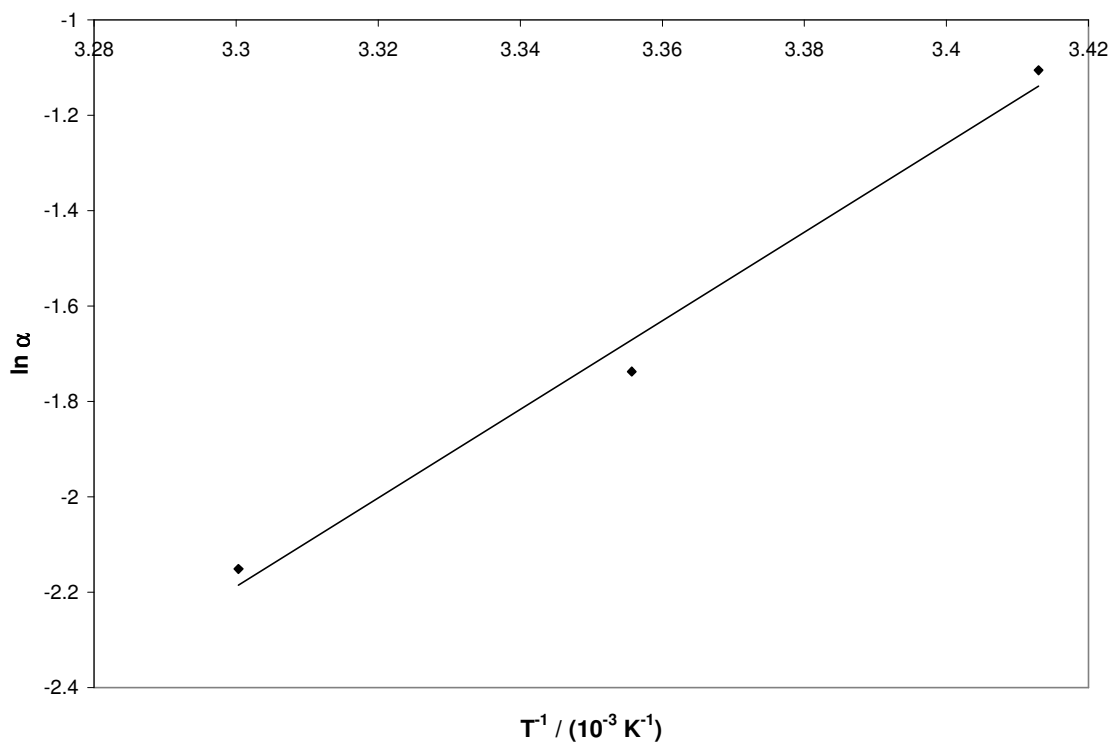


**Fig. 5.14** - Plot of  $\ln \alpha$  versus  $T^{-1}$  where  $\alpha$  is the gradient of an R versus %CO<sub>2</sub> plot as a function of temperature.

As expected and as previously reported<sup>6</sup> in literature, the solvent-based ink exhibits similar temperature sensitivity (*ca.* 7% per °C), typically  $-(28 \text{ to } 80) \text{ kJmol}^{-1}$  and  $-(211 \text{ to } 80) \text{ Jmol}^{-1} \text{ K}^{-1}$  for  $\Delta H$  and  $\Delta S$  respectively.

#### 5.3.1.4 Effect of humidity on CO<sub>2</sub> sensitivity

A study on the effect of humidity on the sensitivity of the MCP/silica/PE CO<sub>2</sub>-indicator revealed no change in  $\alpha$  (sensitivity) over the range 15 - 100 %RH at 21°C, as illustrated in Fig. 5.15. This is not surprising due to the highly hydrophobic nature of the polyethylene.

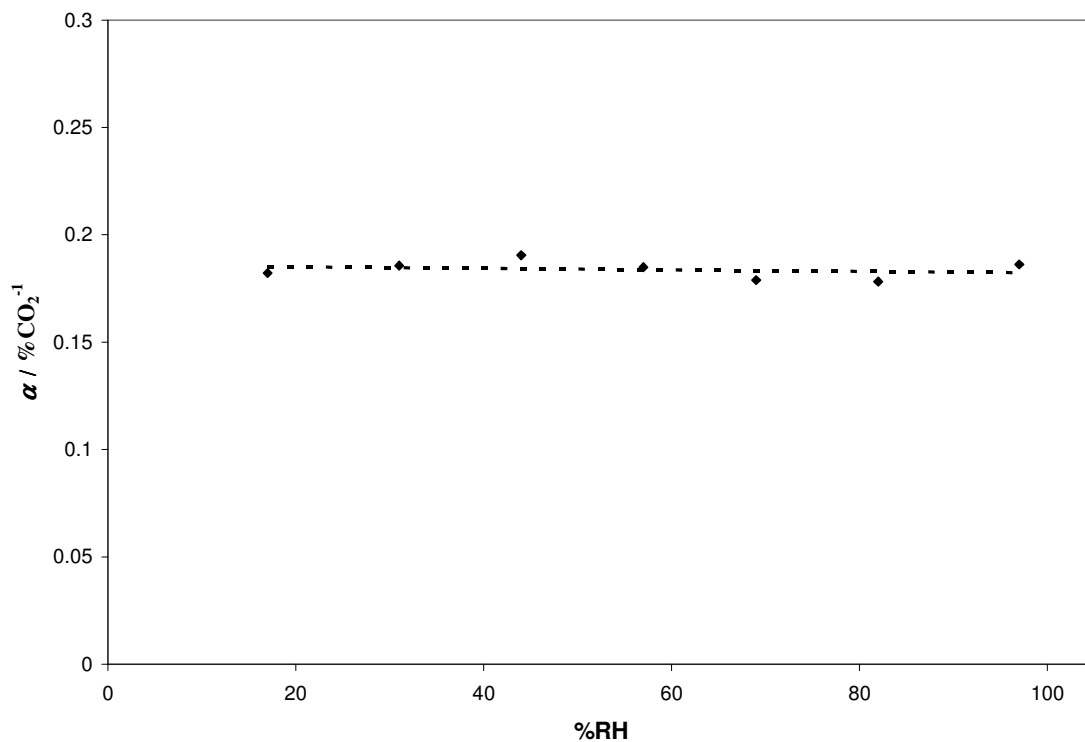


**Fig. 5.15** – Effect of humidity on sensitivity ( $\alpha$ ) for MCP/silica/PE CO<sub>2</sub>-indicator at 22°C.

Previous work reported in Chapter 3 showed that the typical solvent-based indicator is largely insensitive towards humidity over a wide range (20 – 70%RH). Similar findings are reported in the literature for other solvent based sensors.<sup>10</sup>

### 5.3.1.5 Stability

As noted earlier, it is known<sup>6,11,12</sup> that most solvent-based CO<sub>2</sub>-sensitive inks suffer irreversible acidification from interfering acidic gases, such as NO<sub>2</sub> and SO<sub>2</sub>. Indeed, all optical CO<sub>2</sub> indicators that operate *via* a pH changing dye are non-selective with regard to other acidic gases and the indicators reported in this paper are no different. This is a particular problem when it comes to film storage since NO<sub>2</sub> and SO<sub>2</sub> are typically present in an urban environment at levels of 150 and 50  $\mu\text{gm}^{-3}$ , respectively.<sup>12</sup> And so it is an important feature of the MCP /silica pigment plastic



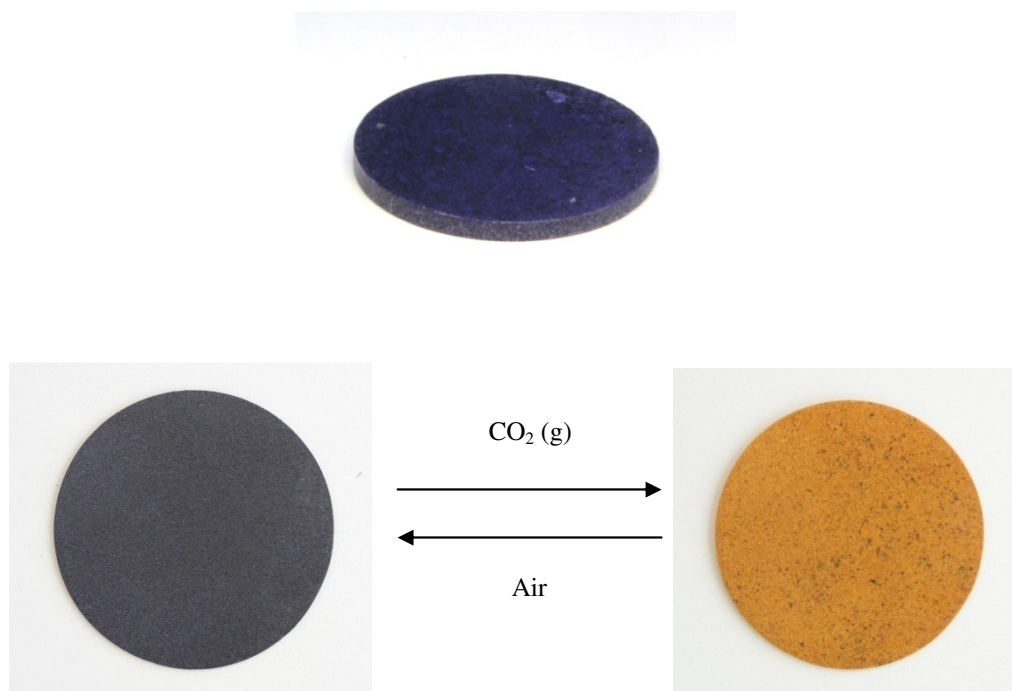
CO<sub>2</sub>-indicator films that they have a much greater longevity compared to that of a conventional solvent -based ink. For example, in our hands a solvent -based, indicator film will typically begin to acidify irreversibly, under ambient conditions within 1 week and be completely unusable within 5 weeks, when stored in a sealed container under ambient conditions. In contrast, the pigment/polymer composite film shows no visual sign of acidification after months of storage under the same sealed ambient, dark, conditions and works as if new. This is a significant advantage of the MCP /silica pigment plastic film indicators. Others<sup>11</sup> have shown the tolerance level of solvent based indicators for these acidic gases is only *ca.* 5 ppm. Interestingly, other work shows that the MCP /silica pigments have much higher tolerances (300 and 30 ppm for NO<sub>2</sub> and SO<sub>2</sub>, respectively), which helps explain their greater longevity when stored under ambient air.

### 5.3.2 Pressed pigment discs

Compressing the silica pigments into a disc using the press was attempted; however the films were extremely brittle. To improve the integrity of the films, wax was added to the silica to assist in the binding. A variety of waxes were investigated including candle wax, candelilla wax, beeswax, stearic acid and tea-light candle wax (thought to be made primarily from paraffin wax i.e. mixture of long chain hydrocarbons). Good discs were produced, but inevitably the response and the recovery of the discs were compromised. It was aimed to keep the disc thickness as low as possible, thereby increasing the permeability. Due to the presence of the wax particles in the silica, a speckled pattern is observed in the films. This can be decreased, to an extent, by mixing and grinding the wax/silica mixture repeatedly, but the wax still prevents a uniform colour change upon exposure to carbon dioxide.

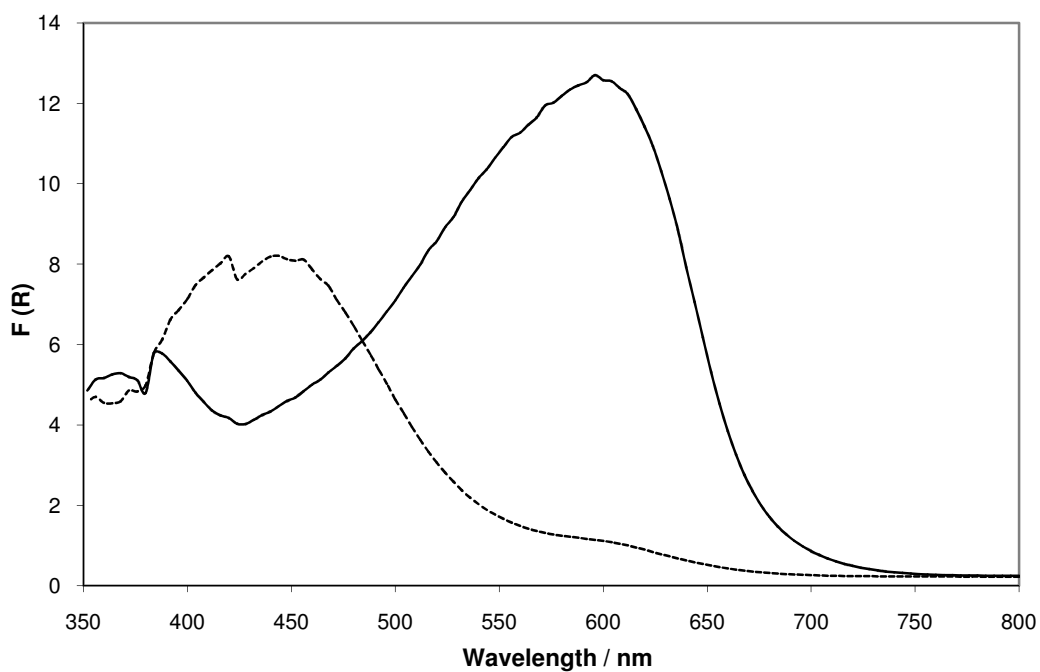
Approximately 0.5 g of a 30% w/w wax/silica mix, pressed at 10 - 12 tons for a few minutes is required to produce a whole, unbroken disc. Thinner discs break very easily, and rarely came out whole.

Below are pictures of the 30% w/w wax silica disc showing the colour change when exposed to CO<sub>2</sub>.



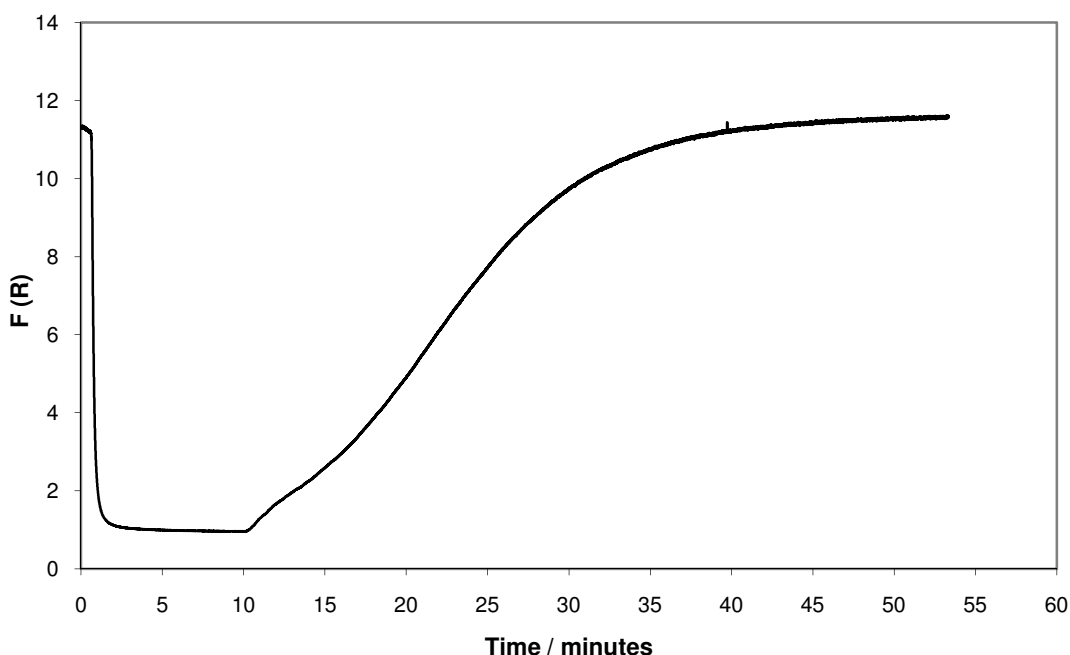
**Fig. 5.16** – Colour change of pressed silica discs when exposed to CO<sub>2</sub> (g).

Fig. 5.17 illustrates the diffuse reflectance spectra of the disc in air (solid line) and in the presence of carbon dioxide (dashed line).



**Fig. 5.17** – Diffuse reflectance spectra of wax/silica disc in the presence of air (—) and also carbon dioxide (- - -) at 22°C.

As previously discussed, the response of the disc to carbon dioxide is reasonable, but the recovery is slower, as observed in Fig. 5.18. The recovery of the discs towards a purge of air is immediate but does not fully recover until after > 40 minutes.



**Fig. 5.18** – Response and recovery of 30% w/w wax/silica disc towards carbon dioxide at 22°C.

The work on pressed disks is interesting but lacks a specific application, which is further hampered by their brittle form. Therefore the main focus of this work is the development of flexible pigmented polymer films.

## 5.4 Application

The incorporation of the CO<sub>2</sub>-sensitive pigment into a flexible and extrudable thermoplastic makes applications in food-packaging highly desirable. Further research and development on the product will hopefully provide thin intelligent plastics capable of giving colourimetric responses indicating the quality of the product held within the package, whilst at the same time being an integral part of the product packaging. Fig. 5.19 below illustrates the intelligent plastic as a leak indicator. The meat was packaged under CO<sub>2</sub> gas and sealed, using a standard industrial heat sealer. As observed in Fig. 5.19, the indicator was initially bright

yellow. The packaging was then intentionally ruptured, causing the MAP gas to leak out. At the same time, the indicator responds to the decrease in CO<sub>2</sub> concentration and slowly reverts back to its deprotonated, blue form.

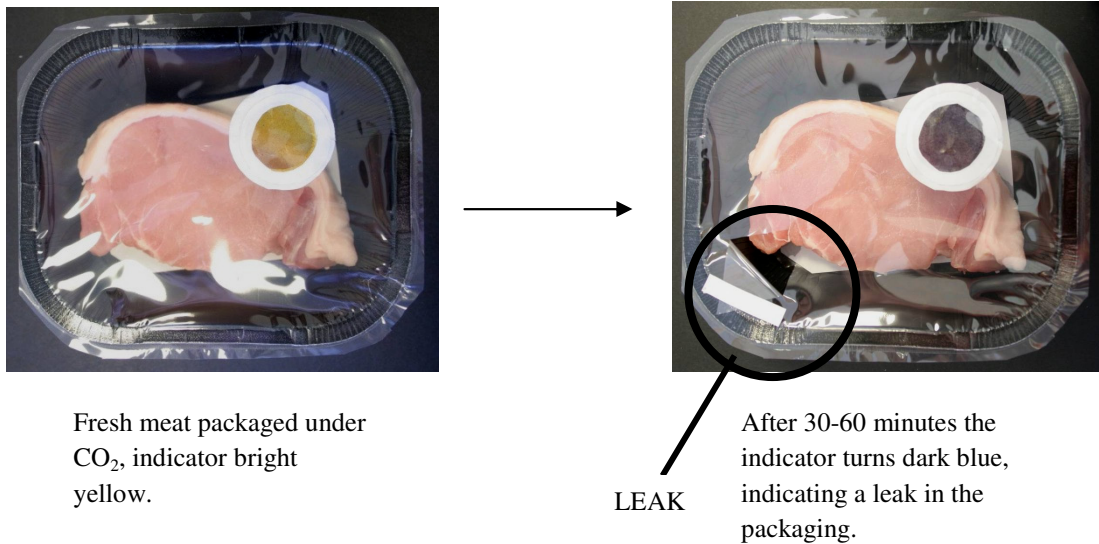


**Fig. 5.19** – Illustration of the intelligent plastic being used as a leak indicator in MAP packaged foods.

## 5.5 Further Work

Due to the success of the initial studies carried out in this project, which resulted in a publication (see appendix) and a published patent, work is now being funded to extend the technology to a commercialisation level, where these indicators can be used in intelligent food packaging. This work has received much interest from the media<sup>13</sup> and subsequently the food packaging industry. The main development of this more recent work is the capability to produce extruded polymer films opposed to heat pressed circular disks. Fig. 5.20 illustrates the steps involved to prepare thin extruded pigmented polyethylene films which have the same sensing capabilities as previously developed. Firstly the pigment is prepared (**A**), which is then mixed with the polymer to form pigmented polymer chips (masterbatch) (**B**), which is then extruded into a thin film (**C**).

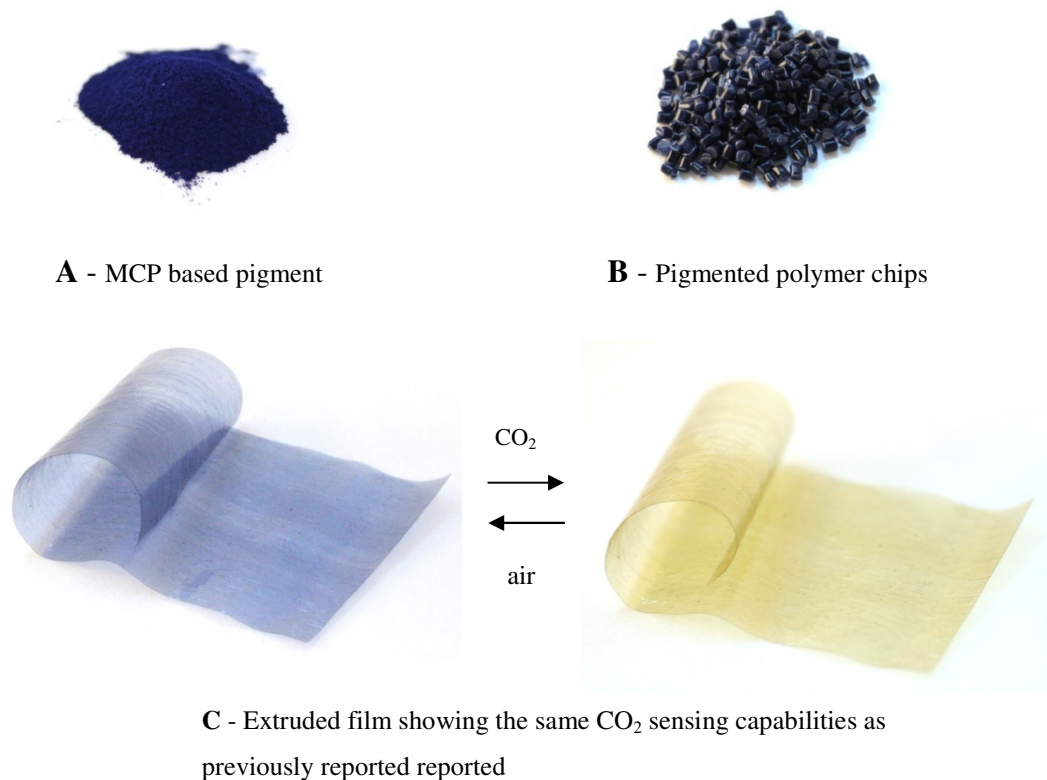


**Fig. 5.20** – Photographs of pigment, polymer chips and extruded MCP film.

## 5.6 Extended work on intelligent pigments and plastics

There is scope to develop a wide variety of intelligent pigments for a number of applications. Although not the main focus of this project, a number of pigments and pigmented polymer films were prepared using a variety of dyes, for a number of applications.

### 5.6.1 Breath responsive pigments

Capnography is the study of  $\text{CO}_2$  levels in exhaled breath, these levels provides vital information during many medical procedures. As discussed in Chapter 1, a number of indicators have been developed to aid the field of capnography. To prepare a pigment able to give a colourimetric response at levels of  $\text{CO}_2$  contained in human breath ( $\sim 5\%$ ), dyes with a higher  $\text{pK}_a$  than *m*-cresol purple were used. The phthalein dyes are a family of dyes which contain a lactone species. In the presence of acid, the ring closes forming a lactone, breaking the conjugation, and hence quenching the colour. The pigments quickly changed colour when breathed upon, as illustrated in Fig. 5.21.

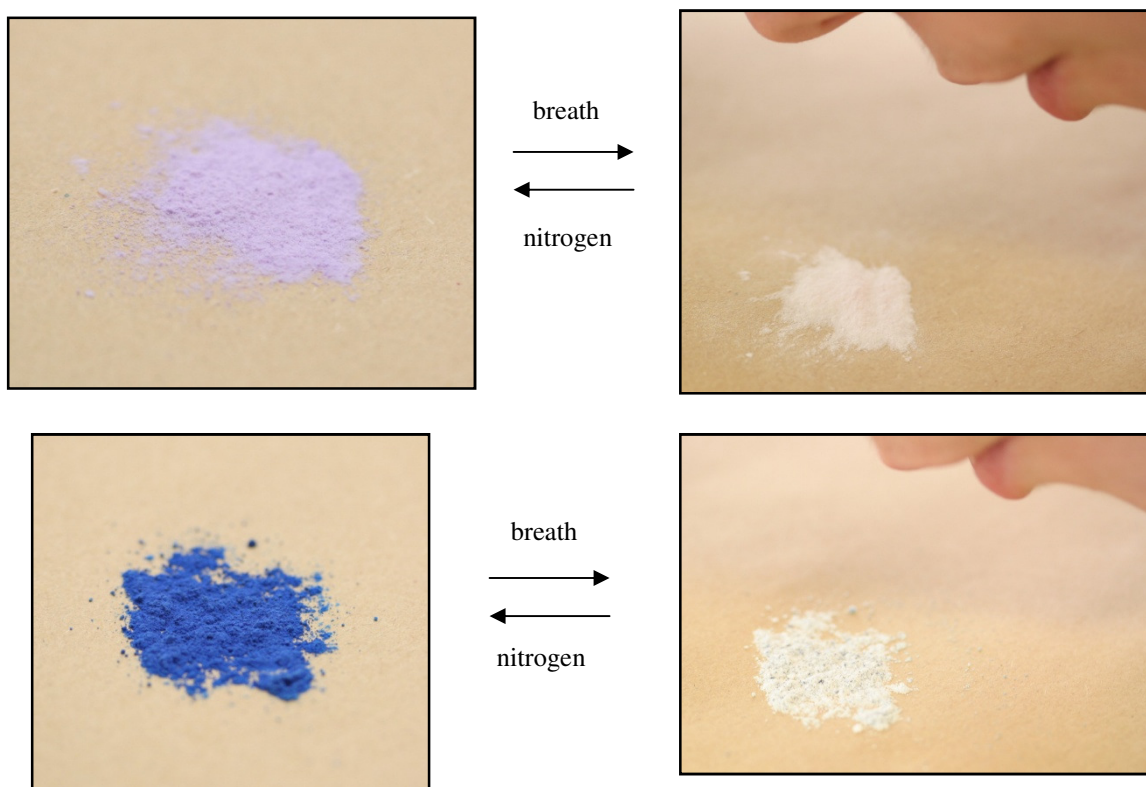


**Fig. 5.21** –  $\text{CO}_2$  pigments responding to levels on  $\text{CO}_2$  contained in human breath. Top: *o*-cresolphthalein based pigment, bottom: thymolphthalein based pigment.

Unfortunately these pigments were found to be too sensitive to CO<sub>2</sub>, slowly changing colour even under ambient levels of CO<sub>2</sub>. After a number of uses, the pigments gradually lost their intense colour as the dye converted to its colourless, acidic form. Hence it was impossible to prepare a pigmented polymer film for CO<sub>2</sub> breath analysis. These problems may be overcome by identifying different dyes, and altering the base concentration contained within the pigment formulation.

### 5.6.2 Oxygen indicating pigments and plastics

The use of semiconductor photocatalysis to create oxygen sensors has been widely studied and reported<sup>14,15</sup> in literature. The application of this technology to create intelligent pigments and their incorporation into polymers, have great potential for use in smart food packaging.

TiO<sub>2</sub> can be easily coated with a redox dye (methylene blue) and a sufficient sacrificial electron donor (DL-threitol), forming a blue pigment which changes colour upon irradiation under UVA light. In a typical experiment, the MB/TiO<sub>2</sub>/DL-Threitol solvent- and water-based powders were exposed to UVA light for approximately 1 minute (or less) to observe a distinct blue to white colour change (Fig. 5.22). Recovery was observed in air.

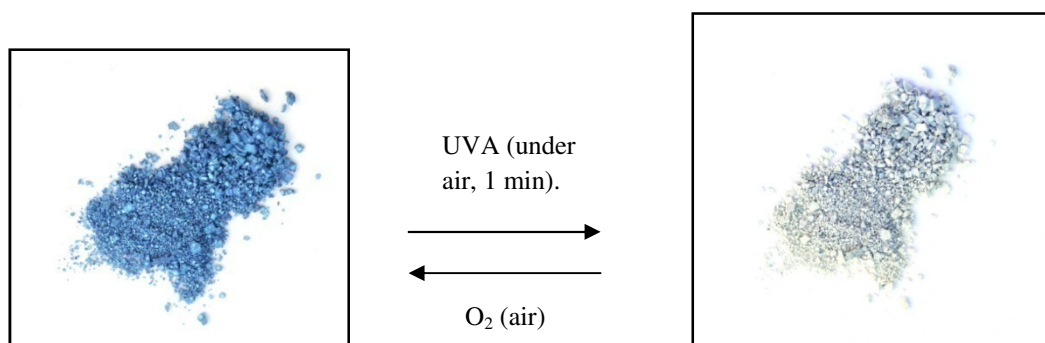


**Fig. 5.22** – Solvent-based MB/TiO<sub>2</sub>/DL-Threitol pigment irradiated under UVA light and its recovery in air.

Full recovery back to the original blue colour of the pigments may take up to an hour in air. A similar colour change is observed when the pigment is dispersed in polyethylene. In a typical experiment the films were exposed to UVA light, under



nitrogen, for approximately 4 - 5 minutes to observe the distinct colour change observed in Fig. 5.23.

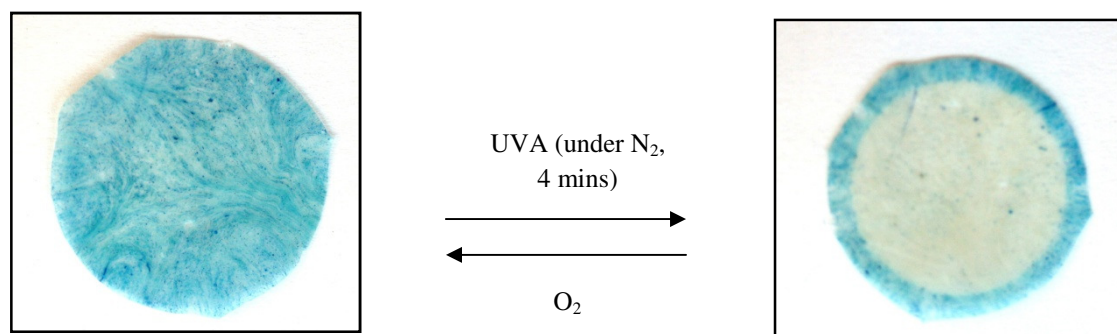


**Fig. 5.23** – Solvent-based intelligent  $O_2$ -indicating plastic irradiated under UVA light and its recovery in air.

This first example of an ‘extrudable’ plastic oxygen indicating sensor proves to be quick to respond and easy to prepare.

It is obvious that there is much scope for the further development, which would hopefully extend the sensitivity and potential for a plastic, extrudable oxygen indicator.

### 5.6.3 Luminescent oxygen indicating pigments and plastics

Many examples of novel fluorescent optical indicators for the detection of oxygen have been reported in literature<sup>4,5,16-19</sup>. The choice of lumophores have been dominated by ruthenium diimine complexes and platinum and palladium porphyrin-based dyes. Typically, a dye solution would be added to a polymer solution, along with a suitable plasticizer. The resulting ink solution would be cast onto glass plate supports, forming a thin sensing film. In this work, luminescent dyes are coated onto silica powders and incorporated into different thermoplastics which results in flexible plastics with luminescent oxygen sensing properties.

Fig. 5.24 illustrates a photograph of a typical dye (Pt (II) OEP) coated powder and a heat pressed plastic film with the silica dispersed throughout the plastic.



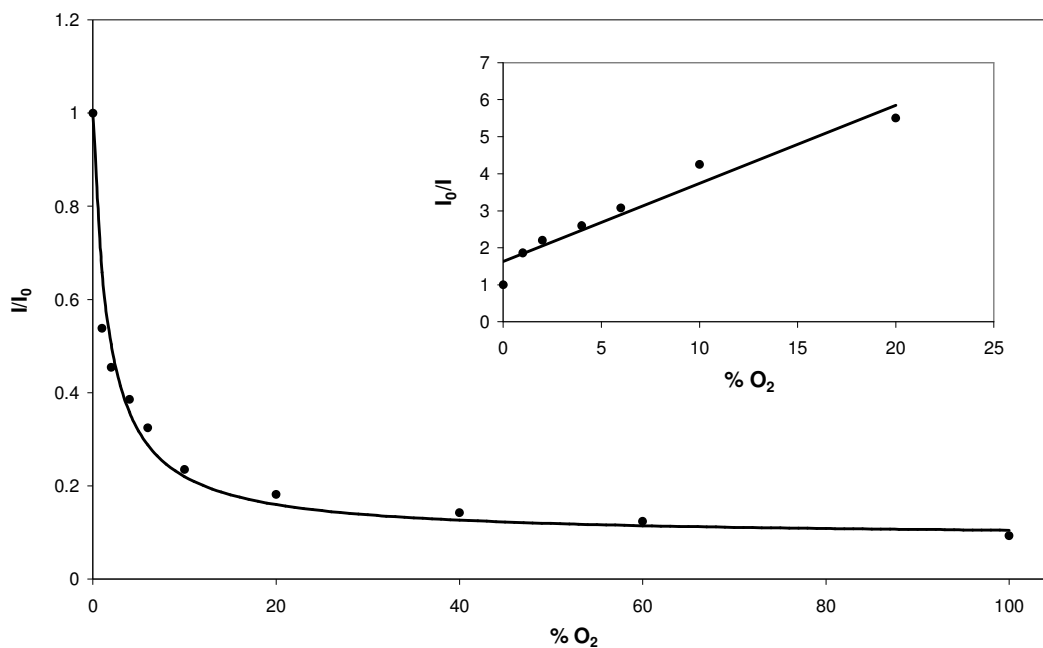
**Fig. 5.24** – Photograph of Pt (II) OEP coated hydrophobic silica and the silica dispersed in a polyethylene film.

In a typical experiment the thin plastic films luminesced under UVA light. The fluorescence was quenched in the presence of oxygen. The change in fluorescence was monitored using a fluorimeter as the oxygen concentration was increased. The results are shown in the form of a Stern-Volmer plot of the variation of emission intensity with ambient partial pressure of oxygen. The results obeyed the Stern-Volmer equation:

$$I_0/I = 1 + K_{sv}pO_2 \quad (5.4)$$

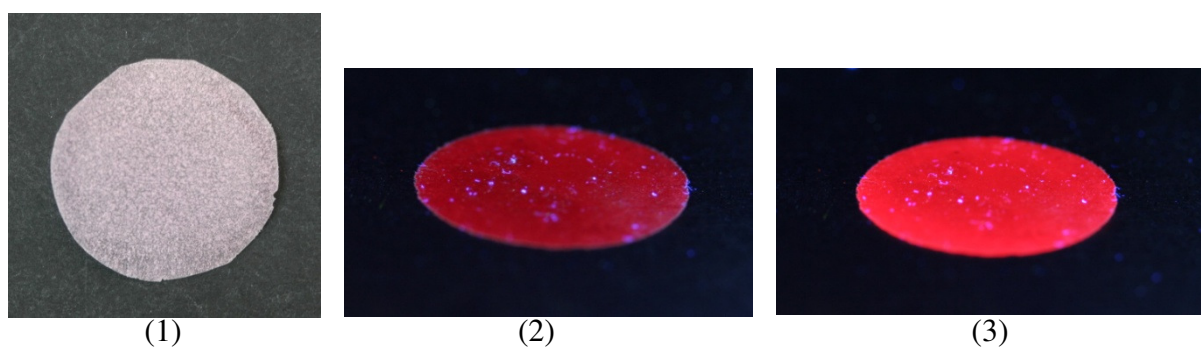
where  $K_{sv}$  is the Stern-Volmer constant.

Fig. 5.25 shows the plot for the Pt (II) OEP/Silica/ Polyethylene sample.



**Fig. 5.25** – Observed change in the relative luminescent intensity at 644 nm ( $\lambda_{\text{excit}} = 535$  nm), as a function of  $p\text{O}_2$  for Pt(II)OEP/Silica/Polyethylene plastic indicator at 22°C. The insert diagram shows the corresponding Stern-Volmer plot of the data, revealing  $m = 0.211$ ,  $c = 1.63$  and  $R^2 = 0.9387$ .

Below are photos of the Pt(II)OEP/Silica/polyethylene sample (1) in normal lighting conditions (2) under UVA light in air and (3) under UVA light in nitrogen.



**Fig. 5.26** - Photographs of the Pt (II) OEP/Silica/polyethylene sample (1) in normal lighting conditions (2) under UVA light in air (20% O<sub>2</sub>) and (3) under UVA light in nitrogen.

From the photos in Fig. 5.26, it is clear that the intensity of luminescence increases as the oxygen concentration decreases. The response to oxygen is further shown in

Fig. 5.27, where the luminescence is quenched when a stream of oxygen is applied to the indicator in the fluorimeter. The luminescence is recovered when a stream of nitrogen is purged over the indicator.

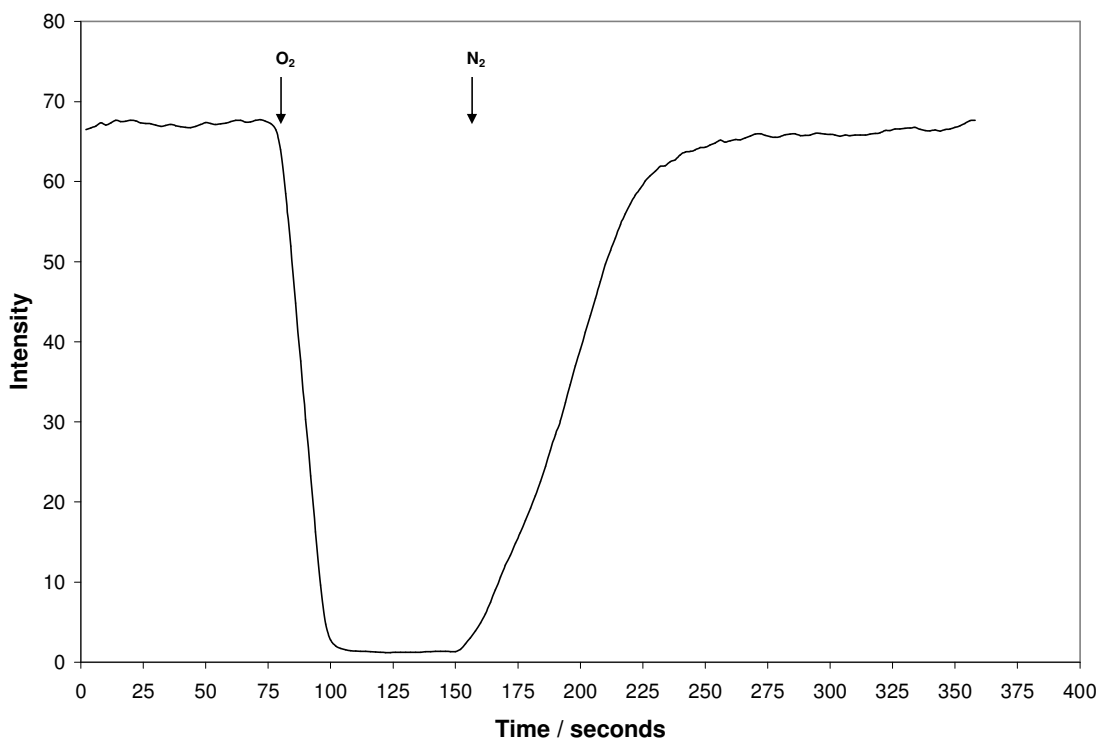
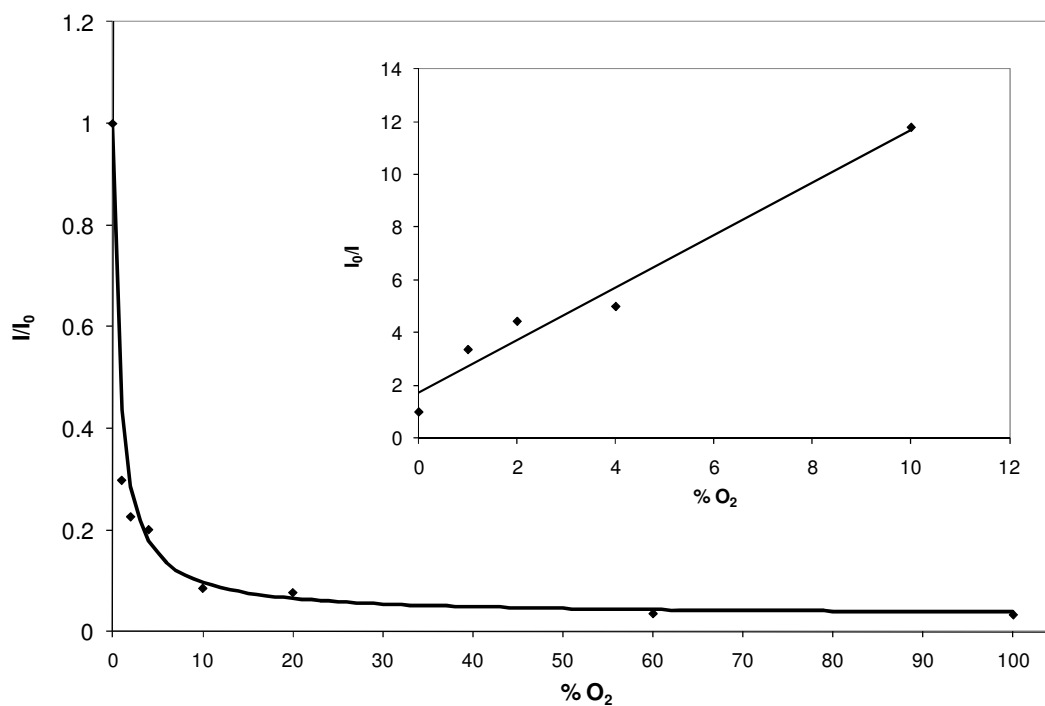


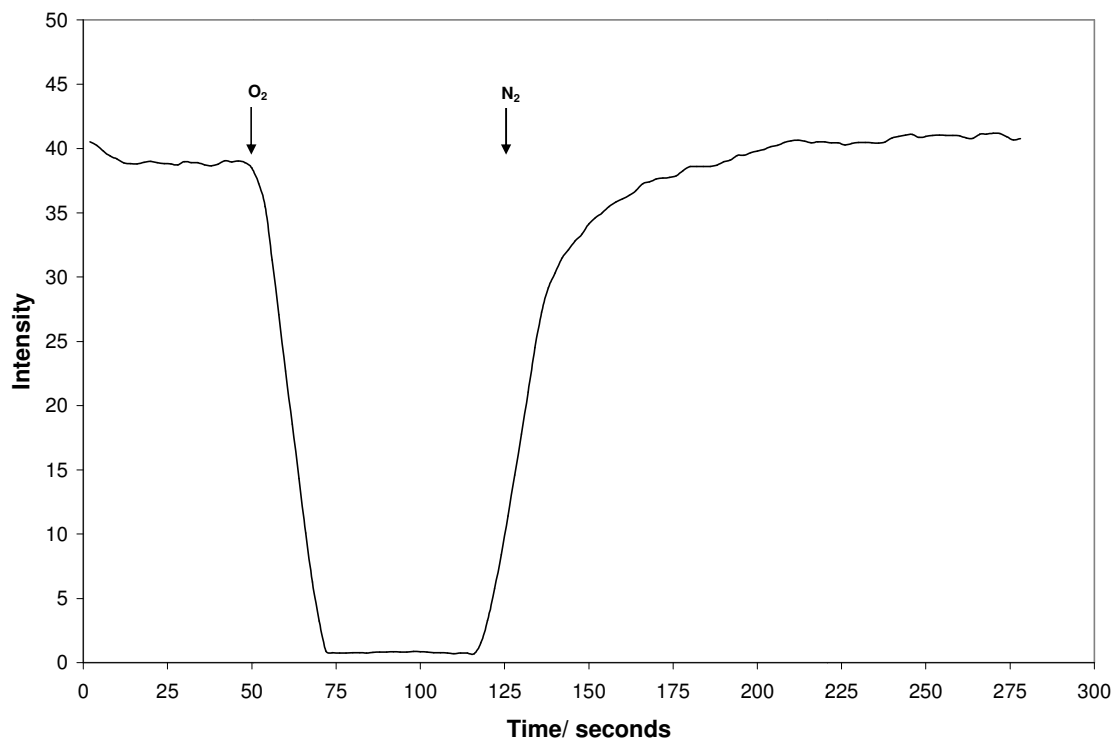
Fig. 5.27 – Response of the indicator to 100% O<sub>2</sub> and recovery at 21°C.

Similar experiments were carried out for a polyethylene oxide film. Fig. 5.28 shows the observed change in the relative luminescent intensity, as a function of  $pO_2$  for the Pt (II) OEP/Silica/Polyethylene oxide sample, along with the Stern-Volmer plot.



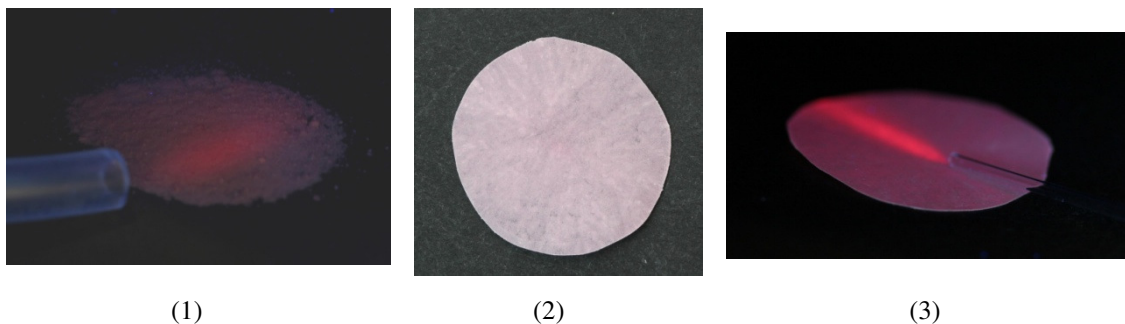
**Fig. 5.28** – Observed change in the relative luminescent intensity at 644 nm ( $\lambda_{\text{excit}} = 535$  nm), as a function of  $pO_2$  for Pt(II)OEP/Silica/Polyethylene oxide plastic indicator at 21°C. The insert diagram shows the corresponding Stern-Volmer plot of the data, revealing  $m = 0.9963$ ,  $c = 1.7195$  and  $R^2 = 0.9697$ .

Fig. 5.29 also illustrates the luminescence quenching by oxygen.



**Fig. 5.29** - Response of the indicator to 100% O<sub>2</sub> and recovery at 21°C.

The photos in Fig. 5.30 show (1) the Pt(II) OEP coated silica luminesce under UVA light when nitrogen is being blown onto the sample, (2) Pt(II)OEP/Silica/polyethylene oxide sample under normal light and (3) the Pt(II)OEP/Silica/polyethylene oxide sample under UVA light with nitrogen being blown onto the sample.



**Fig. 5.30** – (1) Pt(II)OEP coated silica luminescence under UVA light when nitrogen is being blown onto the sample, (2) silica dispersed in polyethylene oxide under normal lighting conditions and (3) the same sample exposed to UVA light with a stream of N<sub>2</sub> being blown onto the surface.

It is evident that this sample is slightly more sensitive than the polyethylene based sample. No luminescence is observed under UVA light until the sample is exposed to nitrogen, showing that the level of oxygen in air is sufficient to quench any luminescence in this system. Whereas luminescence is still observed in the presence of air for the polyethylene based sample, as shown in Fig. 5.26.

Alternatively, various ruthenium based dyes e.g.  $\text{Ru(dpp)}_3^{2+} (\text{Ph}_4\text{B}^-)_2$ ,  $\text{Ru(bpp)(Ph)}_4\text{B}$ ,  $\text{Ru(bpy)}_3^{2+} (\text{Ph}_4\text{B}^-)_2$  can be used instead of Pt(II)OEP. All of the dyes form a yellow powder when adsorbed onto silica. The powders luminesce with an orange glow under UVA light and in the absence of oxygen. They can, like the platinum based sensor, be dispersed into a thermoplastic (e.g. polyethylene) and retain their oxygen sensing capabilities. Fig. 5.31 illustrates the powders and plastics luminescing under UVA light and in the absence of oxygen ( $\text{N}_2$ ). When oxygen gas is blown over the samples the luminescence is quenched.

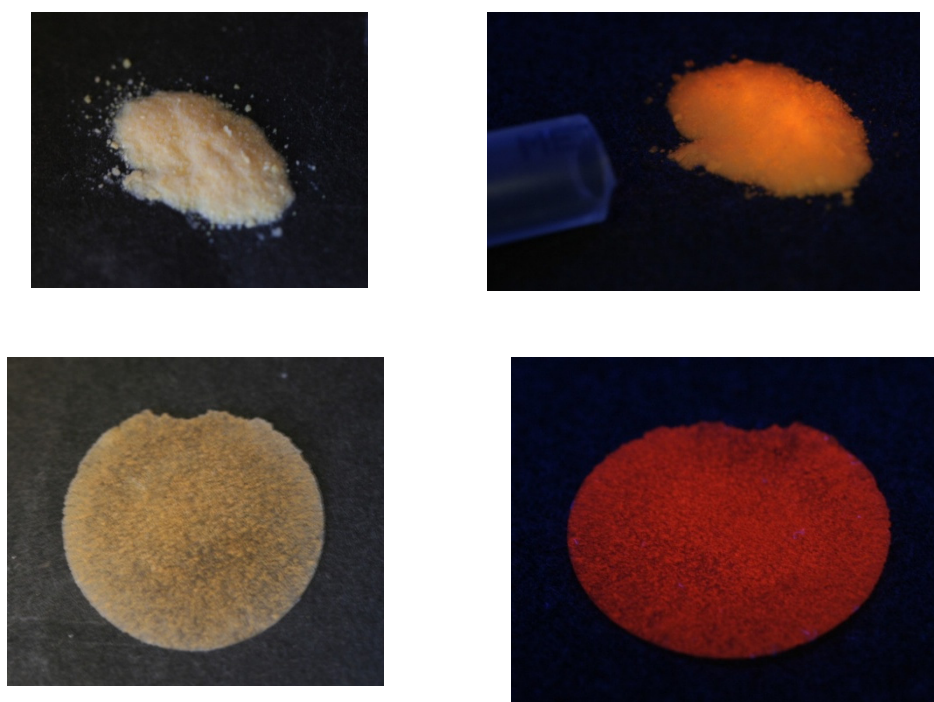


**Fig. 5.31** – Top left:  $\text{Ru(dpp)}_3^{2+} (\text{Ph}_4\text{B}^-)_2$  based powder under ambient conditions, top right: same powder under UVA light and exposed to a stream of nitrogen gas. Bottom left:  $\text{Ru(dpp)}_3^{2+} (\text{Ph}_4\text{B}^-)_2$  based powder dispersed in polyethylene, under ambient conditions, bottom right: same sample under UVA light and exposed to a stream of nitrogen gas.

These luminescent based oxygen indicators once again show the potential for a wide variety of indicators to be incorporated into extrudable polymer films, which extends the sensors' capabilities to be used in a variety of applications.

#### **5.6.4 Volatile amine indicating pigments and plastics**

Although not carried out as part of this work, a complimentary study was carried out in our group where a series on volatile amine indicating pigments and plastics were developed. The primary application of these indicators is to detect spoilage gases (volatile amines), known to be released as meat (particularly fish products) as they spoil. This novel technology allows a more accurate real time analysis of the freshness of the food, instead of relying on set 'use-by' dates. This technology is being developed alongside the intelligent plastic CO<sub>2</sub> indicators.

### **5.7 Conclusions**

It is evident that there is great potential for these new series of intelligent pigments and plastics to make a significant impact on the food packaging market. Intelligent pigments, when dispersed into an extrudable thermoplastic, create a series of commercially relevant indicators. The plastic CO<sub>2</sub> indicator has shown to be stable than previously developed solvent-based indicators. As is common with most CO<sub>2</sub> indicators, the indicator's sensitivity toward CO<sub>2</sub> decreases with increasing temperature. It is quick to respond to CO<sub>2</sub> and recovers in a time which would allow it to be used as an effective lead indicator. It shows no change in sensitivity towards a wide range of humidities. Further work has shown that the potential for these indicators to be developed for a range of analytes is promising. Each indicator has a striking colour change, is quick to respond and can easily be incorporated into traditional packaging materials, allowing a low cost production.



## 5.8 References

1. *Novel food packaging techniques*, Woodhead Publishing Limited, 2003.
2. S. K. Lee, M. Sheridan and A. Mills, *Chem. Mat.*, 2005, **17**, 2744-2751.
3. A. Mills, *Chem. Soc. Rev.*, 2005, **34**, 1003-1011.
4. A. Mills and A. Lepre, *Anal. Chem.*, 1997, **69**, 4653-4659.
5. A. Mills and F. C. Williams, *Thin Solid Films*, 1997, **306**, 163-170.
6. A. Mills, Q. Chang and N. McMurray, *Anal. Chem.*, 1992, **64**, 1383-1389.
7. A. Mills, A. Lepre and L. Wild, *Sens. Actuators B*, 1997, **38-39**, 419-425.
8. A. Mills and Q. Chang, *Anal. Chim. Acta*, 1994, **285**, 113-123.
9. J. Brandrup, E. H. Immergut and E. A. Grulke, *Polymer handbook*, 1999.
10. C. R. Schroeder and I. Klimant, *Sens. Actuators B*, 2005, **107**, 572-579.
11. J.F.Fernandez-Sanchez, R. Cannas, S. Spichiger, R. Steiger and U. E. Spichiger-Keller, *Sens. Actuators B*, 2007, **128**, 145-153.
12. H. N. McMurray, *J. Mater. Chem.*, 1992, **2**, 401-406.
13. <http://www.bbc.co.uk/news/uk-scotland-glasgow-west-12128120>, (accessed, 18/06/11).
14. A. Mills and D. Hazafy, *Analyst*, 2008, **133**, 213-218.
15. S. K. Lee, A. Mills and A. Lepre, *Chem. Commun.*, 2004, 1912-1913.
16. S. R. Ricketts and P. Douglas, *Sens. Actuators B*, 2008, **135**, 46-51.
17. B. F. Lei, B. Li, H. R. Zhang, S. Z. Lu, Z. H. Zheng, W. L. Li and Y. Wang, *Adv. Funct. Mater.*, 2006, **16**, 1883-1891.
18. S. Z. Topal, K. Ertekin, D. Topkaya, S. Alp and B. Yenigul, *Microchim. Acta*, 2008, **161**, 209-216.
19. H. R. Zhang, B. Li, B. F. Lei, W. L. Li and S. Z. Lu, *Sens. Actuator B-Chem.*, 2007, **123**, 508-515.

## Chapter 6: Polyoxometalate based oxygen indicator

---

### 6.1 Introduction

Polyoxometalates (POM) are a large class of inorganic compounds which have been the focus of research for many years.<sup>1</sup> Their interesting redox chemistry attracts the development of such compounds to be used in indicator technologies. Previous work<sup>2,3</sup>, albeit limited, have demonstrated POMs can be incorporated into thin polymer films which change colour upon UV radiation<sup>3</sup>.

Feng and co-workers published<sup>4,5</sup> a number of papers which describe the development of photochromic films which comprise a variety of POMs in a number of polymer matrices (polyacrylamide<sup>6</sup> and bisvinyl-A/N-vinylpyrrolidone crosslinked polymer<sup>4</sup>). Under UV irradiation, such thin films turn blue and the studies note the affect that oxygen has on the reversibility of the colour change; quickened reversibility with increasing oxygen concentration. Interestingly, they do not recognise the potential for such systems to be used as indicators, and do not investigate the characteristics of the colour changes in terms of their ability to indicate an analyte, neither for UV nor oxygen. A similar study<sup>3</sup> was published by Gong *et al.* where they describe a PVA/H<sub>6</sub>P<sub>2</sub>W<sub>18</sub>O<sub>62</sub> hybrid membrane. They report that the colour of the films changed from light blue to deep blue with increasing irradiation time and POM content. The recovery of the films to their original colourless form are reported to be > 50 hours. However, the recovery was fastest for films containing higher quantities of POM. They attribute this trend to the instability of the oxidised state of the organic matrix. Once again, although extensive film characterisation is reported, no specific application is noted.

The aim of this work is to build upon this previous work, extending the capability of POMs to be used as indicators for important, commercially useful analytes, in particular for O<sub>2</sub>. The application of POM-based indicators in the food packaging industry will be investigated.

The formation of heteropolybrowns after a number of consecutive irradiations of polyoxometalates has been observed and reported<sup>6</sup> in literature. Such colour deterioration would be considered an obstacle to the commercialisation of POM-based indicators. Hence, the suppression of such discolouration will be explored.

## 6.2 Experimental

### 6.2.1 Ink and pigment formulations

Unless specified, all chemicals were purchased from Sigma Aldrich in the highest purity available. The water used to make all aqueous solutions was double distilled and deionised. High purity gases were obtained from BOC gases. Spectrophotometric measurements were carried out using a Carey 50 spectrophotometer. Thin films were produced using a spin coating technique, with a Spin Coater Model 4000-1 (Electro-Micro Systems).

A typical phosphotungstic acid ( $\text{H}_3\text{PW}_{12}\text{O}_{40}$ , PWA) ink was prepared by dissolving 3 g of PWA in 1 ml of distilled water and adding this to 2 g of 10% w/v polyvinyl alcohol (MW = 146,000 – 186,000) in water. 500 mg of glycerol were added to the mixture, which was then stirred at room temperature for approximately 30 minutes. The composition of the ink can be summarised as PVA/PWA/glycerol in pphr as follows: 100/1500/25, where pphr = parts per hundred resin.

A glycerol-free version of the PVA/PWA ink was prepared by dissolving 3 g of PWA in 1 ml of distilled water and adding this to 2.5 g of 10% w/v polyvinyl alcohol (MW = 146,000 – 186,000) in water. The mixture was then stirred at room temperature for approximately 30 minutes. The composition of the ink can be summarised as PVA/PWA in pphr as follows: 125/1500 pphr.

A typical PWA-based pigment was prepared by mixing 3.5 g phosphotungstic acid with 2.0 g hydrophobic silica and 2.5 g DL-threitol or 1,6-hexanediol. Approximately 100 ml of acetone were added and the solution sonicated until all of the DL-threitol/1,6-hexanediol was dissolved. The solvent was then removed under reduced pressure and the resulting powder ground until a fine powder was obtained. In order to make the corresponding PWA-based oxygen-indicating plastic, 0.8 g of the hydrophobic *pigment* were added to 4.0 g of powdered polyethylene (Alfa Aesar, LDPE, 1000  $\mu\text{m}$ ) and the mixture ground up using a mortar and pestle. A small sample (*ca.* 0.3 - 0.4 g) of the powder mixture was then heat pressed using a Specac Atlas™ Series Heated Platens at 115°C to create a clear PWA/DL-threitol/silica pigmented polyethylene film (0.1 mm thick).

### 6.3 Results and discussion

Phosphotungstic acid (PWA) has a very high acidity. Investigation of its acidity in acetic acid shows that the three protons dissociate independently rather than sequentially, and the acid sites are of the same strength<sup>7</sup> ( $\text{pK}_a = -13.16$ )<sup>8</sup>. Due to this high acidity, many commonly used polymers are degraded immediately upon contact with PWA. As a consequence, hydroxyethylcellulose (HEC), ethylcellulose (EC) and polyvinyl butyral (PVB) were quickly dismissed as potential polymers for the ink due to their degradation under high acidity. However, polyvinyl alcohol (PVA) and polyacrylamide (PAM) were found to be stable at very low pHs. The structures of these polymers are found in Fig. 6.1.

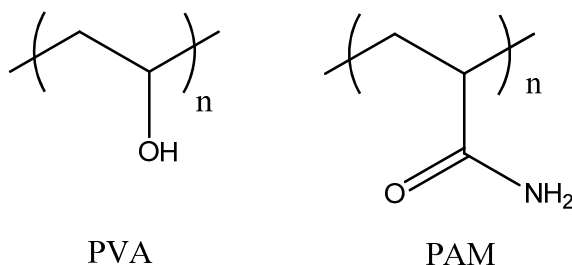


**Fig. 6.1** – Structures of polyvinylalcohol (PVA) and polyacrylamide (PAM).

The sodium salt of phosphotungstic acid (NaPWA) was used in the methylene blue based ink due to its slightly higher pH in solution (typically 10 mg/ml aqueous solutions of phosphotungstic acid and sodium phosphotungstate have pHs of 1.7 and 2.1, respectively). Silicotungstic acid ( $\text{H}_4\text{SiW}_{12}\text{O}_{40}$ ) is another commonly used POM which can be used to prepare the indicators described above. However, results show that indicators containing silicotungstic acid take slightly longer to respond to UVB, compared to phosphotungstic acid, which agrees with studies published in literature<sup>9,10</sup>. Hence, phosphotungstic acid was the preferred choice of POM in all further work.

### 6.3.1 PWA-based oxygen indicator

#### 6.3.1.1 Characteristics of standard PVA/PWA/glycerol indicator

Photographs of a standard PVA/PWA/glycerol indicator were taken before and after irradiation under UVB light and the results are illustrated in Fig. 6.2.

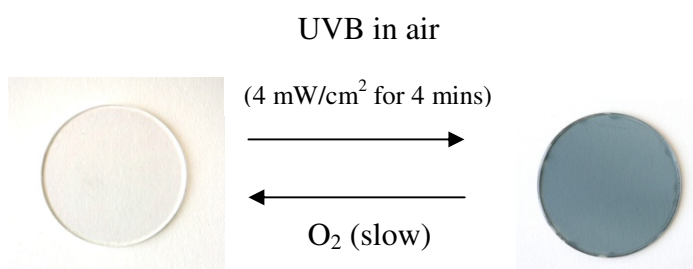


**Fig. 6.2** – Photographs of a standard oxygen indicator.

Fig. 6.3 shows a proposed schematic illustration of the chemical processes involved to produce the colour changes observed in the indicator.

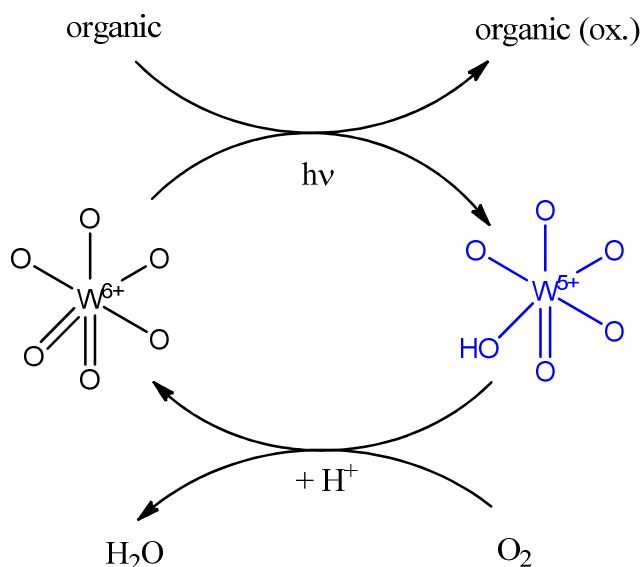


**Fig. 6.3** – Proposed general mechanism involved in the colour change of the indicator from colourless to dark blue.

Upon irradiation with UV light, the POM becomes a powerful oxidising agent, picking up an electron from the glycerol (organic sacrificial electron donor) and forming its characteristic blue colour (see Fig. 6.2). However, in the presence of an oxidant (such as oxygen) this process is reversed. It is this key stage in the reaction schematic which allows POM based materials to be used as UV-activated, oxygen indicators. Without a suitable oxidant, the POM remains in the blue form.

The above ‘standard’ PVA /PWA /glycerol indicator was characterised further. Thus, absorbance spectra of a standard PVA /PWA /glycerol indicator were monitored by UV/vis absorption spectroscopy as a function of irradiation time and the results are illustrated in Fig 6.4. As the film was irradiated under UVB light the formation of the dark blue colour is evident by the formation of the peak at 725 nm, which is due to the formation of  $W^{5+,6}$ , as seen in Fig. 6.3.

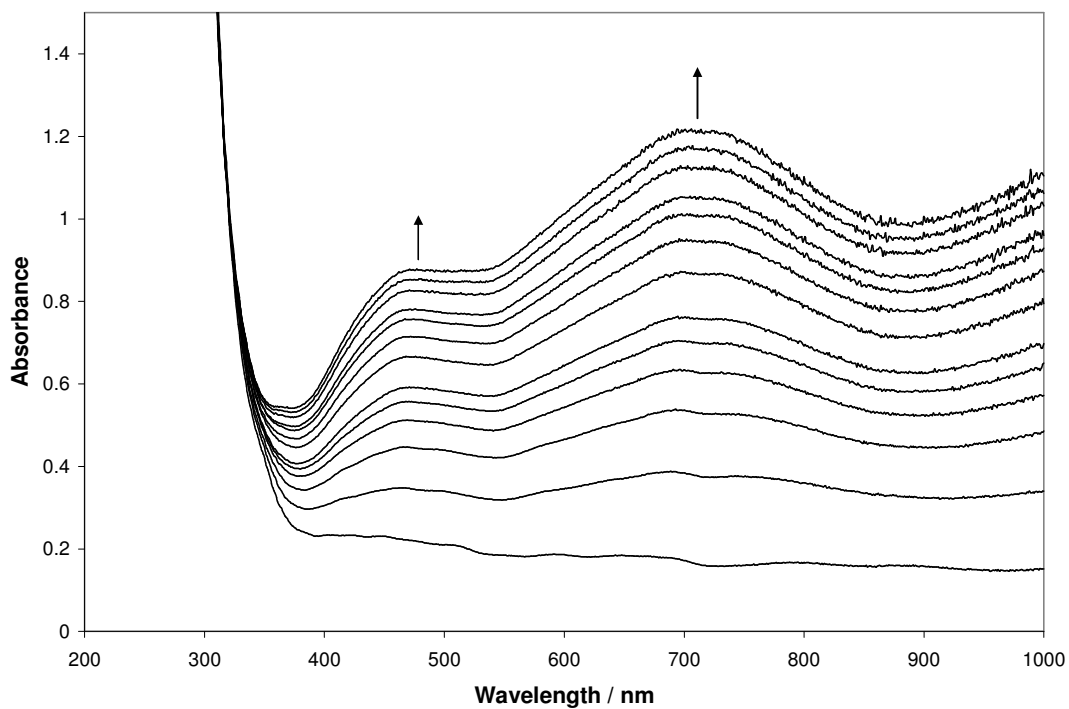


**Fig. 6.4** – UV/vis spectra of the PVA /PWA /glycerol film at different time intervals during irradiation 0, 2, 4, 6, 8, 10, 15, 20, 24, 30, 40, 50 and 60 minutes at 22°C.

The absorption spectrum illustrated in Fig. 6.4 is typical of that of reduced PWA<sup>4,11</sup>. The absorbance of the indicator (at 725 nm) was then recorded during 5 hours of irradiation under UVB light (N<sub>2</sub>) and its response to oxygen in air. The results of this work are shown in Fig. 6.5.

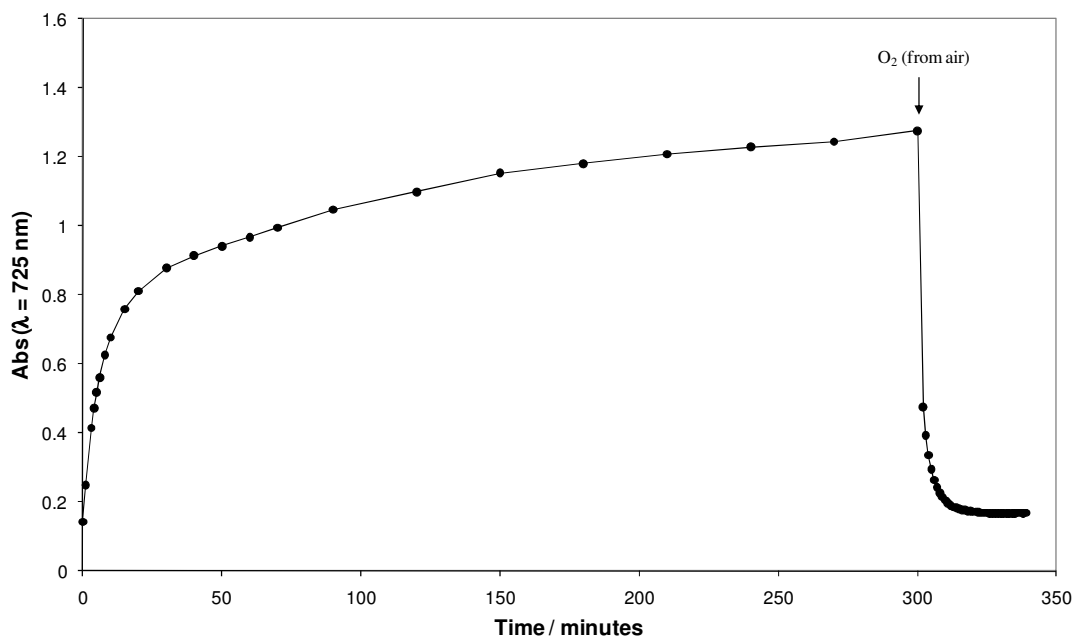
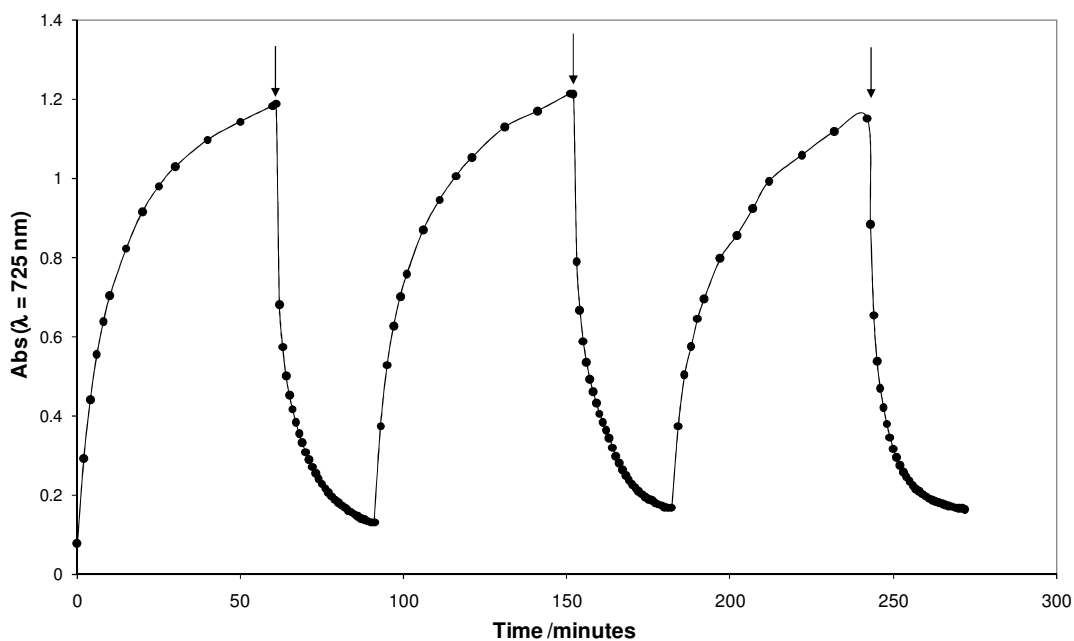


Fig. 6.5 – Irradiation and response of PVA /PWA /glycerol indicator in air at 21°C.

As evident from Fig. 6.2, only after a short time (*ca.* 4 minutes) a distinct colour change is observed. However if the indicator is irradiated for longer, as in Fig. 6.5, the colour change continues, at a slower rate, producing a very dark blue coloured film. Upon exposure to O<sub>2</sub> (from air) the original colourless condition of the PVA/PWA /glycerol film is restored within 20 minutes (see Fig. 6.5).

The indicator can be used repeatedly with no loss in sensitivity, as illustrated by the repeated cycles of irradiation and recovery in Fig. 6.6.





**Fig. 6.6** – Absorbance versus time plot for the typical indicator, when irradiated under UVB light and under N<sub>2</sub>, then left to recover in humid air (~90%RH) at 21°C; the start of the latter is depicted by the ↓ .

### 6.3.1.2 Suitable UV light source

The UV/vis spectra of an aqueous solution of phosphotungstic acid and of a standard PVA /PWA /glycerol ink film were recorded and the results are illustrated in Fig. 6.7. It is apparent from Fig. 6.7 that phosphotungstic acid primarily absorbs light in the UVB region, hence all irradiations were carried out using a UVB light source (~ 4 mW/cm<sup>2</sup>).

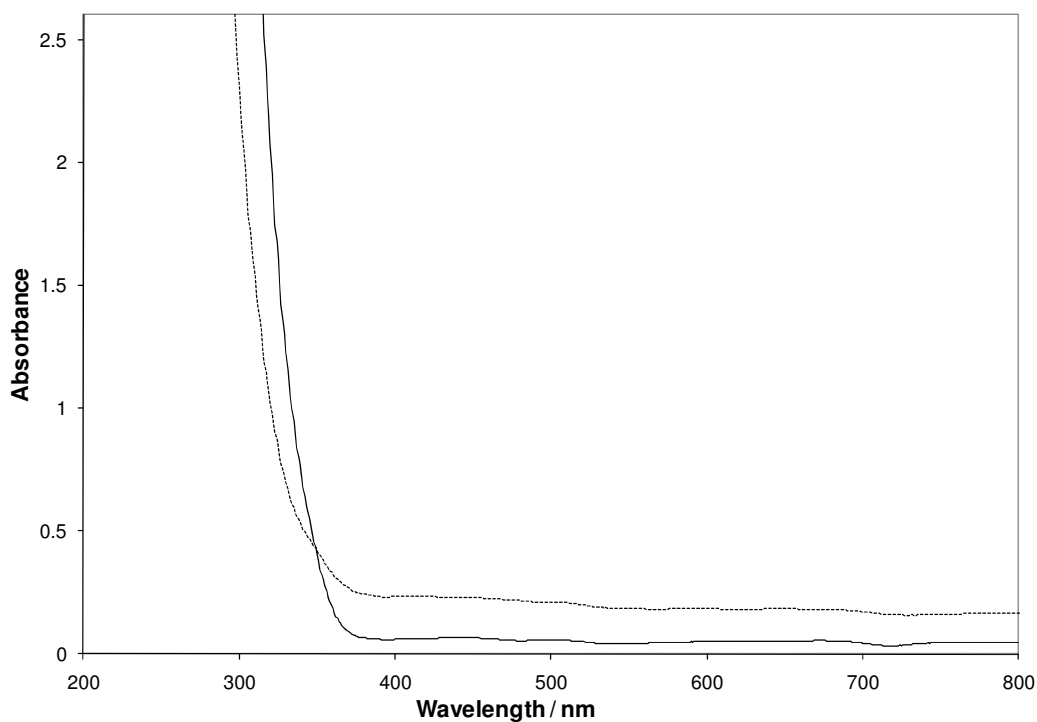


**Fig. 6.7** – Absorbance spectra of aqueous phosphotungstic acid solution (—) and a standard PWA/PVA/glycerol indicator (---) before irradiation.

To investigate the effect of using different wavelengths of UV light, two identical films of ink were spin-coated and one irradiated under UVA and the other under UVB light for 4 minutes. Fig. 6.8 shows photographs of the indicators before and after these irradiations. The film irradiated under the UVB light showed a distinct colour change after 4 minutes, whereas only a small colour change was observed under the UVA irradiation. This confirms that UVA light is not as strongly absorbed by the indicator than UVB light.

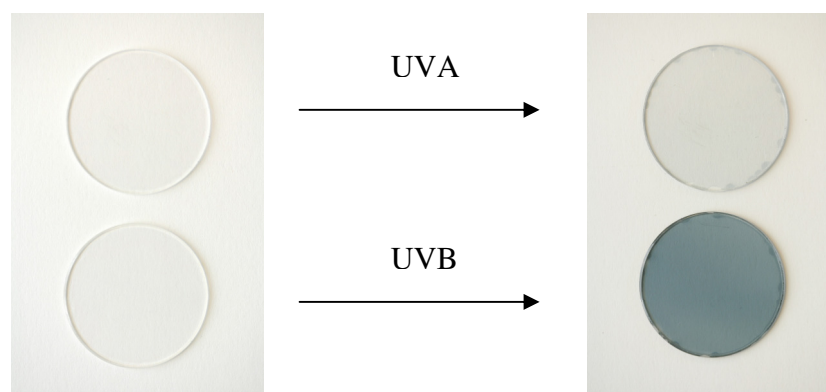


**Fig. 6.8** – Comparison of colour change after irradiation of standard indicator using UVA and UVB light for 4 minutes,  $4 \text{ mWcm}^{-2}$ .

To further confirm the effect of using different wavelengths of UV light, response and recovery profiles for a standard indicator film were recorded under UVA and UVB light and the results of this work are illustrated in Fig. 6.9.

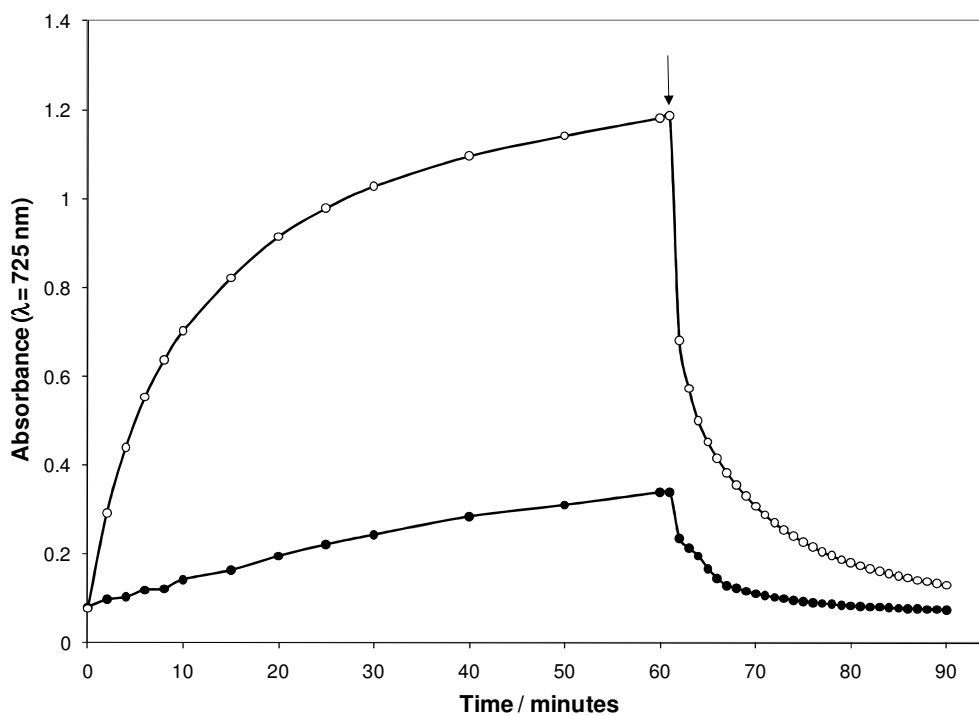


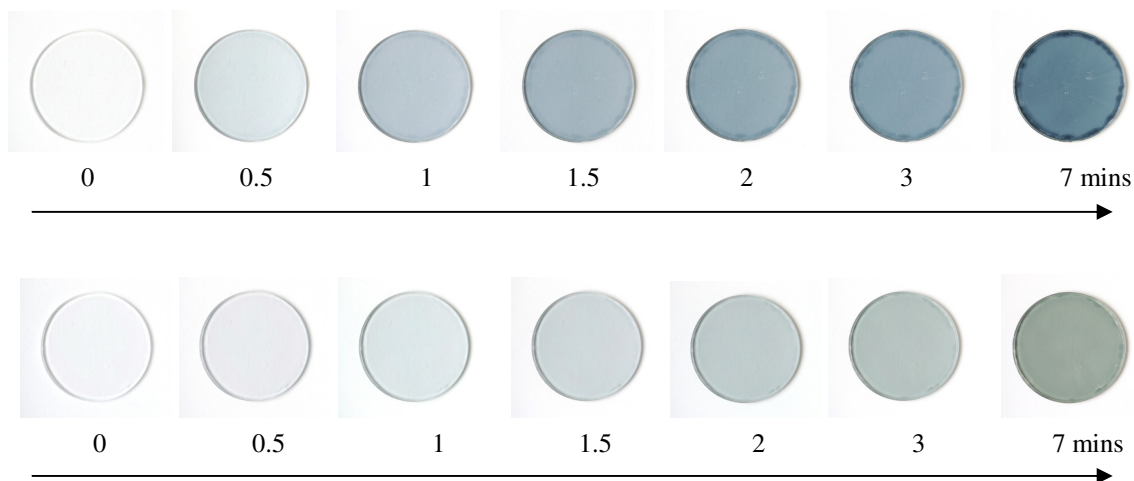
**Fig. 6.9** – Response and recovery of PVA/PWA/glycerol film under UVB (○) and UVA light (●) irradiances at 22°C. Arrow depicts end of irradiation and subjection of the indicator to air (oxygen source).

From these results, the irradiation using UVB light improved the performance of the indicator substantially, as opposed to using UVA. After 60 minutes of irradiation, an absorbance at 725 nm of ~2.4 times greater was obtained using UVB as opposed to the UVA irradiation. This is presumably due to the higher energy of UVB light and its ability to convert  $W^{6+}$  to  $W^{5+}$  more efficiently.

### 6.3.1.3 Effect of glycerol

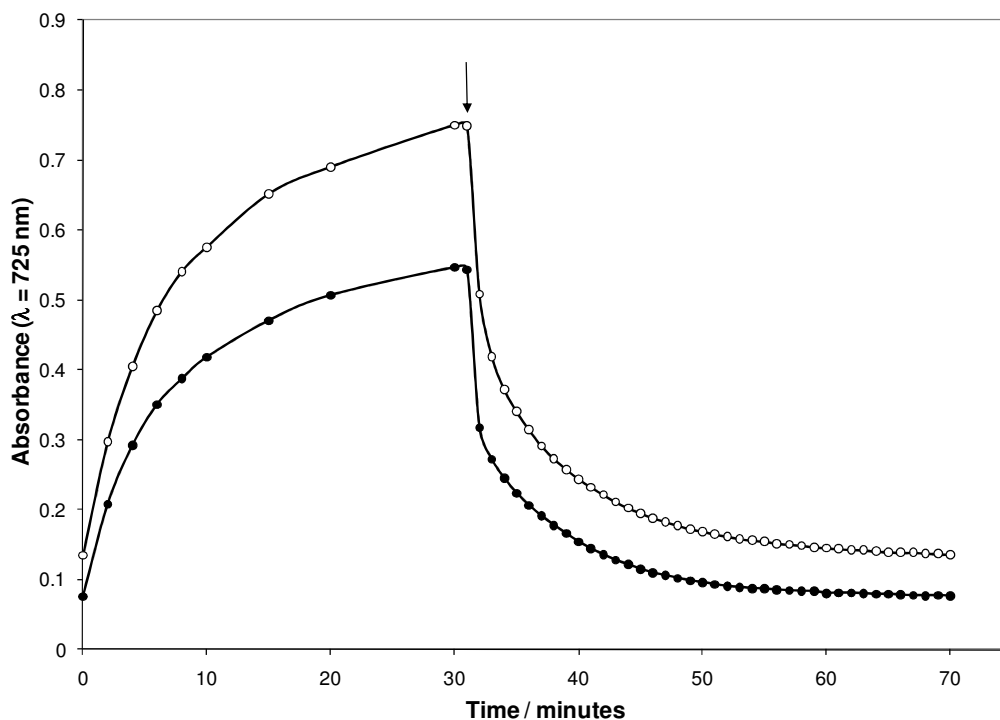
Glycerol has previously been reported<sup>12</sup> to be a good sacrificial electron donor (SED), and has found applications in  $TiO_2$  based oxygen indicating inks. To determine the effect of adding glycerol to the ink, two PVA/PWA films, one with glycerol and one without, were irradiated under UVB light and pictures taken at 30 s

intervals. The inks were prepared according to the experimental section, but substituting 500 mg of 10% w/v PVA for the glycerol in the 'glycerol-free' ink. It is apparent from Fig. 6.10 that the film containing glycerol produces a striking colour change quicker than the film without. It is also evident that the final colour of the indicator containing glycerol is dark blue, whereas the 'glycerol-free' ink turns grey-brown after the same level of irradiation.



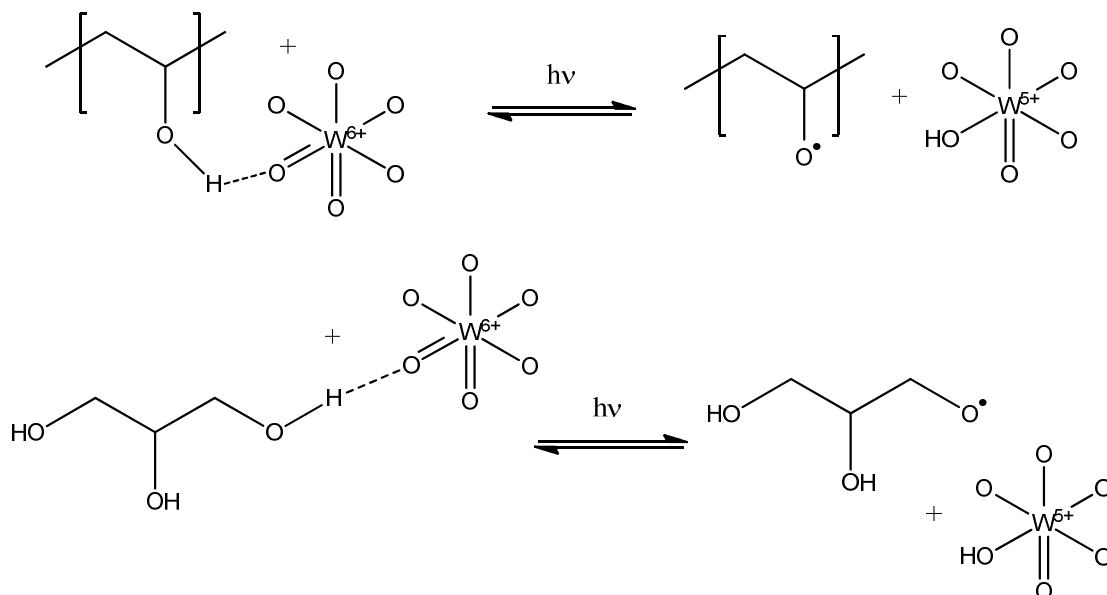
**Fig. 6.10** – Pictures of PVA/PWA films with (top) and without (bottom) glycerol, whilst being irradiated under UVB light.

Fig. 6.11 illustrates the response and recovery of each film (with and without glycerol), whereby the absorbance of the two indicators were measured and compared. It is evident that the addition of glycerol improves the performance of the indicator by ~30%.



**Fig. 6.11** – Response and recovery profiles at 21°C for PVA/PWA films with (○) and without (●) glycerol. Arrow depicts end of irradiation and subjection of indicator to air.

It has been widely reported<sup>3,5</sup> that commonly used polymers (PVA or PAM) can donate electrons to the POM, under a suitable light source, to effect the colour change. The improved performance observed when glycerol is combined into the system, may be due to the more oxidisable nature of the hydroxyl groups on the glycerol compared to those on the polymer. Glycerol has three available hydroxyl groups which can donate electrons. Fig. 6.12 illustrates the reduction of the POM *via* the polymer and the glycerol.



**Fig. 6.12** – Basic reaction mechanism between POM and polymer (PVA) /glycerol to produce the blue  $W^{5+}$  species. <sup>3</sup>

Ultimately the  $-O^\bullet$  species are further oxidised to form  $=O$ , such as aldehydes and ketones and possible carboxylic acids.

#### 6.3.1.4 Effect of humidity on response and recovery

To investigate the effect of humidity on the response and recovery of the indicator, the response and recovery profiles were recorded in dry ( $\sim 0 - 10\%RH$ ) and humid ( $\sim 90 - 100\%RH$ ) conditions. The results of this experiment are shown in Fig. 6.13.

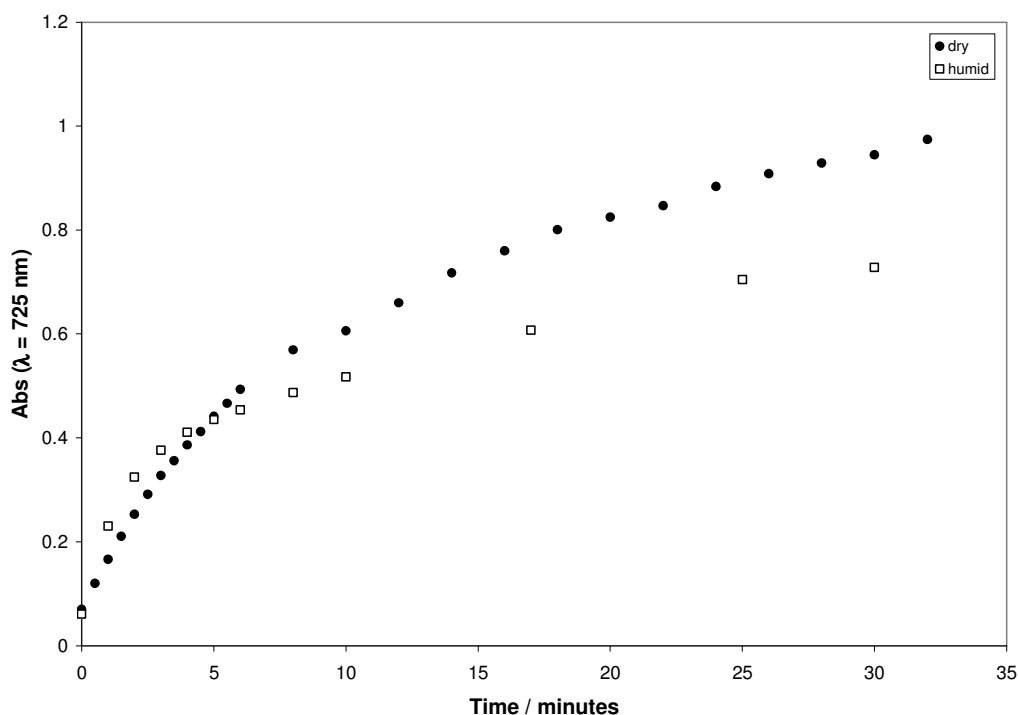


**Fig. 6.13** – Effect of humidity on the irradiation of the standard PVA/PWA/glycerol indicator (● = ~ 0 – 10 %RH and □ = ~ 90 – 100%RH) at 22°C.

The results show that the response of a standard indicator film to UVB irradiation under dry and humid nitrogen gas does not affect the response significantly. The rate was shown to be slightly higher when using dry opposed to humid nitrogen.

Whereas the UV activated step does not appear to be particularly humidity dependent, the recovery step does. This was demonstrated in a study where the air used in the recovery step (i.e. UV activation then exposure to air) was varied in humidity from 0 - 100%RH. The results obtained are illustrated in Fig. 6.14. Under high humidity conditions (~90 - 100%RH), the indicator recovered fully within 25-30 minutes, whereas the indicator recovering under dry conditions only recovered ~15% after 30 minutes.



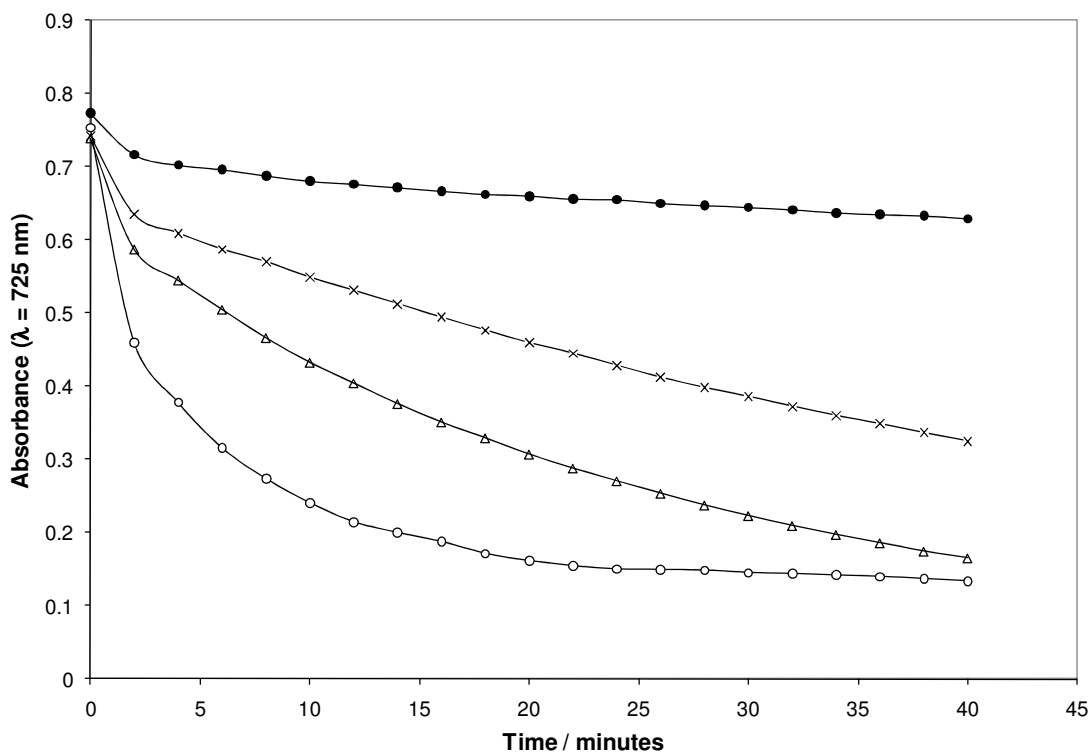


**Fig. 6.14** – Effect of humidity on the recovery of the indicator, where ● = 0, X = 40, Δ = 50 and ○ = 100%RH, at 20°C.

From these results, it can be concluded that the reduction step (irradiation) is largely independent of humidity, whereas the oxidation (colour recovery) is very humidity sensitive. Under dry conditions (~0 – 10 %RH), the rate of oxidation is slow, but fast under high humidity conditions (~50 – 100%RH). This may be due to water acting as a plasticizer, aiding oxygen diffusion through the film.

Due to the significant humidity sensitivity of the indicator, an experiment was carried out to confirm that the indicator was not acting as a humidity indicator, but rather humidity was only facilitated in the recovery process. Fig. 6.15 illustrates an indicator film which has been irradiated under UVB and then exposed to alternate streams of humid nitrogen and humid air (~100 %RH).

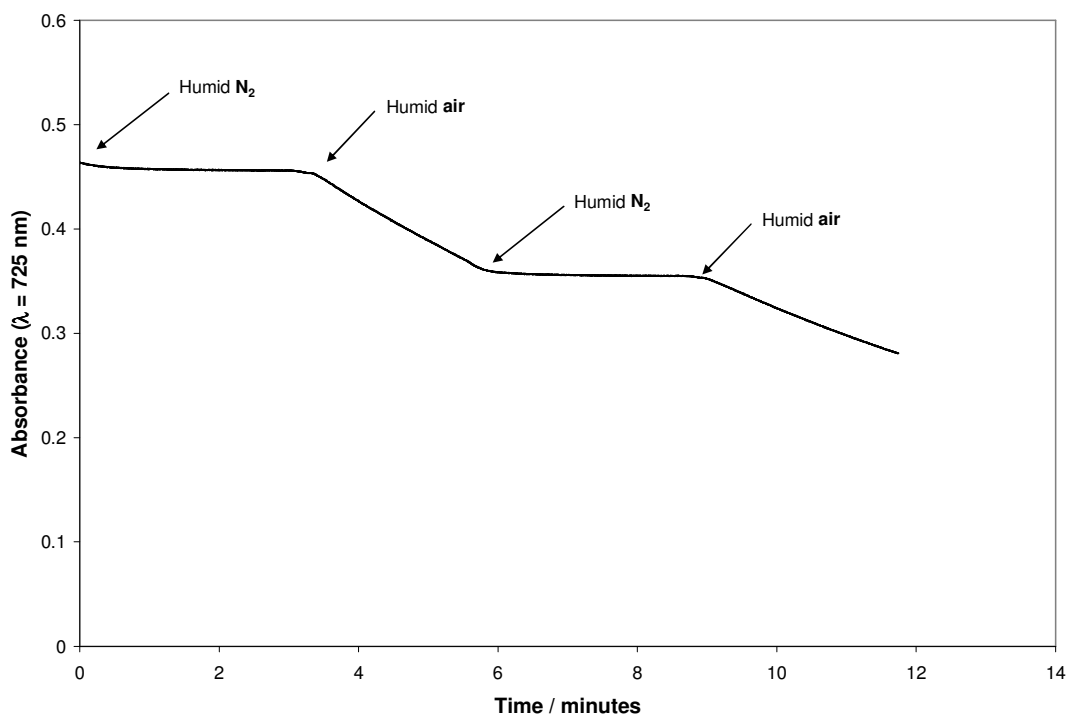


**Fig. 6.15** - The PVA/PWA indicator exposed to alternate streams of humid nitrogen and humid air.

The results show that the photoreduced film does not oxidise (i.e. lose its blue colouration) under nitrogen and high humidity. The presence of high humidity does not therefore contribute to the oxidation process in the absence of O<sub>2</sub>, but rather increases its rate when oxygen is present, as might be expected if it acts as a plasticiser.

#### 6.3.1.5 'De-colouration' of the film

It was observed that freshly prepared indicators are colourless (as inferred from Fig. 6.1), but start to irreversibly change colour to brown, after a number cycles of irradiation and response to oxygen in air. To investigate this, absorbance spectra of a freshly prepared PVA/PWA/glycerol indicator and the same indicator after three cycles of irradiation and response to oxygen, were recorded and the results illustrated

in Fig. 6.16. As indicated on the spectra, a light brown colour forms. This discolouration is known in literature as the formation of a ‘heteropolybrown’<sup>13</sup>. The smaller peak at 460 nm is presumably due to the ‘heteropolybrown’ ion, which is reported to be a further and irreversibly reduced form of PWA, involving  $W^{4+}$ . In contrast to  $W^{5+}$ , it is known<sup>6</sup> that  $W^{4+}$  is not easily oxidised back to  $W^{6+}$ . This agrees with the experimental observations that the brown colour is irreversibly produced.

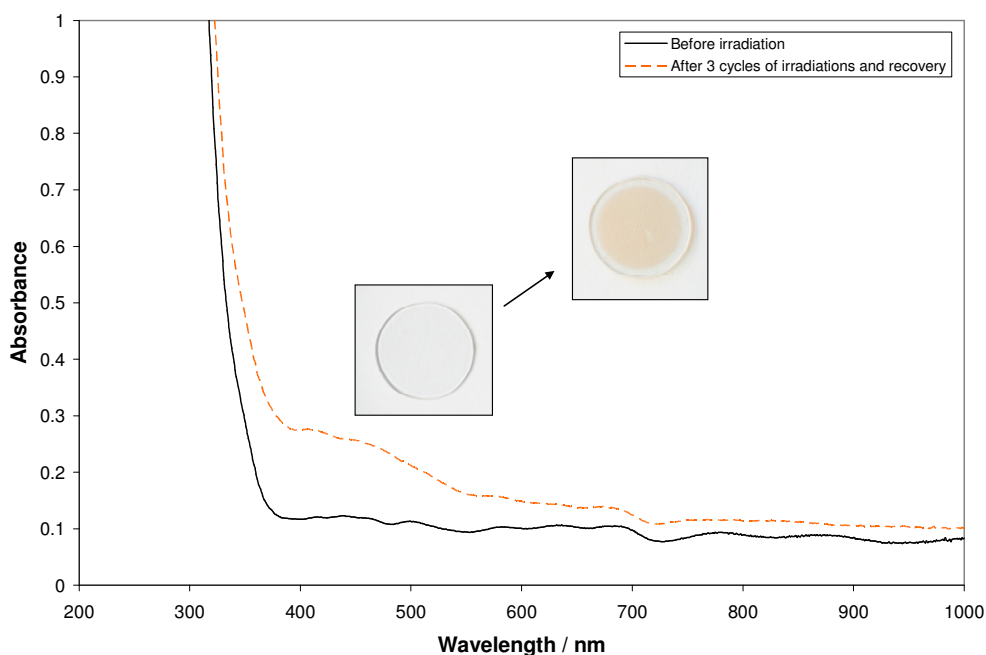
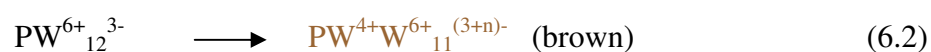
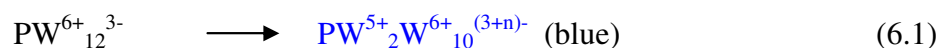


**Fig. 6.16** - Spectra of the indicator before and after three consecutive cycles of irradiation and response to oxygen in air.

Feng *et al.* suggests<sup>6</sup> that under higher energy light sources and for long periods of time, more electrons can be donated (from the polymer in their case) to the POM, leading to heteropolybrowns. The reductions can be written as follows:



where  $n$  refers to the number of accepted electrons.

Since  $W^{5+}$  can easily oxidise back to  $W^{6+}$  in air, the blue colour is only a temporary colour change, which allows phosphotungstic acid based inks to be good optical indicators.

As is evident from the photographs of the films in Fig. 6.17, it has been observed that glycerol reduces the amount of  $W^{4+}$  formed, and so reduces the amount of heteropolybrown formed. After only one cycle of irradiation and recovery, the glycerol-free indicator appears brown, whereas the ink containing glycerol only begins to show the same discolouration after 3 further cycles. This is a significant advantage of the glycerol-based indicators over the previously reported indicators in literature.

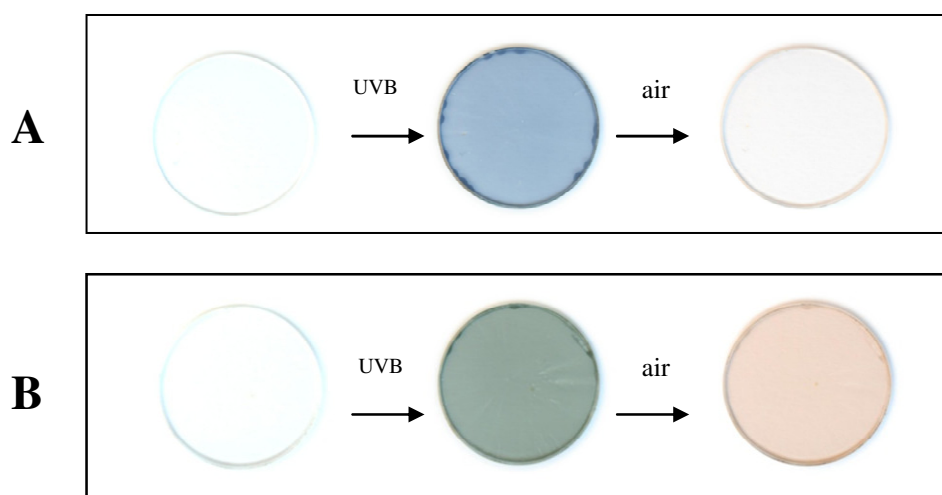













**Fig. 6.17** – Photographs of a glycerol (A) and glycerol-free (B) indicator before and after irradiation under UVB light for 4 minutes, then after their response to oxygen in air.

## 6.3.1.6 Application onto different substrates

To investigate the use of the PVA/PWA/glycerol ink on other substrates other than glass, the ink was coated onto a variety of substrates. The ink was found to be easily applied to paper, as well as other everyday substrates such as glass and plastic (polypropylene). The versatility of the ink allows it to be applied on numerous substrates, which strengthens the potential to be adopted as optical indicators for food packaging applications.

In this experiment the standard PWA ink (as described in 6.2.1) was coated onto standard white printer paper and then irradiated under UVB light ( $4 \text{ mW/cm}^2$  for 4 minutes). The characteristic colour change from colourless to dark grey/blue was observed. The response of the inks to oxygen (i.e. fading of the grey colour) was observed visually and photographs were taken at different time intervals. Samples were stored at both room ( $21^\circ\text{C}$ ) and fridge temperatures ( $4^\circ\text{C}$ ). The results of this study are illustrated in Table 6.1

**Table 6.1** – Response of indicators to oxygen in air at 4 and  $21^\circ\text{C}$ .

	day 0	day 1	day 2	day 3	day 6	day 8
<b><math>4^\circ\text{C}</math></b>						
<b><math>21^\circ\text{C}</math></b>						-

From these results, it is clear that there is a temperature dependence on the recovery of the ink. At room temperature the printed ink on paper is fully recovered after ~2-3

days, whereas the identical sample stored in the fridge takes ~8 days to recover. This is expected since diffusion is a thermally activated process.

It is also interesting to note that the time the indicators take to respond to oxygen are much slower than that observed when the same indicator was applied onto a glass substrate, as in earlier experiments. It is thought that by applying the ink onto paper, the local level of glycerol may have reduced, and since glycerol acts both as a plasticiser and SED, the effect would be to slow down the rate of diffusion of O<sub>2</sub> into the film, hence slower response times to O<sub>2</sub>.

It is expected that by varying the irradiation time, PWA concentration and glycerol concentration, the recovery times may be 'tuned' to produce indicators which respond at times relevant to the specific application. Further work would need to be carried out to fully investigate this.

#### 6.3.1.7 Applications

The detection of oxygen in food packaging is vital, since any variation in concentration from the initial packaging conditions suggests that a leak may be present. Any damage in food packaging will result in an increase in oxygen concentration, which will allow increased microbial growth, hence decreased shelf-life due to accelerated spoilage. Therefore, indicators which detect changes in oxygen concentration within food packaging have significant potential. A number of oxygen indicators for applications in food packaging have been reported and are described in more detail in Chapter 1. Results have shown that POM-based indicators can respond quickly to oxygen, so are useful as indicators which require a relatively quick response time.

However, the main disadvantage of *immediate response* indicators is that they do not allow for the time period where the food is still safe to eat under ambient air conditions (~20% O<sub>2</sub>). The development of *delayed response* oxygen indicators takes

into consideration this time delay before the food begins to deteriorate below the 'fit for consumption' level. One of the disadvantages of best before and use-by dates is that they assume that the food will be stored under its original packaging conditions (i.e. MA). However, as soon as the packaging is opened (intentionally or unintentionally), these conditions are changed, affecting the shelf-life. Although guidelines regarding the products' lifetime after opening are normally indicated on the packaging, they require that the customer remember when the product was opened. Another important point of note is that the lifetime after opening suggested by the manufacturer will vary depending on storage conditions, most notably temperature. A delayed oxygen indicator, which incorporates temperature dependence, would provide the consumer with a more accurate lifetime of the packaged food.

Interestingly, the characteristics shown when the PVA/PWA/glycerol ink was applied onto paper (i.e. slower response to oxygen), suggests that the indicator may have application as a delayed response indicator.

### **6.3.2 POM-based pigments and plastics**

Following on from previous work<sup>14</sup> (Chapter 5), it was attempted to incorporate the O<sub>2</sub> indicator capability, as observed in the PVA/PWA/glycerol ink, into pigment form which could potentially be incorporated into extrudable plastics. The main adaptation which would have to be addressed is an alternative sacrificial electron donor (SED), since glycerol, a viscous liquid at room temperature, has a low melting point. Indeed, a SED which is solid at room temperature would be required. Results from a previous study (unpublished) in our group highlighted suitable solid state compounds which could replace glycerol. DL-threitol and 1,6-hexanediol proved to be the most promising candidates due to their similar structures (see Fig. 6.18) and electron donating ability as glycerol.

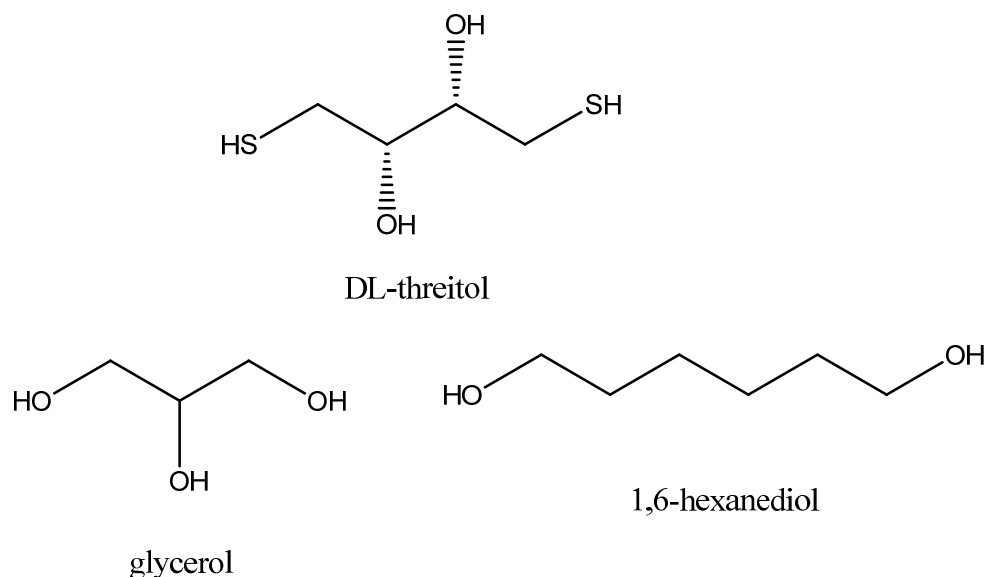


**Fig. 6.18** – Structures of SEDs.

### 6.3.2.1 Effect of SED on colourimetric response

To investigate the dependence of colour change on the quantity of SED contained in the pigment, various batches of pigment were prepared containing differing amounts of 1,6-hexanediol and irradiated under UVB light. Photographs were taken before and after the irradiation, which are illustrated in Fig. 6.19.

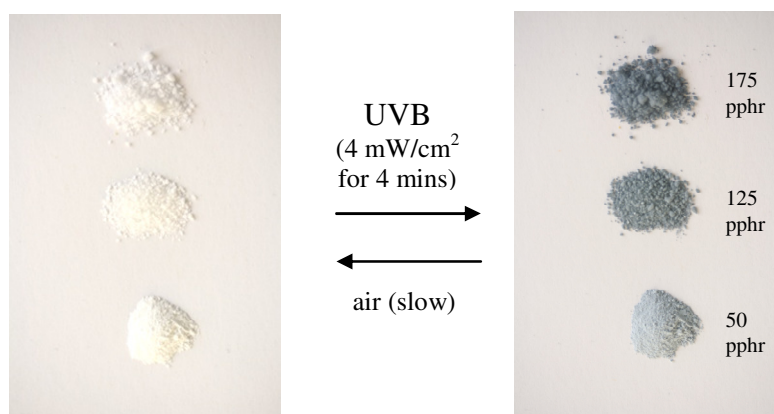


**Fig. 6.19** – Irradiation of PWA pigments with varying levels of SED (1,6-hexanediol) and their response to oxygen in air.



It is evident from the photographs in Fig. 6.19, that the greater the quantity of SED, the darker the colour change. However, as the quantity of 1,6-hexanediol is increased, the pigment become less ‘powdery’ and more ‘waxy’. Such pigments were incorporated into flexible polyethylene films, as described in section 6.2.1. However incorporating pigments containing high quantities of SED posed problems when trying to obtain a well dispersed pigment in polyethylene. Often this leads to a very speckled film as observed in Fig. 6.20. Similar observations were made when using DL-threitol, plus it has a nasty pungent odour, due to the thiol groups.

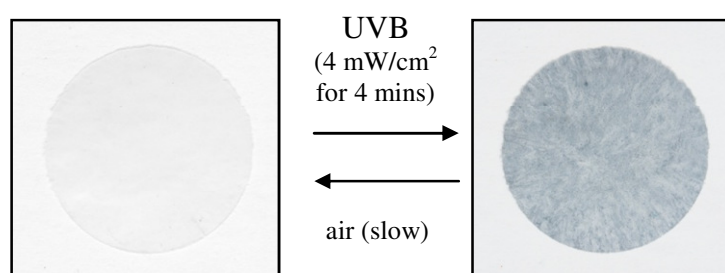


**Fig. 6.20** - Photographs of an O<sub>2</sub>-sensitive pigment incorporated in a polyethylene plastic film, before and after irradiation to UVB light.

To further investigate the effect of SED in the pigmented polymer films, two pigments with different quantities of 1,6-hexanediol (50 and 125 pphr) were combined with PE powder, mixed and heat pressed. Irradiation and response profiles were recorded for each film, using the same method as the ink samples. The results of this work are illustrated in Fig. 6.21, from which it can be concluded that the amount of SED within the pigment, has no affect on the response to UVB light, but affected the recovery of the pigmented film. Greater levels of SED results in an increased rate of recovery.

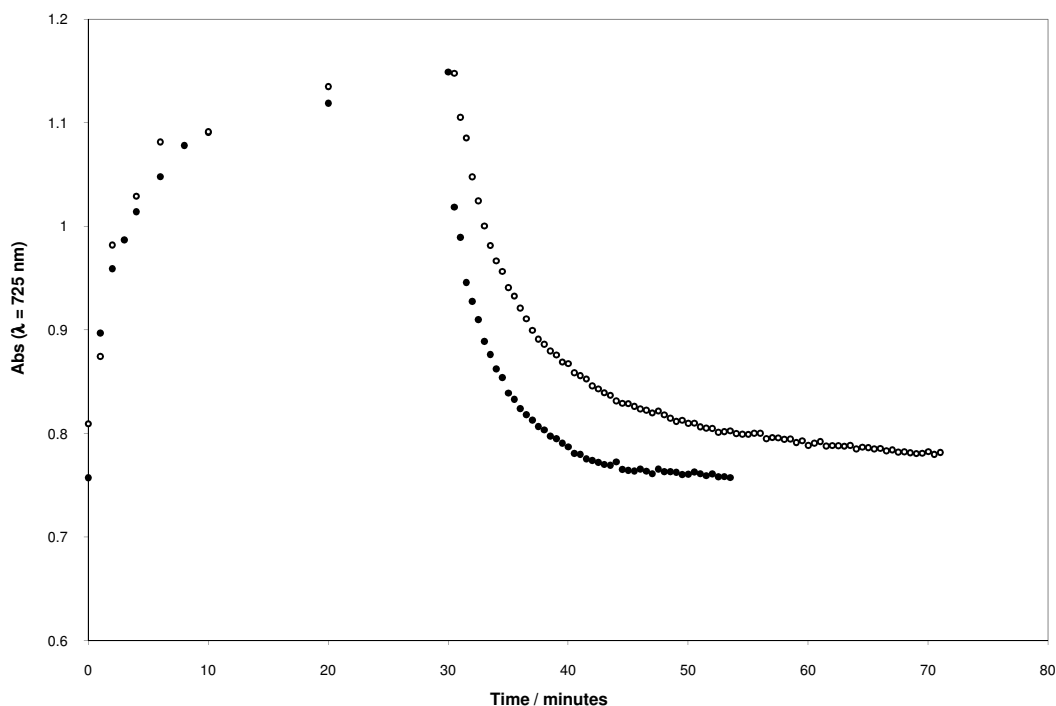


**Fig. 6.21** – Effect of SED quantity on the response and recovery of POM pigment/PE films with 50 (○) and 125 (●) pphr of 1,6-hexanediol, at 21°C.

This observation would be key to the development of delayed oxygen indicators, where it would be necessary to control the colour changes depending on food types. Further work would be needed to explore the lower limit of SED which could be used that would give a rapid activation and the slowest recovery.

## 6.4 Conclusions

A novel polyoxometalate-based indicator for the detection of O<sub>2</sub> has been formulated and characterised. The addition of glycerol to the indicator was found to enhance its characteristics significantly, both in its activation time and longevity. The indicator was shown to have quick activation times (2 - 4 minutes) under UVB light and show a distinctive colour change. Upon application on paper the indicator was shown to have slower response times than previously reported indicators, which may be an advantage in some applications, where a slow, delayed response is desirable, such as

food packaging. Further to this work, it was demonstrated that same O<sub>2</sub> indicating capabilities of the inks can be incorporated into pigments, which can then be combined into flexible polymer films, providing an alternative and possibly more attractive substrate in relation to the possible applications. All indicators are cheap and easy to prepare and shows considerable potential to be developed further for commercially relevant applications.

## 6.5 References

1. E. Papaconstantinou, *Chem. Soc. Rev.*, 1989, **18**, 1-31.
2. J. Chen, Y. Lui, D.-Q. Xiong, W. Feng and W.-M. Cai, *Thin Solid Films*, 2008, **516**, 2864-2868.
3. J. Gong, X.-D. Li, C.-L. Shao, B. Ding, D.-R. Lee and H.-Y. Kim, *Materials Chemistry and Physics*, 2003, **79**, 87-93.
4. J. Chen, Y. Liu, W. Feng and W.-M. Cai, *J. Mater. Sci.: Mater. Electron*, 2008, **19**, 295-299.
5. W. Feng, T. R. Zhang, L. Wei, R. Lu, Y. B. Bai, T. J. Li, Y. Y. Zhao and J. N. Yao, *Mater. Lett.*, 2002, **54**, 309-313.
6. W. Feng, T. R. Zhang, Y. liu, R. Lu and Y. Y. Zhao, *J. Mater. Sci.*, 2003, **38**, 1045-1048.
7. D. Farcasiu and J. Q. Li, *J. Catal.*, 1995, **152**, 198-203.
8. S. Takeshima and T. Kikichi, *Int. Pat.* , 147552, 2009.
9. A. Troupis, E. Gkika, A. Hiskia and E. Papaconstantinou, *C. R. Chim.*, 2006, **9**, 851-857.
10. A. Troupis, T. M. Triantis, E. Gkika, A. Hiskia and E. Papaconstantinou, *Appl. Catal. B-Environ.*, 2009, **86**, 98-107.

11. P. Kormali, A. Troupis, T. Triantis, A. Hiskia and E. Papaconstantinou, *Catal. Today*, 2007, **124**, 149-155.
12. A. Mills, *Chem. Soc. Rev.*, 2005, **34**, 1003-1011.
13. W. Feng, Y. S. Ding, Y. Liu and R. Lu, *Mater. Chem. Phys.*, 2006, **98**, 347-352.
14. A. Mills, G. A. Skinner and P. Grosshans, *J. Mater. Chem.*, 2010, **20**, 5008 - 5010.

## Chapter 7: Polyoxometalate based UV dosimeter

---

### 7.1 Introduction

Recognising the ability of polyoxometalates to be used to develop optical indicators for commercially useful analytes, e.g.  $O_2$  as demonstrated in Chapter 6, it was endeavoured to expand their detecting capability to other important analytes, in particular UV radiation. The detection of UV radiation is of great interest due to the established link between UV exposure from the sun and the subsequent related health defects. The development of personal UVB dosimeters allows a person to monitor the amount of UVB light that has been absorbed by their skin by means of simple colour changes. As discussed in Chapter 1, many types of UVB dosimeters have been reported in literature and indeed some have boasted commercial products<sup>1,2</sup>. However, to our knowledge, POMs have not been used in this capacity. Therefore, a novel POM-based UVB dosimeter is described and the subsequent sensing characteristics reported.

Reversible methylene blue (MB),  $TiO_2$ -based oxygen indicators are well established in the literature<sup>3</sup>. Replacing  $TiO_2$  with a POM would lead to optically clear films as opposed to the opaque character of the previous  $TiO_2$ -based films. The main problem of using polyoxometalate ions (e.g.  $PW_{12}O_{40}^{3-}$ ) alongside commonly used reversible redox dyes (e.g. methylene blue and methyl viologen) is the formation of insoluble ion pairs. The anionic phosphotungstate ion,  $PW_{12}O_{40}^{3-}$ , and cationic methylene blue are both water soluble, but when ion-paired form a very insoluble ion complex ( $MB^+_3PW_{12}O_{40}^{3-}$ )<sup>4</sup>. A formulation is reported which allows these two species to be incorporated into a stable ink without affecting their ability to perform as an indicator for the detection of UVB radiation.

## 7.2 Experimental

### 7.2.1 Ink formulations

Unless specified, all chemicals were purchased from Sigma Aldrich in the highest purity available. The water used to make all aqueous solutions was double distilled and deionised. High purity gases were obtained from BOC gases. Spectrophotometric measurements were carried out using a Carey 50 spectrophotometer. Thin films were produced using a spin coating technique, with a Spin Coater Model 4000-1 (Electro-Micro Systems).

A typical methylene blue (MB)-PWA ink was prepared by dissolving 8 mg of methylene blue in 2 g of 10% w/v polyvinyl alcohol in water (MW = 146,000 – 186,000). To this solution were added 300 mg of glycerol and 120 mg sodium phosphotungstate (NaPWA,  $\text{Na}_3\text{PW}_{12}\text{O}_{40}$ ) dissolved in 1 ml distilled water. The mixture was stirred at room temperature for approximately 30 minutes before use. The composition of the ink can be summarised as PVA/MB/NaPWA/glycerol in pphr as follows: 100/4/60/15 pphr.

The optimised methylene blue (MB)-PWA ink suitable for a personal UV dosimeter was prepared by dissolving 12 mg of methylene blue in 2 g of 10% w/v polyvinyl alcohol in water (MW = 146,000 – 186,000). To this solution were added 300 mg of glycerol and 90 mg of sodium phosphotungstate (NaPWA) dissolved in 1 ml distilled water. The mixture was stirred at room temperature for approximately 30 minutes before use. The composition of the ink can be summarised as PVA/MB/NaPWA/glycerol in pphr as follows: 100/6/45/15 pphr.

## 7.3 Results and discussion

### 7.3.3 POM/Methylene blue based indicator

Efforts were made to solubilise the ion pair complex ( $\text{MB}^+\text{POM}^-$ ) in a range of solvents, but only minimal/no solubility in all solvents was observed. Although Wen *et al.* claim<sup>4</sup> that the methylene blue-phosphotungstate ion complex is soluble in THF, the concentration used in the paper is only  $\sim 0.74$  mM, which is too weak to produce a highly coloured indicator ink. An attempt to produce an ink containing the MB-POM ion pair was carried out. However, the very light coloured film did not undergo any observable colour change under UVB irradiation. To overcome the formation of the insoluble ion-complex, low concentrations of each compound are used, and added to each other dropwise, with stirring. This appears to reduce the formation of the insoluble complex significantly. Due to the high molar absorptivity of methylene blue ( $\epsilon = 76000 \text{ M}^{-1}\text{cm}^{-1}$ )<sup>5</sup>, only a small concentration is required to give a strong blue colour, so a low concentration of the dye still produces an intensely blue coloured ink. Although, the concentration of the sodium phosphotungstate is sufficiently low (e.g. 60 pphr compared to 1500 pphr of the PVA/PWA/glycerol indicators) to not give a dark blue colour when irradiated, it is also sufficiently high to reduce the methylene blue and hence see an observable colour change.

#### 7.3.3.1 Characterisation of standard PVA/MB/NaPWA/glycerol indicator

Photographs of a standard indicator film were recorded before and after irradiation under UVB light. From Fig. 7.1, it is clear that a distinctive colour change takes place.

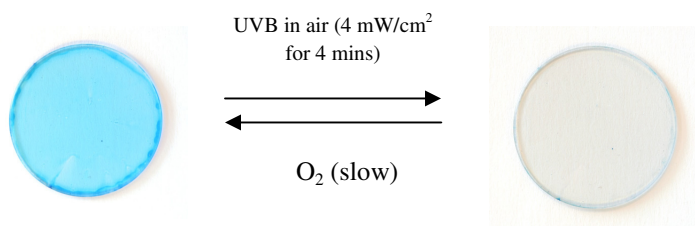


**Fig. 7.1** – Photographs of a standard PVA/MB/NaPWA/glycerol ink film, before and after irradiation under UVB light for 4 mins.

Fig. 7.2 is a schematic illustration of the chemical processes involved to produce the colour changes observed in the indicator. It is clear from the cycle that oxygen is essential to the recovery process.

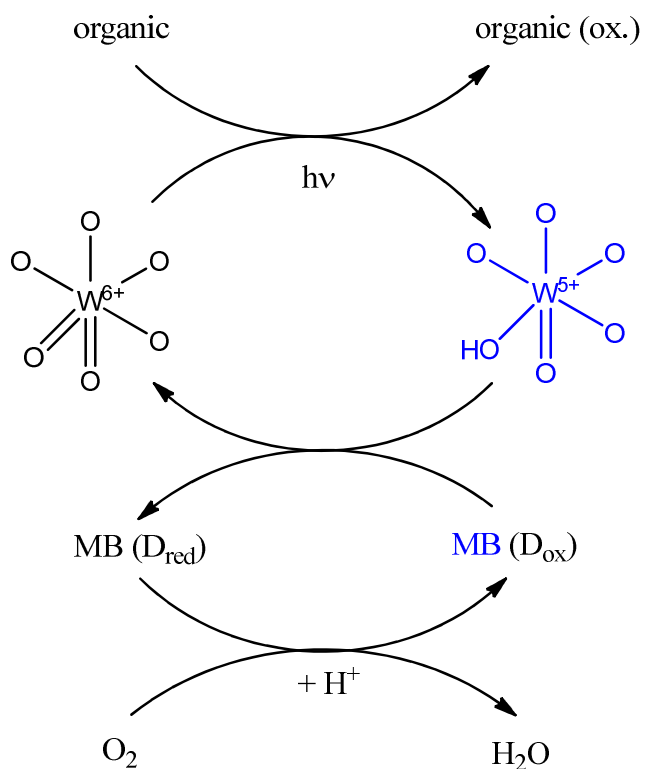


**Fig. 7.2** – Proposed schematic illustration of the cycles involved in the PVA/MB/NaPWA/glycerol indicator.



The absorbance spectra of a standard film were monitored by UV/vis absorption spectroscopy as a function of irradiation time (UVB), under nitrogen gas and the results are illustrated in Fig. 7.3.

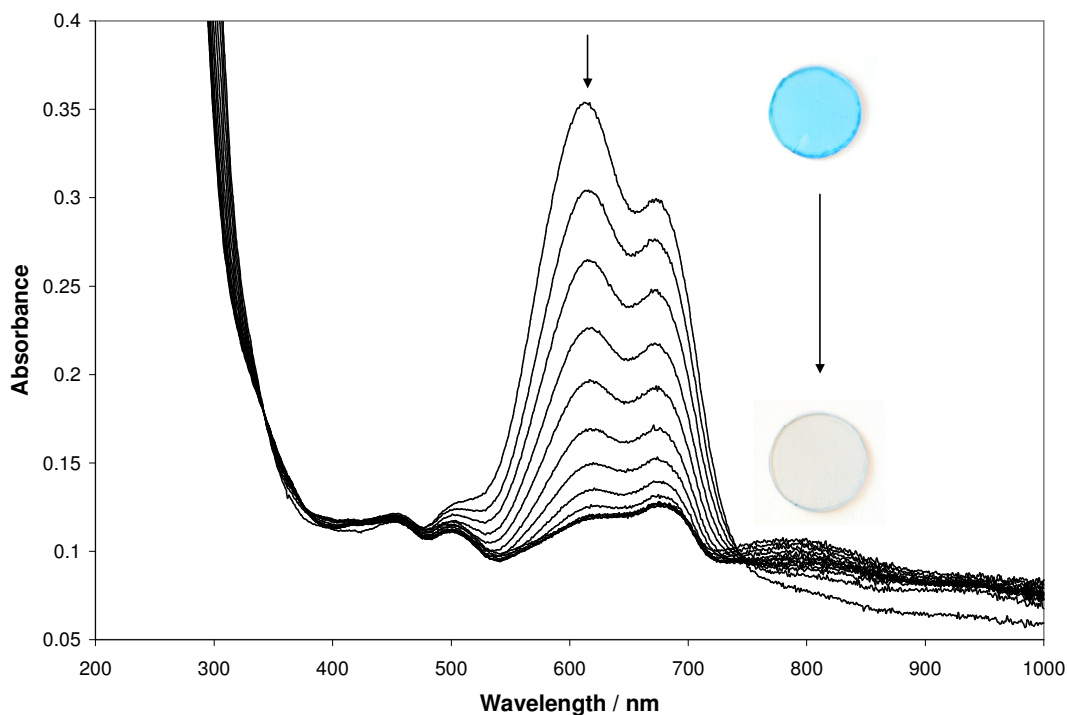


**Fig. 7.3** – UV/vis absorption spectra of the standard PVA/MB/NaPWA/glycerol indicator as a function of irradiation time at 21°C. Spectra were recorded every 15 seconds for 3 minutes.

The results show a gradual decrease in absorbance at 610 nm, illustrative of the colour change from blue to colourless.

A similar irradiation was carried out using UVA light, and the results, along with the UVB irradiation, are illustrated in Fig. 7.4.

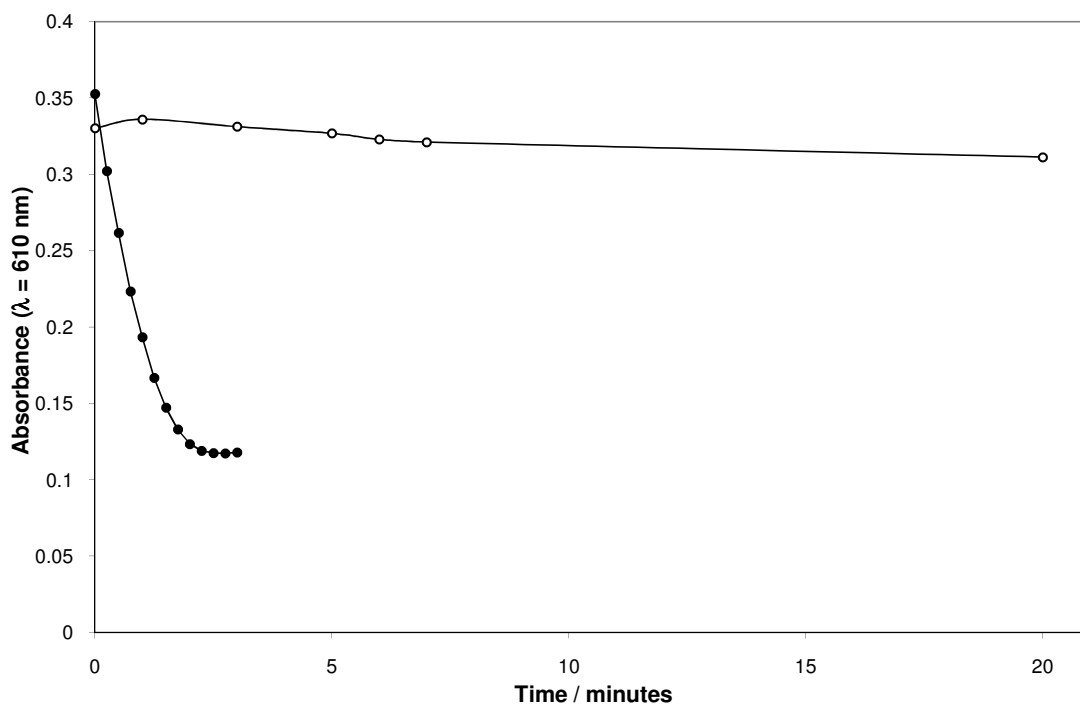


**Fig. 7.4** – Comparison of irradiation of standard PVA/MB/NaPWA/glycerol indicator under UVA (○) and UVB (●) light, at 21°C.

As is indicated in Fig. 7.4, minimal colour change took place, suggesting that UVA light is absorbed much less strongly by the indicator than the UVB light. These results illustrate the potential for this indicator to be used as a UV personal dosimeter, since it is primarily UVB light from the sun which causes the most damage to human skin.

### 7.3.3.2 Indicator response and recovery times

An experiment was carried out where the absorbance of the film at 610 nm was monitored during the irradiation under UVB light under nitrogen and the recovery in air and oxygen respectively. The results of this work are illustrated in Fig. 7.5.

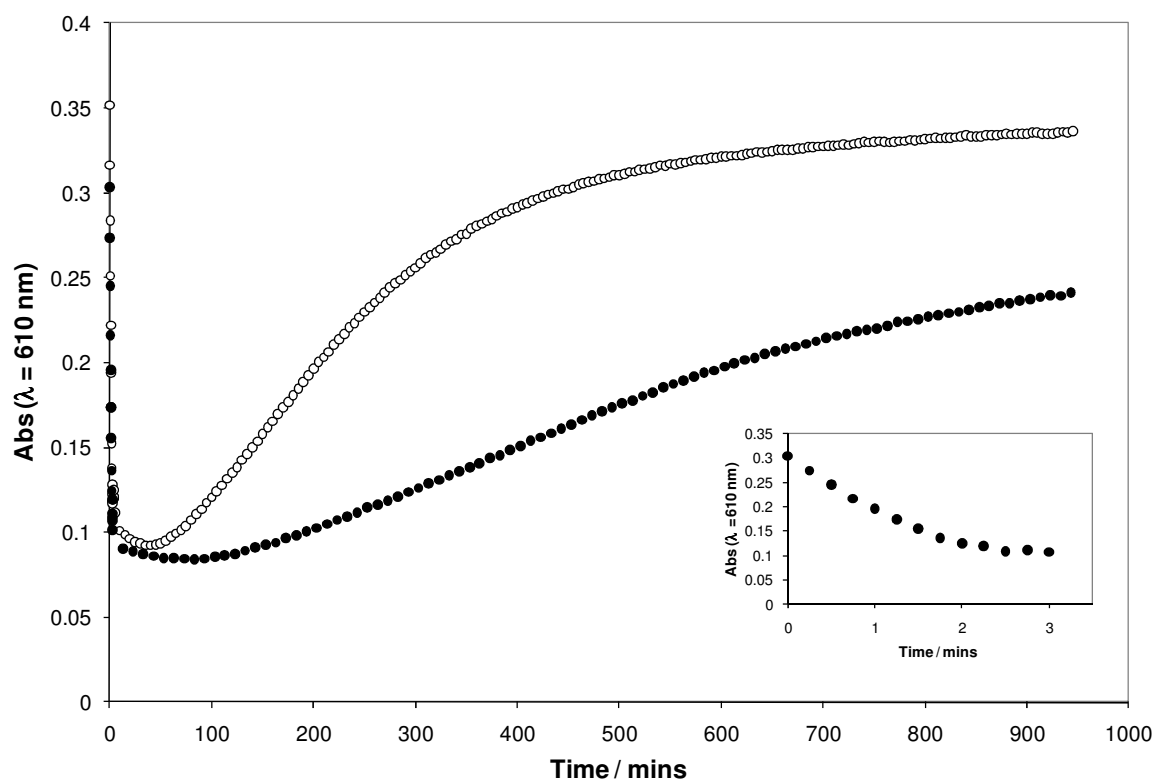


**Fig. 7.5** – Comparison of recovery in air (●) and oxygen (○), after irradiation under UVB light in nitrogen, at 21°C.

Although methylene blue quickly gets reduced to the leuco-form (~2 mins), it has a fairly long recovery back to its original absorbance. It is evident from the results that the concentration of oxygen significantly affects the recovery times, the higher the oxygen concentration, the quicker the recovery. This agrees with the schematic illustration shown in Fig. 7.2.

To investigate how the indicator performs after repeated cycles of irradiation and response to oxygen, an experiment was carried out where the indicator was irradiated with UVB light under  $N_2$  for 4 minutes, then left to recover for 24 hours. This cycle was repeated 4 times and absorbance spectra recorded before and after irradiation, then again after the 24 hour recovery cycle. The results of this work are found in Fig 7.6.

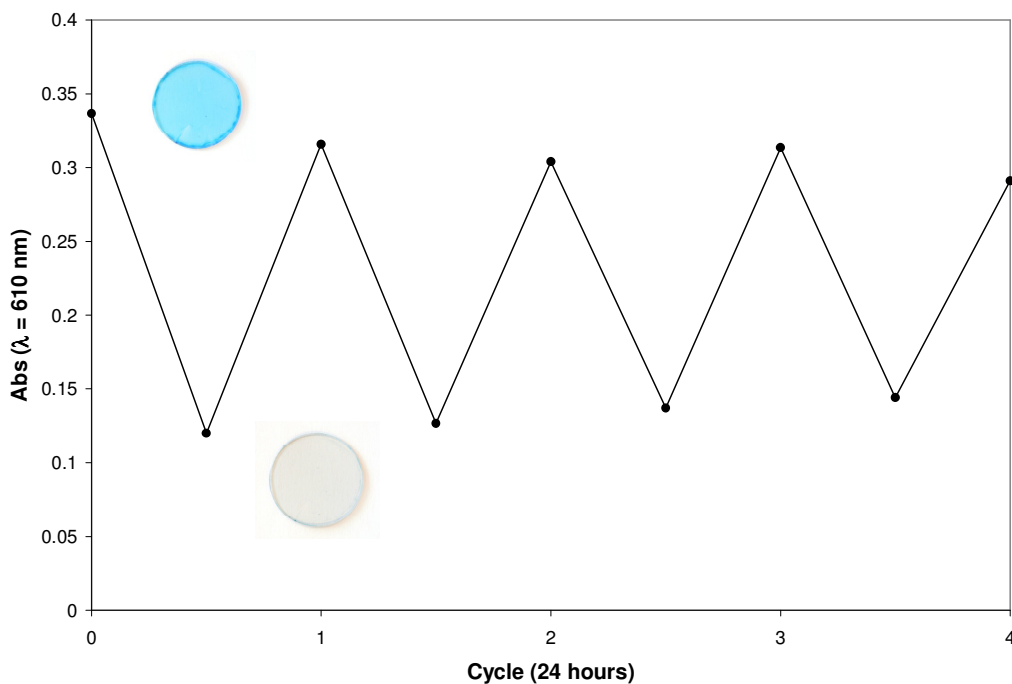


**Fig. 7.6** – Four consecutive cycles of UVB irradiation for 4 minutes and then recovery for 24 hours, at 22°C.

It is clear from these results that the indicator can be used repeatedly with minimal loss in performance.

### 7.3.3.3 Effect of humidity

In another set of experiments, the effect of humidity on the recovery of the indicator after UVB irradiation was investigated. The indicator was irradiated in the normal manner (UVB light 4 mW/cm<sup>2</sup> for 4 mins) and then exposed to air streams with different relative humidities. The results of this work are illustrated in Fig. 7.7.

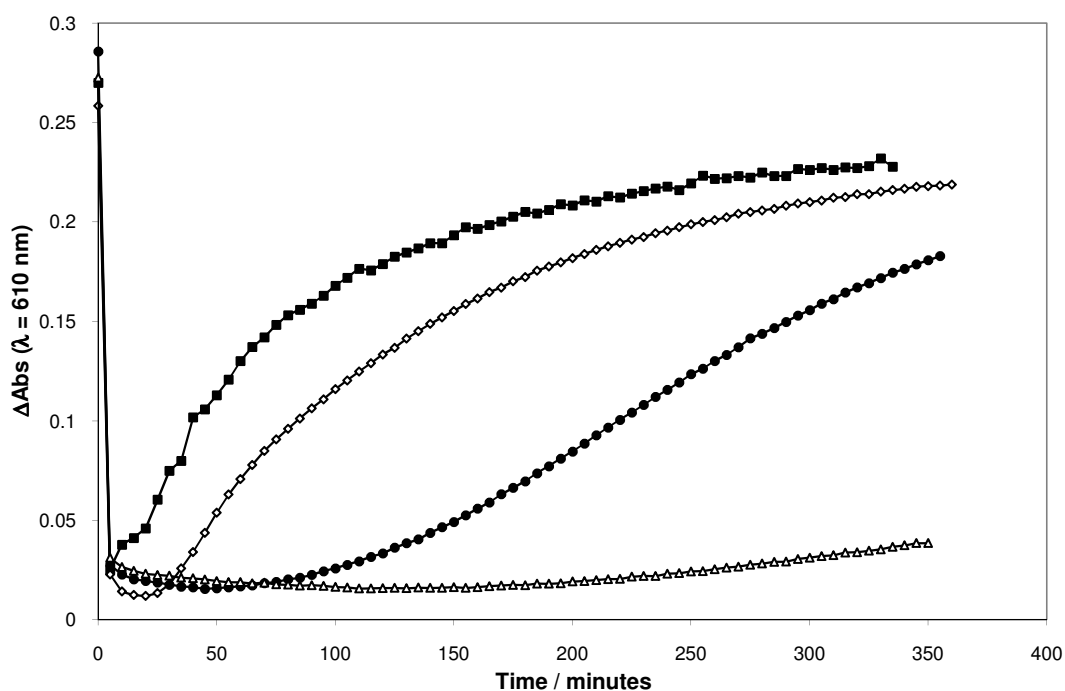
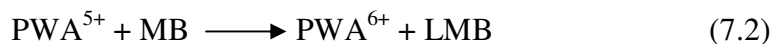


**Fig. 7.7** – Effect of level of humidity in air on the response of indicator after 4 minutes irradiation under UVB light ( $4 \text{ mWcm}^{-2}$ ), where ■ (80%RH), ◇ (50% RH), ● (25%RH) and △ (0%RH), at  $21^\circ\text{C}$ .

From Fig. 7.7, it is evident that humidity plays a significant role in the recovery of the indicator. Under mid to high humidity conditions (50 - 100%RH), the indicator is nearly fully recovered after 5 hours, whereas under low humidity levels (0 - 20%RH) the indicator recovers very slowly. The indicator left in dry air (0%RH) only began to recover some of its initial blue colour after 5 hours. The humidity dependence may be explained by the dependence of water (or  $\text{H}^+$ ) on the rate determining step and the plasticisation effect of water.

It is also evident from Fig. 7.7 that even after the indicator has been removed from the UV light, the absorbance continues to decrease before increasing. Reactions (7.1) – (7.3) summarise the three processes involved which produces the colour change.



From previous studies, it is known<sup>6</sup> that reaction 7.3 is slow at low pH (and quite likely slower in PWA/MB ion pairs). The dip appears to show reaction 7.2 is slow and that after illumination some PWA<sup>5+</sup> is still around to react with MB, hence the delayed response.

#### 7.3.3.4 Indicator optimisation as a personal UV-dosimeter

As discussed at length in Chapter 1, the development of UV indicators which change colour depending on the ‘dose’ of UV light is useful in the development of personal sunburn indicators (i.e. UV dosimeter). In order to optimise the ink to become suitable as a personal UV dosimeter, a series of experiments were carried out using a UV solar simulator.

The effect of the level of glycerol present on the initial rate of the indicators bleaching was investigated. A series of inks were prepared with varying quantities of glycerol in the range 0 - 240 pphr. These inks were then used to produce thin films which were irradiated using a solar simulator at UVI = 5, for 33 minutes, giving an overall MED = 1 (based on skin phototype II). As mentioned previously, glycerol acts as a SED. Presumably, by increasing the level of glycerol (i.e. increasing the quantity of electrons available), the initial rate,  $r_i$ , would increase. The results of this study are presented in Fig. 7.8.

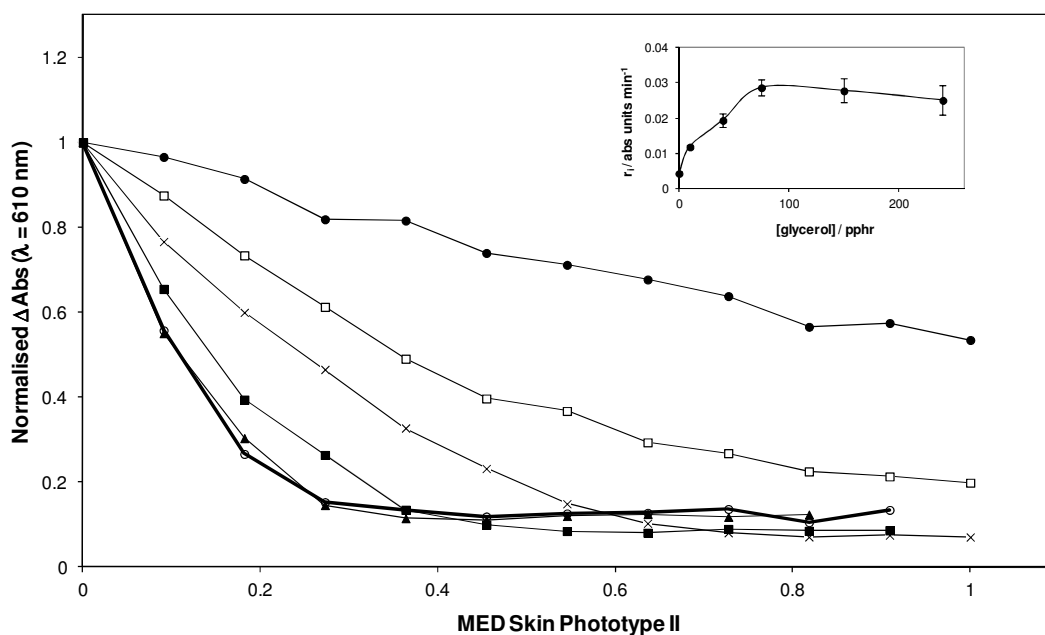


**Fig. 7.8** – Plot of  $\Delta\text{Abs}(\lambda = 610 \text{ nm})$  against MED level of skin phototype II for indicator films containing 0 pphr (●), 10 pphr (□), 40 pphr (×), 75 pphr (■), 150 pphr (○) and 240 pphr (▲) glycerol, at 21°C. Inset diagram shows the variation of initial rate with [glycerol], calculated using the data in the main diagram. MED values on x-axis are directly proportional to irradiation time, with MED = 1  $\equiv$  33 mins.

From these results, an increase in rate is observed up to an optimum concentration of  $\sim 100$  pphr. Increasing the level of glycerol beyond this point did not improve the performance of the indicator. Interestingly, photobleaching is still observed in the absence of glycerol, albeit at a significantly reduced rate. This may be attributed to the electron donating ability of the polymer, PVA.

In a similar manner to the previous experiment, a series of inks were prepared where the level of sodium phosphotungstate was varied and irradiated as before. Studying the proposed schematic illustration in Fig. 7.2 suggests that no colour change will take place if no polyoxometalate is present in the ink and the initial rate increase with increase polyoxometalate concentration. The results are illustrated in Fig. 7.9.

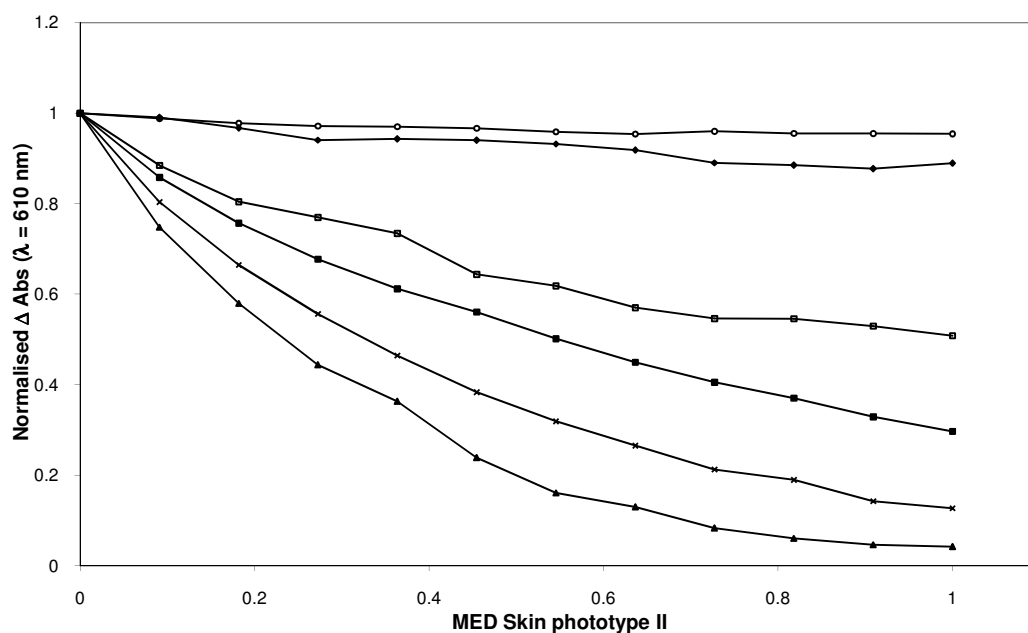


**Fig. 7.9** – Plot of  $\Delta\text{Abs}$  vs. MED Skin phototype II for a series of indicator films containing 0 pphr (○), 30 pphr (◆), 35 pphr (□), 40 pphr (■), 45 pphr (×) and 50 pphr (▲) NaPWA, at 21°C. The ink contained 12 mg methylene blue opposed to the standard 8 mg, in the attempt to make the colour change of the final dosimeter more striking. MED values on x-axis are directly proportional to irradiation time, with MED = 1  $\equiv$  33 mins.

From these results, it is evident that the ink containing no sodium phosphotungstate showed no colour change over the length of irradiation, as expected. Gradually increasing the concentration from 0 to 50 pphr [NaPWA], revealed an increase in initial rate ( $r_i$ ). The plot of [NaPWA] versus initial rate ( $r_i$ ) in Fig. 7.10, illustrates this relationship effectively.



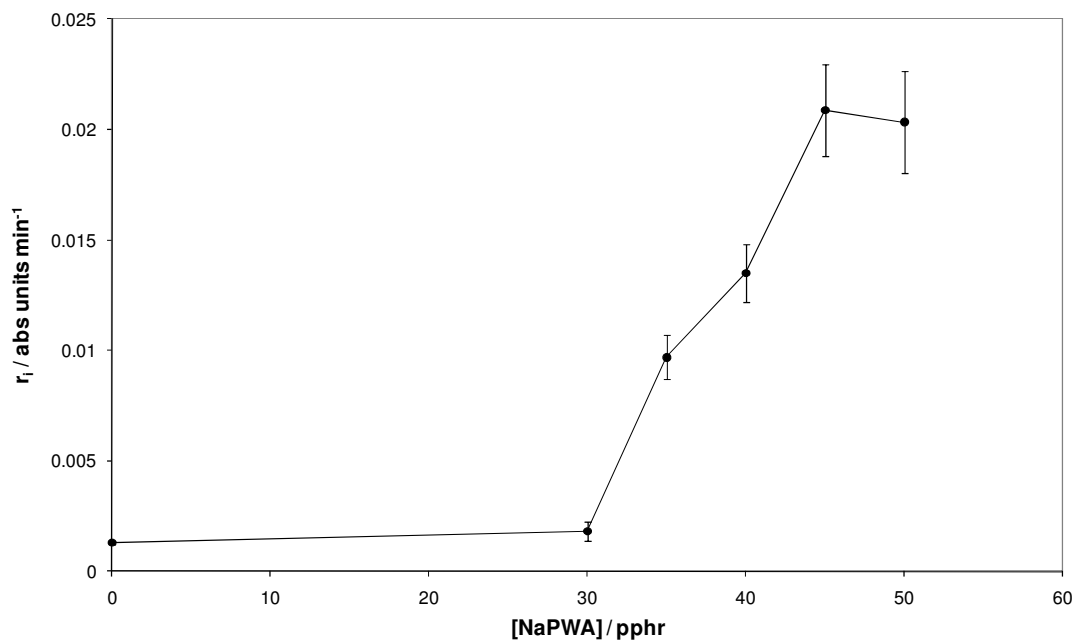


**Fig. 7.10** – Plot of initial rate ( $r_i$ ) vs. [NaPWA], illustrating the optimum concentration of NaPWA.

Interestingly, the initial rate increases minimally between 0 and 30 pphr NaPWA. This may be due to insufficient amounts of PWA available to bind to the  $\text{MB}^+$ . However, further studies would be needed to investigate this relationship.

In order to obtain a distinct colour change between 0 and 1 MED, hence making the indicator suitable as a personal UV dosimeter, the original ink formulation was altered to PVA/MB/NaPWA/glycerol, 100/6/45/15 pphr. Fig. 7.11, shows the variation in absorbance at 610 nm for the original (o) and modified (●) ink.

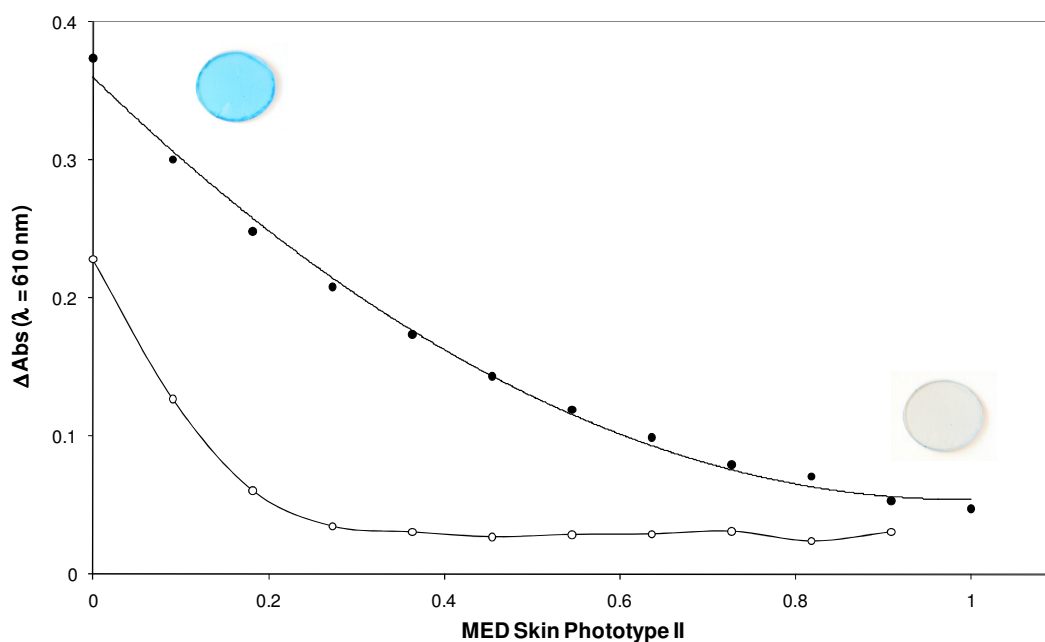


**Fig. 7.11** – Plot of  $\Delta\text{Abs}$  vs. MED for skin phototype II for original (o) and modified (●) ink, at 21°C.

The modified ink, compared to the original ink, has a darker blue colour before irradiation takes place due to the increased dye loading. This provides a more distinct colour change, making it easier to notice when sunburn is about to take place. The decreased concentration of sodium phosphotungstate allows a more gradual colour change, which corresponds to the time skin phototype II will begin to burn (MED = 1). By varying the levels of NaPWA and glycerol, it is possible to make UV dosimeters for other skin phototypes.

In order to create an irreversible UV dosimeter (which would be necessary if used in ambient air), further work would need to be carried out. One possible way to create this would be to apply an oxygen impermeable membrane which would stop the indicator recovering due to the presence of  $\text{O}_2$  in air.

## 7.4 Conclusions

A polyoxometalate-based UV indicator which gradually fades from blue to colourless upon exposure to UV light has been developed. Increasing the amount of

plasticizer was found to increase the rate of response to UVB light. Similarly, increasing the amount of NaPWA, also quickened the rate of response towards UVB light. By fine-tuning these parameters, along with the dye level, it was demonstrated that a UVB personal dosimeter which becomes fully photobleached at different MED levels (for different skin types), can be formulated.

## 7.5 References

1. <http://www.solarsafewristbands.co.uk/>, (accessed, 20/10/10).
2. <http://www.sunsignals.com/>, (accessed, 25/10/10).
3. A. Mills, *Chem. Soc. Rev.*, 2005, **34**, 1003-1011.
4. M. L. Wen, Y. B. Zhao, X. Chen and C. Y. Wang, *Croat. Chem. Acta*, 1998, **71**, 757-764.
5. T. Antony, M. Atreyi and M. V. R. Rao, *Chem.-Biol. Interact.*, 1995, **97**, 199-214.
6. A. Mills, J. Hepburn and M. McFarlane, *ACS Applied Materials & Interfaces*, 2009, **1**, 1163-1165.

## Chapter 8: Summary

---

This research endeavoured to develop new and extend the capabilities of existing indicators for commercially useful analytes, in particular CO<sub>2</sub>, O<sub>2</sub> and UV. Examples of each type of indicator have been developed, characterised and compared to existing technology.

Investigations into the development of water-based colourimetric CO<sub>2</sub> indicators led to the discovery of an indicator with enhanced shelf-life. Characterisation studies of the water-based indicator revealed it to be less sensitive compared to its solvent-based counterpart, but still responding and recovering in commercially useful times. It was found that by increasing the plasticizer (glycerol) content, the indicator's response and recovery times decreased. The indicator's sensitivity was found to decrease with increasing base concentration. As expected, the indicator became less sensitive towards CO<sub>2</sub> with increasing temperature. A demonstration of the ink being loaded into a felt-tipped pen and applied onto a variety of different surfaces was illustrated. Its possible application as a MAP leakage indicator was identified.

A CO<sub>2</sub>-sensitive indicator capable of detecting pressures of CO<sub>2</sub> above ambient pressure was reported. A progressive colour change from deep pink to yellow was demonstrated over a 0 – 8 bar CO<sub>2</sub> pressure range. Increased response and recovery times were observed with increasing humidity levels and an increased sensitivity with decreasing temperatures was observed, as typical for most CO<sub>2</sub>-indicators. The application of this indicator to detect the degree of fizz in a carbonated drink was demonstrated. The indicator was shown to have distinct colour changes between ~ 0 (air), 1 and > 4 bar CO<sub>2</sub>, which correspond to the equilibrium headspace pressures above an empty, flat and fizzy carbonated drink, respectively. An alternative solvent-based ink was also developed and characterised.

The coating of dyes onto particulate inorganic substrates (e.g. silica) led to the development of a range of intelligent pigments. These pigments were then dispersed into an extrudable, thermoplastic polymer, creating a series of flexible intelligent plastics. CO<sub>2</sub>-sensitive plastics were characterised extensively, showing similar sensing abilities as previously reported CO<sub>2</sub>-sensitive inks. O<sub>2</sub> (both colourimetric

and fluorimetric) and UV-sensitive pigments and plastics were also demonstrated, illustrating the scope of the range of analytes which can be detected. Intelligent plastics were reported to have a significant advantage over inks since they can be incorporated more easily into existing substrates i.e. food packaging and medical equipment. A reduction in processing cost was also highlighted as one of the main advantages of this technology, since it eliminates the need for printing. It was suggested that this may increase the likelihood of such indicators being commercialised.

The interesting chemistry of polyoxometalates resulted in the development of two novel indicators. The first colourimetrically detects the presence of oxygen. The indicator was shown to be activated by irradiation of UVB light, creating a colourless to dark blue colour change. Further characterisation revealed that the indicator slowly returns to colourless in the presence of oxygen. As expected, the rate at which this occurs was found to be dependent on the concentration of oxygen. Although the UV activation step was found not to be particularly humidity dependent, the oxidation step was found to be very humidity sensitive. The addition of glycerol (as a SED and plasticiser) was found to reduce the formation of heteropolybrowns, which have been previously reported in earlier work. Interestingly, when the ink was applied onto standard white printer paper, the response towards oxygen was decreased. This was thought to be due to the decreased local concentration of the plasticiser (glycerol). This prompted the possible application as a delayed oxygen indicator, useful in food packaging applications.

The second polyoxometalate-based indicator incorporated the redox dye methylene blue, which gradually turns from blue to colourless when irradiated with UVB light. The effect of humidity on the recovery of the indicator was found to be humidity dependent; increasing humidity increased the rate of recovery. Increasing the glycerol content up to 100 pphr increased the rate of bleaching, however beyond this optimum concentration, no further increase was observed. Similarly, increasing the polyoxometalate content (sodium phosphotungstate), revealed an increase in the initial rate of bleaching. Combining these observations, along with increasing the dye concentration, led to an optimised ink formulation which changed colour between 0

and 1 MED. This allowed the ink to be used as a personal UV dosimeter and more specifically as a sunburn warning indicator. It was noted that a range of sunburn indicators could be developed for different skin types by altering the formulation.

### **Further work**

- Following the interesting work on pigment and plastics in Chapter 5, it is envisaged that a flexible pigmented plastic form of the high pressure CO<sub>2</sub> ink, as described in Chapter 4, would be advantageous in the commercial development of the indicator. Further work to transfer the sensing capabilities of the ink formulation into a pigment and subsequent plastic would need to be carried out. One obvious technical difficulty which would need to be addressed is the identification of an alternative plasticiser, since glycerol is a viscous hygroscopic liquid at room temperature.
- All characterisation of the high pressure CO<sub>2</sub> indicator was carried out in the headspace (i.e. gas phase). However, it is envisaged that the indicator (if appropriately water-proofed) would colourimetrically detect the amount of CO<sub>2</sub> dissolved in the carbonated drink (i.e. fizz). Further work, would need to be carried out to characterise this property fully.
- It was evident in work reported in Chapter 5, that the scope of intelligent pigments and plastics is substantial. Further work to extend the preliminary work carried out on both O<sub>2</sub> (colourimetrically and fluorimetrically) and CO<sub>2</sub> (breath indicator) indicators would be beneficial. Development of pigments and plastics to detect other analytes such as humidity, carbon monoxide and volatile organics would also be very valuable to a range of industries.
- The need for an O<sub>2</sub>-impermeable membrane to be applied onto the UV-dosimeter was highlighted in Chapter 7. This would create an irreversible indicator, which would be necessary to ensure an accurate dosage of UVB light could be indicated by the sensor, when used in ambient conditions (i.e.

~20% O<sub>2</sub>). Further work would investigate this amendment to the indicator design and investigation on how/if it affects any of its indicating properties.

- A range of polyoxometalate-based sunburn indicators for different skin types could be developed by altering the ink formulation. The translation of the ink into a pigmented plastic would also be very useful, since it would enable the indicator to be tuned into a wrist-band type of product.

## Appendix – Published papers

---

- A. Mills and G. A. Skinner, Water-based colourimetric optical indicators for the detection of carbon dioxide, *Analyst*, 2010, **135**, 1912 – 1917.
- A. Mills, G. A. Skinner and P. Grosshans, Intelligent pigments and plastics for CO<sub>2</sub> detection, *J. Mater. Chem.*, 2010, **20**, 5008 – 5010.
- A. Mills and G. A. Skinner, A novel ‘fizziness’ indicator, *Analyst*, 2011, **136**, 894 – 896.



# Water-based colourimetric optical indicators for the detection of carbon dioxide

Andrew Mills\* and Graham A. Skinner

Received 12th January 2010, Accepted 26th May 2010

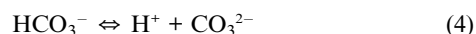
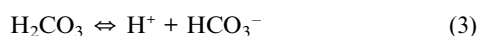
DOI: 10.1039/c000688b

Water-based colourimetric indicator films are shown to have increased operational lifetimes under ambient conditions compared to similar solvent-based counterparts. The response and sensitivity characteristics of a water-based, carbon dioxide-responsive ink are characterised and compared and contrasted to those of a similar solvent-based indicator. The changes in the response characteristics of the ink as a function of the amount of base (sodium hydrogen carbonate) and plasticizer (glycerol) contained in the ink are reported, as are the effects of varying ambient temperature and humidity. The ink is incorporated into a felt tip pen and applied to a number of different substrates, producing a distinct, reversible colour change on all tested surfaces, when a sufficient level of carbon dioxide is present. The possible application of the indicator is discussed briefly.

## Introduction

Colourimetric optical indicators for the detection of carbon dioxide have been studied widely in recent years and their applications are broad and varied (*e.g.* food packaging,<sup>1</sup> medicine<sup>2</sup> and environmental monitoring<sup>3,4</sup>). These indicators are attractive due to their inexpensive manufacture, quick response and recovery times and striking colour changes. This combination of properties renders them suitable for semi-quantitative analysis, with little or no need for supporting analytical equipment (apart from the human eye).

Most colourimetric CO<sub>2</sub>(g) indicators are reliant upon the change in pH which occurs when CO<sub>2</sub>(g) dissolves in water. In aqueous solution this observed pH change is due to the following reactions:



In such indicators, the colour change is usually due to the presence of a pH-sensitive dye which reacts with the protons generated *via* reactions (1)–(4), *i.e.*,



where A is the colour of the deprotonated dye (D<sup>−</sup>) and B is the colour of the protonated form of the dye (HD). Thus, upon exposure of such an indicator to CO<sub>2</sub>(g) at an appropriate level, the pH of the ambient environment decreases sufficiently to

protonate the dye and so cause a measurable and usually observable change in absorbance of the indicator.

Many papers and patents have been published on the development of such colourimetric CO<sub>2</sub> optical indicators,<sup>5–11</sup> with the majority focused on solvent-based (*i.e.* non-aqueous) systems, incorporating a phase transfer agent (PTA) to solubilise the usually lipophilic dye and base.<sup>12</sup> However, it has been noted by many that a major drawback of such systems is their poor shelf-life stability<sup>12–17</sup> when stored under dark, but otherwise ambient, conditions. Thus, typically, the dye in such indicators will, over a period of a few hours/days, change irreversibly to its acidified form, rendering the indicator ineffective. It has been suggested that this irreversible reaction is due to acidification of the film by ambient SO<sub>2</sub> and NO<sub>x</sub>,<sup>16,17</sup> which is possible given typical levels of SO<sub>2</sub> and NO<sub>x</sub> in the atmosphere are in the range ~5 to 10 μg m<sup>−3</sup> and ~40 μg m<sup>−3</sup> respectively.<sup>18</sup> As a result, manufacturers have largely overcome this problem by packaging the indicators in an inert atmosphere,<sup>2,19</sup> but with an obvious added cost to production. Curiously, water-based CO<sub>2</sub> indicators have not been well studied, and we have found recently that such indicators have markedly greater lifetimes, than their solvent-based counterparts, when stored under ambient air conditions. Thus, in this paper we report the characteristics of a typical water-based CO<sub>2</sub> indicator and compare and contrast them with those of an otherwise similar, but solvent-based, CO<sub>2</sub> indicator.

## Experimental

### Materials

All chemicals were purchased from Sigma Aldrich, unless specified, and at the highest purity available. The water used to make all aqueous solutions was double distilled and deionised. The gases were obtained from BOC gases and of high purity. Gas blends were generated using a Cole–Parmer rotameter-based, gas-blender. Spectrophotometric measurements were carried out using a Perkin Elmer Lambda 35 UV-Visible spectrophotometer. All films were produced using a spin coating technique, with a Spin Coater Model 4000-1 (Electro-Micro Systems).

Department of Pure & Applied Chemistry, University of Strathclyde, Glasgow, UK G1 1XL. E-mail: a.mills@strath.ac.uk; Fax: +44 (0)141 548 4822; Tel: +44 (0)141 548 2458

## Methods

A typical water-based *meta*-cresol purple (MCP) ink was prepared by dissolving 0.100 g sodium salt of *m*-cresol purple in an aqueous solution comprising 2.5 ml distilled water and 1 ml of 0.7 M aqueous sodium hydrogen carbonate solution. The solution was stirred for 10–15 minutes, placed in a sonicating bath for 10 minutes, then stirred further until fully dissolved. To 2.0 ml of this solution were added 10 g of 5% w/v aqueous hydroxyethyl cellulose (HEC) solution, 1 ml of the 0.7 M aqueous sodium hydrogen carbonate solution and 1.5 g glycerol; this solution was then stirred at room temperature for 30 minutes. The resulting ink was blue/purple in colour with a viscosity of approximately 1000 cP, as measured using a cone and plate rheometer (6 cm and 0.5°). The composition of the printed form of the water-based ink can be summarised by the ratios of HEC/MCP/NaHCO<sub>3</sub>/glycerol = 100/11/18/300 pphr, where pphr = parts per hundred resin.

A typical<sup>12</sup> solvent based *m*-cresol purple ink was also prepared at the same time by dissolving 0.036 g of *m*-cresol purple in 3 ml methanol and 0.5 ml 1 M tetrabutylammonium hydroxide (TBAH) in methanol. This solution was stirred for 10–15 minutes, placed in the sonicating bath for 10 minutes, then stirred further until all the components were fully dissolved. To 2 ml of this solution were added 10 g of 10% w/v ethyl cellulose in toluene/ethanol (80 : 20) (EC), 1 ml tributyl phosphate (TBP), 0.5 ml of 1 M tetrabutylammonium hydroxide in methanol and a further 0.5 ml methanol; the product was stirred at room temperature for 30 minutes. The resulting ink was dark blue with a viscosity of approximately 900 cP. The composition of the printed EC/MCP/TBAH/TBP ink was 100/2/20/97 pphr.

In preparation of dried colourimetric films of the above inks for CO<sub>2</sub> analysis, 1–2 drops of the ink were placed onto a borosilicate microscope slide and spun-coated at 1000 rpm for 15 seconds. Typical film thicknesses for the water- and solvent-based indicator films were ~1 and ~0.8 μm, respectively, as measured using scanning electron microscopy.

## Results and discussion

### Longevity

As noted earlier, the well-known, limited shelf-life of most solvent-based CO<sub>2</sub> colourimetric films,<sup>13,14</sup> when stored under ambient dark conditions, is an obvious limitation to their application. Thus, longevity experiments were carried out on both the solvent- and water-based CO<sub>2</sub> indicators, whereby their absorbances were measured as a function of time over a period of

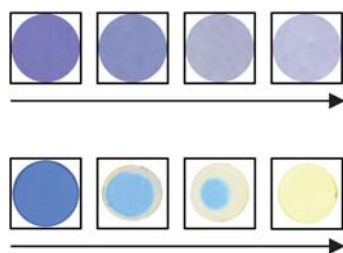


**Fig. 1** Comparison of film deterioration of water-based (top: 0, 4, 8, 12 weeks) and solvent-based indicators (bottom: 0, 1, 3, 5 weeks) when stored in the dark under ambient conditions.

12 weeks when stored in the dark, but under otherwise ambient lab conditions. The results showed that whereas the water-based indicator fades slowly and uniformly over time (but is still blue and working after 35 weeks), the solvent-based indicator fades much more quickly and changes irreversibly to the acidified yellow form of the dye, rendering it ineffective. As illustrated in Fig. 1, the solvent-based films make a characteristic ring pattern during this blue to yellow colour change (yellowing) process.

As noted earlier, it has been suggested that this ‘yellowing’ is due to the irreversible acidification of the dye by interfering acidic gases found in air (*e.g.* SO<sub>2</sub> and NO<sub>2</sub>).<sup>16</sup> It is not clear why the yellowing/acidification occurs from the edge first, spreading inwards. However, additional work shows that the film is at least 20% thinner at the film edge compared to the centre and presumably, the thinner the film the faster the acidification process. Interestingly, for reasons which remain unclear, the process of film fading appears very different for the water-based ink. Thus, in contrast to the solvent-based CO<sub>2</sub> indicator, the water-based indicator, in its faded form, still gives a good, quantifiable colourimetric response to carbon dioxide, even after 9 months of storage.

The loss in colour of either indicator can be moderated if the indicator is stored under a modified atmosphere, as is usually the case for commercial forms of the CO<sub>2</sub> colourimetric indicator.<sup>20</sup> So, as part of this work, the effects of storage conditions on the colours of both solvent- and water-based indicators were further investigated and the results are given in Table 1.

From this work, it appears that by choosing suitable storage conditions, whereby most notably the permeation of permanent, film-acidifying species such as NO<sub>2</sub> and SO<sub>2</sub> is minimised, the longevity of the solvent- and water-based CO<sub>2</sub> indicators can be increased markedly, although the solvent-based film still appears much less stable than its water-based counterpart. From the results in Table 1, the water-based indicator alone appears to possess a significant longevity under ambient conditions and although alternative environments can preserve the indicator longer, they are not essential.

### CO<sub>2</sub> sensitivity of water-based indicator

Photographs of a standard water-based CO<sub>2</sub> ink were recorded in the absence and increasing presence of CO<sub>2</sub> and the results are illustrated below in Fig. 2.

The results of Fig. 2 show that the initial blue indicator film turns increasingly yellow when exposed to a gas stream containing an increasing partial pressure of CO<sub>2</sub>. The process is reversible and so can be repeated many times with no sign of deterioration in indicator response.

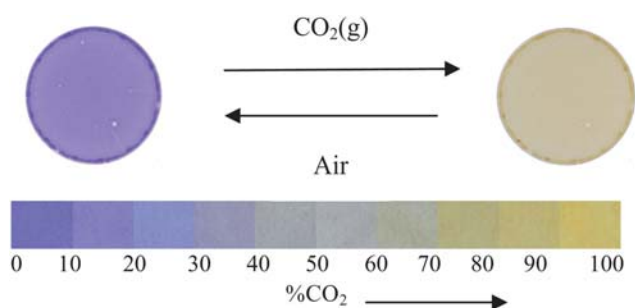
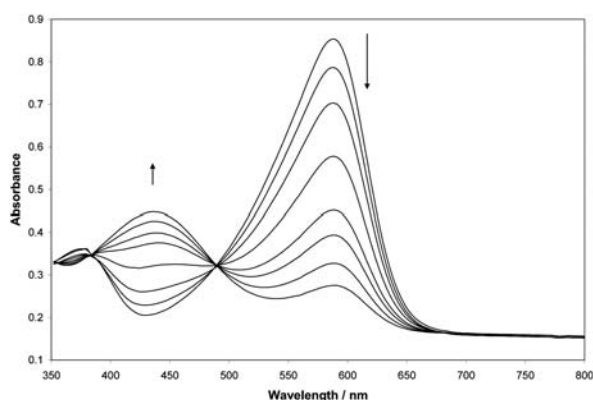
In this work, the absorbance spectrum of a standard CO<sub>2</sub> indicator film was also monitored by UV-Vis absorption spectroscopy as a function of ambient %CO<sub>2</sub> (varied using a gas blender) and the results are illustrated in Fig. 3. A clear isosbestic point is observed (at λ = 490 nm), indicating the conversion of the dye, from its blue, deprotonated form, to its yellow protonated form, by ambient CO<sub>2</sub> involves no other dye species, *i.e.* it is well described by reaction (5) as an equilibrium reaction between D<sup>-</sup> and HD.

It is usual<sup>12</sup> and useful to define the parameter, *R*, based on experimentally measurable absorbance values at λ<sub>max</sub> (due to D<sup>-</sup> alone) at different %CO<sub>2</sub>, as follows:

**Table 1** Summary table of dark storage conditions over 35 weeks for water- and solvent-based CO<sub>2</sub> indicators

Storage conditions	Water-based	Solvent-based
Open atmosphere	Fades, but indicator performs well even after 35 weeks	Irreversible deterioration (yellowing) starts within one week—film permanently yellow and non-functioning within 6 weeks
Sealed under air	Little fading, indicator works well	Irreversible deteriorating (yellowing) starts within 3 weeks—film permanently yellow and non-functioning within 7 weeks
Sealed under vacuum	Little fading, indicator works well	Little fading, indicator works well
Open atmosphere in fridge	Little fading, indicator works well	Starting to deteriorate after 20 weeks storage
Sealed over NaOH pellets	Little fading, indicator works well	Starts to deteriorate after 10 weeks
Sealed under CO <sub>2</sub> <sup>a</sup>	Little fading, indicator works well	Little fading, indicator works well
Sealed under Ar	Little fading, indicator works well	Little fading, indicator works well

<sup>a</sup> For samples stored under CO<sub>2</sub> the films are in their yellow protonated form, but when removed should, within 10 minutes, return to the original blue/purple (deprotonated) colour.

**Fig. 2** Photographs of a standard CO<sub>2</sub> indicator and progressive colour response chart to CO<sub>2</sub>.**Fig. 3** UV/visible absorption spectra of the standard film as a function of %CO<sub>2</sub> at 21 °C, for %CO<sub>2</sub> (from top to bottom at λ<sub>max</sub> (D<sup>-</sup>), 588 nm) of 0, 2, 5, 10, 20, 30, 60, 100%, respectively.

$$R = (\text{Abs}_0 - \text{Abs}) / (\text{Abs} - \text{Abs}_\infty) = [\text{HD}] / [\text{D}^-] \quad (6)$$

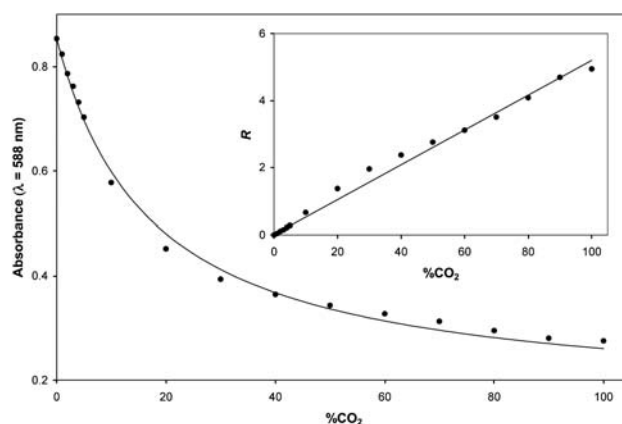
where [HD] and [D<sup>-</sup>] are the concentrations of the protonated and deprotonated forms of the dye, respectively. Abs<sub>0</sub> is the value of absorbance of the dye at λ<sub>max</sub> (D<sup>-</sup>) when %CO<sub>2</sub> = 0 (*i.e.* when all the dye is in its deprotonated form) and Abs<sub>∞</sub> is the absorbance of the film when all the dye has been converted into D<sup>-</sup>, *i.e.*

when %CO<sub>2</sub> = ∞. Since, with the dye concerned, HD does not absorb at λ<sub>max</sub> (D<sup>-</sup>), it is convenient to take Abs<sub>∞</sub> as that of the substrate (microscope slide) alone (*i.e.* no indicator film) at λ<sub>max</sub> (D<sup>-</sup>). From eqn (6) the parameter, *R*, is a measure of the transformation of the dye from the deprotonated to protonated forms and is directly proportional to [HD]/[D<sup>-</sup>].<sup>12</sup> Based on reactions (1)–(5), for such indicators it can be shown<sup>20</sup> that:

$$R = [\text{HD}] / [\text{D}^-] = \alpha \times \% \text{CO}_2 \quad (7)$$

where α is a proportionality constant, which is in turn inversely dependent upon the background base concentration, *i.e.* α vs. 1/[base], used in the film.<sup>21</sup> The absorbance (Abs) vs. %CO<sub>2</sub> plot arising from the data in Fig. 3 is illustrated in Fig. 4, along with the *R* vs. %CO<sub>2</sub> plot, calculated using these data and eqn (6). The linear relationship between *R* and %CO<sub>2</sub> is in accordance with eqn (7) and reveals an α value of 0.052 ± 0.001%CO<sub>2</sub><sup>-1</sup> at 21 °C.

In comparison, a typical solvent-based CO<sub>2</sub> indicator (using the same pH dye) revealed an α value of 0.33 ± 0.01%CO<sub>2</sub><sup>-1</sup> *i.e.* approximately 6 times more sensitive than the water-based

**Fig. 4** Plots of absorbance of film at 588 nm vs. %CO<sub>2</sub> (inset: *R* vs. %CO<sub>2</sub>). Data from Fig. 3. The solid lines are best fits to the data, assuming an α value of 0.052 ± 0.001%CO<sub>2</sub><sup>-1</sup>.

indicator, possibly due to the much greater solubility of CO<sub>2</sub> in the hydrophobic medium of the solvent-based polymer.<sup>22</sup>

### Indicator response and recovery times

In addition to indicator sensitivity (*i.e.* the value of  $\alpha$ ), other key characterisation parameters of any indicator are its response and recovery times. In one set of experiments the typical Abs (D<sup>-</sup>) response and recovery curves for a standard water-based ink were recorded by exposing it to an alternating gas stream of air and 100% CO<sub>2</sub> and the results are illustrated in Fig. 5, from which 90% response and recovery times,  $\tau_{90}$ , of 30 and 120 s, respectively, were determined.

In comparison, the  $\tau_{90}$  response and recovery times of a solvent-based ink were found to be <1 and 3 s respectively. These much shorter values of  $\tau_{90}$  may be due to a much greater plasticizer action of tributyl phosphate compared to that of glycerol.

### Effect of base concentration

The sodium hydrogen carbonate concentration in a typical water-based ink was varied over the range 0.1 M to saturated (*ca.* 1.2 M) to create a series of water-based indicator films and the observed variation in absorbance *versus* %CO<sub>2</sub> recorded for each film is illustrated in Fig. 6. As expected, from other work on solvent-based CO<sub>2</sub> indicators<sup>17</sup> and predicted from reactions (1)–(5),<sup>21</sup> the sensitivity ( $\alpha$ ) of a typical water-based indicator is inversely proportional to [base] as illustrated by the plot of the data in this form shown as the inset diagram in Fig. 6.

### Plasticizer

The use of plasticizers in solvent-based CO<sub>2</sub> film indicators is a common<sup>7,12,14,15</sup> method for decreasing the response and recovery times exhibited by the indicator films, by increasing the rate of diffusion of the CO<sub>2</sub> throughout the film.

Thus, increasing the level of plasticizer (*i.e.* glycerol) in the water-based CO<sub>2</sub> indicator should decrease the response and recovery times of the indicator. This feature was confirmed by the results illustrated in Fig. 7.

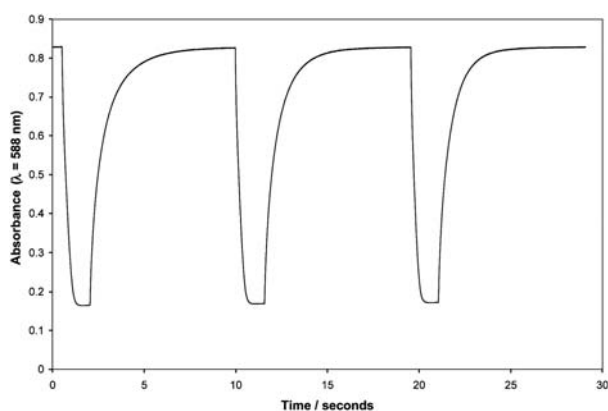


**Fig. 5** Absorbance *versus* time plot for the typical water-based film, when exposed to alternating gas supply of air and 100% CO<sub>2</sub>(g).

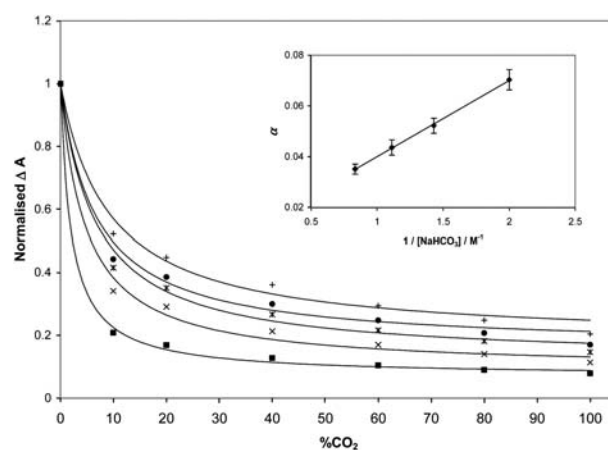


**Fig. 6** Change in normalised absorbance ( $=\Delta\text{Abs}/\Delta\text{Abs}_0$ ) *versus* %CO<sub>2</sub>, as a function of varying sodium hydrogen carbonate concentration (from bottom to top: 0.1, 0.5, 0.7, 0.9 M and saturated respectively). The inset diagram is a plot of  $\alpha$  (from the data in the main diagram) *versus*  $1/[\text{NaHCO}_3]$ .

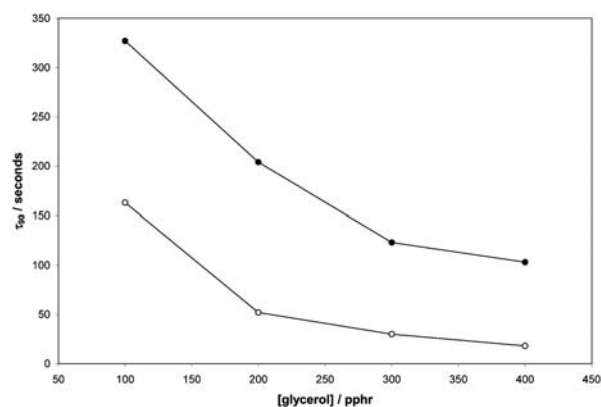


**Fig. 7** Relationship between response/recovery time and glycerol concentration ( $\tau_{90}$  recovery (●) and  $\tau_{90}$  response (○)).

Solvent-based indicators are known to behave similarly using tributyl phosphate as the plasticizer.<sup>15</sup>

### Humidity

Most CO<sub>2</sub> indicators exhibit some sensitivity towards relative humidity.<sup>16</sup> And a brief study of a typical water-based indicator exposed to 0 and 40%CO<sub>2</sub> at different relative humidity (RH) values, spanning the range 25 up to 100%RH at 20 °C revealed a clear increase in  $\alpha$  (*i.e.* sensitivity towards CO<sub>2</sub>) with increasing %RH, as illustrated in Fig. 8. Additional work showed this effect on  $\alpha$ , upon increasing the relative humidity, was completely reversible. In contrast, the solvent-based *m*-cresol purple indicator exhibited an opposite trend in sensitivity with increasing humidity, as illustrated by the results in Fig. 8.

Similar findings to these have been reported by Schröder and Klimant,<sup>16</sup> studying solvent-based CO<sub>2</sub> indicators with either quaternary ammonium or phosphazene bases. That the solvent-based indicator showed little or no sensitivity towards humidity over a wide range (20–70% for the indicator in Fig. 8) is

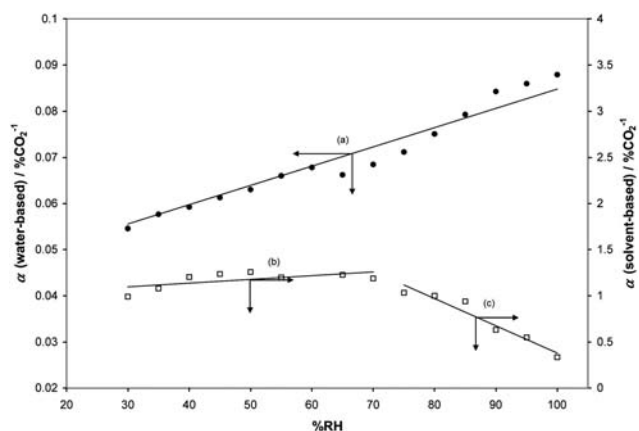


**Fig. 8** Effect of humidity on sensitivity ( $\alpha$ ) for a water-based indicator ( $\bullet$ ) and solvent-based indicator ( $\square$ ). The sensitivity of the water-based ink is directly proportional to %RH (a), whereas that of the solvent-based ink is mostly independent (b) or, at high %RH, negatively affected (c).

suggested<sup>16</sup> to be due to the intrinsic molecules of water associated with the dye–base ion pair, *i.e.*  $D^-Q^+ \cdot xH_2O$ , that enable reaction (5) to take place. In contrast, the same workers found a phosphazene indicator became increasingly  $CO_2$ -sensitive (rather like the water-based indicator reported here) with increasing RH, due to the need for water to promote reaction (5), and the lack of any bound water of hydration in the indicator. Thus, the water-based  $CO_2$  indicator exhibits a similar humidity response as that noted<sup>16</sup> for a phosphazene-based  $CO_2$  indicator, presumably due to the lack of bound water of hydration.

### Temperature

A series of experiments using a water-based  $CO_2$  indicator were carried out in which the absorbance due to the deprotonated dye was monitored as a function of % $CO_2$  for indicators at different temperatures. The data were used to create  $R$  vs. % $CO_2$  plots from which different  $\alpha$  values as a function of temperature were extracted. A Van't Hoff plot of the data, *i.e.*  $\ln(\alpha)$  versus  $T^{-1}$ , revealed a good straight line for which values of  $-27 \text{ kJ mol}^{-1}$  and  $-113 \text{ J mol}^{-1} \text{ K}^{-1}$  were calculated for  $\Delta H$  and  $\Delta S$  respectively for the overall process, *i.e.*



Typical solvent-based  $CO_2$  indicators, have similar values of  $-(28 \text{ to } 80) \text{ kJ mol}^{-1}$  and  $-(211 \text{ to } 80) \text{ J mol}^{-1} \text{ K}^{-1}$  for  $\Delta H$  and  $\Delta S$  respectively.<sup>12,16</sup> Thus, water-based indicators, like solvent-based ones, exhibit a strong temperature dependence, becoming less sensitive with increasing temperature.

### Application to different substrates

Most promising, in terms of possible applications, the indicator can be applied readily (*e.g.* via felt-tipped pens) to a variety of different materials, including ceramics, paper and aluminium foil as illustrated in Fig. 9. A typical, water-based carbon dioxide sensing ink was incorporated into a refillable felt-tipped pen and prepared using a thinner polymer solution and increased dye, base and plasticizer content. This felt-tipped pen ink formulation

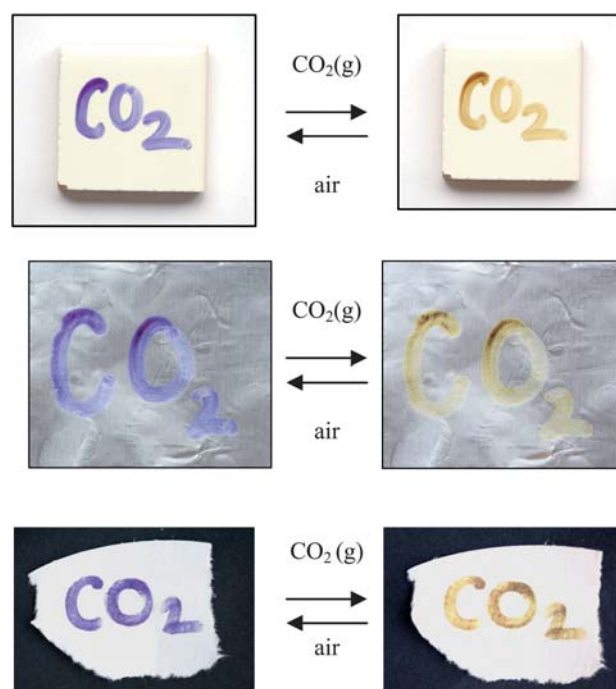


**Fig. 9** Ink applied by pen onto a variety of substrates (top: ceramic tile, middle: cellulose based filter paper, bottom: metal foil), all showing a distinct colour change when exposed to  $CO_2(g)$ .

is summarised as follows: HEC/MCP/ $NaHCO_3$ /glycerol = 100/43/55/750 pphr.

The ink when stored in a sealed container (such as a bottle or pen) under otherwise ambient conditions is very stable, showing no deterioration even after one year. Such an indicator might find applications in modified atmosphere packaging (MAP), with a suitable coating to prevent dye leaching and direct food contact, although the humidity and temperature sensitivity of the ink are drawbacks. Fortunately, in MAP often the food package is maintained at a fixed (usually chilled,  $4^\circ\text{C}$ ) temperature and (for meat and fish) high and largely unchanging %RH. Thus, under such conditions a water-based  $CO_2$  indicator may find applications in MAP, if not as a quantitative indicator of ambient  $CO_2$ , at least as a semi-quantitative  $CO_2$  indicator of the package integrity.

### Conclusions

A water-based  $CO_2$  indicator ink is less sensitive towards  $CO_2$  than its solvent-based counterpart, but much more stable in terms of shelf life. The water-based  $CO_2$  indicator is still quick in its response and recovery ( $\leq 2$  minutes), but rendered less sensitive with increasing base concentration. Increasing the amount of plasticizer improves the indicator's response and recovery times. As is common with most  $CO_2$  indicators, the water-based indicator's sensitivity toward  $CO_2$  decreases with increasing temperature. The response of a water-based  $CO_2$  indicator is directly related to relative humidity, roughly increasing by 80% as the RH is increased from 20% to 100%. In contrast, a solvent-based  $CO_2$  indicator is largely humidity insensitive over the RH range 20–70%; which is an important advantage of the latter. The

water-based inks have much improved operational lifetimes compared to the more, well-studied solvent-based indicators<sup>5,12</sup> and can be applied to a variety of different surfaces, using a simple applicator, such as felt-tipped pen.

## Notes and references

- 1 C. Von Butzingslowen, A. K. McEvoy, C. McDonagh, B. D. MacCraith, I. Klimant, C. Krause and O. S. Wolfbeis, *Analyst*, 2002, **127**, 1478–1483.
- 2 C. G. Fehder, *US Pat.*, 5 166 075, 1992.
- 3 R. A. Kopelman, *US Pat.*, 7 247 493, 2007.
- 4 M. D. DeGrandpre, *Anal. Chem.*, 1993, **65**, 331–337.
- 5 R. Lines, *Int. Pat.*, 075 498, 2007.
- 6 O. Oter, K. Ertekin and S. Derinkuyu, *Talanta*, 2008, **76**, 557–563.
- 7 M. J.-P. Leiner, J. Tusa and I. Klimant, *EP*, 1 965 198, 2008.
- 8 G. C. Upreti, Y. Wang and A. S. H. Kueh, *Int. Pat.*, 079 024, 2008.
- 9 R. Ostrowski and M. P. Debreczeny, *Int. Pat.*, 039 424, 2008.
- 10 Y. Amao and N. Nakamura, *Sens. Actuators, B*, 2004, **100**, 347–351.
- 11 S. M. Borisov, M. C. Waldhier, I. Klimant and O. Wolfbeis, *Chem. Mater.*, 2007, **19**, 6187–6194.
- 12 A. Mills, Q. Chang and N. McMurray, *Anal. Chem.*, 1992, **64**, 1383–1389.
- 13 J. F. Fernandez-Sanchez, R. Cannas, S. Spichiger, R. Steiger and U. E. Spichiger-Keller, *Sens. Actuators, B*, 2007, **128**, 145–153.
- 14 H. N. McMurray, *J. Mater. Chem.*, 1992, **2**, 401–406.
- 15 A. Mills and L. Monaf, *Analyst*, 1996, **121**, 535–540.
- 16 C. R. Schröder and I. Klimant, *Sens. Actuators, B*, 2005, **107**, 572–579.
- 17 B. H. Weigl and O. S. Wolfbeis, *Sens. Actuators, B*, 1995, **28**, 151–156.
- 18 <http://www.scottishairquality.co.uk>, accessed 03/09/2009.
- 19 F. Colin, T. J. N. Carter and J. D. Wright, *Sens. Actuators, B*, 2003, **90**, 216–221.
- 20 A. Mills, A. Lepre and L. Wild, *Sens. Actuators, B*, 1997, **38–39**, 419–425.
- 21 A. Mills and Q. Chang, *Anal. Chim. Acta*, 1994, **285**, 113–123.
- 22 J. Brandrup, E. H. Immergut and E. A. Grulke, *Polymer Handbook*, Wiley-Interscience, 1999.



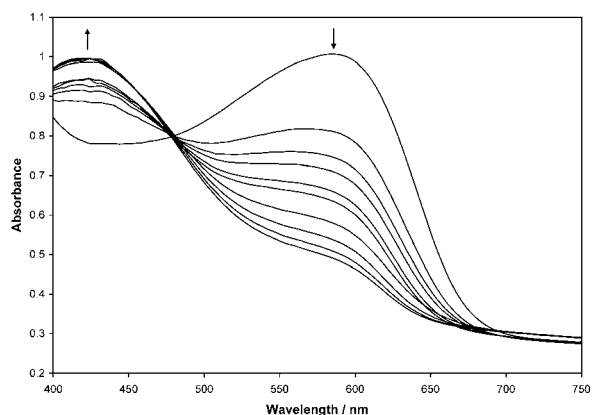


**Fig. 3** UV/visible absorption spectra of the MCP/silica/PE plastic film as a function of %CO<sub>2</sub>, for %CO<sub>2</sub> (from top to bottom) of 0, 1, 2, 3, 4, 5, 20, 30, 60, 100%, respectively. Abs<sub>∞</sub> is ~0.44.

was stirred for at least 30 minutes. The composition of the deposited dried ink film, 0.8 μm thick, in terms of pphr, was EC/MCP/TBAH/tributyl phosphate = 100/4/19.5/97.

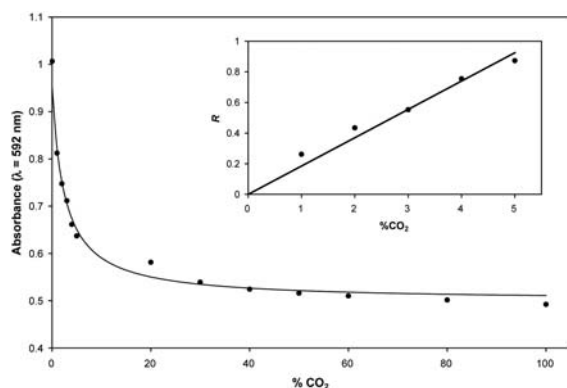
The MCP/silica pigment in polyethylene plastic film is initially blue coloured but, as with the bare pigment (see Fig. 1), it changes to yellow upon exposure to carbon dioxide gas, as illustrated in Fig. 2. This characteristic, blue to yellow, colour change was also observed for the MCP solvent-based ink, which uses the same quaternary base.

Fig. 3 shows the recorded UV-visible spectra of the MCP/silica pigment plastic film as a function of %CO<sub>2</sub>. As with its solvent-based film counterpart, the change in colour, due to λ<sub>max</sub> shifting from 592 to 424 nm, is a result of the MCP<sup>-</sup> forming MCPH *via* reaction (2). The variation in the absorbance due to the MCP in the plastic film as a function of %CO<sub>2</sub> is illustrated in Fig. 4.

It is useful to define the parameter, *R*, which is directly proportional to the ratio of concentrations [MCPH]/[MCP<sup>-</sup>], *via* Beer's law, through the expression:

$$R = (Abs_0 - Abs)/(Abs - Abs_\infty) = [MCPH]/[MCP^-] \quad (3)$$

where Abs<sub>0</sub> is the value of absorbance of the dye at λ<sub>max</sub> (MCP<sup>-</sup>) when %CO<sub>2</sub> = 0 (*i.e.* when the dye is fully in its deprotonated form)



**Fig. 4** Plots of absorbance of MCP/silica pigment plastic film at 592 nm versus %CO<sub>2</sub>. Data from Fig. 3. Solid lines were best fit to the data, revealing an α value of 0.185 ± 0.02%CO<sub>2</sub><sup>-1</sup>.

and Abs<sub>∞</sub> is the absorbance of the film when all the dye has been converted into its protonated form *i.e.* when %CO<sub>2</sub> = ∞. Since MCPH does not absorb at λ<sub>max</sub> (MCP<sup>-</sup>), it is convenient to estimate Abs<sub>∞</sub> at 592 nm. For such indicators it can be shown<sup>3</sup> that:

$$R = [MCPH]/[MCP^-] = \alpha\%CO_2 \quad (4)$$

and the linear relationship between *R* and %CO<sub>2</sub>, as illustrated in the inset diagram in Fig. 4, reveals an α value of 0.185 ± 0.02%CO<sub>2</sub><sup>-1</sup>. A similar experiment carried out on the solvent-based CO<sub>2</sub>-indicator reveals an α value of 0.80 ± 0.08%CO<sub>2</sub><sup>-1</sup>. Since α is a measure of indicator sensitivity, it appears that the solvent-based sensor shows a greater sensitivity (4 times) towards CO<sub>2</sub> compared to the MCP/silica pigment plastic indicator, possibly in part due to the greater permeability of CO<sub>2</sub> (by a factor of *ca.* 9) in ethyl cellulose compared to polyethylene.<sup>8</sup> Although the two indicator systems tested have markedly different dye levels ([dye] = *ca.* 7 times more—in terms of pphr in the solvent based indicator), this is unlikely to be responsible for the difference in sensitivity for two reasons. Firstly, the sensitivity of such indicators is expected<sup>9</sup> to be independent of dye concentration, except at very high dye levels. Secondly, at high dye concentrations the dye will buffer the system and so the indicator would appear less sensitive (not more, as found for the higher dye-containing solvent-based indicator).

The MCP/silica pigment plastic indicator is fully reversible and responds quickly (within a few minutes) when exposed to 100% CO<sub>2</sub>, but has a slow recovery time (*ca.* 2 hours to fully recover). In contrast the solvent-based CO<sub>2</sub>-indicator has response and recovery times of both <1 and 3 s respectively. The above differences between the two indicators are due to the diffusion dependence of indicator film response and recovery times which, as a consequence, will depend upon film thickness and CO<sub>2</sub> permeability. Thus, the much slower recovery time of the polyethylene indicator will be due to its greater film thickness (100 compared to 0.8 μm) and lower CO<sub>2</sub> permeability (different by a factor of *ca.* 9). Both CO<sub>2</sub>-indicators can be used repeatedly without any loss in performance.

As noted earlier, it is known<sup>1,3,10</sup> that most solvent-based CO<sub>2</sub>-sensitive inks suffer irreversible acidification from interfering acidic gases, such as NO<sub>2</sub> and SO<sub>2</sub>. Indeed, all optical CO<sub>2</sub> indicators that operate *via* a pH changing dye are non-selective with regard to other acidic gases and the indicators reported in this paper are no different. This is a particular problem when it comes to film storage since NO<sub>2</sub> and SO<sub>2</sub> are typically present in an urban environment at levels of 150 and 50 ppb, respectively.<sup>10</sup> And so it is an important feature of the MCP/silica pigment plastic CO<sub>2</sub>-indicator films that they have a much greater longevity compared to that of a conventional solvent-based ink. For example, in our hands a solvent-based, indicator film will typically begin to acidify irreversibly, under ambient conditions within 1 week and be completely unusable within 5 weeks, when stored in a sealed container under ambient conditions. In contrast, the pigment/polymer composite film shows no visual sign of acidification after months of storage under the same sealed ambient, dark, conditions and works as if new. This is a significant advantage of the MCP/silica pigment plastic film indicators. Others<sup>1</sup> have shown the tolerance level of solvent based indicators for these acidic gases is only *ca.* 5 ppm. Interestingly, other work shows that the MCP/silica pigments have much higher tolerances (300 and 30 ppm for NO<sub>2</sub> and SO<sub>2</sub>, respectively), which helps explain their greater longevity when stored under ambient air.



MCP/silica pigment plastic films over the range 20–40 °C show a decrease in sensitivity (*ca.* 0.06% per °C) with increasing temperature, similar to that of the solvent-based indicator<sup>3</sup> (*ca.* 7% per °C). This decrease is not unexpected given the nature of the key reaction (2).

It was also found that the MCP/silica pigment plastic indicator shows little or no sensitivity towards relative humidity, presumably due to the extremely hydrophobic nature of the indicator. In contrast, the MCP solvent-based indicator, whilst showing little or no sensitivity over a wide humidity range (typically 20–70%RH), does exhibit a slight decrease in sensitivity for %RH higher than 70%RH. Similar results have been found by others<sup>6</sup> studying other CO<sub>2</sub>-sensitive, solvent-based indicators.

Fast-acting, reversible and stable, intelligent CO<sub>2</sub>-sensitive pigments incorporated into thermoplastics, such as polyethylene, are easy and cheap to prepare. The resulting plastic films exhibit excellent reversibility, a striking colour change and a markedly longer shelf-life than similar, solvent-based CO<sub>2</sub>-sensitive inks. As a consequence they

have great potential for use in a wide range of applications—including food packaging.<sup>11</sup>

## Notes and references

- 1 J. F. Fernandez-Sanchez, R. Cannas, S. Spichiger, R. Steiger and U. E. Spichiger-Keller, *Sens. Actuators, B*, 2007, **128**, 145–153.
- 2 M. J.-P. Leiner, J. Tusa and I. Klimant, *EP*, 1 965 198, 2008.
- 3 A. Mills, Q. Chang and N. McMurray, *Anal. Chem.*, 1992, **64**, 1383–1389.
- 4 A. Mills, A. Lepre and L. Wild, *Sens. Actuators, B*, 1997, **39**, 419–425.
- 5 G. C. Upreti, Y. Wang and A. S. H. Kueh, *Int. Pat.*, 079024, 2008.
- 6 C. R. Schroeder and I. Klimant, *Sens. Actuators, B*, 2005, **107**, 572–579.
- 7 R. Ostrowski and M. P. Debreczeny, *Int. Pat.*, 039424, 2008.
- 8 J. Brandrup, E. H. Immergut and E. A. Grulke, *Polymer Handbook*, Wiley-Interscience, 1999.
- 9 A. Mills and Q. Chang, *Anal. Chim. Acta*, 1994, **285**, 113–123.
- 10 H. N. McMurray, *J. Mater. Chem.*, 1992, **2**, 401–406.
- 11 A. Mills, *Chem. Soc. Rev.*, 2005, **34**, 1003–1011.

Cite this: *Analyst*, 2011, **136**, 894

www.rsc.org/analyst

## A novel 'fizziness' indicator

Andrew Mills\* and Graham A. Skinner

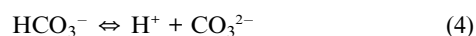
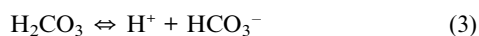
Received 6th August 2010, Accepted 9th December 2010

DOI: 10.1039/c0an00610f

**A novel colourimetric 'fizziness' indicator is described which changes colour depending on the headspace pressure of carbon dioxide above a carbonated liquid.**

The detection of carbon dioxide using colourimetric indicators has been the subject of research over many years and there are numerous examples which show a distinct reversible colour change in the presence of carbon dioxide.<sup>1–7</sup> However, all previous work has focussed on the detection of modest pressures of CO<sub>2</sub>, typically << 1 bar, due to the potential application for such indicators in food packaging or clinical analysis (*e.g.* capnography). In this work, we extend the range of detection to higher pressures and show how this can be used to indicate the degree of 'fizz' in a carbonated drink.

The majority of CO<sub>2</sub> colourimetric indicators are dependent upon the change in pH which occurs when CO<sub>2</sub> dissolves in water. In aqueous solution this observed pH change is due to the following equilibria:



coupled to:



where D<sup>−</sup> and DH are, respectively, the differently coloured deprotonated and protonated forms of a pH-sensitive dye. Thus, upon exposure of such an indicator to CO<sub>2</sub>, the pH of the dye's ambient environment is decreased sufficiently to protonate the dye, so as to cause a measurable and observable change in absorbance of the indicator; the greater the partial pressure of carbon dioxide (*P*<sub>CO<sub>2</sub></sub>) the greater the colour change. The p*K*<sub>a</sub> of the pH dye is critical in determining the sensitivity, and therefore practical operating range, of the colourimetric indicator; the lower the p*K*<sub>a</sub> the less sensitive the CO<sub>2</sub> indicator.<sup>2</sup>

The detection of carbon dioxide at pressures greater than 1 bar is very attractive, not least because it then provides a measure of the 'fizziness' of carbonated drinks, as indicated by the data in Table 1, and therefore, is a useful quality assurance tool to the retailer and the consumer.

Obviously, with such drinks, the headspace pressure decreases everytime the bottle is opened, or decreases with time in the case of faulty packaging; and such, usually unwanted, degassing increases with increasing temperature.

The longer the bottle is left opened—the more CO<sub>2</sub> is lost from the system and the lower the eventual equilibrium headspace pressure due to remaining CO<sub>2</sub>, when the bottle is eventually resealed.

A typical<sup>9</sup> water-based high *P*<sub>CO<sub>2</sub></sub> ink was prepared by dissolving 0.400 g of phenol red (sodium salt, PR) in 10 cm<sup>3</sup> of distilled water and adding 4 cm<sup>3</sup> of 1.0 M sodium hydroxide. The solution was stirred for 10–15 minutes and then 4 cm<sup>3</sup> of this solution added to 6.00 g of 15% w/v polyvinyl alcohol in water (PVA, MW 146 000–186 000), along with 0.600 g glycerol. The resulting solution was stirred at room temperature for at least 30 minutes. The composition of the PVA/PR/glycerol/NaOH ink can be summarised as 100/12.7/66.7/5.6 pphr, where pphr = parts per hundred resin. In order to characterise the dried form of the ink, the ink (bright pink) was spun-coated onto borosilicate glass discs using a spin coater at 2000 rpm for 10 seconds, forming a dry ~2 μm thick film.

The absorbance spectrum of such a standard film of the ink was monitored *via* UV-vis absorption spectroscopy as a function of CO<sub>2</sub> pressure and the results are illustrated in Fig. 1, along with the associated recorded colours of the indicator at the different *P*<sub>CO<sub>2</sub></sub> values.

The absorbance of the dye at the wavelength of its maximum absorbance in its deprotonated, D<sup>−</sup> form, λ<sub>max</sub> (D<sup>−</sup>), 570 nm, as a function of *P*<sub>CO<sub>2</sub></sub>, decreases in a hyperbolic manner as illustrated in Fig. 2. It is usual<sup>3</sup> and useful to define the parameter, *R*, based on experimentally measurable absorbance values at λ<sub>max</sub> (due to D<sup>−</sup>) at different *P*<sub>CO<sub>2</sub></sub>, as follows:

**Table 1** Typical carbonation levels<sup>8</sup>

Degree of 'fizziness'	Approximate <i>P</i> <sub>CO<sub>2</sub></sub> /bar at 20 °C
Flat	~≤1.0
Lightly sparkling	1.5
Typical fizzy drink ( <i>e.g.</i> cola)	3.5
Highly carbonated ( <i>e.g.</i> mixer)	4.0

Department of Pure & Applied Chemistry, University of Strathclyde, Glasgow, UK G1 1XL. E-mail: a.mills@strath.ac.uk; Fax: +44 (0)141 548 4822; Tel: +44 (0)141 548 2458

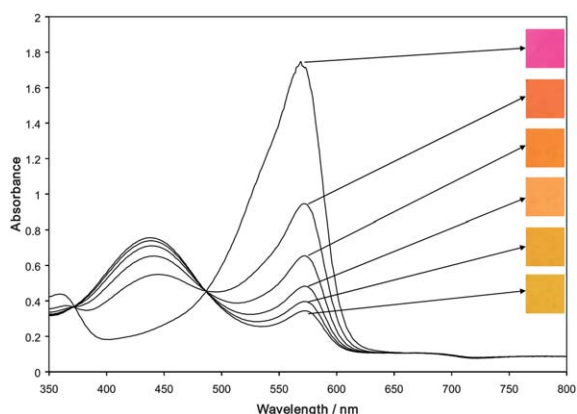


**Fig. 1** UV/visible absorption spectra of the film at different pressures of  $\text{CO}_2$  (from top to bottom: air, 1, 2, 4, 6, and 8 bar respectively).

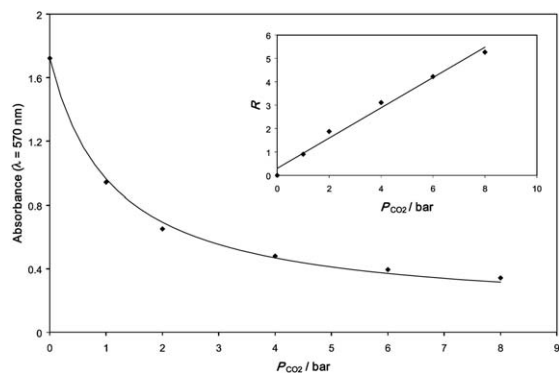


**Fig. 2** Plots of absorbance of the film at 570 nm vs.  $P_{\text{CO}_2}$  (inset:  $R$  vs.  $P_{\text{CO}_2}$ ). Data from Fig. 1. Solid lines are best fits to the data, revealing an  $\alpha$  value of  $0.65 \pm 0.04 \text{ bar}^{-1}$ .

$$R = (\text{Abs}_0 - \text{Abs}) / (\text{Abs} - \text{Abs}_\infty) = [\text{HD}] / [\text{D}^-] \quad (6)$$

where,  $\text{Abs}_0$  is the value of absorbance of the dye at  $\lambda_{\text{max}}(\text{D}^-)$  when  $P_{\text{CO}_2} = 0$  (*i.e.* when all the dye is in its deprotonated form), and  $\text{Abs}_\infty$  the absorbance of the film when all the dye has been converted into its protonated form (HD). Since the protonated form of the dye does not absorb significantly at  $\lambda_{\text{max}}(\text{D}^-)$ , it is convenient to take  $\text{Abs}_\infty$  as that of the substrate (in this case the glass disc) alone (*i.e.* no indicator film) at  $\lambda_{\text{max}}(\text{D}^-)$ .  $R$  is a measure of the transformation of the dye from its deprotonated to protonated form and for such indicators it can be shown<sup>3</sup> that:

$$R = [\text{HD}] / [\text{D}^-] = \alpha P_{\text{CO}_2} \quad (7)$$

where  $\alpha$  is the proportionality constant. The absorbance versus  $P_{\text{CO}_2}$  plot arising from the data in Fig. 1 is illustrated in Fig. 2, along with the  $R$  versus  $P_{\text{CO}_2}$ , calculated using these data and eqn (6). The linear relationship between  $R$  and  $P_{\text{CO}_2}$ , as expected from eqn (7), reveals an  $\alpha$  value of  $0.65 \pm 0.04 \text{ bar}^{-1}$ .

Typical response and recovery times for the indicator when exposed to 3 bar  $\text{CO}_2$  and then back to ambient environment are 22

and 54 minutes, respectively. The indicator is fully reversible and can be used repeatedly without any loss in performance. As a consequence, the response and recovery times of the indicator do not limit its ability to provide an indication of the degree of fizziness of the liquid next time the bottle is opened, provided that time is at least 1 h after the last.

To demonstrate the use of the ink as a 'fizziness' indicator for carbonated drinks, it was coated onto biaxially orientated polypropylene sheets (Goodfellow, 0.075 mm), which had been pre-treated with a 1  $\mu\text{m}$  coating of polyvinyl butyral in ethanol (20% w/v) to improve film adhesion. The samples were then laminated using commercially available PET lamination pouches (150  $\mu\text{m}$  thick) in order to render them waterproof. The use of a polymer substrate and lamination had no significant effect on the film response and recovery times. The product coloured strips were inserted into three standard polyethylene terephthalate (PET) based fizzy drink bottles which had caps adapted with inlet and outlet valves. In each case, one of these valves was linked up to a carbon dioxide cylinder to enable the pressure of carbon dioxide inside the bottle to be controlled externally. One bottle was left at ambient atmospheric conditions, the other pressurised to 1 bar  $\text{CO}_2$ , representing a 'flat' bottle of carbonated juice, and the third to 3 bar  $\text{CO}_2$ , representing a fizzy bottle of carbonated juice (see Table 1). As expected, and as shown in Fig. 3, there was a clear colour difference between the three indicator strips, indicating the difference in pressure. Additional work was carried out using the same indicator, where the contents of a fizzy drink bottle were progressively allowed to lose its fizz (by removing cap and allowing to stand). The results showed the same colour changes as illustrated in Fig. 3, with orange and magenta indicating the extremes of a 'very fizzy' and 'flat' state, respectively, in a commercial carbonated drink.

As is common with most  $\text{CO}_2$ -sensitive inks, a degree of temperature sensitivity is observed, whereby the  $\text{CO}_2$  sensitivity increases with decreasing temperature, but distinct colour differences were still observed between 1 and 3 bar  $P_{\text{CO}_2}$  values over the temperature range 5 to 25  $^\circ\text{C}$ .

In conclusion, a high pressure  $\text{CO}_2$  indicating ink is reported which has potential in the smart packaging of carbonated drinks. The indicators have different, distinct colours when exposed to key different pressures of  $\text{CO}_2$ . An indication of the level of fizziness is provided by observing the colour of the indicator, after the headspace pressure has equilibrated. The ink is stable, easy and cheap to prepare and highly reversible. The waterproof indicators, which may be incorporated in a clear bottle cap, provide a useful guide to the degree of fizziness of carbonated drinks; although, clearly, the indicator should only be used when the product is stored under the manufacturers recommended conditions, since failure to do so would possibly

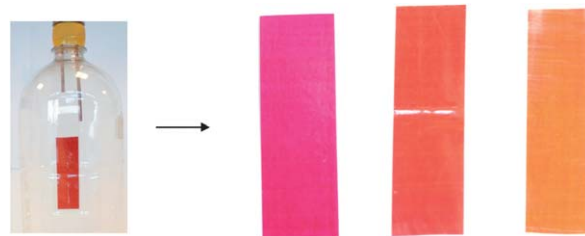


**Fig. 3** Pictures of the laminated ink inside the plastic bottle and the associated colour changes at three different pressures of  $\text{CO}_2$ —air, 1 bar and 3 bar  $\text{CO}_2$  respectively.

compromise the indicator as well as the product. In the case of fizzy drinks it is the recommendation of most manufacturer's to keep the product 'cool and store out of direct sunlight'. Saying that, under ambient room light conditions, or when exposed to AM1.5 solar simulated light for 24 h, the indicator showed no evidence of photobleaching or change of sensitivity.

These indicators have the potential to have a significant impact on areas associated with the measurement of high levels of carbon dioxide, which not only include carbonated drinks but also biotechnology (especially fermentation), refrigeration, dry cleaning, fire extinguishers, aerosols, sewage management and grain storage.

## Notes and references

- 1 H. N. McMurray, *J. Mater. Chem.*, 1992, **2**, 401–406.
- 2 A. Mills and Q. Chang, *Anal. Chim. Acta*, 1994, **285**, 113–123.
- 3 A. Mills, Q. Change and N. McMurray, *Anal. Chem.*, 1992, **64**, 1383–1389.
- 4 G. C. Upreti, Y. Wang and A. S. H. Kueh, *Int. Pat.*, 079024, 2008.
- 5 C. von-Bultzingslowen, A. K. McEvoy, C. McDonagh and B. D. MacCraith, *Anal. Chim. Acta*, 2003, **430**, 275–283.
- 6 B. H. Weigl and O. S. Wolfbeis, *Sens. Actuators, B*, 1995, **28**, 151–156.
- 7 C. G. Fehder, *US Pat.*, 5166075, 1992.
- 8 D. P. Steen and P. R. Ashurst, *Carbonated Soft Drinks—Formulation and Manufacture*, Blackwell Publishing, 2006.
- 9 A. Mills and G. Skinner, *Analyst*, 2010, **135**, 1912–1917.